Obviously influenced by the microarray software movement.

Relate your microarray data into biological pathways with Stratagene's software solutions.

In addition to developing innovative reagents and instrumentation, Stratagene now offers software solutions for life science researchers. We engineer our software so that it is powerful but extremely easy to use, allowing you to focus on your research.

Our Interaction Explorer™ Software (PathwayAssist) enables the building of pathway/biological association networks extracted from scientific literature, while our ArrayAssist® and GeneTraffic® software are specifically designed for analyzing microarray data.

- **Interaction Explorer™ Software (PathwayAssist) – turning microarray data into pathways**
- **ArrayAssist® Software – for complete microarray data analysis**
- **GeneTraffic® Software – data management and analysis for microarray core facilities**

Need More Information? Give Us A Call:

Stratagene USA and Canada
Order: (800) 424-5444 x3
Technical Services: (800) 894-1304

Stratagene Europe
Order: 00800-7000-7000
Technical Services: 00800-7400-7400.

Stratagene Japan K.K.
Order: 03-5159-2060
Technical Services: 03-5159-2070

www.stratagene.com

Ask us about these great products:

Visit **www.stratagene.com/softwaresolutions** for more information or to download trial versions of our software.

STRATAGENE

a spectacular variety of

multiplexed eicosanoids

PGE_2 ELISA (2-hr assay)
Leukotriene C_4 EIA
Thromboxane B_2 EIA
Leukotriene B_4 EIA
8-Isoprostane EIA
CGRP ELISA
Cyclic GMP EIA
Glutathione Assay
Cyclic AMP EIA
PGE_2 EIA
SOD Assay
LPO Assay
Cortisol EIA
Corticosterone EIA
TNFα (human) ELISA

Insulin EIA
Catalase Assay
Substance P ELISA
PGE-Metabolite EIA
PAF Acetylhydrolase Assay
Glutathione Peroxidase Assay
Interleukin 6 (human) ELISA
Testosterone EIA
6-keto $PGF_{1\alpha}$ EIA
Endothelin EIA
Histamine EIA
PGD_2-MOX EIA
$cPLA_2$ Assay
Leptin ELISA
PGE_2 FPIA
11-dehydro Thromboxane B_2 EIA
Creatinine Assay
Estradiol EIA
Interleukin 1β (human) ELISA
Aldosterone EIA
Nitrate/Nitrite Assay
Glutathione S-Transferase Assay
$iPF_{2\alpha}$-VI EIA
Aldosterone EIA
Enterolactone EIA
HDAC Assay
Renin Inhibitor Assay
Protein Carbonyl Assay
Ghrelin (Active) ELISA
PGD_2 FPIA
Vitellogenin ELISA
Leukotriene E_4 EIA

and many more...

Cayman CHEMICAL

www.caymanchem.com/kits

New Platforms for Cayman's Eicosanoid Assays

Several of Cayman's eicosanoid assays are now available on both the Luminex™ and Meso Scale Discovery™ platforms. Both systems provide multiplexing capabilities for the measurement of several analytes from a single small sample.

Luminex:
PGE_2
PGD_2
TXB_2
11-dehydro TXB_2
cysteinyl leukotrienes

MSD:
PGE_2
PGD_2
TXB_2

GE Healthcare

Ni Sepharose™

4x greater binding capacity in histidine-tagged protein purification

Ni Sepharose™ products from GE Healthcare give you the highest binding capacity available for histidine-tagged protein purification. With up to four times the binding capacity, it's no longer pure imagination to dramatically increase your yield, while saving time and costs. Maximum target protein activity is assured, thanks to tolerance of a wide range of additives and negligible nickel ion leakage. The flexibility to use a variety of protocols ensures the highest possible purity. Ni Sepharose 6 FF is excellent for manual procedures such as gravity/batch and easy scale-up, while the HP version is designed for high-performance in automated purification systems – both are available in different formats, including prepacked columns. Outstanding performance has never been easier to achieve.

www.amershambiosciences.com/his

imagination at work

GE10-05

Science

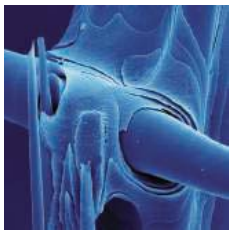

COVER Scanning electron micrograph of an etched sample of the mineral skeleton of the marine glass sponge (genus *Euplectella*), showing the laminated silica cement that holds glassy fibers in place. The design principles of this sophisticated, mechanically stable structure are described on page 275. [Image: J. C. Weaver, D. E. Morse, and J. Aizenberg]

Volume 309
8 July 2005
Number 5732

DEPARTMENTS

NEWS OF THE WEEK

NEWS FOCUS

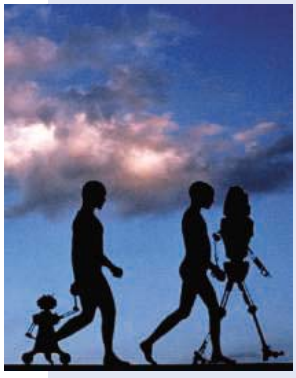

234

247

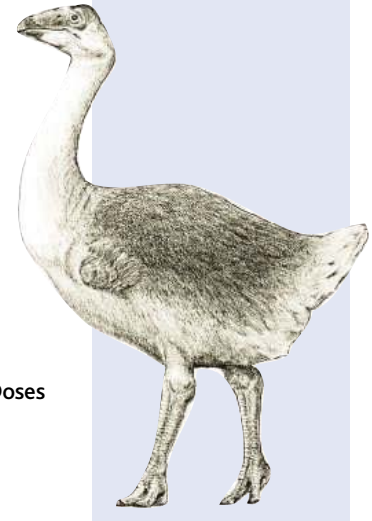

255 & 287

LETTERS

BOOKS *ET AL.*

POLICY FORUM

PERSPECTIVES

REVIEW

Contents continued

Systems Biology — Plasmid DNA Purification

Raising plasmid prep standards again — visual lysis control for greater confidence

New

Insufficient mixing of lysis buffer

Correct mixing of lysis buffer

Correct mixing of neutralization buffer

QIAGEN plasmid kits — now better than ever!

QIAGEN has consistently set the standard for plasmid purification, providing faster preps, higher throughput, more convenience, superior DNA quality for stringent applications, and contract production services. Now our enhanced plasmid prep kits offer even more:

- **Visual lysis control** — a simple color change during cell lysis (blue) and neutralization (colorless), ensures optimal mixing of buffers to give maximum yields of plasmid DNA
- **Color-coded buffer bottles** — easy identification of the correct buffer for added confidence
- **Streamlined handbooks and short protocols** — quickly find the information you need to get rapid results
- **Comprehensive plasmid resource site** — a one-stop Web site containing information on all aspects of plasmid purification at www.qiagen.com/goto/plasmidinfo

Purify your DNA with confidence — use QIAGEN plasmid kits with visual lysis control!

QIAGEN

WWW.QIAGEN.COM

SCIENCE EXPRESS www.sciencexpress.org

BREVIA

263

RESEARCH ARTICLE

REPORTS

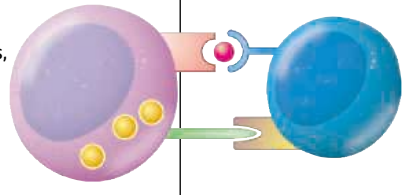

252 & 264

Contents continued


WANTED
revolutionary thinkers
NATIONAL RECONNAISSANCE OFFICE
UNITED STATES OF AMERICA
http://dii4.westfields.net
Specific proposal guidance is outlined in the annual DII Broad Agency Announcement and Government Sources Sought Announcement released each year via the Federal Business Opportunities and DII web sites.

Reports continued

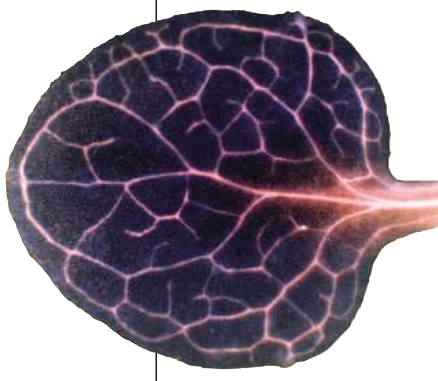

293

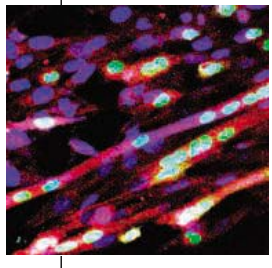

314

AAAS
ADVANCING SCIENCE, SERVING SOCIETY

SCIENCE (ISSN 0036-8075) is published weekly on Friday, except the last week in December, by the American Association for the Advancement of Science, 1200 New York Avenue, NW, Washington, DC 20005. Periodicals Mail postage (publication No. 484460) paid at Washington, DC, and additional mailing offices. Domestic individual membership and subscription (51 issues): $135 ($74 allocated to subscription). Domestic institutional subscription (51 issues): $550; Foreign postage extra: Mexico, Caribbean (surface mail) $55; other countries (air assist delivery) $85. First class, airmail, student, and emeritus rates on request. Canadian rates with GST available upon request, GST #1254 88122. Publications Mail Agreement Number 1069624. **Printed in the U.S.A.**

Change of address: allow 4 weeks, giving old and new addresses and 8-digit account number. **Postmaster:** Send change of address to *Science*, P.O. Box 1811, Danbury, CT 06813–1811. **Single copy sales:** $10.00 per issue prepaid includes surface postage; bulk rates on request. **Authorization to photocopy** material for internal or personal use under circumstances not falling within the fair use provisions of the Copyright Act is granted by AAAS to libraries and other users registered with the Copyright Clearance Center (CCC) Transactional Reporting Service, provided that $15.00 per article is paid directly to CCC, 222 Rosewood Drive, Danvers, MA 01923. The identification code for *Science* is 0036-8075/83 $15.00. *Science* is indexed in the *Reader's Guide to Periodical Literature* and in several specialized indexes.

Contents continued

Need to make a quantum leap in your career?

Then talk to someone who knows science.

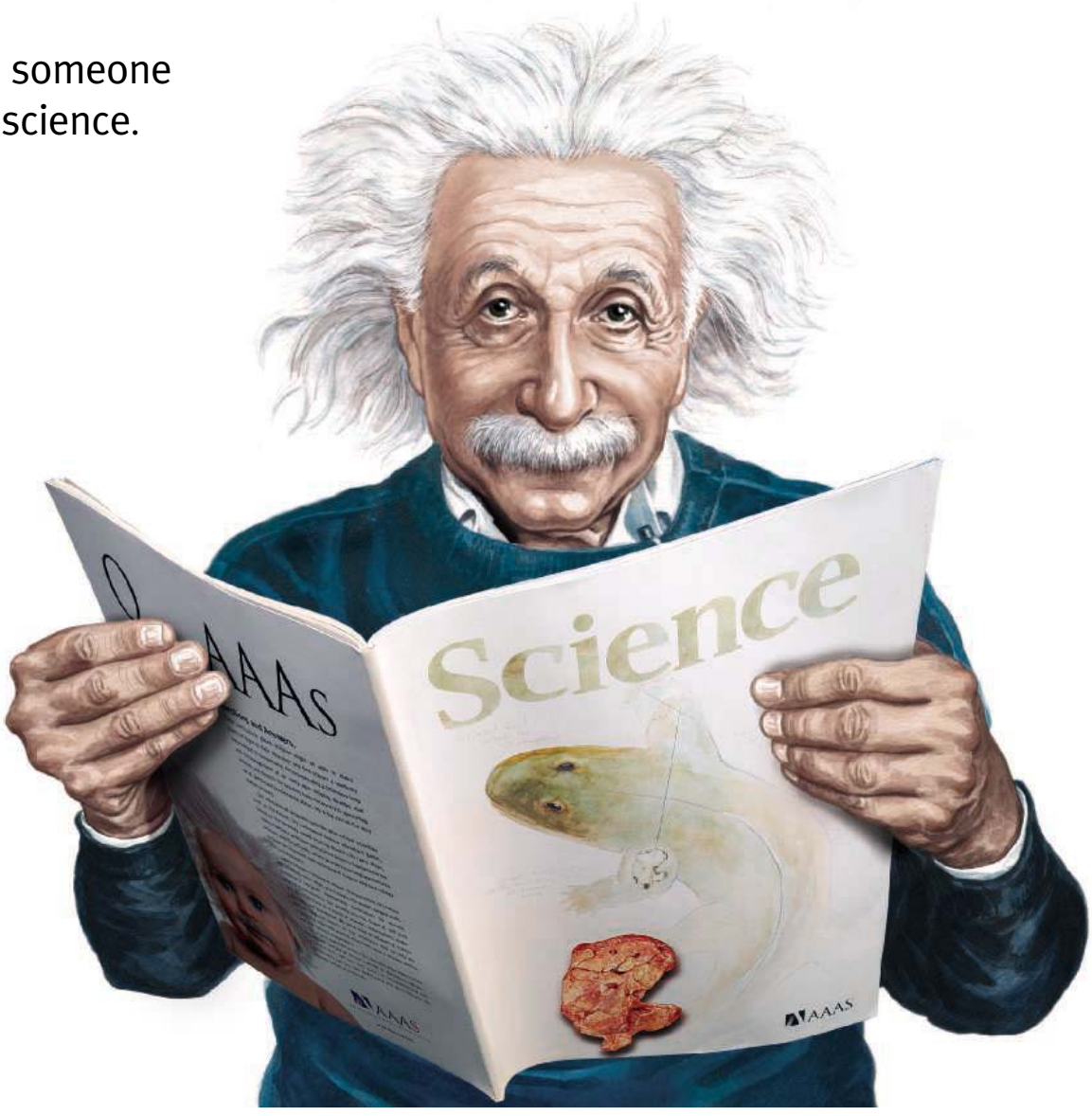

Albert Einstein
1879–1955

If you want to make a big bang in the world of science, it's essential you don't leave your career to chance. At ScienceCareers.org we know science. We are committed to helping you find the right job, and to delivering the advice you need. Our knowledge is firmly founded on the expertise of *Science*, the premier scientific journal, and the long experience of AAAS in advancing science around the world. So if you want a career that's relatively better, trust the specialist in science. Visit ScienceCareers.org.

$E=mc^2$

ScienceCareers.org
We know science AAAS

sciencenow www.sciencenow.org Daily News Coverage

Killer Cells Get a Boost
Protein that helps immune system fight infection has an on/off switch.

African Sand Dunes Are Hot to Trot
Global warming will alter land Africans rely on for ranching and farming.

Catching a Female's Eye
A male butterfly impresses its mate with a bit of sparkle.

Science
www.scienceonline.org

Quarterly Author Index
www.sciencemag.org/feature/data/aindex.shl

Next Wave's pedagogy toolkit.

science's next wave www.nextwave.org Career Resources for Young Scientists

Career Development Center: The Toolkit—Quick 'n' Dirty Pedagogy *R. Austin*
Get a short, nontechnical introduction to the basics of college-level science pedagogy.

Career Development Center: Discovery Corps and Other Transition Awards *GrantDoctor*
Very few fellowships are intended to help scientists make a transition away from the bench.

UK: Starting a Start-Up in the UK, Part 2—Getting the Funds *R. Phillips*
How do you get funding, where can you house your venture, and is it all worth the risk?

France: French Postdocs, Made in USA *E. Pain*
Only 20 percent of French postdocs in the United States intend to stay in North America.

MiSciNet: From Mexicali to Harvard *V. Chase*
A third-year doctoral student talks about his path from minimum-wage jobs to academic researcher.

GrantsNet: International Grants and Fellowships Index *Next Wave Staff*
Here is the latest listing of funding opportunities and competitions happening outside the United States.

science's sage ke www.sageke.org Science of Aging Knowledge Environment

Perspective: T-CIA—Investigating T Cells in Aging *S. Koch, J. Kempf, G. Pawelec*
European program aims to understand immune dysregulation in the elderly.

News Focus: Hair Trigger *R. J. Davenport*
Molecule induces skin cells to construct hair follicles.

News Focus: Odd SOD *M. Leslie*
Out-of-shape proteins speed death in neuron-destroying disease.

Sewing the seeds for new hair.

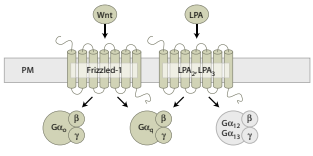

G proteins in β-catenin signaling.

science's stke www.stke.org Signal Transduction Knowledge Environment

Perspective: β-Catenin, Cancer, and G Proteins—Not Just for Frizzleds Anymore *C. C. Malbon*
Lysophosphatidic acid signals through GPCRs to increase cytoplasmic and nuclear accumulation of β-catenin.

Connections Map Overview: Natural Killer Cell Receptor Signaling Pathway *F. Vély and E. Vivier*
A balance of positive and negative signals controls NK cell response.

Connections Map Overview: Natural Killer Cell Receptor Signaling Pathway in Mammals *F. Vély and E. Vivier*
Mice and humans use a similar signaling cascade during activation of NK cells.

Separate individual or institutional subscriptions to these products may be required for full-text access.

Roche Applied Science

Universal ProbeLibrary

Design Your Gene-Expression Assay Today– *Run it Tomorrow!*

Universal ProbeLibrary Workflow

DAY 1

- Identify gene or target sequence of interest
- Design custom assay at **www.universalprobelibrary.com**
- Order assay-specific primers from your preferred oligo supplier for overnight delivery

DAY 2

- Select the appropriate probe from the Universal ProbeLibrary Set in your freezer
- Perform real-time PCR
- Evaluate results

Significantly reduce assay design time – In just seconds, design specific, intron-spanning real-time qPCR assays for human, mouse, rat, *Drosophila*, *Arabidopsis*, *C. elegans*, and primates.

Create cost-effective assays with high specificity for your gene of interest – The Universal ProbeLibrary provides you with probe specificity at prices comparable to SYBR Green I.

Why wait 1–4 weeks for an assay or custom probe? Create a functional, highly specific, optimized assay overnight using pre-validated Universal ProbeLibrary probes. Choose individual probes or a complete set of 90 probes stored in your freezer.

No special hardware or unique reaction conditions required – Employ standard PCR protocols on any real-time PCR instrument.

For detailed information on the Universal ProbeLibrary and to design your next qPCR assay, visit **www.universalprobelibrary.com**

Roche Diagnostics

Roche Diagnostics GmbH
Roche Applied Science
68298 Mannheim
Germany

edited by Stella Hurtley and Phil Szuromi

Nanophases and Electron Correlations

Some of most interesting condensed matter phenomena, such as high-temperature superconductivity and colossal magnetoresistance in transition metal oxides, occur in materials that have strongly correlated electrons. In addition, these materials often exhibit nanoscale phases that are spatially inhomogeneous. **Dagotto** (p. 257) reviews recent research in strongly correlated systems and argues that such materials are similar to other complex systems where new behavior emerges from the interaction of competing phases. Understanding these interactions and controlling the complex pattern formation in these materials will enable the emergence of novel functional properties.

Tiny Glass Engineers

Nature often has to make use of less than ideal construction materials because they are the only ones at hand. To compensate, organisms develop tricks to overcome the inherent weaknesses of these materials. **Aizenberg *et al.*** (p. 275; see the cover and the Perspective by **Currey**) have looked at the mineral-based skeleton of a deep-sea, sediment-dwelling sponge that is primarily made of glass. *Euplectella* uses a myriad of engineering tricks to overcome the brittle nature of glass and shows seven levels of hierarchical structure that span from the nanometer to the micrometer scale.

A Bite Out of C_{60}

The initially surprising stability of C_{60} has been justified by the precise arrangement of five- and six-membered rings in the framework. Although larger clusters, such as C_{70}, have been prepared, most smaller structures would require expanded rings, such as heptagons, in the skeleton. The associated strain has kept efficient synthesis of such compounds out of reach. **Troshin *et al.*** (p. 278) used a fluorinating agent, based on a cesium lead oxyfluoride salt, and synthesized milligram quantities of the elusive C_{58} clusters on heating with C_{60}. Two stable isolated compounds, $C_{58}F_{18}$ and $C_{58}F_{17}CF_3$, were characterized by mass spectrometry and by infrared and nuclear magnetic resonance spectroscopy. The data support a closed framework containing a seven-membered ring.

Moving Electrons Locally

The electrical conductivity of metals is understood in terms of delocalized band structures, but an alternative conductivity model, proposed by Pauling and modified by Anderson, suggests that conductivity can also arise in some materials in a localized way by the formation of resonating valence bond (RVB) structures that alternate between neutral species and ionic pairs. **Pal *et al.*** (p. 281) prepared a molecular solid based on the spirobiphenalenyl molecules that are neutral free radicals. The material has a high conductivity (0.3 siemens per centimeter), and extended Hückel calculations and magnetic susceptibility measurements indicate that the materials are metallic and have no band gap. However, the conductivity is slightly activated, and electronic spectra show an energy gap of 0.34 electron volt. The authors argue that these properties are best explained by viewing the material as a Mott insulator whose conductivity arises through an RVB ground state, unlike ion radical organic conductors.

Probing Coupling Between Quantum Dot Pairs

Manipulating exchange coupling between two electrons in coupled two-dot system is a fundamental concept in a spin-based quantum computing. Placing an electron on one dot affects the charging energy, and therefore the population dynamics of the other dot. However, these energies have not been well studied for realistic double-dot devices. **Hatano *et al.*** (p. 268) describe experiments and theory of electron tunneling in parallel through a hybrid vertical-lateral double-dot device. Depending on the alignment of the electronic states in the left and right dots, which can be tuned with gates, the additional electron can be localized in either dot or delocalized between the two. The two-quantum-dot system presented here should provide useful information for realistic implementations of quantum information processing using coupled quantum dots.

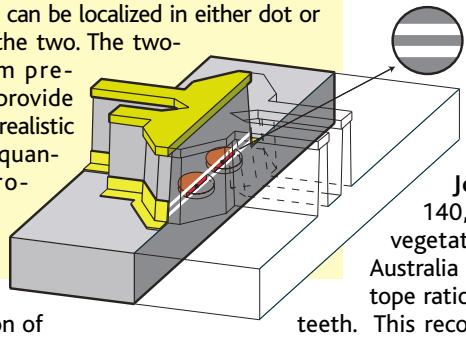

CREDIT: HATANO *ET AL.*

Australian Entry Evidence

Long climate and environmental records have been difficult to obtain from Australia. Humans arrived there about 50,000 years ago, just at the limit of radiocarbon dating. Whether their arrival led to the demise of much of Australia's distinct megafauna has been debated. **Miller *et al.*** (p. 287; see the Perspective by **Johnson**) have now obtained a 140,000-year record of the paleovegetation from three distinct sites in Australia based on the stable carbon isotope ratios of emu eggshells and wombat teeth. This record shows that shortly after the proposed human arrival, the emus and wombats were forced to eat more shrubs instead of grasses.

A Warning from Warmer Oceans

Observations have shown that the upper parts of all of the oceans of the world have become warmer during the past 50 years, and such warming could only have been caused by the absorption of huge amounts of heat. **Barnett *et al.*** (p. 284, published online 2 June 2005; see the Perspective by **Hegerl and Bindoff**) examine the patterns of warming on an ocean-by-ocean basis, as a function of amount, location, and time, and discuss the physics responsible for the observed trends. The patterns of warming can be reproduced accurately by two different climate models only if radiative forcing caused by increases in atmospheric greenhouse gases is included.

Expanding the Professional Cell Staff

Antigen-presenting cells (APCs) chew up proteins and offer the resulting fragments of peptide, along with a suite of stimulatory molecules, to cells of the γδ T cell receptor (TCR) lineage to produce activated T cells armed and ready to clear the corresponding infection. Few cell types are known to be potent "professional" APCs, and at the very top of the stack are dendritic cells (DCs). **Brandes *et al.*** (p. 264, published online 2 June 2005; see the Perspective by **Modlin and Sieling**) now expand this realm to include a subset of noncon-

CONTINUED ON PAGE 219

Q AAAs

Who's helping build the future of science?

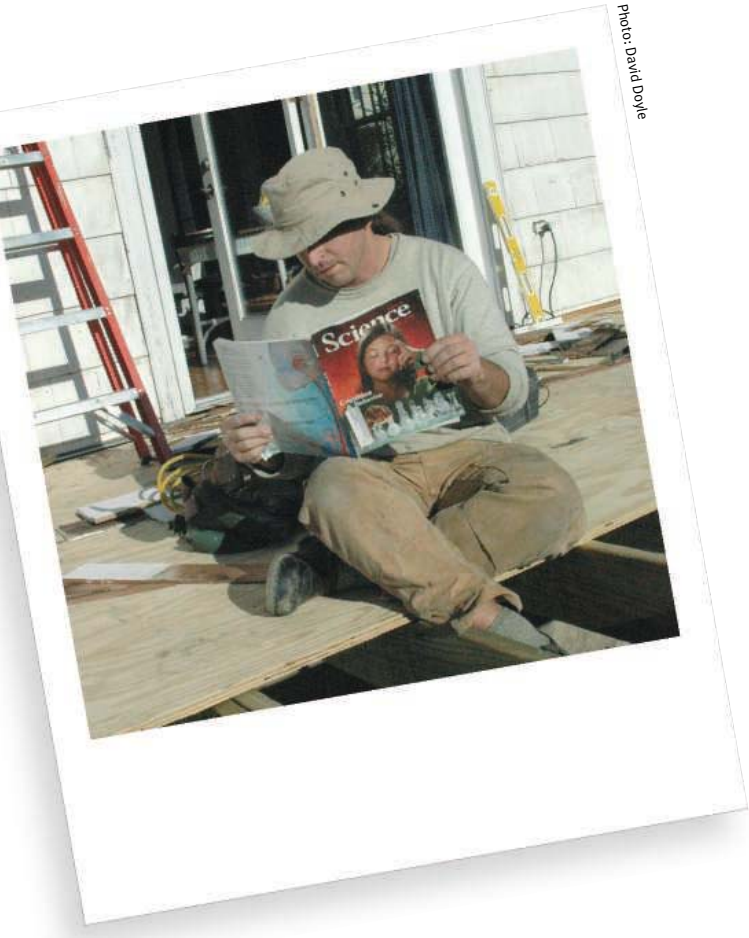

Photo: David Doyle

"I read my *Science* on the work site. Formerly a chemist, I found my true calling in woodworking, but I still try to keep up with advances in science. Reading *Science* also helps me answer questions from colleagues in the building trades about the safety and efficacy of the diverse materials we encounter."

Milton Trimitsis, carpenter and AAAS member

AAAS is committed to advancing science and giving a voice to scientists around the world. We work to improve science education, promote a sound science policy, and support human rights.

Helping our members stay abreast of their field is a key priority for AAAS. One way we do this is through *Science*, which features all the latest breakthroughs and groundbreaking research, and keeps scientists connected wherever they happen to be. Members like Milton find it essential reading.

To join the international family of science, go to www.aaas.org/join.

To see other member photos, please visit:
http://promo.aaas.org/memberpics.shtml

Milton Trimitsis

AAAS
ADVANCING SCIENCE, SERVING SOCIETY

www.aaas.org/join

ventional human T cells bearing the TCR. These cells react vigorously to microbial stimulation and when induced to do so in cell culture, became extremely efficient at presenting different types of antigen to their γδ T cell counterparts. The cells appeared to traffic antigen to the same cellular compartments as DCs and up-regulated an equivalent array of stimulatory and homing molecules. As well as contributing directly to innate immunity, T cells may also represent important instigators of adaptive immune responses.

Controlling the Layout

Successful adaptation and evolution of land plants relied on the acquisition of the stomatal complex, which allows efficient gas exchange for photosynthesis and respiration while minimizing water loss. In the epidermis of higher plants, stomatal complexes differentiate nonrandomly from precursor cells through rounds of asymmetric division. **Shpak *et al.*** (p. 290) now find that three *Arabidopsis* ERECTA family leucine-rich repeat receptor-like kinases, which are known to promote cell proliferation and organ growth, play overlapping but distinct roles to control stomatal patterning. The complexity of this signaling pathway illustrates how the interplay of moderate effects can lead to different outcomes in a developmental process.

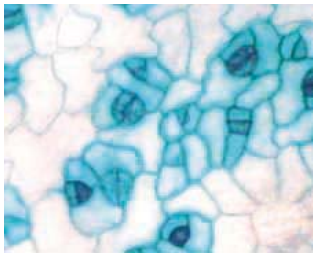

CREDIT: SHPAK *ET AL.*

When It's Spring Again

How does the plant know when its springtime? **Imaizumi *et al.*** (p. 293) now add some of the molecular details to the fascinating subcellular signaling process involved as plants respond to increases in daylength. As the days lengthen, so does the window of opportunity through which one protein, expressed in a daily cyclical pattern, can degrade its target. With longer days, the target suffers increasing degradation, removing its repression of the protein CONSTANS, thus allowing flowering to proceed.

Slip Sliding Away

Eukaryotic cells contain organized microtubule arrays that orchestrate polarized cellular behaviors. Fission yeast cells grow longitudinally and require a polarized distribution of their interphase microtubules along the long, growing axis of the cell. **Carazo-Salas *et al.*** (p. 297) describe how cytoplasmic microtubular arrays are arranged via microtubule sliding during interphase. An evolutionarily conserved, minus-end–directed molecular motor kinesin Klp2 is responsible for this sliding. The mechanism plays an important role in generating the highly polarized microtubules in fission yeast, and similar mechanisms may be exploited by other eukaryotes.

Poetry in Motion

The cooperative organization of dynamic biological processes often requires coordination via chemical signaling. **Riedel *et al.*** (p. 300) found that when attached to a surface, a critical number of sperm cells self-organized into a hexagonally packed array of rotating vortices where each vortex consisted of about 10 hydrodynamically synchronized cells forming a quantized rotating wave. This spatial-temporal pattern of entrained sperm cells formed in the absence of chemical cell-cell signaling, leading to a new coordination concept of cooperative cilia and flagella. Thus, single cells and microorganisms can be hydrodynamically coordinated without the need for chemical signaling.

Sensing Friend or Foe

Ants secrete and recognize specific blends of hydrocarbons in the cuticle, which enable them to display aggressive behavior toward non-nestmates. This identification process is thought to occur at a higher neural level. **Ozaki *et al.*** (p. 311, published online 9 June 2005) have found chemosensory sensilla in the ant antenna that respond to cuticle hydrocarbon blends from non-nestmates, and identify a protein that may carry the compounds to sensory receptors in the sensilla. This finding suggests that chemical information is also processed peripherally.

Launch Your Discovery with MISSION™ RNAi

Introducing the MISSION shRNA Library of The RNAi Consortium

The RNAi Consortium (TRC), based at the Broad Institute of MIT and Harvard, is developing pre-cloned MISSION shRNA libraries targeting the human and mouse genomes. As a member of TRC, Sigma-Aldrich is a principle collaborator and global supplier of the lentiviral based shRNA vector collections for use in transient or stable transfection, as well as viral particle generation. The complete libraries will target 15,000 human and 15,000 mouse genes.

You'll Discover:

- *~35,000 clones available targeting diverse gene families*
- *Renewable resource compared to siRNA*
- *Long term knockdown and phenotypic studies*
- *Lentiviral particles facilitate silencing in difficult cell lines*
- *Sequence-verified clones*

*Experience the **MISSION shRNA** libraries for yourself.*
*Search our target gene database at: **sigma-aldrich.com/mission_px4***

Plus, register to receive our latest literature and updates on upcoming product formats and gene family sets.

MISSION™ RNAi

Member of *The RNAi Consortium*

sigma-aldrich.com

LEADERSHIP IN LIFE SCIENCE, HIGH TECHNOLOGY AND SERVICE
SIGMA-ALDRICH CORPORATION • BOX 14508 • ST. LOUIS • MISSOURI 63178 • USA

SIGMA®

Redefining Science

Why are scientists so upset about the growing movement to bring "intelligent design" (ID) into science classrooms and public education venues such as science museums, zoos, and theme parks? As we mark the 80th anniversary of the Scopes trial,* the pressure to teach ID as a scientific alternative to evolution has been gaining ground in many U.S. states. There is also increasing ID activity in Latin America and Europe. Are scientists so insecure that they are afraid to subject the core concepts of evolution to public scrutiny? Not likely. They're accustomed to that. Scientific theories and principles are routinely subjected to close examination and systematic testing. Moreover, scientists are notoriously argumentative and enjoy debating theories with one another.

The problem is that ID advocates attempt to dress up religious beliefs to make them look like science. By redefining what is and isn't science, they also put the public—particularly young people—at risk of being inadequately prepared to live in modern society. Twenty-first–century citizens are regularly required to make decisions about issues that have heavy science- and technology-related content, such as medical care, personal security, shopping choices, and what their children should be taught in school. To make those choices wisely, they will need to distinguish science-based evidence from pseudoscientific claims.

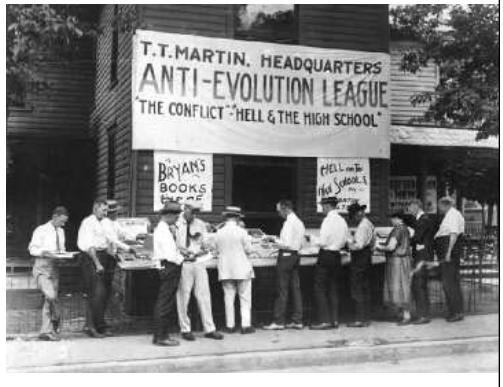

There is an important distinction between a belief and a theory. ID is cast by its proponents as a scientific theory, an alternative to evolution, but it fails the criteria for achieving that status. In our business, a theory is not an educated guess nor, emphatically, is it a belief. Scientific theories attempt to explain what can be observed, and it is essential that they be testable by repeatable observations and experimentation. In fact, "belief" is a word you almost never hear in science. We do not believe theories. We accept or reject them based on their ability to explain natural phenomena, and they must be testable with scientific methodologies.

ID advocates often attempt to denigrate evolution as "just a theory." In one sense that's true. Evolution *is* only a theory, but so is gravity. People often respond that gravity is a fact, but the fact is that your keys fall to the ground when dropped. Gravity is the theoretical explanation that accounts for such observed facts. Scientific theories such as evolution and gravity are accepted only after they have been subjected to validation through repeated observation and experiment, vetted extensively through the peer review process. ID can pass none of these tests. Its proponents assert its scientific standing without undertaking the scientific processes that are required to establish it.

At the same time, it is important for scientists to acknowledge that not all questions can be answered by science. Scientific insights are limited to the natural world. For reasons of their own, some scientists argue with some passion that there could not have been an intelligent designer behind the process of evolution. In fact, we cannot answer that question scientifically, because it is a matter of belief that is outside our realm.

By keeping ID out of the science venue, are we attempting to stifle it? On the contrary, I believe it is appropriate to teach about belief-based concepts like ID in humanities courses, in classes comparing religious points of view, or in philosophy courses that contrast religious and scientific approaches to the world. However, what is taught in science class should be limited to science. Redefining science to get a particular belief into the classroom simply isn't educationally sound.

Just as the scientific community has broad responsibilities to monitor the integrity with which its members conduct their work, it also must take some responsibility for the uses of science and for how it is portrayed to the public. That requires us to be clear about what science is and to distinguish clearly between scientific and belief systems, in schools and in various public venues devoted to science. Otherwise, we will fail in our obligation to our fellow citizens and to the successor generations of students who will depend on science for their future.

Alan I. Leshner
Chief Executive Officer
American Association for the Advancement of Science
Executive Publisher, Science

10.1126/science.1116621

*From 10 to 25 July 1925, John Scopes was on trial for teaching the theory of evolution in a Tennessee public school. Scopes was convicted of breaking a state law against the teaching of evolution, though the decision was later overturned on a technicality. The law was repealed in 1967.

edited by Stella Hurtley

EARTH SCIENCE

Water Water Everywhere?

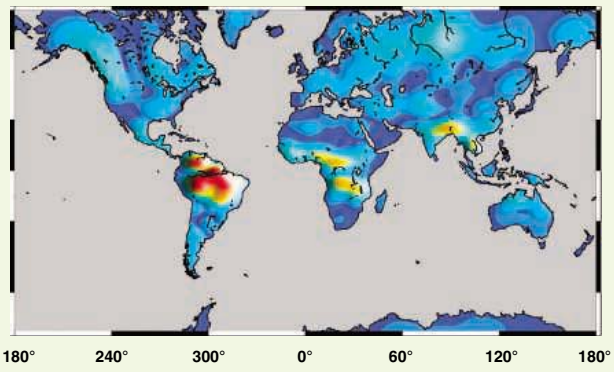

Water levels across the globe.

Seasonally, the amount of water stored on and in the upper part of the various land areas and river basins varies greatly. These changes are enough to produce subtle differences in the distribution of mass over Earth, which produce slight effects in its local gravity. To detect these slight variations, the satellite mission GRACE flies twin satellites in formation, which communicate with each other, increasing sensitivity greatly. It has been recording global gravity since its launch in March 2002, producing essentially monthly data sets.

Ramillien *et al.* present an analysis of Earth's terrestrial hydrosphere using the GRACE data for the past 2 years, and attempt to separate out water in snow, groundwater, surface water, and soil water. By inversion, and with precipitation data, this also provides information on net evapotranspiration, an important climate parameter. Although the data resolution is still undergoing improvement, large-scale monthly hydrologic changes are evident over Earth's major river basins, and evapotranspiration seems to be more seasonal in tropical basins than in purely equatorial ones. — BH

Earth Planet. Sci. Lett. **235**, 283 (2005).

ECOLOGY/EVOLUTION

Dolphin Culture

Wild bottlenose dolphins in Shark Bay, Western Australia, have been shown to break off pieces of marine sponge, which they then wear over their closed snouts while probing for fish concealed in the seabed. It has been uncertain whether this "sponging" behavior, which is apparently confined almost entirely to a subset of females, is transmitted genetically or culturally, or whether it reflects ecological preferences of individuals for foraging in particular locations. It is difficult to make direct observations of social learning in wild animals (especially underwater); instead, attempts may be made to rule out alternative explanations. Krützen *et al.* show that ecological explanations for sponging are unlikely, as spongers and nonspongers (both male and female) forage in the same deep channels. Genetic data gathered from almost 200 individual dolphins, coupled with mating behavioral observations of the animals over a 14-year period, indicate that none of the plausible modes of single-locus inheritance could account for transmission of the behavior. Nevertheless,

Sponger in action.

mitochondrial DNA data indicate that sponging is passed on through a single matriline and that all spongers are closely related. It seems possible that all spongers are descended from a recent, innovative "sponging Eve," whose daughters and granddaughters have learned the behavior from their mothers. — AMS

Proc. Natl. Acad. Sci. U.S.A. **102**, 8939 (2005).

NEUROSCIENCE

Cannabis Use Impairs Brain Development

During early brain development hippocampal activity is driven by two excitatory neurotransmitters, glutamate and GABA. Because GABA does not have the usual inhibitory function it has in the mature brain, other systems need to be in place to stabilize the activity of neuronal networks and prevent the potential danger of runaway excitation that may lead, for example, to epileptic activity. Potential candidates for such a system are the endocannabinoids: endogenously produced metabolites capable of activating the brain's cannabinoid (CB) receptors. Bernard *et al.* investigated endocannabinoid signaling during the first postnatal week in the rat hippocampus, an age that corresponds, in terms of brain development and physiological activity, to the last trimester of pregnancy in humans. Endocannabinoids were released by both interneurons and pyramidal cells in the CA1 region of the hippocampus, activating CB1 receptors and reducing GABA release. Interfering with endocannabinoid signaling during pregnancy either by smoking cannabis or by using recently developed CB1 receptor antagonists may thus affect the normal brain development of the fetus and the newborn child. — PRS

Proc. Natl. Acad. Sci. U.S.A. **102**, 9388 (2005).

IMMUNOLOGY

Fatty Obstacle to TB Immunity

Immunopathology caused by the chronic production of inflammatory cytokines is normally avoided through a number of counterinflammatory pathways. Some of these depend on lipid mediators known as lipoxins, including lipoxase A4 (LXA4), which is derived via 5-lipoxygenase (5-LO)–mediated biosynthesis.

Bafica *et al.* explored whether the 5-LO pathway might influence the course of experimental *M. tuberculosis* infection, and found that LXA4 was indeed generated at significant levels in the sera of infected mice. Genetic deficiency in 5-LO increased the ability of animals to control infection, with a reduction in bacterial counts and increase in survival of animals after infection. This was accompanied by amplification of hallmark inflammatory cytokines, including IFN-γ and IL-12, as well as nitric oxide synthase 2, which is an important factor in host resistance to *M. tuberculosis*. Treatment of

CREDITS: (TOP) RAMILLIEN *ET AL., EARTH PLANET. SCI. LETT.* **235**, 283 (2005); (BOTTOM) MICHAEL KRÜTZEN, UNIVERSITY OF ZÜRICH

5-LO–deficient mice with a lipoxin analog reversed resistance. 5-LO is already being assessed as a therapeutic target in asthma, and this study suggests that 5-LO inhibition may also help to control chronic infectious diseases. — SJS

J. Clin. Invest. **115**, 1601 (2005).

PROTEIN CHEMISTRY

An Easy Switch

Protein secondary structure changes from α helices to β sheets appear to play a key role in diseases such as Alzheimer's disease. Metal ions such as Cu^{2+} and Zn^{2+} may be partly responsible for these conformational changes. Pagel *et al.* have now developed a simple peptide model to investigate the influence of metal ions on secondary structure changes.

The authors have designed a peptide that, depending on the solvent, can form either a two-helix dimer or a β-sheet structure. In a modified version of the peptide, histidine residues are incorporated to encourage metal complexation in the β-sheet configuration. The peptides were exposed to Cu or Zn ions, under conditions that normally favor α-helix formation. Whereas the original peptide did not change structure, the histidine-substituted peptide converted to a β-sheet structure. This process could be reversed by introducing a metal scavenger, proving that metal complexation was responsible for the structural change. The system will be useful for systematic studies of the impact of metals on peptide secondary structure. — JFU

Org. Biomol. Chem. 10.1039/b505979h (2005).

CHEMISTRY

Catalysts Taking Turns

Enzymes can be highly selective in promoting reactions of just one enantiomer from a racemic mixture. In dynamic kinetic resolution, a second catalyst is added to rapidly interconvert the starting enantiomers, so that eventually the chiral catalyst guides every molecule in the mixture to a single enantiomer of product. Now van As *et al.* have adapted this technique to form chirally pure oligoesters from racemic monomers. They use a lipase enzyme to catalyze ring-opening polymerization of 6-methyl-ε-caprolactone. The ring-opening liberates an alcohol center that can open another lactone; however, the enzyme selects for attack of an (R)-alcohol on an (S)-lactone. A ruthenium catalyst then racemizes the ring-opened alcohol so that, as the reaction proceeds,

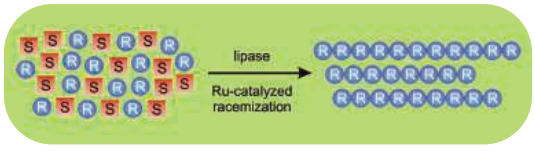

Reaction scheme.

the enzyme adds an (S)-center to the end of the growing chain, and the metal swaps the configuration of this center to enable further chain growth. Decomposition of the pentamer and chromatographic analysis revealed 92% selectivity for (R)-configurations in the backbone. The results are an important contribution toward generating a novel route toward enantiopure polyesters. — JSY

J. Am. Chem. Soc. 10.1021/ja052347d (2005).

HIGHLIGHTED IN *SCIENCE*'S SIGNAL TRANSDUCTION KNOWLEDGE ENVIRONMENT

Science's stke www.stke.org

Before the Rods and Cones

Rods and cones in the mouse retina, which are necessary for image formation, become responsive to light on the 10th day after birth (P10). The intrinsically photosensitive retinal ganglion cells (ipRGCs) express the photopigment melanopsin and can detect brightness. By assaying the responses of retinas loaded with a fluorescent calcium indicator, Sekaran *et al.* examined the early postnatal development of light responses. About 5.4% of cells in the ganglion cell layer responded to 470-nm light at P4 to P5, whereas about 13.7% responded at P0 to P1. The response to light was not affected by pharmacological blockade of glutamate receptors but was absent in retinas from mice that lacked melanopsin. The fraction of light-responsive cells at birth and at P4 to P5 was greater than found in adults. The density of melanopsin-expressing cells was lower at P14 and in adults than earlier in development, peaking at about P4 to P5. ipRGCs project to the suprachiasmatic nucleus of the hypothalamus (SCN), and functional connections from ipRGCs to the SCN were present at P0. Thus, in mice, the ability to detect light substantially predates the ability to form images. — EMA

Curr. Biol. **15**, 1099 (2005).

CREDITS: VAN AS *ET AL.*, *J. AM. CHEM. SOC.* 10.1021/JA052347D (2005)

www.sciencemag.org

Science

1200 New York Avenue, NW
Washington, DC 20005
Editorial: 202-326-6550, FAX 202-289-7562
News: 202-326-6500, FAX 202-371-9227

Bateman House, 82-88 Hills Road
Cambridge, UK CB2 1LQ
+44 (0) 1223 326500, FAX +44 (0) 1223 326501

SUBSCRIPTION SERVICES For change of address, missing issues, new orders and renewals, and payment questions: 800-731-4939 or 202-326-6417, FAX 202-842-1065. Mailing addresses: AAAS, P.O. Box 1811, Danbury, CT 06813 or AAAS Member Services, 1200 New York Avenue, NW, Washington, DC 20005

INSTITUTIONAL SITE LICENCES please call 202-326-6755 for any questions or information

REPRINTS Ordering/Billing/Status 800-635-7171; Corrections 202-326-6501

PERMISSIONS 202-326-7074, FAX 202-682-0816

MEMBER BENEFITS Bookstore: AAAS/BarnesandNoble.com bookstore www.aaas.org/bn; Car purchase discount: Subaru VIP Program 202-326-6417; Credit Card: MBNA 800-847-7378; Car Rentals: Hertz 800-654-2200 CDP#343457, Dollar 800-800-4000 #AA1115; AAAS Travels: Betchart Expeditions 800-252-4910; Life Insurance: Seabury & Smith 800-424-9883; Other Benefits: AAAS Member Services 202-326-6417 or www.aaasmember.org.

science_editors@aaas.org (for general editorial queries)
science_letters@aaas.org (for queries about letters)
science_reviews@aaas.org (for returning manuscript reviews)
science_bookrevs@aaas.org (for book review queries)

Published by the American Association for the Advancement of Science (AAAS), *Science* serves its readers as a forum for the presentation and discussion of important issues related to the advancement of science, including the presentation of minority or conflicting points of view, rather than by publishing only material on which a consensus has been reached. Accordingly, all articles published in *Science*—including editorials, news and comment, and book reviews—are signed and reflect the individual views of the authors and not official points of view adopted by the AAAS or the institutions with which the authors are affiliated.

AAAS was founded in 1848 and incorporated in 1874. Its mission is to advance science and innovation throughout the world for the benefit of all people. The goals of the association are to: foster communication among scientists, engineers and the public; enhance international cooperation in science and its applications; promote the responsible conduct and use of science and technology; foster education in science and technology for everyone; enhance the science and technology workforce and infrastructure; increase public understanding and appreciation of science and technology; and strengthen support for the science and technology enterprise.

INFORMATION FOR CONTRIBUTORS

See pages 135 and 136 of the 7 January 2005 issue or access www.sciencemag.org/feature/contribinfo/home.shtml

EDITOR-IN-CHIEF **Donald Kennedy**
EXECUTIVE EDITOR **Monica M. Bradford**
DEPUTY EDITORS **R. Brooks Hanson, Katrina L. Kelner**
NEWS EDITOR **Colin Norman**

EDITORIAL SUPERVISORY SENIOR EDITORS Barbara Jasny, Phillip D. Szuromi; SENIOR EDITORS Gilbert J. Chin, Lisa D. Chong, Pamela J. Hines, Paula A. Kiberstis (Boston), Beverly A. Purnell, L. Bryan Ray, Guy Riddihough (Manila), H. Jesse Smith, Valda Vinson, David Voss; ASSOCIATE EDITORS Marc S. Lavine, Jake S. Yeston; ONLINE EDITOR Stewart Wills; CONTRIBUTING EDITOR Ivan Amato; ASSOCIATE ONLINE EDITOR Tara S. Marathe; BOOK REVIEW EDITOR Sherman J. Suter; ASSOCIATE LETTERS EDITOR Etta Kavanagh; INFORMATION SPECIALIST Janet Kegg; EDITORIAL MANAGER Cara Tate; SENIOR COPY EDITORS Jeffrey E. Cook, Harry Jach, Barbara P. Ordway; COPY EDITORS Cynthia Howe, Alexis Wynne Mogul, Sabrah M. n'haRaven, Jennifer Sills, Trista Wagoner; EDITORIAL COORDINATORS Carolyn Kyle, Beverly Shields; PUBLICATION ASSISTANTS Chris Filiatreau, Joi S. Granger, Jeffrey Hearn, Lisa Johnson, Scott Miller, Jerry Richardson, Brian White, Anita Wynn; EDITORIAL ASSISTANTS Ramatoulaye Diop, E. Annie Hall, Patricia M. Moore, Brendan Nardozzi, Michael Rodewald; EXECUTIVE ASSISTANT Sylvia S. Kihara; ADMINISTRATIVE SUPPORT Patricia F. Fisher

NEWS SENIOR CORRESPONDENT Jean Marx; DEPUTY NEWS EDITORS Robert Coontz, Jeffrey Mervis, Leslie Roberts, John Travis; CONTRIBUTING EDITORS Elizabeth Culotta, Polly Shulman; NEWS WRITERS Yudhijit Bhattacharjee, Jennifer Couzin, David Grimm, Constance Holden, Jocelyn Kaiser, Richard A. Kerr, Eli Kintisch, Andrew Lawler (New England), Greg Miller, Elizabeth Pennisi, Charles Seife, Robert F. Service (Pacific NW), Erik Stokstad; Carolyn Gramling, Genevra Ornelas, Cathy Tran (interns); CONTRIBUTING CORRESPONDENTS Marcia Barinaga (Berkeley, CA), Barry A. Cipra, Adrian Cho, Jon Cohen (San Diego, CA), Daniel Ferber, Ann Gibbons, Robert Irion, Mitch Leslie (NetWatch), Charles C. Mann, Evelyn Strauss, Gary Taubes, Ingrid Wickelgren; COPY EDITORS Linda B. Felaco, Rachel Curran, Sean Richardson; ADMINISTRATIVE SUPPORT Scherraine Mack, Fannie Groom BUREAUS: Berkeley, CA: 510-652-0302, FAX 510-652-1867, New England: 207-549-7755, San Diego, CA: 760-942-3252, FAX 760-942-4979, Pacific Northwest: 503-963-1940

PRODUCTION DIRECTOR James Landry; SENIOR MANAGER Wendy K. Shank; ASSISTANT MANAGER Rebecca Doshi; SENIOR SPECIALISTS Vicki J. Jorgensen, Jessica K. Moshell; SPECIALISTS Jay R. Covert, Stacey Ferebee; **PREFLIGHT** DIRECTOR David M. Tompkins; MANAGER Marcus Spiegler; SPECIALIST Jessie Mudjitaba;

ART DIRECTOR Joshua Moglia; ASSOCIATE ART DIRECTOR Kelly Buckheit; ILLUSTRATOR Katharine Sutliff; SENIOR ART ASSOCIATES Holly Bishop, Laura Creveling, Preston Huey, Julie White; ASSOCIATE Nayomi Kevitiyagala; PHOTO RESEARCHER Leslie Blizard

***SCIENCE* INTERNATIONAL**

EUROPE (science@science-int.co.uk) EDITORIAL: INTERNATIONAL MANAGING EDITOR Andrew M. Sugden; SENIOR EDITOR/PERSPECTIVES Julia Fahrenkamp-Uppenbrink; SENIOR EDITORS Caroline Ash (Geneva: +41 (0) 222 346 3106), Stella M. Hurtley, Ian S. Osborne, Peter Stern; ASSOCIATE EDITOR Stephen J. Simpson; EDITORIAL SUPPORT Emma Westgate; Deborah Dennison ADMINISTRATIVE SUPPORT Janet Clements, Phil Marlow, Jill White; NEWS: INTERNATIONAL NEWS EDITOR Eliot Marshall DEPUTY NEWS EDITOR Daniel Clery; CORRESPONDENT Gretchen Vogel (Berlin: +49 (0) 30 2809 3902, FAX +49 (0) 30 2809 8365); CONTRIBUTING CORRESPONDENTS Michael Balter (Paris), Martin Enserink (Amsterdam and Paris); INTERN Mason Inman

ASIA Japan Office: Asca Corporation, Eiko Ishioka, Fusako Tamura, 1-8-13, Hirano-cho, Chuo-ku, Osaka-shi, Osaka, 541-0046 Japan; +81 (0) 6 6202 6272, FAX +81 (0) 6 6202 6271; asca@os.gulf.or.jp JAPAN NEWS BUREAU: Dennis Normile (contributing correspondent, +81 (0) 3 3391 0630, FAX 81 (0) 3 5936 3531; dnormile@gol.com); CHINA REPRESENTATIVE Hao Xin, + 86 (0) 10 6307 4439 or 6307 3676, FAX +86 (0) 10 6307 4358; haoxin@earthlink.net; SOUTH ASIA Pallava Bagla (contributing correspondent +91 (0) 11 2271 2896; pbagla@vsnl.com); CENTRAL ASIA Richard Stone (+7 3272 6413 35, rstone@aaas.org)

EXECUTIVE PUBLISHER **Alan I. Leshner**
PUBLISHER **Beth Rosner**

FULFILLMENT & MEMBERSHIP SERVICES (membership@aaas.org) DIRECTOR Marlene Zendell; MANAGER Waylon Butler; SYSTEMS SPECIALIST Andrew Vargo SENIOR SPECIALIST Pat Butler; SPECIALISTS Laurie Baker, Tamara Alfson, Karena Smith

BUSINESS OPERATIONS AND ADMINISTRATION DIRECTOR Deborah Rivera-Wienhold; BUSINESS MANAGER Randy Yi; SENIOR BUSINESS ANALYST Lisa Donovan; BUSINESS ANALYST Jessica Tierney; FINANCIAL ANALYST Michael LoBue, Farida Yeasmin; RIGHTS AND PERMISSIONS: ADMINISTRATOR Emilie David; ASSOCIATE Elizabeth Sandler; MARKETING: DIRECTOR John Meyers; MEMBERSHIP MARKETING MANAGER Darryl Walter; MARKETING ASSOCIATE Julianne Wielga; RECRUITMENT MARKETING MANAGER Allison Pritchard; ASSOCIATES Mary Ellen Crowley, Amanda Donathen, Catherine Featherston; DIRECTOR OF INTERNATIONAL MARKETING AND RECRUITMENT ADVERTISING Deborah Harris; INTERNATIONAL MARKETING MANAGER Wendy Sturley; MARKETING/MEMBER SERVICES EXECUTIVE: Linda Rusk; JAPAN SALES AND MARKETING MANAGER Jason Hannaford; SITE LICENSE SALES: DIRECTOR Tom Ryan; SALES AND CUSTOMER SERVICE Mehan Dossani, Catherine Holland, Adam Banner, Yaniv Snir; ELECTRONIC MEDIA: INTERNET PRODUCTION MANAGER Lizabeth Harman; ASSISTANT PRODUCTION MANAGER Wendy Stengel; SENIOR PRODUCTION ASSOCIATES Sheila Mackall, Amanda K. Skelton, Lisa Stanford; PRODUCTION ASSOCIATE Nichele Johnston; LEAD APPLICATIONS DEVELOPER Carl Saffell

PRODUCT ADVERTISING (science_advertising@aaas.org); MIDWEST Rick Bongiovanni: 330-405-7080, FAX 330-405-7081 • WEST COAST/W. CANADA B. Neil Boylan (Associate Director): 650-964-2266, FAX 650-964-2267 • EAST COAST/E. CANADA Christopher Breslin: 443-512-0330, FAX 443-512-0331 • UK/SCANDINAVIA/FRANCE/ITALY/BELGIUM/NETHERLANDS Andrew Davies (Associate Director): +44 (0)1782 750111, FAX +44 (0) 1782 751999 • GERMANY/SWITZERLAND/AUSTRIA Tracey Peers (Associate Director): +44 (0) 1782 752530, FAX +44 (0) 1782 752531 JAPAN Mashy Yoshikawa: +81 (0) 33235 5961, FAX +81 (0) 33235 5852 ISRAEL Jessica Nachlas +9723 5449123 • TRAFFIC MANAGER Carol Maddox; SALES COORDINATOR Deiandra Simms

CLASSIFIED ADVERTISING (advertise@sciencecareers.org); U.S.: SALES DIRECTOR Gabrielle Boguslawski: 718-491-1607, FAX 202-289-6742; INTERNET SALES MANAGER Beth Dwyer: 202-326-6534; INSIDE SALES MANAGER Daryl Anderson: 202-326-6543; WEST COAST/MIDWEST Kristine von Zedlitz: 415-956-2531; EAST COAST Jill Downing: 631-580-2445; LINE AD SALES Emnet Tesfaye: 202-326-6740; SENIOR SALES COORDINATOR Erika Bryant; SALES COORDINATORS Rohan Edmonson, Christopher Normile, Joyce Scott, Shirley Young; INTERNATIONAL: SALES MANAGER Tracy Holmes: +44 (0) 1223 326525, FAX +44 (0) 1223 326532; SALES Christina Harrison, Suitlana Barnes; SALES ASSISTANT Helen Moroney; JAPAN: Jason Hannaford: +81 (0) 52 789 1860, FAX +81 (0) 52 789 1861; PRODUCTION: MANAGER Jennifer Rankin; ASSISTANT MANAGER Deborah Tompkins; ASSOCIATE Amy Hardcastle; SENIOR TRAFFICKING ASSOCIATE Christine Hall; SENIOR PUBLICATIONS ASSISTANT Robert Buck; PUBLICATIONS ASSISTANT Natasha Pinol

AAAS BOARD OF DIRECTORS RETIRING PRESIDENT, CHAIR Shirley Ann Jackson; PRESIDENT Gilbert S. Omenn; PRESIDENT-ELECT John P. Holdren; TREASURER David E. Shaw; CHIEF EXECUTIVE OFFICER Alan I. Leshner; BOARD Rosina M. Bierbaum; John E. Burris; John E. Dowling; Lynn W. Enquist; Susan M. Fitzpatrick; Richard A. Meserve; Norine E. Noonan; Peter J. Stang; Kathryn D. Sullivan

AAAS
ADVANCING SCIENCE, SERVING SOCIETY

NetWatch

edited by Mitch Leslie

FUN

How Does Your Garden Grow?

If snails or slugs are chomping your garden, offer them a beer. Attracted to yeast in the liquid, the mollusks will trail right into a dish of beer and drown, sparing your garden from their depredations. Other seemingly strange plant-care suggestions, such as composting nail clippings, also get the thumbs up at the Science of Gardening, a new exhibit from the Exploratorium in San Francisco, California. With the museum's usual flair, the site harvests tidbits on everything from the bacteria that maintain soil fertility to the origins of our modern plant varieties. Iceberg lettuce's firm, round head allows it to endure rough handling during harvest and transportation, for example. A clever section explores the relationship between plants and their pollinators with mock love letters between the parties—followed by a scientific explanation of what's happening. "You appeared in the thousand facets of my eyes" reads a letter from a bumblebee to a lavender flower.

www.exploratorium.edu/gardening

EDUCATION

Cleaning Up Chemistry

Today, even chemists who can't keep their lawn alive can have a green thumb. Green chemistry is a growing movement to reduce industry's use of hazardous raw materials and release of noxious byproducts. Teachers looking for lab and classroom resources on green chemistry can drop by this new directory from the University of Oregon, Eugene. The site links to lab procedures, tutorials, and Environmental Protection Agency software for identifying green chemicals and reactions. For example, a novel procedure for bleaching paper replaces chlorine—which spawns toxins such as dioxin—with hydrogen peroxide, which breaks down into water and oxygen. Listings also include abstracts of articles in the *Journal of Chemical Education*.

greenchem.uoregon.edu/gems.html

DATABASE

Reading Between the Lines

Cancer biologists rely on immortal populations of tumor cells to uncover the mechanisms behind uncontrolled growth and test potential new drugs. But these cell lines, which are passed from lab to lab, might have picked up fresh DNA glitches over the years, and different lines might have mixed with cells from other sources. Now, a team at the Sanger Institute in the U.K. that has been working to characterize more than 600 cell lines has released its first data. The collection indicates which of four major genes involved in cancer, including the tumor-fighter *p53*, is faulty in each of the lines. Visitors can also peruse a list of lines that are likely descended from each other and find out whether a line has lost copies of a particular gene.

www.sanger.ac.uk/genetics/CGP/CellLines

IMAGES

Watch the Skies

A pair of swirly lenticular clouds (right) hovers over the Front Range of the Rocky Mountains in Colorado. Often mistaken for UFOs by the gullible, the oval clouds condense on the downwind sides of mountains as speeding air crosses the summit. You'll find hundreds more shots of weather, natural disasters, pollution, and related subjects at this gallery from the University Corporation for Atmospheric Research in Boulder, Colorado. Follow a tornado slashing across north Texas, watch a tropical downpour in Africa, or see an eroded Hawaiian beach. Visitors can use the images free for education or research.

www.ucar.edu/imagelibrary

EXHIBITS

Body Works

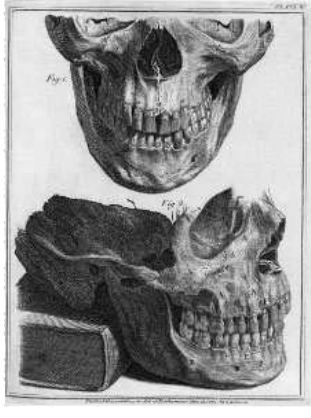

The 16th through 19th centuries were a boom time for anatomy, as doctors began to apply scientific methods to analyze human structure. Anatomical illustration also blossomed as artists strove for greater accuracy, added color, and burnished their craft in other ways. Anatomia, an online exhibit from the University of Toronto Libraries in Canada, showcases this period with 4500 medical plates from 95 texts published between 1522 and 1867. These views of the jaw (left) come from the 1778 version of *The Natural History of the Human Teeth* by the British "surgeon extraordinary" John Hunter (1728–1793), who minted the terms "molar," "incisor," and "bicuspid." Some illustrations are interactive: For instance, you can open the heart to see its internal architecture.

link.library.utoronto.ca/anatomia/application/index.cfm

Send site suggestions to netwatch@aaas.org. Archive: www.sciencemag.org/netwatch

CREDITS (TOP TO BOTTOM): THE EXPLORATORIUM; CARLYE CALVIN/UNIVERSITY CORPORATION FOR ATMOSPHERIC RESEARCH; UNIVERSITY OF TORONTO LIBRARIES

NEWS

This Week

PAGE 231
Waterfowl succumb to bird flu

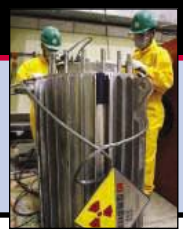

233
Low-level radiation effects

PLANETARY SCIENCE

Deep Impact Makes a Lasting Impression on Comet Tempel 1

Splat! Mission accomplished. The two-part Deep Impact spacecraft—a bulletlike hypervelocity impactor and its watchful mothership—performed flawlessly on 4 July, punching a hole in the icy dirtball of comet Tempel 1 in full view of all the world.

In the first hours, at least, the collision revealed none of the hoped-for secrets of the solar system's formation; real science doesn't always make for instant science. But mission scientists have no doubt that Deep Impact returned much of the raw data they need. "We do impact cratering simulations [in the lab] in pieces," says team member Peter Schultz of Brown University in Providence, Rhode Island. At Tempel 1, "we saw all the pieces come together in one giant event." Eerily, the real thing bore a fair resemblance to computer animations based on lab experiments and numerical simulations.

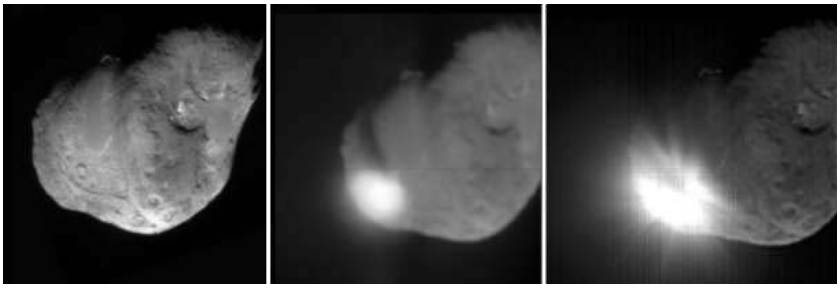

On target. A fireball (brightest splotch) expands above comet Tempel 1 as a vertical column of debris (shadow cast toward top) rises from the collision with Deep Impact.

Deep Impact wasn't always unalloyed fun for team members. The cost-constrained, PI-led Discovery mission had a checkered history of cost overruns, near-fatal reviews by NASA headquarters, and technical problems, including an onboard computer that had to be rebuilt. "We were very close to being canceled," says PI Michael A'Hearn of the University of Maryland, College Park. All the scrutiny may have paid off, however. Despite bumpy trials early on, the computer and its comet-targeting software deftly homed the impactor in on Tempel 1's nucleus, snapping pictures down to the last 3 seconds before impact.

The death-plunge pictures were revealing. The nucleus of Tempel 1 "looks very different from Wilt 2's or Borrelly's," says A'Hearn. Those are the other two comet nuclei closely imaged by spacecraft. Unlike on those nuclei, "a lot of things on Tempel 1 look like [impact] craters," he says. A band of smooth terrain of unknown origin wraps around the waist of the elongate, 14-kilometer-long body. Other features include topography that formed when the sun ate away at primordial ice in layered strata, said A'Hearn.

The encounter had a rather conventional outcome, considering that this spring scientists "didn't have a clue" what was going to happen, as A'Hearn put it (*Science*, 27 May, p. 1247). Tempel 1 didn't just swallow up the impactor, the way something as accommodating as a marshmallow might. Nor did it form a small, bowl-shaped crater, the way a strong material would. In the images returned by the afternoon of the first day, the first sign of contact was a very small, faint dot of a flash, says Schultz. That was the impactor, a ▶

SCIENTIFIC PUBLISHING

Britain's Research Agencies Endorse Public Access

Starting in October, all investigators funded by the big eight research agencies in Britain may be required to put their papers and meeting talks in a free public archive "at the earliest opportunity, wherever possible at or around the time of publication." An oversight group, Research Councils UK (RCUK), handed down this formula last week as its final proposal after months of consultation with interested groups. By one estimate, it would cover half of all U.K.-funded research.

Despite the mandatory tone, journals will find some wiggle room that may allow them to keep their usual embargoes. RCUK says its mandate is "subject to copyright and licensing arrangements" that can restrict what authors do (www.rcuk.ac.uk/access/index.asp). RCUK spokesperson Heather Weaver said this phrase recognizes that "publishers vary" in how they handle rights, and the government is setting no fixed time frame for free data release—other than "as soon as possible."

Advocates for the open-access movement praised the RCUK announcement. Some think it comes closer to their goals than a policy announced earlier this year by the U.S. National Institutes of Health (NIH), which merely encourages authors to put papers in the U.S. PubMed Central database within 12 months of publication (*Science*, 29 April, p. 623, and 11 February, p. 825). Peter Suber—a professor of philosophy at Earlham College in Richmond, Indiana, and leader of the Public Knowledge advocacy group in Washington, D.C.—described it as "an excellent policy" because it is mandatory, unlike NIH's. But he says the copyright "loophole … will allow publishers to impose embargoes."

Publishers, whose revenues are threatened by the open-access movement, found fault with the RCUK approach. A group representing 320 nonprofit, academic, and scientific society journals—the Association of Learned and Professional Society Publishers in Clapham, U.K.—released a critique on 30 June by Executive Director Sally Morris (www.alpsp.org/RCUKResponse.pdf). Among other concerns, it warns that the open-access trend may "siphon off" subscriptions to society publications.

RCUK specifies only that papers should be put in "an appropriate e-print repository (either institutional or subject-based), wherever such a repository is available." More than 50 qualify in Britain alone. RCUK officials say this and other fine points will be worked out in consultations through 31 August, before the policy takes effect this fall. **–ELIOT MARSHALL**

CREDIT: NASA/JPL-CALTECH/UMD

clothes-washer-size, copper-laden bullet, penetrating the surface. After 150 milliseconds, a "really bright flash" saturated the flyby spacecraft's camera. The impactor had penetrated the nucleus and vaporized, and now a ball of incandescent comet vapor was expanding above the surface.

At the same time, the shadow of a growing vertical column fell across the nucleus, apparently cast by material shooting out of the penetration hole like a roman candle, says Schultz. A curtain of ejecta zoomed upward as the curtain expanded outward across the nucleus, "just like the movies" based on the experiments, says Schultz: "It looks so similar to the experiments." That implies to Schultz that Tempel 1 is not armored by a thick hard crust, as some had imagined, but wrapped in a soft, dusty layer.

Still, team members had yet to identify the much-anticipated crater hidden beneath suspended impact dust. Further image processing should reveal it, A'Hearn said. Schultz thinks it will be big. "Now we have to go back and do more complicated experiments and compare them with numerical simulations," he says. So far, he and his colleagues have hardly mentioned the spectroscopic data that in coming months should reveal the composition of freshly exposed primordial material—presumably the same stuff that made up the planets. That analysis will take much longer than an instant. **–RICHARD A. KERR**

ANTHROPOLOGY

A New Skirmish in the Yanomamö Wars

Sensational accusations that anthropologists mistreated Venezuela's Yanomamö Indians while studying them continue to roil the American Anthropological Association (AAA). Last week, AAA members voted 846–338 to rescind the association's report on the charges, which were leveled almost 5 years ago in journalist Patrick Tierney's book *Darkness in El Dorado*. Although opposition to the referendum was "very vocal," says Thomas Headland, an anthropological consultant to SIL International in Dallas, Texas, who supported it, "I guess there's a silent majority among the 11 or 12 thousand members of the AAA."

Tierney's book set off a firestorm with its charges that researchers had "devastated" the Yanomamö, who live near the headwaters of the Orinoco River. The most explosive allegation—that prominent anthropologist Napoleon Chagnon of the University of California, Santa Barbara, and the late geneticist James V. Neel exacerbated and possibly caused a lethal 1968 measles epidemic—was quickly shown to be implausible (*Science*, 29 September 2000, p. 2251; 19 January 2001, p. 416). But researchers continued to battle over a host of other claims, including that Chagnon's widely known depictions of the Yanomamö as "fierce" and violent had provided intellectual cover to people trying to take over their land.

In February 2001, AAA appointed a task force to "conduct an inquiry" into the growing storm. If the measure was intended to quell the dispute, it failed. Released in July 2002, the task force's 325-page final report exonerated Chagnon of the most serious charges (*Science*, 19 July 2002, p. 333) but argued that his association with a group of wealthy, allegedly corrupt Venezuelans was "unacceptable on both ethical and professional grounds" because visitors made many illicit trips to Yanomamö villages "without any quarantine procedures or other protections for the indigenous peoples." More importantly, the task force concluded that Chagnon's "representations [of the Yanomamö as 'fierce'] have been damaging" to them.

Misrepresented? Napoleon Chagnon's depiction of the Yanomanö as "fierce" and violent continues to divide anthropologists.

CREDIT: ANTONIO MALI

Almost immediately, anthropologists Thomas Gregor of Vanderbilt University in Nashville, Tennessee, and Daniel Gross of the World Bank in Washington, D.C., attacked the task force. In two critiques in the *Chronicle of Higher Education* and *American Anthropology* (the flagship AAA journal), Gregor and Gross scoffed that the investigation was "a model of ineptitude." The five-member committee, Gregor says, based its conclusions "on biased interviews of selected, unrepresentative Indians." Not consulted, Chagnon's defenders note, were indigenous leaders such as Jaime Turon, elected head of the Upper Orinoco district, who wrote in a 2003 open letter that Chagnon and his associates, far from hurting the Yanomamö, "were the only ones that helped us … in the 1960s and 1970s."

Gross and Gregor obtained the 50 signatures AAA bylaws require to hold a referendum on the report. "We were not attempting to mount a defense of Mr. Chagnon," Gross wrote in an e-mail to *Science*—indeed, they have attacked each other's ideas in print since the 1970s. "However, Chagnon [and Neel] were subjected to a process that was highly loaded ideologically and in which they had no way of defending themselves."

Despite the strong rejection of the task force report, few expect a cease-fire in the Yanomamö wars. Robert Borofsky of Hawaii Pacific University in Honolulu has said AAA should keep "evaluating the charges"; Brazilian director José Padilha is filming a BBC documentary on the affair for broadcast in early 2006. Raymond Hames of the University of Nebraska, Lincoln, says Chagnon is a "lightning rod" for the conflicts now rending anthropology. The field is bitterly split, he says, between "people who try to do science and people who believe that science is impossible or—with a postmodern ring—is actually an unethical thing to do, a hegemonic tool of Western imperialism." Chagnon's high-profile ▶

eppendorf PhysioCare Concept criteria 7 and 8

- Effective maintenance
- Professional workshops
- Training programs
- Worldwide service
- Ergonomics approved by TÜV

Progressive philosophy.

Simple maintenance – Total support

PhysioCare Concept pipettes.
Since the introduction of the first industrially manufactured piston-stroke pipette in 1961, Eppendorf has been continually expanding and refining its range of liquid handling systems and customer support offers.

High-precision, easy-to-use pipettes and professional technical and application services are the reasons why you can place your confidence in us.

TÜV Rheinland approved our manual pipettes as: ergonomic, user-friendly and user tested.

PhysioCare concept

Check out how good your pipette really is!
PhysioCare Concept™ website
www.physiocare-concept.info

eppendorf

In touch with life

Your local distributor: www.eppendorf.com/worldwide · Application Hotline: +49 180-3 66 67 89
Eppendorf AG · Germany · +49 40 538 01-0 • Eppendorf North America, Inc. 800-645-3050

support of a data-driven view of anthropology, Hames—a Chagnon collaborator—and other anthropologists say, has made him a special object of opprobrium to the field's postmodern flank.

Chagnon further "infuriated people," Gross says, when he argued (*Science*, 26 February 1988, p. 985) that Yanomamö men "who had killed had higher reproductive success"—an evolutionary explanation for the high levels of violence Chagnon said he observed. The claim, Gross says, simultaneously drew the ire of researchers suspicious of what they saw as "crude biological determinism" and activists who believed that the depiction of the Yanomamö as warlike, which they believed inaccurate, "directly harmed" them.

Inflamed by Chagnon's sometimes hot-tempered personal style, these conflicts have led to divisions that are unlikely to be resolved quickly. Indeed, Leslie Sponsel of the University of Hawaii, Manoa, one of Chagnon's most outspoken detractors, calls the vote "simply another smoke screen to distract attention from the multitude of diverse allegations made by Tierney, some of which were confirmed by various investigations."

Although Chagnon calls himself "pleased" by the vote, he believes that "activist anthropologists" will continue to use ethical charges "as a social and political weapon." Meanwhile, he believes the AAA task force may actually have "worsened the plight of the Yanomamö because the [Venezuelan government] has, as a consequence of AAA actions, been shut off to researchers who might be more genuine and effective in their efforts to help them."

–Charles C. Mann

SPANISH SCIENCE

Madrid Heart Center to Be Rescued

Barcelona, Spain—Hoping to recover from a calamitous start, Spain's Ministry of Health is using private money to rescue a troubled heart research facility in Madrid. When the Spanish Cardiovascular Research Center (CNIC) got tangled in management problems last year, the director was let go. Now the government has recruited a prominent new chief—cardiologist Valentin Fuster of the Mount Sinai School of Medicine in New York City—and signed up five companies to help float the project for 10 years.

Double duty. Valentin Fuster will lead research in New York City and Madrid.

CREDITS (TOP TO BOTTOM): NIH; MOUNT SINAI

CNIC slipped into limbo in May 2004 following a dispute between the government and acting chief Salvador Moncada, an expert in nitrous oxide who heads the Wolfson Institute for Biomedical Research at University College London. Moncada challenged a court-issued reprimand over travel costs. He and CNIC then parted ways, and almost a year ago, Health Minister Elena Salgado began searching for a new leader, a spokesperson says. On 27 June, she announced that Fuster, a Spanish national, had agreed to return to Spain to help relaunch CNIC and become director on a date to be determined.

To help revive the project and sustain it through 2015, she said, five big companies with no stake in health products or the drug industry have agreed to kick in €170 million, 35% of a new sustaining fund of €500 million. The remaining 65% will come from the health ministry. Salgado describes the project as "an innovative joint venture between the government and the private sector." The deal also will make it possible to inaugurate CNIC's new €60 million building on 1 September.

Fuster says he plans six major research departments devoted to areas such as tissue regeneration, stem cell studies, heart embryogenesis, and basic genetics and proteomics. He aims to hire 200 scientists on government salaries; they will also receive bonuses based on productivity, to be financed with company money. There will be no place for the unproductive, he says. The involvement of the private sector is a "breakthrough," adds Fuster, noting that it is a first for Spain. According to the health ministry, the companies will share in rights to CNIC's medical discoveries.

Fuster says he intends to split his time between Mount Sinai, where he is in charge of 41 basic and clinical scientists, and CNIC. He plans "a highly aggressive scientific interrelation" between CNIC and Mount Sinai—as well with other U.S. and European centers. For example, Salk Institute developmental biologist Juan Carlos Izpisúa-Belmonte is reportedly discussing plans to work with CNIC on embryonic stem cells from a new base at Barcelona's Centre of Regenerative Medicine.

It is a "very good initiative," says stem cell researcher Jordi Petriz of Barcelona's IDIBAPS Institute. "But it remains to be seen how CNIC will be sustained at the long term."

–Xavier Bosch

Xavier Bosch is a science writer based in Barcelona.

ScienceScope

NIH Fires Critic of AIDS Trials

A federal researcher who raised concerns about a clinical trial and misconduct at the National Institutes of Health (NIH) has been sacked.

Jonathan Fishbein, a safety official at the National Institute of Allergy and Infectious Diseases (NIAID), claimed in last year that record-keeping problems with a Uganda-based trial of the AIDS drug nevirapine were covered up. (An Institute of Medicine report later found that the trial was scientifically valid.)

Fishbein has also alleged sexual harassment at NIAID (*Science*, 29 April, p. 613). Fishbein, who was suspended in February 2004 for poor performance, was terminated on 1 July—12 days before the end of his 2-year probationary period.

Senate Finance Committee leaders Charles Grassley (R–IA) and Max Baucus (D–MT) protested Fishbein's firing in a letter to NIH Director Elias Zerhouni and suggested that it "may be an act of retaliation." Two other lawmakers have sent similar letters. Aspects of the case are under investigation by Congress and several federal agencies, including NIH.

–Jocelyn Kaiser

Stem Cells Face Vote in Senate

Following the House's lead, the Senate is poised to pass a bill to loosen up President George W. Bush's stem cell policy. Last week, stem cell supporters Tom Harkin (D–IA) and Arlen Specter (R–PA) said in a press conference that Senate Majority Leader Bill Frist (R–TN) had promised them a vote this month. "We're hoping for an up-or-down vote" on the same measure the House passed (H.R. 810) (*Science*, 3 June, p. 1388), said Harkin. At the same time, the Senate will likely vote to increase support for stem cell research with umbilical cords and bone marrow.

Harkin predicts that the bill will pass the Senate with enough votes to withstand the veto Bush promises. Meanwhile, Frist and others are seeking to give NIH more money to study alternative ways to generate embryonic-like stem cells without destroying embryos (see p. 240).

–Constance Holden

STRUCTURAL BIOLOGY

Ten Centers Chosen to Decode Protein Structures

An ambitious and costly plan to churn out protein structures shifted into its second phase last week, as the National Institutes of Health (NIH) announced roughly $300 million in new awards. The Protein Structure Initiative (PSI) aims to deposit up to 5000 new protein structures in a public database.

Roughly $200 million will go to four large-scale centers that, much like the centers that sequenced the human genome, will crank out protein structures as rapidly as possible. It's a labor-intensive task: Until recently, a single protein structure could take a year to decipher. The rest of the money goes to six "specialized" centers that will focus on how to handle some of the most challenging proteins, including potential drug targets.

PSI was launched as a pilot project 5 years ago to send protein biology into a new realm. Protein structures can shed light on both normal and deviant molecular pathways and on how divergent species, from bacteria to humans, overlap in their biology (*Science*, 11 March, p. 1554). But the initiative drew fire from researchers who felt that taking snapshots of an isolated protein's structure reveals little about its function.

PSI's expansion hit another snag this year, when a tight NIH budget forced PSI to scale down its current awards from $75 million a year to about $60 million (compared with $68 million for each of the last 2 years of the pilot project). "We had to make reductions in awards to the centers," says PSI director John Norvell of the National Institute of General Medical Sciences. The four large-scale centers will each receive roughly $9 million to $10 million a year for the next 5 years; specialized centers will garner $3 million to $4 million a year.

The Winners*

$48 million–$53 million (over 5 years)

Scripps Research Institute
Argonne National Laboratory
Structural Genomix
Rutgers University

$12 million–$20 million (over 5 years)

DeCODE Biostructures
University of Wisconsin, Madison
Hauptman-Woodward Medical Research Inst.
University of California, San Francisco
Los Alamos National Laboratory
New York Structural Biology Center

* Institutions at which the winners are based.

Protein boost. Four large-scale and six specialized centers will take part in PSI.

Awardees say they are trying to drive costs downward. "Our goal would be to get to less than $10,000 per protein," says Lance Stewart, vice president of the company deCODE Biostructures in Bainbridge Island, Washington, and the leader of one of the new specialized centers. Currently, he says, deducing structures of bacterial proteins can cost $100,000; more complex eukaryotic ones can soar to 10 times that.

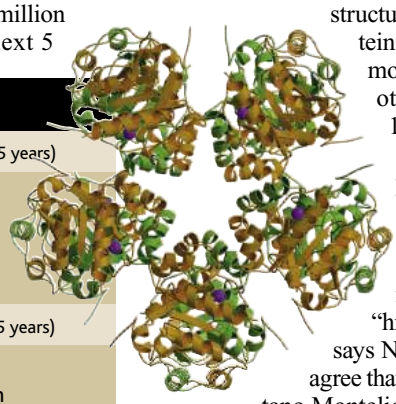

Having deciphered structures for more than 1100 proteins, most of them bacterial, PSI is now looking to the "higher hanging fruit," says Norvell. Researchers agree that won't be easy. Gaetano Montelione of Rutgers University in Piscataway, New Jersey, who directs the Northeast Structural Genomics Consortium, says his success rate for deducing eukaryotic protein structures is 1%, compared with 10% for bacteria; eukaryotic proteins, he says, don't grow well in *Escherichia coli* bacteria, the method used to purify them.

Montelione expects to boost his eukaryotic protein yield, though, and will likely need to: His large-scale center will focus on protein networks in cancer biology, and he has already drawn up hit lists of proteins that drive tumor growth. **–JENNIFER COUZIN**

BIOSECURITY

New Panel to Offer Guidance on Dual-Use Science

Most biologists don't spend much time thinking about whether their co-workers in the lab are trustworthy or whether a terrorist might profit from the paper they're about to submit. But a newly formed U.S. committee has begun considering how life scientists should deal with such questions.

Meeting in Bethesda, Maryland, last week for the first time, the panel hopes to develop guidelines—such as codes of conduct—for "dual use" research in the life sciences that will strike a balance between limiting risks and preserving scientific freedom. "If we don't do this carefully, we run the risk of losing what's really the greatest scientific engine the world has ever seen," says panelist Paul Keim of Northern Arizona University in Flagstaff.

The 24-member interagency panel, created in March 2004 and led by the Department of Health and Human Services (HHS), is an outgrowth of a 2004 National Academies report that looked at the potential misuse of biotechnology in the wake of the deadly 2001 anthrax letter attacks. As White House Homeland Security Council official Rajeev Venkayya told the committee last week, 2 years ago "there was an increasing sense of angst" on the council that some newly published studies, such as synthesizing viruses from scratch, could be misused. The academies' report, he said, helped stave off calls for more "draconian" measures.

Selecting the panelists took more than a year, however, and its membership was only unveiled at last week's meeting. The roster is studded with scientific stars as well as intelligence, biosafety, and bioweapons experts. Harvard University microbiologist Dennis Kasper is chair of the panel, officially the National Science Advisory Board for Biosecurity. Its 2-year charter runs out next March but is expected to be extended.

The panel's goal is to create "a culture of responsibility," says National Institute of Allergy and Infectious Diseases Director Anthony Fauci, an ex officio member. It is modeled on HHS's Recombinant DNA Advisory Committee, which was created 30 years ago to address concerns about the risks of genetic engineering.

One big challenge is a definition of dual use. The academies' report included case studies of seven potentially controversial experiments, such as modifying a microbe to make it resistant to drugs. But it did not consider studies that analyze the country's vulnerability to attack, such as a paper modeling use of botulinum toxin to poison the U.S. milk supply that the *Proceedings of the National Academies of Sciences* published last week despite concerns from HHS. The board also will tackle guidelines for journals, codes of scientific conduct, international collaborations, and advice for studying synthetic genomics.

Observers are cautiously optimistic about what the board will achieve. "I just don't know if they're going to be able to muster the courage to take steps that are sufficiently strong," says Ed Hammond of the Sunshine Project, a bioweapons watchdog group based in Austin, Texas. **–JOCELYN KAISER**

CREDIT: NIH/NIGMS; (INSET) MYCOBACTERIUM TUBERCULOSIS CENTER

AVIAN INFLUENZA

Potentially More Lethal Variant Hits Migratory Birds in China

When China reported in mid-May that the H5N1 avian influenza virus had caused the deaths of 1000 or more migratory birds at a breeding ground in western China, ornithologists worldwide were alarmed. "It is the biggest and most extensively mortal avian influenza event ever seen in wild birds," says David Melville, an ornithologist in New Zealand. Now, in a paper published online by *Science* this week (www.sciencemag.org/cgi/content/abstract/1115273), Jinhua Liu of the College of Veterinary Medicine in Beijing and colleagues there and at five other Chinese institutions report that the outbreak at Lake Qinghai in western China appears to have been caused by a new H5N1 variant that may be more lethal to wild birds, as well as to experimentally infected mice. Similar findings, from different groups, were published online this week by *Nature*. The results suggest that the virus is evolving and raise the possibility that surviving birds could spread it over an even wider geographic area, endangering more poultry and increasing the chances of further genetic changes that could spark a deadly human pandemic.

Liu and colleagues fully sequenced four isolates recovered from various bird species and found them all to be very similar but distinct from any H5N1 sequences posted in GenBank. George Gao, a virologist at the Chinese Academy of Sciences' Institute of Microbiology and the corresponding author, says the evidence suggests that the genetic changes account for the increased mortality, although more data are needed to be certain.

The researchers also tested the pathogenicity of the virus by using it to infect mice, which succumbed more quickly than mice infected with other H5N1 strains. "This shows that [the virus] is also more pathological for mammals," says Ilaria Capua, a virologist at the Istituto Zooprofilattico Sperimentale delle Venezie in Legnaro, Italy. This does not necessarily mean that humans will be more easily infected or that the virus can be passed from human to human, she says.

The outbreak raises other questions, including how the virus got to this sparsely populated corner of China. Since H5N1 appeared, researchers have debated whether migratory birds can spread it. Some aquatic birds are known to host strains of the virus with no or minimal symptoms. But the United Nations' Food and Agriculture Organization says there is no evidence tying outbreaks in poultry to wild birds. Still, Capua suggests that migratory birds from different regions might have carried several less pathogenic H5N1 strains to the "melting pot" environment of the lake, where this new variant emerged. Melville counters that abundant evidence shows that human activity—transporting poultry, poultry products, and even contaminated crates—can spread avian flu viruses over seemingly improbable distances.

A more pressing question is where these migratory birds might carry the virus next. Melville says that bar-headed geese, one of the infected species, fly several thousand kilometers to wintering grounds in India, potentially dropping the virus along the way. For many other species that breed at Qinghai, the understanding of migration routes "is very rudimentary," he says.

Breeding ground. Flu experts worry that migratory birds infected with a new strain of the H5N1 virus, like the bar-headed goose (*left*), might carry it far from their breeding ground at Lake Qinghai.

But "dead ducks don't fly," he adds, quoting an essay on wild birds and flu by Hong Kong–based ornithologist Martin Williams—meaning that if this new strain kills all the birds it infects, it is not going to travel very far. A priority, says Melville, should be determining if surviving birds are carrying a weakened strain of the virus, or if some species or individual birds are carrying the same variant with minimal health effects. "These are the important questions," says Gao, whose team is gearing up to answer them by collecting additional samples from healthy birds over the next couple of months.

–DENNIS NORMILE

CREDIT (INSET): © 2005 JOHN WHITE

ScienceScope

Petition Presses E.U.

More than 12,000 scientists have signed a petition calling for increased research funding. This spring, the European Commission proposed doubling the European Union's research budget—to $84 billion over 7 years—but disagreements over the entire E.U. budget have threatened to scuttle those plans (*Science*, 24 June, p. 1848).

Science is the first to go when budgets are tight, says Frank Gannon, president of the European Molecular Biology Organization, which helped draft the petition, which asks E.U. leaders for a "significant increase."

–GRETCHEN VOGEL

Bunker Buster Fight Looms

The Senate and the House are at odds over a White House plan to study a new nuclear weapon for underground targets. Last week, the Senate approved $4 million for a feasibility study of the Robust Nuclear Earth Penetrator (RNEP) as part of a $31.2 billion spending bill for energy and water projects. "What is the harm in getting the study?" asked John Warner (R–VA) during floor debate.

In May, the House voted to strike RNEP funding for the project and put the program in the Pentagon, which does not do nuclear research. "It's our hope ... what happened last year will happen this year, and they'll go with the House version," said Joe Volk, executive secretary for the Friends Committee on National Legislation, a Quaker lobby in Washington, D.C., that opposes nuclear weapons.

–ELI KINTISCH

European *BRCA2* Patent Lives On

The European Patent Office has let stand a patent filed by the biotech firm Myriad Genetics in Salt Lake City, Utah, on the breast cancer gene *BRCA2*. Opponents of the patent—including a group of gene-testing clinics—had argued that Myriad's discovery was not innovative and that it discriminated against an ethnic group. Specifically, the European Society of Human Genetics (ESHG) in Vienna, Austria, objected to a legal claim that applies only to "Ashkenazi Jewish women" (*Science*, 24 June, p. 1851).

According to ESHG member Gert Matthijs of the Catholic University of Leuven, Belgium, European doctors will have to ask a woman if she is Ashkenazi before offering to test for *BRCA2*—and change procedures if she says she is. Myriad's opponents may appeal the latest ruling, issued on 29 June.

–ELIOT MARSHALL

RESEARCH MANAGEMENT

Scientists Say Genome Canada's Cofunding Rules Stymie Good Ideas

OTTAWA, CANADA—Does it make sense to reject a study of whether poplar trees can help mitigate global warming simply because the trees were going to be planted anyway? That Zen-like question has become a rallying cry for scientists protesting rules about cofunding of research proposals in Canada.

Last month, Genome Canada rejected a proposal from University of Toronto botanist Malcolm Campbell to team up with the Canadian Forest Service (CFS) on an $18.4 million poplar genomics initiative that would have examined the role of the trees as carbon sinks or feedstock for biofuels. It was one of 27 ideas shot down in the first of a two-stage process that focused on the financial, rather than scientific, merits of each application. Some 66 proposals remain in the running for $132 million in this, the third round of funding from Genome Canada.

The rejected scientists fell victim to a flawed process, say 39 prominent researchers who last month released a public letter suggesting that cofunding may be undermining the country's ability to support cutting-edge research (*Science*, 24 June, p. 1867). "It does sound like sour grapes," admits Campbell, who says he was lured home last fall from Oxford University in the U.K. because of the "promising" environment created by a raft of new Canadian programs such as Genome Canada. "But it's sour because one does not expect when formulating a scientific proposal to have it evaluated first on the grounds of management criteria."

But Martin Godbout, president of Genome Canada, says the complaints have no merit. Cofunding is essential for stretching scarce resources, he says, and is an integral part of Genome Canada's mission to collaborate with provincial and local governments, industry, and private foundations. ▶

Growing unhappiness. Malcolm Campbell and other Canadian scientists don't like how Genome Canada weeds out grant proposals.

PESTICIDE TESTING

EPA Draft Rules for Human Subjects Draw Fire

Efforts by the Environmental Protection Agency (EPA) to adopt ethical guidelines for controversial testing of pesticides on humans have run into trouble.

Last week, the Senate, as part of a measure setting the agency's 2006 budget, voted to bar EPA from using any such studies in its regulatory decisions. The House had passed an identical amendment in May, although differences in the two bills must still be reconciled. And a leaked version of draft regulations has already drawn criticism from scientists who say the rules don't go far enough. "This document is not about protecting human subjects," says toxicologist and environmental activist Ellen Silbergeld of Johns Hopkins University in Baltimore, Maryland.

In one corner. Senator Barbara Boxer offered one of two Senate amendments that send mixed signals to EPA.

The issue of human testing flared up in 1998, when the Environmental Working Group, an advocacy organization in Washington, D.C., released a report questioning whether it was ethical for EPA to use studies based on volunteers being fed pesticides to help determine how to regulate the compounds. In 2001, EPA turned to the National Academies for advice. The academies' study, published last year, concluded that some research was acceptable under certain conditions (*Science*, 27 February 2004, p. 1272).

Meanwhile, EPA had begun to work on rules that would extend a federal ethics code for human research to studies not conducted or funded by EPA. Last week, Representative Hilda Solis (D–CA) and Senator Barbara Boxer (D–CA), who introduced the EPA amendments in their respective bodies, made public a copy that was scheduled for release in August.

Critics are unhappy with the scope of the rules to protect pregnant women and children. The ethical requirements would only apply to studies conducted to identify or quantify a toxic effect, with the results intended for EPA's use. The agency could still draw upon other studies in which the subjects might have been harmed from exposure to small doses of a substance, says John Hopkins pediatrician Lynn Goldman, who headed EPA's pesticides program from 1993 to 1998.

Another worry is that EPA is setting the bar too low by declaring that it will reject only those studies that fail to "substantially" comply with ethical guidelines. EPA can still decide to accept a study if it decides that the ethical flaws are outweighed by public health benefits. "That's an enormous loophole," Goldman says.

According to the leaked draft regulation, EPA would also consider using research conducted before the rules are put in place, if that research provided useful knowledge not attainable any other way and met the prevailing ethical standards at the time. But that's not good enough, says Goldman: "We need to make sure we're not going down a slippery slope."

The critics' biggest concern is that the rules ignore an academies' recommendation to create an outside expert panel to review proposals for pesticide tests and determine if they would be ethically acceptable. EPA believes that approach would "unnecessarily confine EPA's discretion to adopt more effective or efficient approaches in the future," according to the leaked draft.

The agency's stance does have its backers in Congress. In addition to Boxer's measure, the Senate passed an amendment offered by Senator Conrad Burns (R–MT) for EPA to stay the course and issue final rules within 6 months. And because Burns chairs the spending panel that oversees EPA's budget, his view could very well prevail when the House and Senate work out differences between the two bills later this summer. —**ERIK STOKSTAD**

CREDIT (TOP): W. COLE/UNIVERSITY OF TORONTO

"Cofunding works," he asserts. He also defends the initial screening, saying that it was needed to cope with the heavy workload and that it won't affect which proposals ultimately receive funding.

The letter writers, including some whose proposals were rejected, argue that a "committee of accountants" scoured applications for any flaw that might be used as an excuse to whittle the field. In Campbell's case, the agency decided that the CFS contribution amounted to trees that would be planted regardless of whether the project proceeded. "We all sat there, with our mouths agape, literally, for a minute," says Campbell, describing his team's reaction in a meeting with the due-diligence review committee. "We were at a complete loss as to how this did not qualify," he added, noting that the project had passed muster with two of Genome Canada's five regional genomics centers.

John Bergeron, chair of the department of anatomy and cell biology at McGill University in Montreal, couldn't understand why a KPMG accountant who chaired the review committee viewed as an apparent conflict of interest the housing of mice for Bergeron's proteomic studies of liver diseases at a company associated with his team. "It was so weird," says Bergeron. "You're sitting there, and you're saying: What's going on? This is wacko."

Godbout doesn't think so. Most of the projects rejected demonstrated a poor understanding of the goal of cofunding, he says, which is to generate novel funding sources. Another problem, he suggests, is that the results were delivered differently this year: Applicants who failed the financial review were informed immediately that they were out of the running. In previous years they were not notified until the winners had been chosen, leaving some with the impression that they'd failed the scientific review. "Next time, we will again run these two processes in parallel, within the same week," Godbout announced. But he predicted that "the outcome will be the same."

Regardless of which projects are chosen, Lou Siminovitch, an eminence grise within Canadian genetics and professor emeritus at the University of Toronto, fears that cofunding programs put too great an emphasis on grantsmanship and wooing potential investors to the detriment of science. "They're making people spend so much time at their desks that they have no time to innovate," he frets. **–WAYNE KONDRO**

Wayne Kondro is a freelance writer in Ottawa.

EPIDEMIOLOGY

Radiation Dangerous Even at Lowest Doses

A new National Research Council (NRC) report* finds that although the risks of low-dose radiation are small, there is no safe level. That conclusion has grown stronger over the past 15 years, says the NRC committee, dismissing the hypothesis that tiny amounts of radiation are harmless or even beneficial.

The risk of low-level radiation has huge economic implications because it affects standards for protecting nuclear workers and for cleaning up radioactive waste. The Biological Effects of Ionizing Radiation VII (BEIR VII) panel examined radiation doses at or below 0.1 sieverts (Sv), which is about twice the yearly limit for workers and 40 times the natural background amount the average person is exposed to each year. For typical Americans, 82% of exposure stems from natural sources such as radon gas seeping from Earth; the rest is humanmade, coming mostly from medical procedures such as x-rays.

In its last report on the topic in 1990, a BEIR panel calculated risks by plotting cancer cases and doses for survivors of the two atomic bombs dropped on Japan in World War II. Risks appeared to increase linearly with the dose. Based on evidence that even a single "track" of radiation can damage a cell's DNA, the panel extrapolated this relationship to very low doses to produce what is known as the linear no-threshold model (LNT).

Some scientists have challenged this LNT model, however, noting that some epidemiological and lab studies suggest that a little radiation is harmless and could even stimulate DNA repair enzymes and other processes that protect against later insults, an idea known as hormesis (*Science*, 17 October 2003, p. 378).

But the 712-page BEIR VII report finds that the LNT model still holds. The panel had the latest cancer incidence data on the bomb survivors, as well as new dose information.

CREDIT: GETTY IMAGES

Risky business. A new review verifies that even radiation levels well below those encountered by nuclear workers can raise cancer risk.

Committee members also reviewed fresh studies on nuclear workers and people exposed to medical radiation, all of which supported the LNT relationship. The model predicts that a single 0.1-Sv dose would cause cancer in 1 of 100 people over a lifetime. Such risks should be taken into account, the report cautions, when people consider full-body computed tomography scans, a recent fad that delivers a radiation dose of 0.012 Sv.

At the same time, notes panelist Ethel Gilbert, an epidemiologist at the National Cancer Institute in Bethesda, Maryland, "we can't really pinpoint" the risk at the lowest doses. The BEIR VII panel examined the latest evidence for a threshold. But it found that "ecologic" studies suggesting that people in areas with naturally high background radiation levels do not have elevated rates of disease are of limited use because they don't include direct measures of radiation exposures. The panel also concluded that animal and cell studies suggesting benefits or a threshold for harm are not "compelling," although mechanisms for possible "hormetic effects" should be studied further.

Toxicologist Ed Calabrese of the University of Massachusetts, Amherst, a vocal proponent of the hormesis hypothesis, says the panel didn't examine enough studies. "It would be better if more of the details were laid out instead of [hormesis] just being summarily dismissed," he says. The panel's chair, Harvard epidemiologist Richard Monson, acknowledges that the long-running debate over the LNT model won't end with this report, noting that "some minds will be changed; others will not." **–JOCELYN KAISER**

* *Health Risks from Exposure to Low Levels of Ionizing Radiation: BEIR VII Phase 2* books.nap.edu/catalog/11340.html

The goal of much of modern medicine and culture is effectively to stop evolution. Is that happening?

Are Humans Still Evolving?

The news made headlines around the world: Blonds were going extinct. According to CNN and other media, a World Health Organization (WHO) study concluded that the gene for blond hair, which was described as recessive to dominant genes for dark hair, would disappear in 200 years. The BBC announced that the last natural blond would be born in Finland and suggested that those who dyed their hair might be to blame, because "bottle blonds" were apparently more attractive to the opposite sex than natural blonds were and thus had more children.

Fortunately for blonds, the whole story turned out to be a hoax—"a pigment of the imagination," as the *Times of India* later put it. WHO announced that it had never conducted such a study, and hair color is probably determined by several genes that do not act in a simple dominant-recessive relationship. The story, which may have originally sprung from a German women's magazine, apparently simply leaped from one media outlet to another.

Although the story was untrue, the ease with which it spread reflects popular fascination with the evolutionary future of our species, as well as the media's appetite for evolutionary pop science. Today, Oxford University geneticist Bryan Sykes is receiving voluminous coverage for his book, *Adam's Curse*, which predicts that continuing degeneration of genes on the Y chromosome will leave men sterile or even extinct in 125,000 years. Many biologists say that the question they most often receive from students and the public is "Are humans still evolving?"

To many researchers, the answer is obvious: Human biology, like that of all other living organisms on Earth, is the result of natural selection and other evolutionary mechanisms. Some say the question itself betrays a misunderstanding of how evolution works. "The very notion that … we might not be evolving derives from a belief that all other life forms were merely stages on the way to the appearance of humans as the intended end point," says primatologist Mary Pavelka of the University of Calgary in Canada.

Modern mismatch. Overbite is widespread among modern humans, but evolution may not be to blame.

But other scientists point out that in developed countries, culture, technology, and especially medical advances have changed the evolutionary rules, from survival of the fittest to the survival of nearly everyone. The result, they say, is a "relaxation" of the selective pressures that might have operated 50 or 100 years ago. "Biologically, human beings are going nowhere," says anthropologist Ian Tattersall of the American Museum of Natural History in New York City. University College London geneticist Steven Jones agrees. "The central issue is what one means by 'evolving,' " Jones says. "Most people when they think of evolution mean natural selection, a change to a different or better adapted state. In that sense, in the developed world, human evolution has stopped."

Yet millions of people in developing countries continue to live under the combined stresses of poverty and disease. Under these conditions, even skeptics of ongoing human evolution agree that natural selection may be favoring genes that confer resistance to disease or enhance reproductive fitness in other ways. Indeed, researchers are now tracking how deadly maladies such as AIDS and malaria exert selective pressure on people today. "As long as some people die before reproducing or reaching reproductive age, selection is likely to be acting," says geneticist Chris Tyler-Smith of the Sanger Institute near Cambridge, United Kingdom.

Even in developed countries, where survival tends to be prolonged for almost all, recent studies suggest that there are still genetic differences among people in fertility and reproductive fitness, an indication that natural selection is operating. "The question 'Are humans still evolving?' should be rephrased as 'Do all people have the same number of children?' " says Pavelka. "The answer is that we do not make equal contributions to the next generation, and thus we are still evolving."

Over the past few years, a wealth of new data has begun to illuminate how natural selection has shaped—and may still be shaping—humanity. The human genome project and genetic data from people around the world have powered an explosion of research seeking signs of natural selection in human DNA. "A lot of the tools we are now using to search for selection were developed by people working on flies and other organisms," says evolutionary geneticist Bruce Lahn of the University of Chicago. "But once researchers began to discover examples of ongoing selection in humans, it opened the door and gave them confidence that they could find even more."

CREDITS (TOP TO BOTTOM): GETTY IMAGES; M. MÖLLENBERG/ZEFA/CORBIS

So far, the number of confirmed cases of genes under recent selective pressure is only "a handful," says Tyler-Smith. But that is likely to change once the results of the International HapMap Project, a multination effort to determine worldwide variation in the human genome, are released later this year. Because genetic variation is the raw material on which natural selection works, favoring certain alleles over others, Tyler-Smith says the HapMap should "give us an overall view of the regions of the genome that have been under selection."

Drifting toward modernity?

To science-fiction fans, the future of human evolution conjures up visions of dramatic changes in our bodies, such as huge brains and skulls. "Many people see us continuing on the righteous path of increasing intelligence," says Pavelka. "But we will not head in the direction of larger brains and crania as long as infants are required to pass through a woman's pelvis to get into the world."

Whatever lies in our evolutionary future, scientists agree that the modern human body form is largely the result of evolutionary changes that can be traced back millions of years. The uniquely human lineage dates from about 6 million years ago, and many studies have demonstrated that our divergence from chimpanzees was accompanied by strong selective pressure, for example on the human brain. Yet researchers caution that not all morphological changes—the ones we can see in body shape and size—are the result of natural selection; some may not be due to genetic evolution at all. For example, the increase in average height seen in many developed nations over the past 150 years or so is probably due mostly to better diets rather than natural selection.

Even very early evolutionary changes in the hominid line were not necessarily due to natural selection. Take the hominid face, which has changed dramatically in the past 3 million years from the heavy-jawed mugs of the australopithecines to the relatively small and gracile skulls of modern humans. Anthropologist Rebecca Ackermann of the University of Cape Town in South Africa and anatomist James Cheverud of the Washington University School of Medicine in St. Louis, Missouri, analyzed hominid faces over time, using formulas that model natural selection as well as random genetic drift, in which some traits or alleles become more common simply through chance. They concluded last December in the *Proceedings of the National Academy of Sciences* (*PNAS*) that natural selection probably drove the evolution of facial form up to the birth of early *Homo*. But they also found that genetic drift could explain most of the changes in the human face after the birth of *Homo* about 2.5 million years ago. "Selective pressures on the face may have been released" when humans began using tools and so did less biting and chewing, says Ackermann.

Cold adapted. Natural selection may have favored the Buriats' broad skulls.

The take-home lesson, she says, is that "genetic drift has played an important role in shaping human diversity. This is evolution, too." Drift has continued to shape modern human faces and skulls in the more recent past, according to other studies. For example, researchers have examined regional differences in head shape—parameters such as width of the skull, height of the nose, and length of the jaw—to see whether certain traits were favored by natural selection in response to differences in climate or environment. In most cases, the differences among populations turned out to be no more than expected due to random drift. But there are a few exceptions: Anthropologist Charles Roseman of Stanford University in California last year reported in *PNAS* that the skulls of the Buriat people of Siberia are broader than predicted by random drift. Broad skulls have smaller surface areas and so may be an adaptation to cold climates. That fits with previous work by anthropologist John Relethford of the State University of New York College at Oneonta. Relethford concludes that random drift and migration can explain cranial differences in "most cases," with the exception of people like the Buriat and Greenland Eskimos, who live in very cold environments.

Although the evolution of measurable traits such as modern human skull shape may be due to random drift, some changes in human body form may have more to do with cultural and environmental factors such as diet. "Over the past 10,000 years, there has been a significant trend toward rounder skulls and smaller, more gracile faces and jaws," notes anthropologist Clark Larsen of Ohio State University in Columbus. Most of the change, says Larsen, is probably due to how we use our jaws rather than genetic evolution. With the rise of farming, humans began to eat much softer food that was easier to chew. The resulting relaxation of stress on the face and jaw triggered changes in skull shape, Larsen says. He adds that the dramatic and worldwide increase in tooth malocclusion, tooth crowding, and impacted molars are also signs of these changes: Our teeth are too big for our smaller jaws. Numerous studies show that non-Western people who eat harder textured foods have very low rates of malocclusion, he notes. Similar changes are found in monkeys fed hard and soft diets. "With the reduction in masticatory stress, the chewing muscles grow smaller, and thus the bone grows smaller," Larsen says. "It is not genetic but rather reflects the great plasticity of bone. It is a biological change but heavily influenced by culture."

Signs of selection

Even if random drift and other nongenetic forces have helped shape modern humans, there is

Candidates for Recent Selection in Humans

GENE OR GENETIC LOCUS	HYPOTHESIZED SELECTIVE PRESSURE
Lactase	Improved nutrition from milk
G6PD	Protection against malaria
Duffly blood group	Protection against malaria
Hemoglobin C	Protection against malaria
TNFSF5	Protection against malaria
CCR5	Protection against smallpox and AIDS
H2 haplotype	Unknown but only in Europe
DRD4	Cognition and behavior
MAOA	Cognition and behavior
AGT	Protection against hypertension
CYP3A	Protection against hypertension
TAS2R38	Bitter taste perception

CREDITS (TOP TO BOTTOM): GETTY IMAGES/AFP; IMAGE: CDC

Battle for survival. AIDS and other deadly diseases may spur a rise in resistant gene alleles.

growing evidence that natural selection has also played an important role, even if its effects have been more subtle. Human evolution researchers are now mining the riches of genomic data to spot genes subject to recent selective pressures (*Science*, 15 November 2002, p. 1324). Geneticists have a large arsenal of "tests of selection" at their disposal, all of which exploit the genetic diversity of human populations to determine whether individual alleles or larger blocks of the genome—called haplotypes—are behaving as would be expected if they were only subject to random drift and were not under selection.

Some tests look for evidence that mutations in an allele that alter the protein it codes for have been favored over those that cause no change; others examine whether certain alleles are more common than expected. A fairly new and powerful approach compares the frequency of an allele in a population with the genetic diversity within a haplotype to which it belongs. If the allele is common due to random drift over a long time, the adjacent region of the genome should show considerable variation due to genetic recombination, the exchange of DNA between chromosomes during meiotic cell divisions. But if the variation is less than expected, the allele may have risen to high frequency in a much shorter period of time—a telltale sign of selection. "These tools are powerful," says Lahn. "Where we are lagging behind is in good data."

By deploying such methods, geneticists have identified more than two dozen genes that appear to have come under selective pressures since the rise of *Homo*, and several of them may still be subject to such pressures today. Some of these favored alleles apparently arose at highly critical periods in human evolution. Such is the case of *FOXP2*, the so-called speech gene, which is implicated in the ability to talk, shows signs of strong selection, and arose no more than 200,000 years ago, coinciding closely with the first appearance of *Homo sapiens* (*Science*, 16 August 2002, p. 1105). Other genes under selection are linked to cognition and behavior, and still others are involved in defense against diseases such as hypertension, malaria, and AIDS (see table, p. 235).

In some cases, the new tests for selection have helped nail down long-suspected cases of evolutionary adaptation. One classic example is lactase persistence, the inverse condition of so-called lactose intolerance. Most adults cannot drink milk because they produce little lactase, the enzyme that breaks down lactose, which is the major sugar in milk. But a sizable number of people can, and their geographical distribution correlates closely with the spread of domesticated cattle out of the Near East. Thus, more than 70% of Europeans, who have a long history of drinking milk, have lactase persistence, as do some African pastoralists. In contrast, the percentage is very low in most of sub-Saharan Africa and Southeast Asia.

Last year, researchers clinched the case for selection at the lactase gene. A team led by genome researcher Joel Hirschhorn of Harvard Medical School in Boston identified a haplotype more than 1 million nucleotide base pairs long that includes the lactase gene and confers lactase persistence on people who carry it. This form of the haplotype is found in nearly 80% of Europeans and Americans of European ancestry but is absent in the Bantu of South Africa and most Chinese populations. Hirschhorn and colleagues concluded from the unusual length of the DNA block that it is young, because it has not yet been broken up by genetic recombination. They calculate in the June 2004 issue of the *American Journal of Human Genetics* that this haplotype came under very strong selective pressure beginning between 5000 and 10,000 years ago, corresponding to the rise of dairy farming. Thus a cultural and technological change apparently fostered a genetic one. "This is one of the best examples of recent selection in humans," says Tyler-Smith.

Although being able to drink milk as an adult has its pleasant side, as any chocolate-shake lover can testify, most people in the world get along fine without the beverage. Yet in some cases, having a certain allele can be a matter of life or death. Thus, the genes most likely to be under strong selective pressure today are probably those involved in providing resistance to infectious disease, says Sarah Tishkoff, a geneticist at the University of Maryland, College Park. "In Africa, people are dying daily [of infectious disease], and those who have genotypes that confer some resistance are going to have more offspring. That is natural selection in action."

AIDS and malaria are arguably the worst scourges of humankind today, and they may both be exerting selective pressure on African genomes. Several genes have alleles that provide resistance to malaria, including those that code for hemoglobin C and an allele of the so-called Duffy blood group found only in sub-Saharan Africa; accumulating evidence suggests that they have both been under recent selective pressure. Four years ago, Tishkoff and colleagues showed that two different alleles of a gene called *glucose-6-phosphate dehydrogenase* (*G6PD*) have also been favored by strong selective pressure. The mutant alleles, A^- and Med, are found only where malaria is or recently was a problem and offer resistance against malaria, although they can cause blood diseases.

Tishkoff and her co-workers used the known geographical variations in the *G6PD* gene to estimate that the A^- allele probably arose in Africa about 6300 years ago and then spread rapidly across the continent; the Med allele, found in southern Europe, the Middle East, and India, is estimated to be only about 3300 years old (*Science*, 20 July 2001, pp. 442 and 455). These estimates are consistent with archaeological evidence that malaria only became a major health problem after the invention of farming, when the clearing of forests left standing pools of water in which the vector for the disease, the *Anopheles* mosquito, could breed. Thus a cultural change again led to a genetic one.

CREDIT: ASSOCIATED PRESS

The case of AIDS, and the virus that causes it, HIV, suggests that the selective advantage of a gene can shift over time. As HIV infects T cells in the blood, it docks onto a cell surface receptor called CCR5. In the mid-1990s researchers discovered that a mutation in the *CCR5* gene provides strong protection against AIDS in homozygotes, people who have two copies of the protective allele. The mutation, called delta 32, is found in up to 13% of European populations but is extremely rare in other groups, including Africans. Researchers dated the origins of the delta 32 mutation in humans to about 700 years ago and concluded that a strong selective event resulted in its spread; this finding was confirmed in 2001 using sophisticated selection tests.

Yet because the AIDS epidemic dates only from the late 1970s at the earliest, researchers believe that the selective pressure on the delta 32 mutation must have been from some other factor. Researchers have debated whether the plague or smallpox, both of which ravaged European populations in the past, is more likely, although some recent studies have leaned toward smallpox.

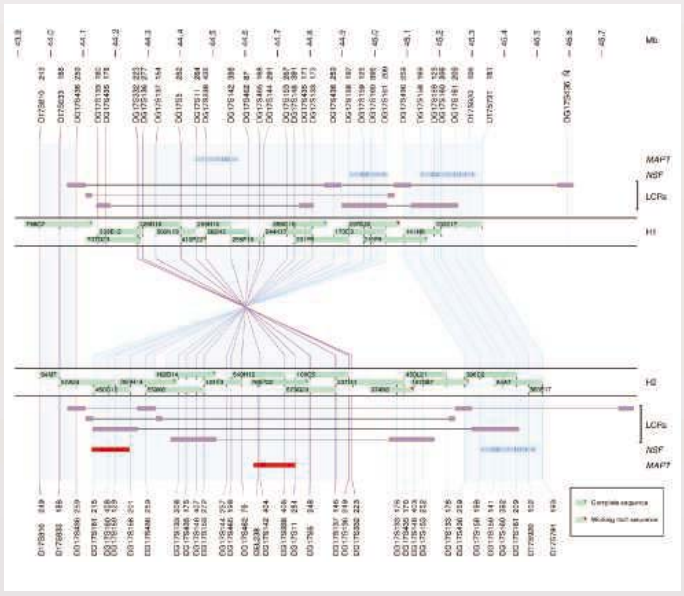

Baby boost. Women with an inversion in this region of chromosome 17 have more children.

Icelanders evolving?

Although researchers scouring the human genome for signs of natural selection have uncovered a few examples, direct evidence that a particular allele actually boosts reproduction—the sine qua non of natural selection—is hard to come by in humans. But that's just what researchers were able to do in one dramatic study in Iceland. For the past several years, scientists at deCODE Genetics, a biotechnology company based in Reykjavik, Iceland, have been gathering genetic information on the nation's 270,000 citizens, in a government-approved effort to isolate disease genes (*Science*, 24 October 1997, p. 566). In the course of this research, deCODE researchers discovered a variant of human chromosome 17 in which a 900,000 - nucleotide-base-pair stretch of DNA was inverted; this inversion was associated with a previously identified haplotype called H2, which they estimate arose 3 million years ago. H2 carriers make up about 17.5% of Icelanders and 21% of Europeans, but only about 6% of Africans and 1% of Asians.

To see whether the relatively high frequencies in Europeans represented natural selection, the team genotyped 29,137 Icelanders born between 1925 and 1965. When these data were correlated with the island's extensive genealogical database, the evidence for positive selection was stunning: As the team reported in the February 2005 issue of *Nature Genetics*, female H2 carriers had about 3.5% more children than H1 carriers. "This study has large implications," says anthropologist Osbjorn Pearson of the University of New Mexico, Albuquerque. "The European version of the H2 haplotype could sweep the entire human population if it conveyed the same reproductive advantage in other people and environments." But deCODE CEO and research team co-leader Kári Stefánsson says the low frequencies of H2 outside Europe suggest that for some reason, its advantages are limited to that continent. "Why, I can't tell you," he says.

There are several genes in the H2 region, but it is not at all clear which ones cause H2 carriers to have more children; one nearby gene is implicated in pregnancy complications. The deCODE team is looking at the genes to see whether differences in expression might create the selective advantage. One lead, Stefánsson says, is that H2 carriers also show a higher rate of recombination during meiosis. In an earlier study, his team found that mothers with high oocyte recombination rates also tend to have more children, possibly because this genetic shuffling helps protect against errors in meiosis, which are a major cause of miscarriage in older mothers. H2 carriers also appear to live longer on average. "It is fascinating to think that there might be an advantage associated with a DNA variant at both ends of life," Stefánsson says.

Our evolutionary future

To many researchers, the limited but growing evidence that natural selection is currently acting on the human genome means that humans are still evolving, even if in subtle ways. But can we actually predict the course of future evolution, à la Sykes's disappearing males or the vanishing blonds? Most researchers' predictions are considerably more narrow and cautious and are tied to known selective pressures.

For example, researchers predict that delta 32 and other protective CCR5 mutations may become more common in populations widely infected with HIV, especially in Africa. "If there are no more advances in the treatment of AIDS and people continue to die, we would expect selection pressure to increase [the mutations'] frequency over time," says Tyler-Smith, who adds that he sees "no reason why they should not go to fixation"—that is, replace all other alleles of the gene.

Whether or not these patterns will make a significant difference in the way humans look or live is another question. "There will be minor fluctuations over time and space in the makeup of local human gene pools as humans respond to local conditions," predicts Tattersall, "but they won't be directional. I find it hard to foresee that under current conditions a qualitatively new kind of human is ever likely to emerge. But if conditions change, all bets are off."

Evolutionary predictions are tied to speculation about just what kind of environment we may face. Some researchers suggest that changing climate conditions may diminish the benefits of culture and medicine, creating a new era of natural selection. "There has been a relaxation in selective pressures in industrialized societies," says evolutionary geneticist Peter Keightley of the University of Edinburgh, U.K. "But our ability to sustain that relaxation is probably temporary. We are using up our energy resources, our population is growing, and the climate is changing. All this is bound to lead to greater difficulties and renewed selective pressures."

Despite such concerns, however, most scientists remain leery of long-term forecasts, in part because of the way evolution works. "Evolution is not directed towards a goal," says Tyler-Smith. "It always takes the short-term view, operating just on what allows us to survive and reproduce better in this generation." For now, predicting humanity's evolutionary future may be little more than crystal ball gazing—better suited to science fiction than scientific research.

–MICHAEL BALTER

CREDIT: *NATURE GENETICS* **37**, 129-137 (2005)

Teaching Qubits New Tricks

A novel approach to storing information could give computers with near-magic powers a boost toward reality

Quantum computers will shatter the encryption that makes Internet commerce safe, search databases at unthinkable speeds, and crank out ciphers that nature itself guarantees secure—if they can be built. For years, scientists thought that would never happen because the same laws of physics that make quantum computers so powerful seemed to make a practical prototype impossible. But in 1995, when they discovered a means of preserving fragile quantum information despite those laws, quantum computing took a step closer to reality. The heart of the discovery was a way to correct errors in quantum information without destroying the information itself. These so-called quantum error correcting codes lie at the heart of quantum-computer research.

Now physicist Ray Laflamme and colleagues at the University of Waterloo in Ontario, Canada, have mathematically reframed quantum error correction in a way that shows that seemingly distinct approaches to it are really the same. This insight could make quantum error correction more efficient and may well push the field toward a much deeper understanding of the limits of quantum information.

"I think this is a very nice advance," says Peter Shor, a mathematician and physicist at the Massachusetts Institute of Technology. "Whether it's a giant leap or just a substantial step forward remains to be seen."

Information, whether it's classical bits stored on silicon or quantum "qubits" inscribed on a cluster of atoms, is extremely perishable. Nature spreads it throughout the environment, diluting it, filling it with errors, and making it unreadable. The ravages of time tend to flip bits and turn precious information into useless gobbledygook. For classical computers, the solution is simple: Make a backup. Then, if nature corrupts your original data, you can restore it from the copy. This is the most rudimentary form of error-correction, and every computer and digital communications device bristles with ever more sophisticated ways of ensuring that data gets stored or moves from place to place without being corrupted. The packets your computer sends over the Internet are padded with error-correcting information; the files on your hard drive are flush with extra data to protect from random bit flips; even your cell phone has means of detecting and compensating for damaged data that it receives.

But in quantum mechanics, copying is impossible, thanks to the "no-cloning rule": You can't duplicate information with perfect fidelity. The act of measuring a quantum object—such as an atom in a delicate state of superposition—destroys the original as you transfer its information to another medium. Any attempt to clone a chunk of quantum information is doomed to failure.

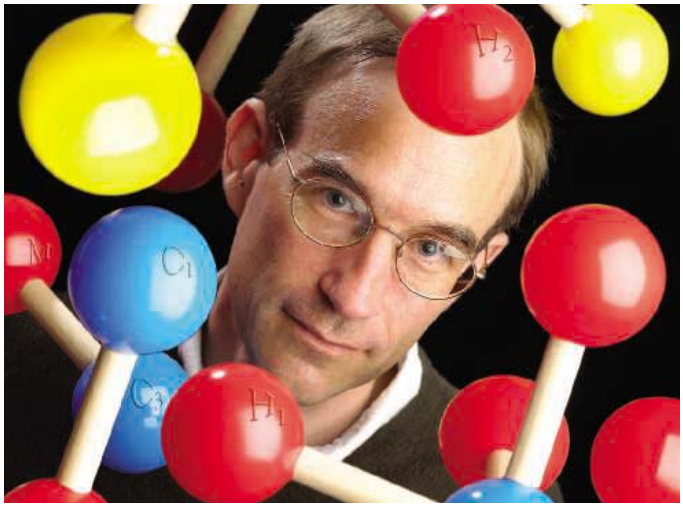

Better way. Ray Laflamme and colleagues showed that "qubits" of data last longer when not stored on quantum objects such as atoms.

As a result, many theorists believed that it would be impossible to correct errors in quantum information. Laflamme was one of the naysayers. "I tried to write a paper about it, saying that you would not be able to build a quantum computer," he says. But a colleague scooped Laflamme and published first. "I was upset, so I decided to poke some holes in the argument," he says.

In the mid-1990s, Shor, Laflamme, and a number of other physicists began to realize that there was a way to correct errors without violating the laws of quantum theory. "What we were thinking at the time was that the way we encode information in physical systems—a qubit upon an atom or a photon—was not very reliable," says Laflamme. Instead, scientists realized, they could spread a qubit over several quantum objects such as atoms or photons at once. The key was to store the information not on a single object but in the relationship among those objects; technically, the collection of objects shares a single quantum state that encodes the information. Unlike information stored on a single object, information inscribed upon such a collection can be made error-resistant without running afoul of the no-cloning rule, because it doesn't need to be copied or read.

In a paper recently published in *Physical Review Letters*, Laflamme and colleagues took the principle of abstraction a step further. Instead of storing information on relationships between quantum objects, they argued, one should store it on the relationship among the relationships. "It's getting more abstract, getting further away from the physical system," Laflamme acknowledges. "But the usual quantum gates can do this easily, and it has some very neat applications."

Using this "operator" formalism, Laflamme says, physicists can make error-correcting codes with smaller ensembles of atoms (or photons or other quantum objects) than ever before, thanks to the improved efficiency that the method allows. The new mathematical structure also enabled Laflamme to prove that several seemingly different quantum-computational methods for controlling errors are really the same. "Some other methods of error corrections were proposed that are more passive," says William Wootters, a physicist at Williams College in Williamstown, Massachusetts. Instead of actively correcting errors as they occur, physicists can pick a setup in which, under certain conditions, the information they inscribe on the system is immune from errors. "It seemed to be a different approach," Wootters says. "This paper shows that you can reduce the passive kind to the active kind." That means that physicists might now be able to borrow powerful tools from each of these areas and apply them to the others.

"We're not sure yet what the real power of this technique is," says Laflamme. "We haven't found the killer application." Nevertheless, it's clear that the abstract approach will give theorists a concrete ability to explore new facets of a decade-old idea. "It allows us to understand that quantum error correction is much richer than we had thought," he says.

–CHARLES SEIFE

CREDIT: BRYN GLADDING

Biologist Helps Students Get a Leg Up on Scientific Inquiry

Scott McRobert's research on how temperature affects the development of toads gives second-graders a chance to dip into real science

PHILADELPHIA, PENNSYLVANIA—Elizabeth places a small plastic cup filled with water on an electronic weighing machine and presses a button to adjust its reading to zero. With help from amphibian biologist Scott McRobert, the 7-year-old dips a fishnet into a bucket swarming with tadpoles and brings up a wriggling specimen that she then nudges into her cup. After recording the animal's weight on a white sheet, she holds the cup aloft against the light to examine the tadpole's body as it swims around. "It's in stage 2 of development," she announces proudly to McRobert, observing that the animal's hind legs have just begun to bud.

Elizabeth and her fellow second-graders at Friends' Central School here are helping McRobert investigate the effect of temperature on the metamorphosis of toad tadpoles. A professor at nearby Saint Joseph's University, McRobert has pursued the relationship between temperature and breeding success among amphibians for more than a decade. His assistants are usually graduate students. This spring, however, during a visit to the school to pick up his daughter, a second-grader here, he noted the toads in a small, shallow pond on campus. That discovery led him to pursue a second, educational goal in addition to his scientific one. "I want these students to not only learn about science," he says, "but also give them the opportunity to be scientists."

The project began in April, when students transferred some of the eggs laid in the pond into two tanks kept indoors and began monitoring their development. As the eggs hatched and the tadpoles grew, developing first tiny hind legs, then knees and front legs, the students kept daily journals of the animals' size, weight, and stage of development. The day the first two tadpoles of the study completed metamorphosis and clambered to the rim of their individual cups, "you would have thought we'd elected a new president," says Barbara Cole, one of two second-grade science teachers at the school. "It became a subject of hallway conversation among the staff."

As those tadpoles developed, McRobert monitored two other batches of eggs at his lab kept at two different temperatures. Last month he shared his findings with the students: The tadpoles in the school tanks had taken an average of 23 days to transform into tiny, frail toadlets, whereas those in the cooler tank at his lab had metamorphosed in 29 days and were, as a result, much larger.

Catching them young. Scott McRobert and second-grade students with their research subject.

Those results weren't surprising. Nonetheless, McRobert says that the correlation between temperature and developmental rate for this species is significant scientifically. "This is a study I would have done with my graduate students," says McRobert, who conducted a similar study on poison dart frogs in Costa Rica 10 years ago to document the optimum temperature for their breeding success.

Cole and McRobert say most of the 60 students involved in the experiment seem to have absorbed its fundamental message, namely, that animals undergo change after they are born and that environmental conditions can affect development. That insight showed up as the children learned about African animals in their regular science class, say their teachers. "When learning about crocodiles, the kids wanted to know if babies hatched in the sand stayed there or moved into the water," says Loren Ratinoff. "They were clearly reflecting on what they'd learned during the toad project." Previous classes, she noted, limited their questions to the size and color of adult animals.

The project may have also nurtured deductive reasoning skills. When a toadlet failed to climb out of its cup after completing metamorphosis and drowned, one student speculated about a larger phenomenon at work. "Maybe the toadlets grow front legs because they need to get out of the water when they develop lungs," he said. Another student wondered if tadpoles developed faster in warmer environments because "when it's warm, the water dries up, and they have no choice but to breathe in the air." McRobert—who conducted the study on his own time and without additional resources—says he "would have been happy if one of my graduate students had said that."

The teachers say the study may have also given the students a more concrete understanding of what science is. "Scientists observe things and write things down," according to one student. Another says she wants to become a scientist "because scientists make stuff to help the environment, and it's fun to make new stuff."

Regardless of what the students learn, the project is likely to help them academically, says Arthur White, a professor of science education at Ohio State University in Columbus. "The memory of the tadpole study could help many of these kids stick through the difficult science classes they will encounter in middle school and high school," White says.

McRobert is hoping for exactly that kind of outcome. "I am in science today because my fifth-grade science teacher allowed me to take care of a big tank of turtles he had at the back of his office," he says. Perhaps one day, his daughter and some of her classmates will be able to say the same thing about their tadpoles.

–YUDHIJIT BHATTACHARJEE

CREDITS (TOP TO BOTTOM): SCOTT MCROBERT; DAWN OVALLE

Embryo-Free Techniques Gain Momentum

Ethical concerns about research involving embryos have been driving the search for other ways to derive stem cells, and results may soon be on the horizon

SAN FRANCISCO, CALIFORNIA—As Californians work to get money flowing into the stem cell initiative that the state's voters approved last fall (see sidebar, p. 241), political pressure is growing in Washington, D.C., to find ways to conduct such research without involving embryos. In theory, the problem is straightforward: A skin cell has all the same genes as an embryonic stem (ES) cell, but different patterns of them are turned on. Scientists would like to be able to control gene expression with enough precision to turn a skin cell, say, directly into a genetically matched line of ES cells.

The perfect answer remains elusive, but many scientists believe that sometime in the coming decade, they will know enough about cellular "reprogramming" to bypass some of the steps required today. "In 10 to 15 years, we will induce transformation directly and will no longer need embryos or oocytes at all," predicts Kevin Eggan of Harvard University.

It may come even sooner, given mounting congressional support and recent scientific advances. At the June meeting of the International Society for Stem Cell Research,* Eggan presented his team's latest work using human ES cells to reprogram the gene expression of human fibroblast cells—moving toward the goal of creating genetically matched pluripotent cell lines without using oocytes or creating a new embryo. The team used polyethylene glycol to fuse the two kinds of cells, forming so-called tetraploid cells with twice the normal number of chromosomes. When grown into cell lines, the fused cells behaved like ES cells, Eggan reported, expressing characteristic genes, differentiating into embryoid bodies in culture, and forming so-called teratomas in immune-compromised mice—even forming patches of hair on the normally bald animals.

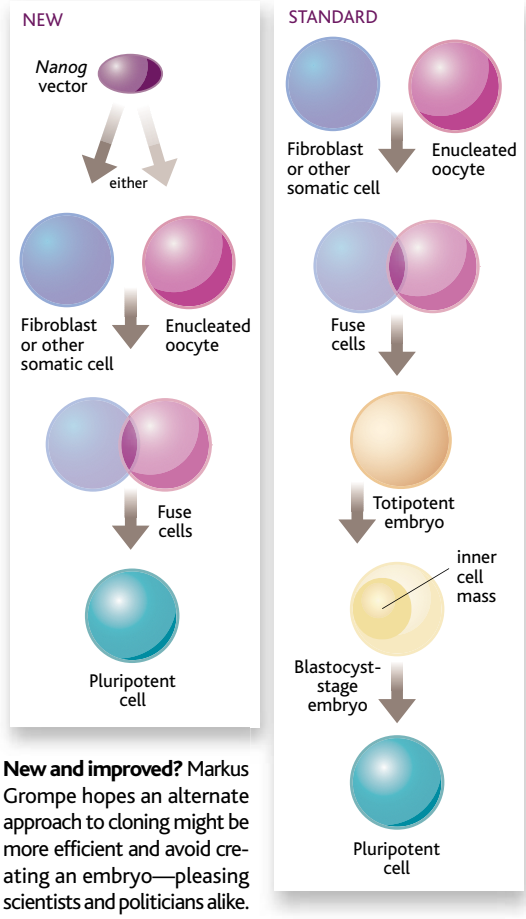

New and improved? Markus Grompe hopes an alternate approach to cloning might be more efficient and avoid creating an embryo—pleasing scientists and politicians alike.

Scientists have known for several years that ES cells can fuse with somatic cells to produce stem cell–like hybrids (*Science*, 15 March 2002, p. 1989), and previous studies had shown that several key tissue-specific genes turned off in the fused nucleus while key embryonic genes turned on. But Eggan and Chad Cowan of Doug Melton's group at Harvard went a step further, using gene expression arrays for detailed analyses of the hybrid cell lines. The cells, they found, had an almost identical expression profile to that of normal ES cells and one very different from that of fibroblast cells. "There is no longer transcription of fibroblast genes," Eggan says, "and there aren't any deficits of ES cell genes." Apparently, he says, "the ES cell nucleus can win the battle" between the two sets of chromosomes.

Eggan says the fused cell lines he described at the meeting were made with ES cells that Melton derived, and his work with them uses no NIH funding. He adds that the group has generated other lines using an NIH-approved ES cell line, and work with those cells would be eligible for NIH funding.

"The data that he's generated are beautiful," says George Daley of Harvard Medical School and Children's Hospital in Boston. "It establishes the principle that there are factors in the human ES cell that will reprogram. But the devil is in the details," such as whether the ES cell's DNA is required to accomplish the reprogramming—and if so, whether it might be removed afterward to create a cell line with just the genome of the original somatic cell.

Another option for reprogramming somatic cells that might be eligible for NIH funding comes from Markus Grompe of Oregon Health and Science University in Portland. It is a slightly different take on the idea of "altered nuclear transfer" that Stanford physician and bioethicist William Hurlbut proposed to the President's Council on Bioethics last fall (*Science*, 24 December 2004, p. 2174). In Hurlbut's proposal, a gene required for early embryonic development would be deleted or knocked out so that the nuclear transfer would produce a cell incapable of developing into a fetus. Some people objected to the idea, saying it would create disabled embryos rather than the "nonembryonic entity" Hurlbut described.

In an editorial in the *Wall Street Journal* on 20 June, Grompe and bioethicist Robert George of Princeton University in New Jersey propose that instead of knocking out a critical gene, scientists could overexpress a gene, such as *nanog*, that is crucial to ES cells, either in the somatic cell or in the oocyte. The resulting fusion of the two would, in theory, produce a cell with the expression pattern of an ES cell rather than that of a just-fertilized egg—essentially, going directly from a somatic cell to a pluripotent stem cell without forming anything resembling an early embryo.

Although some scientists dismiss this idea as "mere semantics" not worth the extra trouble, Grompe says the strategy might have practical benefits beyond its political appeal. Studies have shown that ES cells are better cloning donors than are more mature cells, he notes, so perhaps boosting the level of a key pluripotency gene in the somatic cell would prime the cell and make the process even more efficient.

The idea has won the support of a number of conservative bioethicists, including those who expressed reservations about Hurlbut's

CREDIT: K. BUCKHEIT/*SCIENCE*

* Held in San Francisco, 23–27 June.

California Institute: Most Systems Go

SAN FRANCISCO, CALIFORNIA—Hounded by lawsuits and threatened by legislation that some fear could cripple it, the California Institute for Regenerative Medicine (CIRM), created by the state's voters last fall, is nonetheless proceeding apace—if not exactly on schedule. "We're not going to flame out," neuroscientist Zach Hall, the interim director, assured *Science* last week during the third annual meeting of the International Society for Stem Cell Research.

"We have made tremendous progress," claims Hall, who's been on the job for 4 months. CIRM now has some 15 employees, including neuroscientist and stem cell expert Arlene Chiu, recruited from the National Institutes of Health (NIH) in Bethesda, Maryland. Hall says CIRM, which is currently advertising for program and review officers, hopes to have 15 scientists on board within the next couple of years. Blood stem cell expert Stuart Orkin of Harvard University has agreed to chair the peer review working group that includes 15 non-California scientists and seven patient advocates.

Handout imminent. CIRM Director Zach Hall says the first grants will go out this fall.

CIRM backers were clearly relieved last month when state democratic Senator Deborah Ortiz agreed not to press for a vote—at least for now—on a proposal to amend the rules governing the institute in ways that many believe would make it impossible to run. But hers is not the only impediment; the courts also have to rule on two lawsuits before the state can begin selling the bonds that will finance the initiative. Both suits—one that claims that CIRM is unconstitutional, and a second that argues that fertilized eggs should be treated as "persons"—are thought to have dim prospects of success. Nonetheless, the suits mean substantial delays. "I've heard anything from 6 months to 2 years," says Hall.

Although the $3 billion initiative appears to be mired down, its leaders are steadfastly upbeat. The deadline for applications for the first round of training grants was 1 July, and Hall says that CIRM still plans to award 200 3-year fellowships at 18 institutions in November, to the tune of $45 million. "We're going to go ahead and award them even if there's no [bond] money," says Hall. Bay Area real estate mogul Robert Klein, who spearheaded Proposition 71 and continues to direct start-up efforts, told *Science* that the CIRM is actively looking for $100 million in "bridge" funding. He points out that he raised $28 million to pass Prop. 71, and now that he can promise that donations will actually go to research, he is confident he can drum up a lot more.

Meanwhile, the institute's governing board has set up a new legislative subcommittee to come up with "policy enhancements" that they hope will satisfy Ortiz and her backers. Recommendations are scheduled to go to the full board on 12 July. Hall believes most of the differences with Ortiz—who is concerned about conflicts of interest, public access to decision-making, and Californians' access to the fruits of the research—can be resolved. Originally, Ortiz wanted outside peer reviewers to publicly disclose all financial ties to biotech-related ventures. She appears to have relented on this point, says Hall, who notes that CIRM policies already go beyond NIH requirements by asking reviewers to list any companies in which they have more than a $5000 investment. But that information would not be made public.

Ortiz also pushed for some grant deliberations to be made public—an action that horrified many scientists. Tampering with peer review "would cripple [CIRM's] ability to operate," said Stanford biologist Paul Berg. But now everyone, including Ortiz, agrees that peer-review meetings should be closed, says Hall. He cautions, however, that if the real business goes on in closed meetings and the public meeting of the Independent Citizens' Oversight Committee just looks like a rubber stamp, the public may object. The solution, Hall believes, will be for the peer reviewers to give scores, just like NIH does, to grants recommended for funding and to worthy grants that are not recommended for funding. The final funding decisions will then be made at open meetings, allowing a patient advocate, for example, to make a case for a project that wasn't recommended for funding.

The biggest sticking point is how to satisfy intellectual-property concerns while heeding Ortiz's demand that CIRM "ensure" that any new treatments be "accessible and affordable to low-income residents." According to Hall, this concept goes beyond the institute's mandate—and in any case, no one knows how to ensure that a treatment will be affordable. The latest wording is that CIRM will "seek to" ensure affordability. But that is still problematic, says Hall, as it "presents another target for litigation."

But optimism reigns as institutions all over California ramp up their stem cell capabilities. Stanford University's 3-year-old center, for instance, plans to hire a half-dozen scientists and just lured ear stem cell researcher Stefan Heller of Harvard. The University of California (UC), San Francisco, which distributes a number of cell lines, is planning to establish an "embryo bank" to supply excess embryos, eggs, and sperm from fertility clinics to California researchers; it will also be sending scientists to South Korea to learn the nuclear transfer techniques of Woo Suk Hwang. UC Los Angeles plans to spend $20 million in the next 5 years to establish the Institute for Stem Cell Biology and Medicine, with 12 new faculty positions. Hong Kong philanthropist Li Ka Shing just donated $40 million to UC Berkeley for a new research center focused on emerging scientific fields including stem cell biology. And in southern California, four institutions—UC San Diego, the Burnham Institute, the Salk Institute, and the Scripps Research Institute—have formed the La Jolla Stem Cell Initiative. All will be vying for money from CIRM, which aspires to become the world epicenter of stem cell research.

–CONSTANCE HOLDEN

technique. If Grompe's idea works, says Tadeusz Pacholczyk, a molecular biologist and priest at the National Catholic Bioethics Center in Philadelphia, Pennsylvania, the somatic nucleus would only be reprogrammed to a pluripotent state—able to become all tissue types in the body—without reaching the totipotent state in which a cell can form a complete new embryo.

Support seems to be growing in Washington as well. On 30 June, Representative Roscoe Bartlett (R–MD) introduced a bill that would fund animal studies to test the ideas, and Rick Santorum (R–PA), one of the Senate's strongest opponents of embryo research, has said he might include funding for such work in an omnibus spending bill.

"I would welcome any infusion of resources," says Daley, "as long as it's not used as an excuse to further delay funding for the methodology we know works today," such as the nuclear transfer techniques reported by scientists in South Korea. "You move ahead on all fronts. Scientists will in the end use what works best."

–GRETCHEN VOGEL

CREDIT: C. HOLDEN/*SCIENCE*

Random Samples

Edited by Jennifer Couzin

Fake Meteor Exposed

A metal object long regarded as a famous meteorite, and displayed in a Madrid museum since the 1940s, is apparently nothing more than a ball of steel. The Los Blázquez meteorite was donated to the Geomining Museum by José María Melgar, a mining company employee and meteorite aficionado. The discoverer was said to be the eminent Spanish geologist Casiano de Prado, who died in 1866.

But when curators Tomás Crespo and Rafael Lozano began cataloging the collection a few years ago, the supposed extraterrestrial metal did not respond to magnetic tests, as authentic meteorites do, the pair report in the June issue of the journal *Boletín Geológico y Minero*. The artifact turns out to be made of austenitic steel, an industrial alloy invented 16 years after de Prado's death. The object will remain on display—but with a new and accurate label, says Crespo.

Butterfly Sparkle Lures Mates

Some male butterflies have small, reflective patches dotting their wings. Resembling eyes with white "pupils" that reflect ultraviolet (UV) light, the spots are thought to confuse predators. But the butterflies, members of the species *Bicyclus anynana*, also sport the eyes on their inner—and more hidden—dorsal wings, suggesting an additional purpose: setting females aflutter. Antónia Monteiro, a biologist at the University at Buffalo in New York, her graduate student Kendra Robertson, and their colleagues scrutinized more than 1800 butterflies from the lab's colony. When the researchers blacked out some insects' "pupils" with paint, they found that females flocked to males

whose pupils remained visible. UV reflection seemed to be the draw: Dabbing the pupils with a UV-absorbing pigment was a turnoff for females, the team reports online 6 July in the *Proceedings of the Royal Society B: Biological Sciences*. Males with more UV reflectivity probably appear younger and healthier, attracting mates, says Robertson.

"The results are convincing, and the outcome is amazing," says Ronald Rutowski, a biologist at Arizona State University in Tempe. But one wrinkle, he points out, is that the amount of UV light available in the environment can change from one habitat to the next.

Isotopes of Cattle Feed

Wondering if that steak on your plate came, as advertised, from a contented cow that spent its days munching tender grass in a pasture? German researchers have taken an old technique—carbon isotope testing—and successfully applied it to a cow's feeding history.

A team led by grasslands scientist Hans Schnyder of the Technical University of Munich collected tail hair samples from three to five cows from each of 13 farms in Upper Bavaria. The sites ranged from organic farms where cows ate only grass to heifer-fattening feed lots that relied mainly on corn.

Because of differences in photosynthesis, the ratio of carbon-13 to carbon-12 is higher in corn than in grass. And, indeed, the isotopic signal in the cow hair matched that of their feed, the group reports in the August issue of *Agriculture, Ecosystems, and Environment*. "What's really novel is that we were able to show that you can differentiate [types of farming]," says Schnyder. The method would work just as well in meat or milk, he adds.

John Maas, who studies cattle nutrition and health at the University of California, Davis, says the approach is promising but needs to be validated on a broader scale.

Monkey See, Monkey Abuse

Rhesus macaques are supplying clues about how abusive behavior passes from parents to their children, with a new study suggesting that the link is environmental, not genetic.

Like humans, rhesus macaques that are abused as infants are more likely to become abusive parents, tossing, crushing, and biting their offspring. The monkey-human parallels piqued the interest of Dario Maestripieri, a behavioral biologist at the University of Chicago.

Maestripieri housed 14 female infants with adoptive mothers, some abusive and others not. Seventeen other monkeys stayed with their biological mothers, some of whom were abusive. He followed them for 5 years. The result: Being raised by an abusive mother, adoptive or not, made a difference in their behavior as adults. Nine of 16 infants cared for by abusive mothers became abusive parents, whereas none of those paired with nonabusive mothers did. The study appeared in the 27 June online *Proceedings of the National Academy of Sciences*.

Still, the study doesn't rule out genetics, says Joseph McClay, a geneticist at the Virginia Institute for Psychiatric and Behavioral Genetics in Richmond. Some individuals may be genetically predisposed to become abusive, he says, and the trait may be exacerbated by early environmental influences.

CREDITS (TOP TO BOTTOM): W. H. PIEL; TOMÁS CRESPO AND RAFAEL LOZANO; YERKES NATIONAL PRIMATE RESEARCH CENTER

Edited by Yudhijit Bhattacharjee

JOBS

Pandemic blocker. The next job for a public health expert who steered Hong Kong through the 1997 avian influenza epidemic and the 2003 outbreak of severe acute respiratory syndrome (SARS) is to prepare for a global flu pandemic.

Margaret Chan has been chosen by the World Health Organization (WHO) to help its 192 member countries "mitigate mortality and reduce social and economic disruption" from an anticipated influenza pandemic. Chan, who joined WHO 2 years ago from the Hong Kong Department of Health, plans to use her contacts to strengthen WHO's pandemic preparedness efforts throughout Asia, where the H5N1 avian influenza virus is believed to be endemic. "But I keep reminding myself that [a pandemic] can emerge from any country or any part of the world," she says.

Janelia's first crop. Bioinformatics whizzes, a worm brain mapper, and a scientist who built a flight simulator for fruit flies are among the first seven group leaders recruited by the Howard Hughes Medical Institute's Janelia Farm, a $500 million research campus set to open in mid-2006 in Ashburn, Virginia. The glass-roofed, snake-shaped laboratory will bring up to 300 physical and biological scientists together in 24 groups to figure out how neuronal circuits work and come up with new imaging technologies.

The bent is quantitative: Of the group leaders hired so far, five studied physics or math in college and later moved on to biology. The complete list is neuroscientists Dmitri Chklovskii and Karel Svoboda of Cold Spring Harbor Laboratory in New York; bioinformaticists Sean Eddy of Washington University in St. Louis, Missouri, and Eugene Myers of the University of California, Berkeley; protein imager Nikolaus Grigorieff of Brandeis University in Massachusetts; neurogeneticist Julie Simpson of the University of Wisconsin, Madison; and neurobiologist Roland Strauss of the University of Würzburg, Germany, who models insect flight.

Still ticking. Handprints from children at the development center he championed, an honorary law degree from the agency's general counsel, and a photograph of a plateau in Antarctica that now bears his name are just three of the many going-away presents that Joseph Bordogna received last week as he ended 14 years at the National Science Foundation (NSF), the last nine as the agency's longest-serving deputy director.

Serving under four NSF directors, Bordogna was known for both his attention to detail and his labors on the agency's evolving strategic vision. NSF Director Arden Bement presented the 72-year-old electrical engineer with a clock, then quickly noted that "Joe isn't a clock watcher. He comes to work when the sun rises and leaves when it sets."

Bordogna plans to continue that pace at the University of Pennsylvania, where he reclaims his endowed chair in engineering. He'll also be working with new president Amy Gutmann on implementing her strategic plan for the university.

THEY SAID IT

"I would prefer to call [it] oocyte genome replacement."

—Developmental biologist Roger Pedersen suggesting a new name for research cloning, a term that stem cell researchers say has drawn undesirable political attention to their field. Others have suggested "somatic cell nuclear transfer."

AWARDS

Abolishing hunger. Living in a relocation camp with other Japanese Americans during World War II, Gordon Sato grew corn and vegetables on a patch of land in the California desert at the age of 14. The experience inspired a lifelong interest in agriculture under harsh conditions, which led Sato (right) to develop a technique for cultivating mangrove trees using seawater on the Eritrean coast. Last week, that achievement earned the 77-year-old biochemist the $460,000 Blue Planet Prize, awarded by Japan's Asahi Glass Foundation.

Launched in the 1980s, Sato's Eritrean project has led to the development of 700,000 hectares of mangrove plantations, which could be used as a pasture to rear sheep and goats and lift millions of people out of hunger and poverty. The work has demonstrated that seawater agriculture can be profitable and a means for sustainable development in some of the world's poorest regions, says Sato, adding that it's time for the world to think about "implementing far-out ideas such as converting the Sahara into a mangrove forest."

The foundation awarded another Blue Planet Prize to British geologist Nicholas Shackleton for his contributions to paleoclimatology, including a technique to analyze the fluctuations in the size of ice sheets during the past 1.8 million years. He too will receive $460,000.

Got any tips for this page? E-mail people@aaas.org

CREDITS (TOP TO BOTTOM): SOURCE: ASAHI GLASS FOUNDATION; SOURCE: WHO; MARY HANSON/NSF

LETTERS

When the World Is Not Your Oyster

THE DECLINE OF THE EASTERN OYSTER *Crassostrea virginica* in Chesapeake Bay from overfishing, disease, and habitat degradation is well documented (*1*–*3*). Oysters provided important ecological and economic benefits to the Chesapeake Bay states of Maryland and Virginia, which have poured millions of dollars into their restoration (*4*). Recently, these states have effectively conceded that restoration has been ineffective (*5*), and they are developing an Environmental Impact Statement (EIS) to evaluate alternatives for increasing oyster populations (*6*). Under the EIS, the preferred (proposed) action is to introduce diploid populations of an Asian oyster, *Crassostrea ariakensis*, into the Bay. Such an introduction could occur in 2006 (*7*).

Eastern oysters (*Crassostrea virginica*) are in decline in the Cheseapeake Bay.

Adjacent states currently have no recourse to prevent (or alter) such an introduction despite the likelihood of being affected by it. A recent National Academy of Sciences (NAS) study that examined the proposed introduction concluded: "The existing regulatory and institutional framework is not adequate for monitoring or overseeing the interjurisdictional aspects of open-water aquaculture or direct introduction of *C. ariakensis*. There is no federal legislation that gives specific criteria for regulating the introduction of a nonnative marine species… there is no statutory mechanism for resolving differences among the interests of affected states" [(*4*), p. 7].

Delaware Bay, the estuary just north of Chesapeake Bay, has experienced a similar decline in its once lucrative oyster fishery (*8*). Delaware and New Jersey, which border Delaware Bay, have not given up on native oyster restoration. They object to the Chesapeake introduction of nonnative species because reproductively viable populations in Chesapeake Bay would make the spread of *C. ariakensis* outside of the Bay, by unintended or deliberate means, "highly likely" (*4*). Currently, New Jersey and Delaware have no regulatory role in an introduction in the Chesapeake. In a joint statement, they have taken the position that the introduction is premature and that they would like Maryland and Virginia to fund further research on the little-known basic life history of the oyster before any introduction (*9*).

Federal legislation could provide a mechanism to address this loophole by establishing a process for the governors of any states potentially affected by an intentional introduction to appeal to either the U.S. Fish and Wildlife Service or the National Marine Fisheries Service. If the federal agency was not satisfied with the biosecurity measures accompanying the proposed introduction, that agency could block the introduction, with judicial review for dissatisfied parties in the federal courts. The pending reauthorization of the federal Invasive Species Act could provide a forum for discussion of these or similar changes in federal law, to provide a better-coordinated and better-focused approach to intentional introductions.

J. JED BROWN,[1] RICHARD HILDRETH,[2]* SUSAN E. FORD[3]*

[1]Delaware River Fisheries Coordinator's Office, United States Fish and Wildlife Service, 2610 Whitehall Neck Road, Smyrna, DE 19977, USA. E-mail: Jed_Brown@fws.gov. [2]University of Oregon Ocean and Coastal Law Center, 1515 Agate Street, Eugene, OR 97403–1221, USA. E-mail: rghildre@law.uoregon.edu. [3]Haskin Shellfish Research Laboratory, Rutgers University, 6959 Miller Avenue, Port Norris, NJ 08349, USA. E-mail: susan@hsrl.rutgers.edu

*Members of the National Academy of Sciences panel on Nonnative Oysters in the Chesapeake Bay

References and Notes

1. J. B. C. Jackson *et al.*, *Science* **293**, 629 (2001).
2. C. L. MacKenzie, in *The History, Present Condition, and Future of the Molluscan Fisheries of North and Central America and Europe, vol. 1, Atlantic and Gulf Coasts*, C. L. MacKenzie Jr., V. G. Burrell Jr., A. Rosenfield, W. L. Hobart, Eds. (NOAA Tech. Rep. 127, U.S. Department of Commerce, Washington, DC, 1997), pp. 141–169.
3. B. J. Rothschild, J. S. Ault, P. Goulletquer, M. Heral, *Mar. Ecol. Prog. Ser.* **111**, 29 (1994).
4. Committee on Nonnative Oysters in the Chesapeake Bay, National Research Council, *Nonnative Oysters in the Chesapeake Bay* (National Academies Press, Washington, DC, 2004).
5. See www.dnr.state.md.us/dnrnews/infocus/infocus/oysters.asp
6. U.S. Army Corps of Engineers, Notice of Intent to Prepare an Environmental Impact Statement for the Proposed Introduction of the Oyster Species, Crassostrea ariakensis, Fed. Reg. 69 (no. 2), 330 (5 Jan. 2004) (available at http://a257.g.akamaitech.net/7/257/2422/05jan20040800/edocket.access.gpo.gov/2004/04-73.htm).
7. See www.dnr.state.md.us/dnrnews/infocus/eisschedule.html.
8. S. E. Ford, in *The History, Present Condition, and Future of the Molluscan Fisheries of North and Central America and Europe, vol. 1, Atlantic and Gulf Coasts*, C. L. MacKenzie Jr., V. G. Burrell Jr., A. Rosenfield, W. L. Hobart, Eds. (NOAA Tech. Rep. 127, U.S. Department of Commerce, Washington, DC, 1997), pp. 119–140.
9. See www.dnrec.state.de.us/DNREC2000/Admin/Press/Story1.asp?PRID=1507.

Regulating Mercury: What's At Stake?

THE U.S. ENVIRONMENTAL PROTECTION Agency (EPA) has issued a new rule regulating mercury emissions from power plants. But is the rule sensible?

The best way to answer this question is to tote up the benefits and costs of the rule and compare them. The EPA did not do such an exercise when it issued its proposed rule, so we did our own analysis.

We started with the two alternatives that EPA had on the table. One called for a 30% reduction in mercury emissions by 2008 through the use of command-and-control regulation—where all utilities must meet the same standard. A second was a cap-and-trade program that would reduce emissions 70% by 2018; this was the proposal that the Bush administration adopted in its final rule. It puts a cap on mercury emissions but lets firms sort out the least costly way to achieve those emission reductions. That option appears to cost about $15 billion less than the command-and-control approach while achieving roughly the same environmental outcome.

Is the cap-and-trade program really worth it? We estimate that the costs will be somewhere in the neighborhood of $4 billion on the basis of existing models. There is a lot of uncertainty in these estimates because some of the technologies needed to reduce mercury emissions are not commercially proven.

The main benefit from reducing mercury emissions from power plants is an increase in IQ. But the chain of reasoning that takes us from power plant reductions to IQ increases is uncertain. The basic idea is that reduced mercury emissions will reduce mercury in waterways, which will reduce mercury in fish, which will reduce mercury in pregnant mothers who eat fish, which will make newborns smarter.

We tried to quantify this information, recognizing there are major potential weaknesses in most links in the chain. We find some points worth noting. First, shutting down all

domestic coal-fired power plants would reduce U.S. mercury deposition by less than 20%, which is not likely to make a big dent in the problem (*1*). Second, if all power-plant mercury emissions in the United States were eliminated, we estimate that IQ points of newborns could go up by about 0.01 points, which is tiny by almost any measure (*1*).

When we try to monetize that benefit, based on evaluating parental decisions to reduce blood lead levels in children, we get numbers on the order of $100 million. This assumes there is a strong link between mercury consumption and IQ—an issue that has not been resolved in the scientific community.

While it is possible that we left some key benefits out of the equation, such as less heart disease, it is unlikely that we left so many out that the scales would tip the other way. The bottom line is that $100 million in benefits is a lot less than $4 billion in costs, so regulating mercury does not look like a good idea.

We take away three lessons from this exercise. First, when the benefits of a policy intervention are likely to be small, the probability of making things worse should be carefully considered before regulating.

Second, if an administration wants to promote accountability and transparency in the policy process, it should require agencies to estimate the key impacts of a regulation before that regulation is finalized, so interested parties can comment.

Third, citizens may not want a government or regulatory apparatus that focuses on making the most efficient use of society's limited resources. Nonetheless, when the resource inefficiencies are so great, we think it behooves our elected officials, as well as voters, to understand the implications of their decisions. Spending several billion dollars on a regulation that yields few social benefits means that we have several billion dollars less to spend on other things that could do a lot more good.

TED GAYER[1] AND ROBERT W. HAHN[2]

[1]Public Policy Institute, Georgetown University, 3520 Prospect Street, NW, Washington, DC 20007, USA. [2]American Enterprise Institute–Brookings Joint Center, 1150 17th Street, NW, Washington, DC 20036, USA.

Letters to the Editor

Letters (~300 words) discuss material published in *Science* in the previous 6 months or issues of general interest. They can be submitted through the Web (www.submit2science.org) or by regular mail (1200 New York Ave., NW, Washington, DC 20005, USA). Letters are not acknowledged upon receipt, nor are authors generally consulted before publication. Whether published in full or in part, letters are subject to editing for clarity and space.

Reference

1. T. Gayer, R. W. Hahn, "Designing Environmental Policy: Lessons from the Regulation of Mercury Emissions" (Regulatory Analysis 05-01, AEI-Brookings Joint Center, Washington, DC, March 2005).

The Long Search for Black Holes

IN READING THE PERSPECTIVE ON INTER-mediate-mass black holes ("The hunt for intermediate-mass black holes," G. Fabbiano, 28 Jan., p. 533), one may come away with the impression that much has been written about them, but that no one has gone to the telescope to take an optical spectrum to see what these ultraluminous x-ray sources (ULXs) really are.

Actually, investigators have taken spectra of some of these optically identified ULXs (*1*–*3*). So far, they have all been associated with high-redshift quasars. With the recent addition of a $z = 2.11$ ULX/quasar only 8 arc seconds from the nucleus of a low-redshift Seyfert galaxy, the score now stands: high-redshift quasars = 26, black hole binaries = 0. Since ULXs in galaxies were thought to be black hole binaries, this is a startling result.

The observational demise of a theoretical hypothesis that ULXs = black hole binaries is not so extraordinary. But what is extremely important is that these objects have been accepted as belonging to the low-redshift galaxies in which they are found. That means these high-redshift quasars have been accepted to be at the same distance as nearby low-redshift galaxies. Now that is news!

HALTON ARP

Max-Planck-Institut für Astrophysik, 85741 Garching, Germany.

References

1. H. Arp, C. M. Gutierrez, M. Lopez-Corredoira, *Astron. Astrophys.* **418**, 877 (2004).
2. P. Galianni *et al.*, preprint available at http://arxiv.org/abs/astro-ph/0409215.
3. P. Galianni *et al.*, *Astrophys. J.* **620**, 88 (2005).

Response

I APPRECIATE THE POINT RAISED BY ARP, AND I am aware of the identification with background high-redshift quasars of some bright x-ray sources near low-redshift galaxies, the former of which could be otherwise classified as ULXs. The identification of candidate ULXs (I here use the term "ULX" to indicate sources in the associated galaxies, i.e., presumably at the same redshift) with quasars excluded these sources from the bona fide ULX sample that is discussed in my Perspective. Virtually all ULX candidates in early-type galaxies are likely to be background quasars [(*1*–*3*); see Arp's references (*1*–*3*)].

The ULXs discussed in my Perpective are associated with star-forming galaxies. In fact, their presence seems to be associated with intense star formation activity. Overall, the number of these ULXs greatly exceeds the expected number of background quasars. In the Antennae galaxies alone, 14 such sources are found, and at these fluxes, it is unlikely that even one could be a background quasar. In the cases where optical identifications exist, early-type stars or ionized nebulae in the parent galaxies are found (*4*–*8*). A large number of these ULXs remain to be optically identified. If they were identified with high-redshift quasars, given that on statistical grounds we expect them to reside in the associated galaxies, it would indeed be a change of paradigm discovery.

GIUSEPPINA FABBIANO

Harvard-Smithsonian Center for Astrophysics, 60 Garden Street, MS 6, Cambridge, MA 02138, USA.

References

1. J. A. Irwin, J. N. Bregman, A. E. Athey, *Astrophys. J.* **601**, L143 (2004).
2. A. Ptak, E. Colbert, *Astrophys. J.* **606**, 291 (2004).
3. C. M. Gutierrez, M. Lopez-Correidoira, preprint available at http://arxiv.org/abs/astro-ph/0502290.
4. M. W. Pakull, L. Mirioni, preprint available at http://arxiv.org/abs/astro-ph/0202488.
5. T. P. Roberts *et al.*, *Mon. Not. R. Astron. Soc.* **342**, 709 (2003).
6. M. R. Goad *et al.*, *Mon. Not. R. Astron. Soc.* **335**, L67 (2002).
7. J.-F. Liu *et al.*, *Astrophys. J.* **580**, L31 (2002).
8. J.-F. Liu *et al.*, *Astrophys. J.* **581**, L93 (2002).

Encouraging Discovery and Innovation

FOR THE LATTER PART OF THE 20TH CENTURY, the United States was the global leader in discovery and innovation, allowing it (even with a well-paid workforce) to remain competitive commercially, to maintain defense superiority, and to serve as the world's leader in science and technology.

The world has changed. The emergence of a potent combination of low-priced and highly talented, technically sophisticated workforces in countries like India and China challenges the ability of the United States to maintain its technological superiority. The negative trade balance with countries such as China, and the increasingly high scientific and technological productivity that studies are finding from countries such as China and India, are some indicators of the global technological superiority shift that is starting to emerge.

To remain competitive, we need to accelerate our radical discovery and innovation. Large technical databases and algorithms to exploit the contents of these databases will enhance systematic identification and acceleration of radical discovery and innovation (*1*–*4*). These techniques all access large technical databases of multidisciplinary information for radical discovery and innovation.

Unfortunately, these efforts are fragmented, not well coordinated, and not well funded. At the present pace, many years will be required before they come to fruition. A major opportunity is falling between the cracks.

We need a Manhattan Project for radical discovery and innovation in the United States. This would be a coordinated, well-funded effort, with minimal bureaucratic overhead. The full infrastructure required for systematically accelerating discovery and innovation would be addressed, including people development, technique development, tool development, database development and access, and, especially, incentives for pursuing the interdisciplinary studies necessary for such radical discovery and innovation (*5*). Given the progress of the rest of the world on discovery and innovation, we need to start this project now to stay in the race.

RONALD N. KOSTOFF

Office of Naval Research, 875 North Randolph Street, Suite 1425, Arlington, VA 22217, USA.

References

1. R. N. Kostoff, "Systematic acceleration of radical discovery and innovation in science and technology" (DTIC Technical Report Number ADA430720, Defense Technical Information Center, Fort Belvoir, VA, 2005) (available at www.dtic.mil/).
2. D. R. Swanson, N. R. Smalheiser, *Artif. Intell.* **91** (no. 2), 183 (1997).
3. See www.innovationbp.com/pages/348061/.
4. See www.triz-journal.com/.
5. R. N. Kostoff, "Science and technology metrics" (DTIC Technical Report Number ADA432576, Defense Technical Information Center, Fort Belvoir, VA, 2005) (available at www.dtic.mil/).

Keeping Medical Research Ethical

IN HIS ESSAY "IT TAKES A VILLAGE: MEDICAL research and ethics in Mali" (4 Feb., p. 679), O. K. Doumbo raises important issues on the ethics of medical research, especially in resource-poor areas like Africa. One issue not discussed is the unavoidable reality that local communities may participate in research with the idea that, by becoming subjects, they are in fact buying "insurance." They may hope to ensure that they are in the good books of the research team so that they will be given special treatment when they or their children fall sick. Although this could be seen as a benefit of participating in research, it raises the question of whether the subjects can truly have given informed consent without coercion. Another issue is the influence and power that a research institute in a poor community has over the local populace. A research institute will inevitably be a local employer and consumer of locally produced materials. In this kind of power imbalance, how does one really negotiate informed consent? The challenges of observing ethical standards when the subject community is already so vulnerable are very difficult to overcome.

OBY OBYERODHYAMBO

PATH, ACS Plaza, Lenana Road, Post Office Box 76634–00508, Nairobi, Kenya.

CORRECTIONS AND CLARIFICATIONS

Letters: "Reassessing U.S. coral reefs" (17 June, p. 1740). In the second letter in this exchange, there should have been another author listed in addition to Amit Huppert. The second author is Andrew R. Solow, and his affiliation is Marine Policy Center, Woods Hole Oceanographic Institution, MS 41, Woods Hole, MA 02543, USA.

News of the Week: "Celera to end subscriptions and give data to public GenBank" by J. Kaiser (6 May, p. 775). Richard Gibbs' affiliation was incorrect in the article. He is at Baylor College of Medicine in Houston, Texas.

News of the Week: "Two-thirds of Senate backs more research" by E. Kintisch (6 May, p. 777). A Department of Energy spokesman was misquoted in the story as saying that President George W. Bush had requested a 10% increase over 2005 funding levels for DOE's Office of Science. The spokesperson actually said that the proposed increase was 1%.

ANIMAL BEHAVIOR

Following Their Instincts

Sharon Kingsland

Niko Tinbergen, a founder of the modern science of animal behavior, surprised Richard Burkhardt in 1979 by describing the field he helped to create as a "curious ragbag." *Patterns of Behavior*, Burkhardt's study of the creation and evolution of ethology from the early 20th century to the 1970s, explores how difficult it was for Tinbergen and other animal behaviorists to shape this mixed assortment of scientific problems into a new discipline. In addition to Tinbergen, a Dutch naturalist who developed an outstanding research program at Oxford University in the 1950s, the other central figure in this endeavor was his Austrian mentor and collaborator, Konrad Lorenz, who after years of struggle acquired his own Max Planck Institute at Seewiesen, Germany. Lorenz, a visionary and intuitive thinker, provides a contrast to Tinbergen, who brought experimental rigor and precise language to the study of behavior. Lorenz was charming but could be dogmatic, sensitive to criticism, and prone to sweeping generalization, while Tinbergen, a more rigorous and modest person, worked hard to keep lines of communication open with colleagues and to understand and adjust to their criticisms. In 1973 they shared the Nobel Prize in physiology or medicine with Karl von Frisch, renowned for his analysis of the dance language of bees.

Patterns of Behavior
Konrad Lorenz, Niko Tinbergen, and the Founding of Ethology
by Richard W. Burkhardt Jr.
University of Chicago Press, Chicago, 2005. 648 pp. $80. ISBN 0-226-08089-7. Paper, $29, £20.50. ISBN 0-226-08090-0.

Burkhardt, a historian of science at the University of Illinois at Urbana-Champaign, emphasizes that ethology had to be deliberately constructed as a discipline. He compares the careers of Lorenz and Tinbergen with those of several other American and British pioneers in the study of animal behavior, whose efforts fell short of creating a new field that had independent status. Lorenz succeeded in part because of his narrowly biological approach: he focused on innate or instinctive behaviors and the mechanisms that triggered instinctive responses. Instincts were, he believed, like the organs of the body, and the comparative study of behavior could offer clues to evolutionary relationships. Experimenting with the phenomenon known as "imprinting," he showed that young animals did not instinctively recognize members of their own species but could become attached to whatever individuals they were exposed to at a crucial stage in their development. Famously, Lorenz imprinted a group of young geese on himself, so that they followed him about as though he were their parent.

Lorenz's work in the mid-1930s marked him as an original thinker, who redefined the concept of instinct and promoted a comparative evolutionary approach to behavior. Yet there was a dark side to his vision. As the Nazis gained power, Lorenz curried favor with authorities in order to advance his career, and he appeared to embrace many of the racist ideas underlying National Socialism. He began to write about racial purity (arguing that racial mixing was deleterious), and he held that humans had an innate ability to recognize what was beautiful and ethical in other humans. His willingness to extrapolate from studies of birds to humans and the racist implications of those extrapolations raise troubling questions about the worldview that underlay his research. To be sure, Lorenz maintained that he did not see the full horror of Nazism until quite late and at that point he turned away from it. Nonetheless, his postwar disclaimer that he did not deserve criticism—on the grounds he was never a card-carrying Nazi— is disquieting because he ducks the issue of whether his published views, which he never recanted, supported Nazi ideology. Tinbergen clearly perceived Lorenz as "Nazi-infected" even though he viewed his friend as a basically honest man. Burkhardt handles the question of Lorenz's politics, or perhaps political naivety, fairly. Rather than condemning him as a racist, Burkhardt makes it clear that Lorenz was so convinced that his theories were universal truths that he was dangerously oblivious to the way his science reflected his cultural context. Lingering concerns about the ideological basis of Lorenz's biology prompted criticism from American behaviorist Daniel Lehrman in the postwar period (*1*). One can appreciate from Burkhardt's account how the mid-1970s debate over sociobiology became instantly politicized, for interpretations of behavior that smacked of biological determinism were already deeply suspect.

Tinbergen met Lorenz in 1936, began a collaborative study of bird behavior with him in 1937, and then reestablished their friendship when Lorenz returned to Austria after nearly four years as a Russian prisoner following the war's end. Tinbergen built on Lorenz's work as he "colonized" England ethologically. He worked tirelessly to make sure the field would grow in a coordinated and productive fashion, and he published the first ethology text (*2*) in 1951. Tinbergen emphasized experimental analysis, focusing on the physiological mechanisms underlying behavior. But he was concerned that ethology should not resolve itself into physiology. The study of natural history, based on painstaking observation of animals in their natural context, was an important source of insight and new information. Like other contemporary naturalists, notably Ernst Mayr, Tinbergen tried to preserve the balance between natural history and experimental science and promoted the centrality of evolutionary problems to the study of behavior. By the late 1950s, when the models proposed by Lorenz and Tinbergen were being attacked, the challenge was to respond creatively to criticism and maintain good relations with the critics. Tinbergen's scientific brilliance was matched by his social awareness.

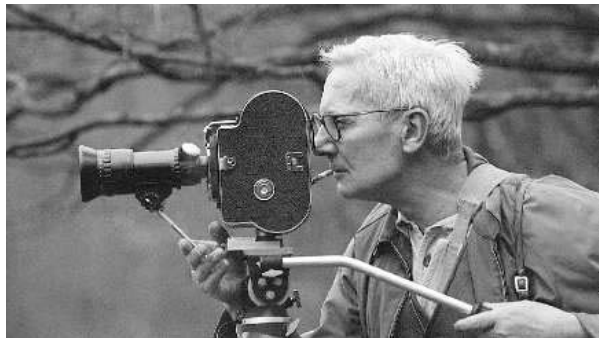

Filming in the field. Tinbergen enjoyed considerable success as a maker of educational nature films, such as *Signals for Survival* (1968).

Patterns of Behavior offers more than a nuanced history of the origins of ethology. The juxtaposition of the stories of Tinbergen

The reviewer is in the Department of the History of Science and Technology, Johns Hopkins University, 3505 North Charles Street, Baltimore, MD 21218, USA. E-mail: Sharon@jhu.edu

CREDIT: LARY SHAFFER

and Lorenz provides an intriguing case study of how the advancement of scientific fields depends as much on the management of the social relations among scientists as on intellectual brilliance and institution-building.

References
1. D. S. Lehrman, *Q. Rev. Biol.* **298**, 337 (1953).
2. N. Tinbergen, *The Study of Instinct* (Clarendon, Oxford, 1951).

10.1126/science.1112557

ANTHROPOLOGY

Is This How the West Won?

Michael Balter

Jared Diamond is a biologist at the University of California, Los Angeles; a member of the U.S. National Academy of Sciences; and the author of the Pulitzer Prize–winning book *Guns, Germs, and Steel* (*1*). Now he is also the star of a three-part series, based on the book, that airs this month on the Public Broadcasting Service (PBS) in the United States. The series details Diamond's influential yet controversial explanation for why the world is divided into haves and have-nots—the principal reason, he maintains, is geography: At the end of the last Ice Age, about 11,500 years ago, prehistoric hunter-gatherers living amongst the wild ancestors of today's domesticated plants and animals—most notably the wheat, barley, sheep, goats, and cattle native to the Near East—were ideally situated to invent farming and amass the agricultural surpluses that fueled the rise of civilization and technology. Meanwhile, the unfortunate inhabitants of geographic regions with few domesticable species—such as Africa and the New World—lagged behind in their development; even worse, they eventually fell victim to armies of (mostly European) colonizers whose technologically superior weaponry allowed them to subjugate entire continents. Adding to this onslaught of guns and steel, Diamond argues, were the ravages of deadly diseases that the invaders brought with them, such as smallpox, to which Europeans had developed some immunity (often through their long coexistence with domesticated animals) but which felled native peoples by the millions.

Guns, Germs, and Steel
Lions Television, London, for National Geographic Television and Films, Washington, DC. Three one-hour episodes. On PBS, Monday evenings, 11 to 25 July 2005.

The reviewer is a Paris-based writer for *Science* and author of *The Goddess and the Bull: Çatalhöyük, An Archaeological Journey to the Dawn of Civilization*. Web site: www.michaelbalter.com

Diamond's thesis is one of the most widely discussed big ideas of recent years, and deservedly so. For one thing, it is an explicitly anti-racist explanation for social and economic inequalities on a global level, an explanation that dispenses with subtle and not-so-subtle assumptions about the inherent superiority of Europeans and their descendants. The have-nots, Diamond counters, are simply those whose prehistoric ancestors were dealt an unlucky draw of the geographical cards. The book, a best-seller in both the original and paperback editions, is required reading in many university courses. It has stimulated considerable debate; for that reason alone a film version, which will undoubtedly reach an even wider audience than the book, seems justified. And it would be churlish to deny Diamond the star treatment he receives in the film, even if one repeated scene of the biologist cruising down a river in Papua New Guinea—while the narrator, actor Peter Coyote, tells us dramatically that Diamond is "on a quest" to understand the roots of power—seems just a bit too focused on the person rather than the ideas.

More worrying, however, is the fact that during all of Diamond's journeys—which take him across the globe by boat, train, airplane, and helicopter, with film crew in tow—the viewer is told only once (at the end of the first hour) that there are scholars who disagree with his thesis. Nor are any of these dissenters ever interviewed, even though a number of other experts and personalities appear in the film to bolster Diamond's viewpoint. This imbalance is a disservice to television viewers, who are surely sophisticated enough to hear challenges to Diamond's ideas without losing track of the plot line. The omission might not be so serious if Diamond had only recently presented his thesis, but over the eight years since the book was first published its tenets have been much debated. Indeed, it is usually assigned to university students precisely so that they can discuss the merits of Diamond's arguments. In 2001, for example, Cornell University in New York required all of that year's incoming undergraduates to read *Guns, Germs, and Steel* as part of a new student reading project (*2*). Members of Cornell's anthropology department organized a campus-wide debate about the book and raised a number of important questions—including whether the geographic vagaries of 11,000 years ago are sufficient to explain why hundreds of millions of human beings live in dire poverty today.

Diamond's quest: the source of power.

CREDIT: COURTESY LIONS TELEVISION AND NATIONAL GEOGRAPHIC TELEVISION AND FILMS

The film opens with Diamond in Papua New Guinea, where he has conducted research for many decades and become an expert on the island's birds. The viewer is told that Diamond's quest began more than 30 years ago, when a man named Yali, whom the biologist "met on a beach," asks him, "Why you white man have so much cargo and we New Guineans have so little?" In the book, Diamond explains that Yali was a "remarkable local politician," but in the film we are told nothing about Yali or who he was. Instead, an actor playing Yali looms before the camera intoning what Diamond calls "Yali's question," which Diamond will spend the ensuing years trying to answer. Here, the film makes its first misstep: In fact, Yali was the charismatic leader of an indigenous post–World War II movement in New Guinea, sometimes called the cargo cult, that sought to acquire more European goods [readers wanting to know more can consult anthropologist Peter Lawrence's *Road Belong Cargo* (*3*)]. By portraying Yali as an anonymous native on the beach, rather than the sophisticated leader he was, the filmmakers inadvertently exaggerate the (albeit important) cultural differences between New Guinea and Western societies.

Fortunately, this scene is followed by some of the film's strongest sequences, in which Diamond and the narrator (aided by interviews with several respected experts on the "Neolithic Revolution") explain the origins of agriculture in the Near East. The viewer gets to visit two important Neolithic excavations in progress, including 11,500-year-old Dhra' in the Jordan Valley, one of the earliest farming villages ever discovered. Meanwhile, Diamond points out, to convincing effect, that out of 14 large

BROWSINGS

The Archaeology of Colonial Encounters. Comparative Perspectives. *Gil J. Stein, Ed.* School of American Research Press, Santa Fe, NM, and James Curre, Oxford, 2005. 457 pp. $60. ISBN 1-930618-43-3. Paper, $24.95. ISBN 1-930618-44-1. £17.95. ISBN 0-85255-980-1. School of American Research Advanced Seminar.

Whereas the topic of colonization has been approached largely through studies of European expansion, this volume offers a broader view. The contributors discuss colonial activities of earlier state societies in the Old World (Mesopotamia, Phoenicia, Greece, and Rome) and indigenous states in the Americas (Teotihuacan, Wari, Tiwanaku, and Inca) as well as Spanish colonialism in Mesoamerica and Spanish and Russian settlements in California. In considering these cases, the authors examine the colonial encounters from the perspectives of the colonies themselves, the colonies' homelands, and the host societies. They recognize great diversities in both the reasons for the establishment and the actual functioning of colonial settlements. For example, there are substantial differences between settlements that remain distinct from the host societies and the development of long-term rule over an alien people.

Bicycling Science. Third Edition. *David Gordon Wilson, with contributions by Jim Papadopoulos.* MIT Press, Cambridge, MA, 2004. 457 pp. $55, £35.95. ISBN 0-262-23237-5. Paper, $22.95, £14.95. ISBN 0-262-73154-1.

This expanded and updated edition of a classic work offers a comprehensive introduction to bicycle technology. It begins with a short historical survey intended to quash many widespread myths. After covering the physiology and biomechanics of generating human power to propel two-wheeled vehicles, Wilson considers the problem of keeping bicyclists cool. A series of chapters then explores aspects of bicycle physics: power and speed, aerodynamics, bearings and tires, braking, balancing and steering, power transmission, and stresses and materials. The book ends with glimpses at unusual human-powered machines—including designs for record speeds, watercraft, airplanes, and helicopters—and a look to the future of human-powered vehicles. The information Wilson provides may be most appreciated by bicycle designers and builders, but it is likely to interest anyone who competes, commutes, or just likes to have fun on two wheels.

How to Clone the Perfect Blonde. Using Science to Make Your Wildest Dreams Come True. *Sue Nelson and Richard Hollingham.* Quirk, Philadelphia, 2004. 272 pp. Paper, $16.95. ISBN 1-59474-008-9.

How to Clone the Perfect Blonde. Making Fantasies Come True with Cutting-Edge Science. Ebury, London. Paper, £7.99. ISBN 0-09189-747-5.

Readers seeking a how-to manual for realizing their fantasies must be warned of the authors' bait-and-switch approach in this exploration of speculative topics from the edges of current science. The title chapter, for example, is actually a factual account of what cloning involves that covers aspects such as techniques, difficulties, Dolly, the difference between identical genotypes and phenotypes, and why claims to have cloned humans are most unlikely. Other chapters consider humanoid robots, teleportation, beautiful bodies, genetically modified foods, time machines, cyborgs, black holes, and living forever. In places, the humor is overdone or requires a UK background. Nonetheless, the fast-paced, engaging presentation offers a great deal of information in a way that a broad audience should find both enjoyable and effective.

mammals domesticated by humans over the millennia since Dhra' was founded, none come from Africa or North America, and only one (the llama) comes from South America. Moreover, Diamond argues, farming was able to spread both east and west from its origins in the Near East (and eventually to North America) because points on the globe that share the same latitude share the same day length and often a similar climate and vegetation.

So far, so good. But in the second segment, the film falters badly by devoting almost the entire hour to a day in November 1532, when 168 Spaniards led by the conquistador Francisco Pizarro massacred 7,000 Incans in the highlands of Peru and captured their emperor, Ataxalpa. This horrific episode is intended to demonstrate how the Spaniards' skills on horseback (the horse being one of the 14 domesticated animals), combined with their technological ability to produce swords of fine tempered steel, could overcome the superior numbers of Ataxalpa's 80,000-man army. Yet despite several entertaining sequences featuring a swashbuckling expert swordsman and horseback rider who demonstrates how the conquistadors cut down the Incas, we are also told that the Spaniards attacked a peaceful gathering and that Ataxalpa had made the fatal decision not to arm his men with their bronze weapons that day. This raises at least two questions: First, whether the Spaniards would have won had they faced Ataxalpa's army in a real battle. Second, why, even if the Europeans did have the ability to wipe out the Incans, they were willing to carry out such terrible acts. Is conquest of other peoples a logical outcome of technological superiority? Today, most of us would argue against any such notion. Here lies a major weakness in Diamond's entire thesis—it fails to explain the conscious decisions that humans make when they resort to violent conquest.

In the third and final hour, Diamond travels to Africa—as indeed he must if the film is to be honest to its message. His quest takes him to a town in northern Zambia, one of the world's poorest countries, where both AIDS and malaria are taking a devastating toll. While talking to a malaria expert in a clinic where up to seven children die each day, Diamond suddenly breaks down in sobs. The moment is genuine, spontaneous, and moving; the decision of the filmmakers to leave it in is, of course, a deliberate one. Yet I think it was the correct decision. Whether Diamond is right or wrong about the reason, much of the world's population is suffering terribly from disease, warfare, and other causes. And no matter what the causes, something has to be done about that suffering. Diamond himself makes this point at the end of the film:

> …the message is a hopeful one; it's not a deterministic, fatalistic one that says forget about Africa and underdeveloped areas. It says there are specific reasons why different parts of the world ended up as they did, and with understanding of those reasons, we can use that knowledge to help the places that historically were at a disadvantage.

That, at any rate, is a statement that most everyone can agree upon.

References

1. J. Diamond, *Guns, Germs, and Steel: The Fates of Human Societies* (Norton, New York, 1997).
2. See www.provost.cornell.edu/g_g_s.htm.
3. P. Lawrence, *Road Belong Cargo: A Study of the Cargo Movement in the Southern Madang District, New Guinea* (Manchester Univ. Press, Manchester, UK, 1964).

10.1126/science.1116063

ECONOMICS

Individual Accounts: Lessons from International Experience

J. Michael Orszag and Peter R. Orszag

The United States is undergoing a debate over whether part of its Social Security system should be replaced with individual accounts. Advocates of this approach, including the Bush administration, have cited international experience as demonstrating its advantages (*1*). However, every country adopting individual accounts has encountered significant problems.

Most advanced economies have some sort of a defined-benefit public retirement program funded on a pay-as-you-go basis (*2*). In other words, benefits do not depend on financial market returns and are financed by concurrent taxation rather than previous saving. Most industrialized countries also have individual accounts in addition, at least on a voluntary, tax-preferred basis. The relative importance of these two components varies, with Western European countries like France and Germany providing generous defined benefits; Australia, New Zealand, and Ireland having much smaller defined-benefit programs; and the United States somewhere in between (see the figure, this page, which includes disability payments).

Individual accounts assume a variety of forms around the industrialized world (*3*). Most are not meaningfully integrated with the public defined-benefit program and are typically voluntary. In the United States, for example, voluntary tax-preferred accounts like 401(k) plans and IRAs (individual retirement accounts) are privately administered and not integrated in any significant manner with the public defined-benefit program (*4*). As a result, the accounts serve as an optional supplement rather than a partial replacement for a public defined benefit foundation.

Countries that include accounts within a public program typically make the accounts mandatory, in part to reduce complexities about how the account component interacts with the defined-benefit component. Sweden and Switzerland represent examples of this approach (*5*). In Australia, employers have been required to contribute to individual accounts for most workers since 1992. These accounts represent the only earnings-related component of the Australian pension system (*6*).

Among the industrialized economies, the United Kingdom is unique in allowing individuals to opt out of a public defined-benefit program and into individual accounts, as has been proposed by the Bush administration in the United States. In the United Kingdom, workers choosing the account option direct part of their payroll taxes into an account held with a financial institution; their defined benefit at retirement is then reduced to reflect this choice (*7*).

The administration's proposal for the United States calls for the accounts to be run by the government; among the other countries with individual accounts, only Sweden has adopted this approach. In Sweden, the public program includes an individual account component for all workers; out of a total payroll tax equal to 18.5% of wages, 2.5% of wages is contributed to an account administered by a government agency (*8*).

To evaluate the experience of these countries with accounts, we examine the three key stages of individual account systems: participation and contribution rates, asset accumulation, and payout.

Participation and Contribution Rates

In voluntary account systems, participation and contribution rates have often posed surprising problems. (In mandatory systems, participation and contributions can be set by policy fiat.) Part of the problem is that people do not appear to behave as rationally as is often assumed in economic models. The introduction in 1988 of voluntary individual accounts in the United Kingdom, for example, was followed by a wave of aggressive sales practices by financial intermediaries. The result was the so-called mis-selling scandal, in which individuals were frequently induced to choose an inappropriate account (*9*). In response to what has been called the "biggest financial scandal in the United Kingdom," the government forced the financial services industry to pay more than 12 billion pounds in compensation to the individuals involved (*10*).

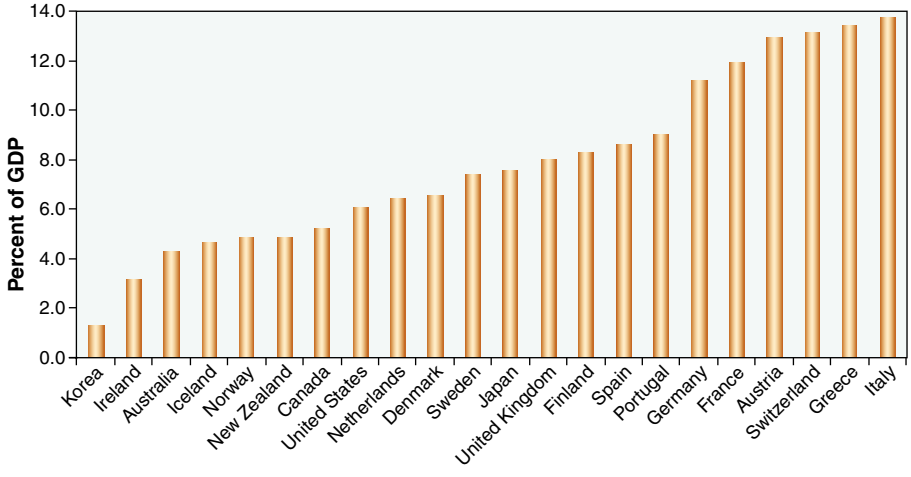

Public pension defined-benefit payments as share of GDP, 2001. [Source (*28*)]

The lack of fully rational individual behavior in the mis-selling example is widely replicated in other settings. For example, in the United States, a significant minority of households is not saving adequately for retirement. Yet research has demonstrated that such under-saving could result in large part from inertia. For example, if workers are automatically included in a 401(k) plan unless they choose not to participate, participation is much higher than if workers must affirmatively sign up for the plan (*11*, *12*). Similarly, workers are more willing to make larger contributions if they had previously committed to doing so (*13*). In Sweden, the overwhelming majority of new participants in the individual accounts

J. M. Orszag is with Watson Wyatt LLP, Reigate Surrey RH2 9PQ, UK; e-mail: mike.orszag@watsonwyatt.com. P. R. Orszag is with the Brookings Institution, Washington, DC 20036, USA; e-mail: porszag@brookings.edu

choose the default fund (*14*). Clearly the reality is different from conventional economic theory, which suggests that in the absence of switching costs, individuals will make fully rational decisions unaffected by the presence of a default (*15*).

Asset Accumulation

Assets within an individual account available at retirement are determined by contributions, financial returns, and administrative costs. The higher the net return on the account, all else being equal, the larger the payout at retirement. In the United States, the geometric average annual equity return (adjusted for inflation) between 1900 and 2000 was 6.7% (*16*). The historical experience in the United States, however, is atypical. Equity returns internationally have been substantially lower (*17*). Furthermore, the higher expected return on equities compared with safer investments reflects their riskiness. Stocks are consistently associated with risk: 15-year returns in the United States have ranged between –2% and 13% since 1885 (*18*). These risks are often exacerbated by poor investment decisions (*19*).

Administrative costs also affect asset accumulation: The relevant return for an individual is after fees and expenses have been subtracted. In most individual account systems, these administrative costs historically have proven to be high. In the United Kingdom, administrative costs were on track to reduce account balances at retirement by more than 30% (*20*) before the government recently introduced fee regulations. In Australia, administrative costs amount to more than 1% per year (*21*), which would reduce account balances at retirement by about 20%. By some estimates, administrative fees have been somewhat lower in Sweden, in part because the system is centralized and government-run and in part because individuals are not charged the entire cost of administering the accounts (*22*).

Finally, if an individual account is voluntary and integrated with the public defined-benefit program, the defined benefit is typically adjusted in some fashion to offset the deposit of payroll revenue into the account. Under the administration's proposal for accounts in the United States, for example, workers opting to deposit payroll taxes into an account today would pay back those funds, accumulated at a 3% real interest rate, through reductions in Social Security benefits at retirement. To achieve an increase in retirement income, individuals must thus accumulate more in their account than the present value, at retirement, of the benefit offsets. If future domestic returns match past international returns, the return on a mixed portfolio of stocks and bonds (with the stock share declining as the worker ages) would fall below the 3% real interest rate more than 70% of the time (*23*). A question for political economists is whether, if a large share of the population winds up losing under the accounts, political pressure would unwind specified reductions in future Social Security benefits.

Payout Phase

Because individual accounts in most countries are relatively new, very few are currently paying out significant sums to retirees. Policy-makers have therefore not yet faced some of the serious challenges associated with the payout stage, which can become particularly complex (*24*). In defined benefit systems, pensions are often payable for life. In individual account systems, individuals can purchase life annuities upon retirement, but such purchase is not mandatory in most countries. Where purchase is not compulsory, take-up is low, and therefore, annuities markets are small; indeed, in the United Kingdom, which has compulsory annuitization, the annuities market is larger than the rest of the world's combined (*25*). Mandatory annuitization, however, may not be sustainable, in part because of political pressures to allow accounts to be bequeathed (annuitizing an account means that the funds cannot be passed to heirs). Another major issue is whether annuity pricing should be uniform, given significant mortality differentials across socioeconomic and other population subgroups. If annuitization is not required, however, take-up tends to be low, meaning that many workers are exposed to the risk of outliving their assets. This risk may be exacerbated by uncertainties over future life expectancy improvements, the degree of which has been the subject of serious disagreement among demographers (*26*, *27*).

Conclusion

As demographic trends have increased costs in traditional defined pension schemes, policy-makers have sought new approaches to cope with an aging population. About 20 years ago, countries started experimenting more actively with individual accounts. At the time, such accounts seemed attractive, perhaps because there not yet had been any significant negative experiences (or significant positive ones, for that matter). It has since become apparent that individual accounts have entailed significant problems in every developed country that has implemented them. These problems indicate that more work is needed both in practice, to make accounts work better, and in research, to achieve better alignment between economic theory and observed behavior.

References and Notes

1. See N. G. Mankiw, "Social Security reform: National saving and macroeconomic performance in the global economy," speech delivered at the Council on Foreign Relations, 18 January 2005; available at www.whitehouse.gov/cea/20050118-Mankiw—CFR.pdf.
2. Social Security Administration, "Social Security programs throughout the world," available at www.ssa.gov/policy/docs/progdesc/ssptw/index.html
3. We focus on the countries included in the Organization for Economic Cooperation and Development.
4. W. G. Gale, J. B. Shoven, M. J. Warshawsky, *Private Pensions and Public Policies* (Brookings Institution Press, Washington, DC, 2004).
5. Other countries, such as Singapore, have defined contribution programs that are not "individual accounts" because they offer little or no individual choice over investments.
6. H. Bateman, G. Kingston, J. Piggott, *Forced Saving: Mandating Private Retirement Provision* (Cambridge Univ. Press, Cambridge, UK, 2001).
7. R. Blundell, C. Meghir, S. Smith, in *Social Security Programs and Retirement Around the World: Micro Estimation*, J. Gruber and D. Wise, Eds. (Univ. of Chicago Press, Chicago, 2004), pp. 643–689.
8. S. Engstrom, A. Westerberg, *J. Pension Econ. Finance* **2**, 225 (2003).
9. R. Disney, E. Whitehouse, "The personal pensions stampede" (IFS Report R40, Institute for Fiscal Studies, London, 1992).
10. N. Cohen, "A bloody mess," *American Prospect* Online, 11 January 2005; available at www.prospect.org/web/page.ww?section=root&name=ViewWeb&articleId=8997.
11. B. Madrian, D. Shea, *Q. J. Econ.* **116** (no. 4), 1149 (2001).
12. J. Choi *et al.*, in *Tax Policy and the Economy*, vol. 16, J. Poterba, Ed. (MIT Press, Cambridge, MA, 2002), pp. 67-113.
13. R. Thaler, S. Benartzi, *J. Polit. Econ.* **112** (no. 1, pt. 2), S164 (2004).
14. J. Turner, "Individual accounts: Lessons from Sweden," [Issue Brief 60, Public Policy Institute, American Association of Retired Persons (AARP), Washington, DC, May 2003].
15. O. S. Mitchell, S. P. Utkus, in *Pension Design and Structure: New Lessons from Behavioral Finance*, O. S. Mitchell and S. P. Utkus, Eds. (Oxford Univ. Press, Oxford, UK, 2004), pp. 3–41.
16. E. Dimson, P. Marsh, M. Staunton, *Triumph of the Optimists: 101 Years of Global Investment Returns* (Princeton Univ. Press, Princeton, NJ, 2002).
17. S. J. Brown, W. N. Goetzmann, P. Jorion, *J. Finance* **54**(3), 953 (1999).
18. G. Burtless, testimony before House Budget Committee, 11 May 1999.
19. M. Murthi, J. M. Orszag, P. R. Orszag, in *New Ideas About Old Age Security*, R. Holzmann and J. Stiglitz, Eds. (World Bank, Washington, DC, 2001)
20. A. Munnell, A. Sundén, *Coming Up Short: The Challenge of 401(k) Plans* (Brookings Institution Press, Washington, DC, 2004).
21. H. Bateman, O. S. Mitchell, *J. Pension Econ. Finance* **3**(1), 63 (2004).
22. E. Palmer, in *Coping with the Pension Crisis: Where Does Europe Stand?*, M. Feldstein and H. Siebert, Eds. (Univ. of Chicago Press, Chicago, 2002).
23. R. Shiller, "The life-cycle personal accounts proposal for Social Security: a review" (Working Pap. 11300, National Bureau of Economic Research, Cambridge, MA, May 2005).
24. V. Reno, M. J. Graetz, K. S. Apfel, J. Lavery, C. Hill, Eds., *Uncharted Waters: Paying Benefits from Individual Accounts in Federal Retirement Policy*, (National Academy of Social Insurance, Washington, DC, 2005).
25. M. Cardinale, A. Findlater, M. Orszag, "Paying out pensions: A review of international annuities markets" (Research report RU07, Watson Wyatt Worldwide, Reigate, Surrey, UK, 2002).
26. Olshansky *et al.*, *N. Engl. J. Med.* **352**(11), 1138 (2005).
27. J. Oeppen, J. W. Vaupel, *Science* **296**, 1029 (2002).
28. Data Chart EQ5.1, available at www.oecd.org/dataoecd/34/11/34542691.xls

10.1126/science. 1113199

IMMUNOLOGY

Now Presenting: γδ T Cells

Robert L. Modlin and Peter A. Sieling

Our immune system recognizes and generates specific responses to both foreign and self molecules called antigens. Whether the antigen is a peptide, lipid, carbohydrate, or other small organic molecule, it elicits a cellular response that requires two distinct elements: an antigen-presenting cell that appropriately displays an antigen on its surface, and the corresponding T cell that detects the presented material. This recognition by T cells involves a variable cell surface structure called the T cell receptor (TCR) that, when activated by antigen, spurs T cells to mount a multifaceted immune response. Most T cells bear a TCR heterodimer composed of α and β chains. A smaller population of peripheral T cells has a TCR composed of γ and δ chains (*1*), but function largely like αβ T cells in their ability to recognize antigen with their TCRs, perform similar cellular functions, and retain an immunologic "memory" of these responses when exposed to the same antigen later. On page 264 in this issue, Brandes *et al*. provide surprising evidence that human γδ T cells, unlike αβ T cells, can also act as potent antigen-presenting cells (*2*). This raises the intriguing possibility that the γδ T cell repertoire provides an additional mechanism of antigen presentation that could rapidly trigger the αβ T cell immune response.

Since the discovery of γδ T cells, immunologists have been trying to understand why the immune system needs two distinct sets of TCR-bearing cells. In the mouse, there are various resident populations of γδ T cells in peripheral tissues including skin, gut, and uterus. Each tissue has its own specific subset of γδ T cells, based on which variable (V) gene is used to generate the TCR. These γδ T cells express "canonical" TCRs, meaning that the normally hypervariable region of the TCR that is generated by rearrangement of germ line DNA is constant. Resident γδ T cells are thought to represent a first line of defense against infection and provide tissue-specific immune function, including the regulation of wound healing (*3*, *4*). However, in humans, tissue-specific γδ T cells are not as prominent, nor are they restricted in TCR gene usage. Indeed, the adult human γδ T cell repertoire is dominated by a polyclonal population that bears the Vγ2Vδ2 TCR. This constitutes ~2 to 4% of peripheral blood T cells. Vγ2Vδ2 T cells recognize phosphorylated isoprenoid presursors and alkylamines, molecules conserved in metabolic pathways from many species including plants, pathogens, and primates (*5*, *6*). These cells expand during infection by many different infections including nontuberculous mycobacteria. But nothing especially remarkable about the immune function of human Vγ2Vδ2 T cells had been suspected. In fact, similar to αβ T cells, Vγ2Vδ2 T cells release cytokines, lyse target cells, and secrete the antimicrobial peptide granulysin (*7*–*10*). They also regulate the maturation of a subset of antigen-presenting cells called dendritic cells, as well as antibody-mediated responses (*10*–*12*).

Human γδ T cells were previously shown to present nonpeptide antigen to other γδ T cells, although antigens were apparently not processed through the cellular pathway that so-called "professional" antigen-presenting cells (dendritic cells and B cells) use (*13*). Brandes *et al*. now provide evidence that activated Vγ2Vδ2 T cells efficiently process and display peptide antigen to αβ T cells, displaying features of the professionals (*2*). A key point is that the activated Vγ2Vδ2 T cells express cell surface proteins required for antigen presentation, including costimulatory and major histocompatibility complex (MHC) class II molecules, at levels similar to that of dendritic cells and greater than that of αβ T cells. The authors also demonstrate that activation of Vγ2Vδ2 T cells by a variety of nonpeptide antigens leads to the accumulation of MHC class II molecules in specific intracellular endosomal com-

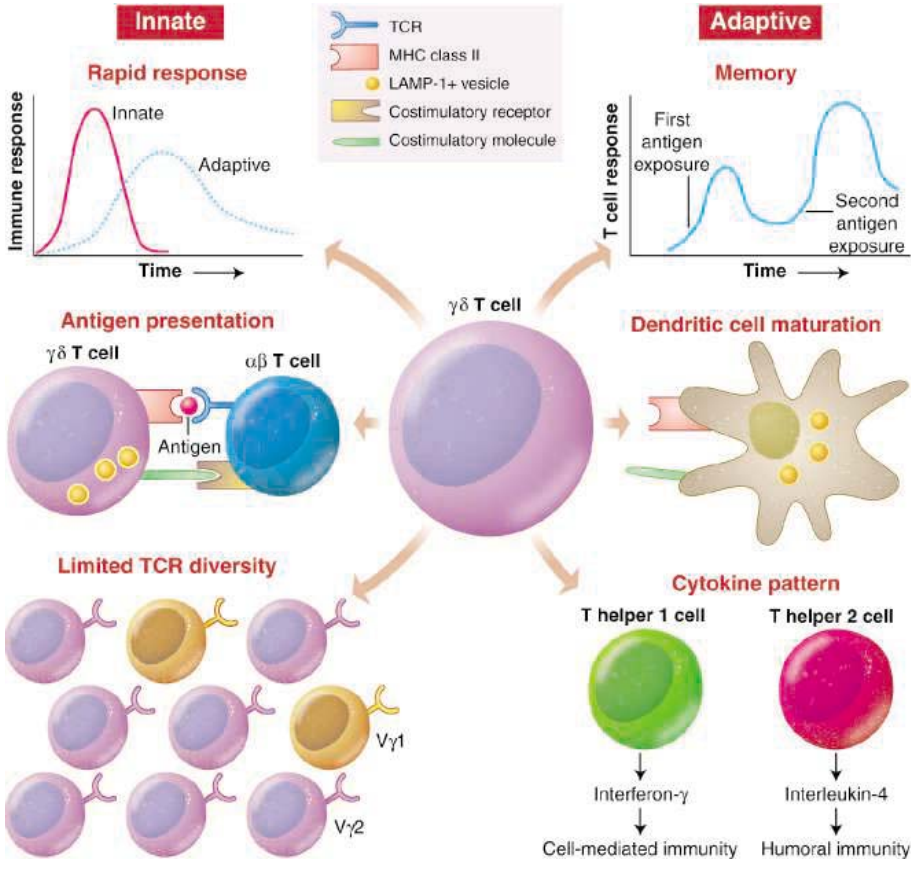

CREDIT: PRESTON HUEY/*SCIENCE*

γδ T cells function in the innate and adaptive immune responses. γδ T cells exhibit functions consistent with both adaptive and innate immunity. Like dendritic cells, they present antigen to αβ T cells (*2*).

The authors are in the Division of Dermatology and Department of Microbiology, Immunology and Molecular Genetics, David Geffen School of Medicine, University of California–Los Angeles, Los Angeles, CA 90095, USA. E-mail: rmodlin@mednet.ucla.edu

partments (identified by expression of a protein called LAMP-1+), a process that is critical for optimal antigen presentation to MHC class II–restricted αβ T cells. It may be that because of their prevalence in peripheral blood, γδ T cells are the first antigen-presenting cells to accumulate at the site of disease, before dendritic cells can be recruited or locally differentiated. There is no evidence, however, that Vγ2Vδ2 T cells function as antigen-presenting cells in vivo—this is understandably difficult to study in humans. Whether murine γδ T cells have antigen-presenting capabilities is also difficult to predict given the differences between the human and mouse γδ T cell populations.

A current dogma in immunology is the division of the immune system into innate and adaptive responses, leading to the assignment of cells and receptors to one or the other system. The innate system is rapid, employing cells with germ line–encoded pattern recognition receptors that directly kill microbial invaders. The innate immune system also instructs the adaptive immune response by the release of cytokines and the efficient presentation of antigen. In contrast, the adaptive immune response is slow, and requires gene rearrangement and clonal selection of receptors on T and B cells that develop immunologic memory. The experiments of Brandes *et al*. provide new information about the categorization of γδ T cells.

γδ T cells have characteristics of adaptive immunity: They express rearranged surface receptors, generate immunologic memory (*14*), and induce dendritic cell maturation. Their effector functions are also similar to those of αβ T cells (see the figure). Nonetheless, γδ T cells also may be classified as part of the innate immune system because they respond rapidly, have limited TCR gene usage, and express TCRs that act as pattern recognition receptors for phosphorylated isoprenoid precursors and alkylamines. Brandes *et al*. demonstrate that γδ T cells are professional antigen-presenting cells in vitro, forming a unique link between innate and adaptive immune responses. Perhaps γδ T cells, which belong to both immune systems, represent a conserved, primitive form of immunity.

References

1. M. B. Brenner *et al.*, *Nature* **322**, 145 (1986).
2. M. Brandes, K. Willimann, B. Moser, *Science* **309**, 264 (2005); published online 2 June 2005 (10.1126/science.1110267).
3. J. Jameson *et al.*, *Science* **296**, 747 (2002).
4. A. Hayday, R. Tigelaar, *Nat. Rev. Immunol.* **3**, 233 (2003).
5. Y. Tanaka, C. T. Morita, E. Nieves, M. B. Brenner, B. R. Bloom, *Nature* **375**, 155 (1995).
6. J. F. Bukowski, C. T. Morita, M. B. Brenner, *Immunity* **11**, 57 (1999).
7. G. A. Follows, M. E. Munk, A. J. Gatrill, P. Conradt, S. H. Kaufmann, *Infect. Immun.* **60**, 1229 (1992).
8. P. F. Barnes *et al.*, *Infect. Immun.* **61**, 197 (1993).
9. M. E. Munk, A. J. Gatrill, S. H. E. Kaufmann, *J. Immunol.* **145**, 2434 (1990).
10. F. M. Spada *et al.*, *J. Exp. Med.* **191**, 937 (2000).
11. J. Ismaili, V. Olislagers, R. Poupot, J. J. Fournie, M. Goldman, *Clin. Immunol.* **103**, 296 (2002).
12. M. Brandes *et al.*, *Blood* **102**, 3693 (2003).
13. C. T. Morita *et al.*, *Immunity.* **3**, 495 (1995).
14. Y. Shen *et al.*, *Science* **295**, 2255 (2002).

10.1126/science.1115264

MATERIALS SCIENCE

Hierarchies in Biomineral Structures

John D. Currey

Most animals mineralize at least part of their bodies, usually for skeletal support. Various minerals are used, with calcium carbonate, silica (glass), and calcium phosphate being the most common. Despite this diversity of materials, there is one nearly constant feature: Almost all biomineralized structures are highly hierarchical, that is, the structure is different at many different length scales. On page 275 of this issue, Aizenberg *et al*. (*1*) show how the glassy sponge *Euplectella*, which uses silica as its skeletal building block, makes a skeleton of extraordinary structural and mechanical refinement with many levels of hierarchy.

Euplectella is a deepwater sponge whose glassy skeleton is a hollow cylinder. On the first level of structural hierarchy, nanometer-sized particles of silica are arranged around an organic axial filament. On the second level, alternating layers of silica and organic material form spicules. On the third level, these small spicules are bundled together to form larger spicules. On the fourth level, the larger spicules are arranged in a grid, with struts in longitudinal, circumferential, and diagonal directions, resisting all load modes (see the figure). In the mature animal, these larger spicules are coated with a cementing layer of silica. On the fifth level, this grid is wrapped into a curved cylinder. Finally, on the sixth level, helical surface ridges further resist torsion and stiffen the structure (*2*).

The precise mechanical consequences of the arrangement of the *Euplectella* skeleton have yet to be worked out in detail, but most are self-evident. Perhaps the most remarkable feature of this skeleton is at level four. Theoretical analysis by Deshpande *et al.* (*3*) has shown that mass and metabolic effort can be minimized for a given stiffness by having anti-shear diagonal struts in every other square. This is the pattern shown by *Euplectella* (see the figure, left and middle panels).

The structural complexity of the *Euplectella* skeleton is not quite matched by other skeletons, but the characteristic hierarchy is. In a mammalian bone, at the lowest level, nanometer-sized crystals of carbonate apatite are embedded in, and surround, the fibrous protein collagen. At the next level, these mineralized fibers lie bundled together and attached to each other. At the next level, these fibers come together to form lamellae with a width of ~2 μm. The lamellae have various patterns; a very common one is a secondary osteon, in which concentric lamellae form cylindrical struc-

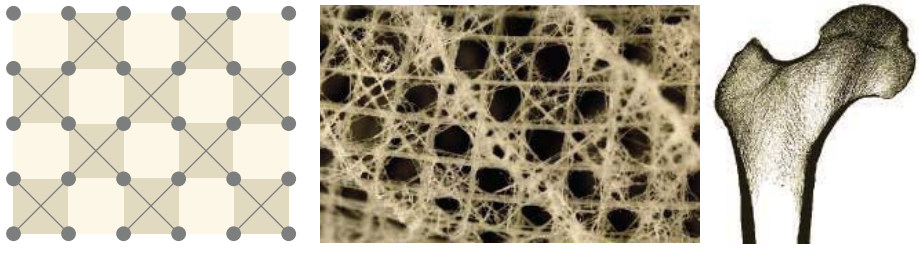

How to resist loads. (**Left**) Arrangement of a square network that is stiff in shear, even though half the cells are not stiffened. [Modified from (*3*)] (**Middle**) In the *Euplectella* skeleton, only half the squares are crossed by shear-stiffening fibers. The sides of the squares are ~3 mm long. (**Right**) Microradiograph of a section of the head of a human femur (*9*), showing the cortical bone (solid black around the outside) and the trabecular bone inside. The direction of the bony trabeculae is related to the direction of the loads on the bone during walking.

The author is in the Department of Biology, University of York, York YO10 5YW, UK. E-mail: jdc1@york.ac.uk

tures, ~200 μm in diameter, surrounding a central blood vessel. Compact bone, solid to the naked eye, is modified in places to form trabecular bone, which consists of many struts; the spaces between the struts are filled with marrow (see the figure, right panel). These struts are not randomly arranged, but are related to the direction of loads on the bone. The mechanical and other properties of bone depend on the interaction of all levels of organization (*4*).

Two more examples of the structural hierarchy of biominerals are the teeth of sea urchins and the "crossed-lamellar" structure of many mollusk shells. The crossed-lamellar structure consists almost entirely of calcium carbonate in the crystalline form of aragonite, with a tiny amount of organic material between the crystals. It has five levels of organization, and the structures are arranged with high precision to prevent the traveling of cracks (*5*, *6*). Sea urchin teeth have fewer levels of hierarchy, but their structure is very similar to that of fiber-reinforced plastics. However, they consist of a composite in which fibers and matrix are chemically identical, being made of calcite, although the crystals differ greatly in size and orientation, with a layer of organic material surrounding the fibers (*7*). Furthermore, the magnesium content of the calcite increases toward the middle of the tooth, markedly increasing its hardness. The resulting differential wear produces a self-sharpened tooth.

The main mechanical function of these hierarchical arrangements, almost certainly, is to produce interfaces that will open up in the presence of potentially dangerous cracks, deflecting the cracks and making their travel energetically expensive. This makes biomineralized skeletons surprisingly tough, given that they are made almost entirely of mineral. Bone is a special case, having less mineral than most other biomineralized skeletons; it can be remarkably tough.

Apart from their hierarchical arrangement, two other features of biominerals contribute to the superior mechanical properties of skeletons made from them. First, at the lowest level, they are often made of tiny crystals that are smaller than the "Griffith length" necessary for cracks to spread (*8*). Second, the precision with which they can be laid down (changing their main orientation over a few micrometers, for instance) allows exquisite adaptations to the loads falling on the skeletons.

The particular mineral used in a skeleton—calcite, aragonite, apatite, silica, or others—is probably much less important than the precise way in which the mineral is arranged in space. Aizenberg *et al.* show this very clearly for the *Euplectella* skeleton, although the organic component is also crucial for providing clear interfaces between the layers.

References and Notes

1. J. Aizenberg *et al.*, *Science* **309**, 275 (2005).
2. This paragraph reflects the author's view of the levels of hierarchy in *Euplectella*; the levels do not quite agree with those specified in (*1*).
3. V. S. Deshpande, M. F. Ashby, N. A. Fleck, *Acta Mater.* **49**, 1035 (2001).
4. J.-Y. Rho, L. Kuhn-Spearing, P. Zioupas, *Med. Eng. Phys.* **20**, 92 (1998).
5. J. D. Currey, A. J. Kohn, *J. Mat. Sci.* **11**, 1615 (1976).
6. S. Kamat, H. Kessler, R. Ballarini, M. Nassirou, A. H. Heuer, *Acta Mater.* **52**, 2395 (2004).
7. R. Z. Wang L. Addadi, S. Weiner, *Philos. Trans. R. Soc. London. B* **352**, 469 (1997).
8. H. J. Gao, B. Ji, L. Jäeger, E. Arzt, P. Fratzl., *Proc. Natl. Acad. Sci. U.S.A.* **100**, 5597 (2003).
9. C. R. Jacobs, M. E. Levenston, G. S. Beaupré, G. C. Simo, D. R. Carter, *J. Biomech.* **28**, 449 (1995).

10.1126/science.1113954

OCEAN SCIENCE

Warming the World's Oceans

Gabriele C. Hegerl and Nathaniel L. Bindoff

Rising greenhouse gas concentrations in the atmosphere are trapping more infrared radiation near Earth's surface. This extra radiation is expected to warm Earth's surface and lower atmosphere, but observations indicate that most of the heat is transported into the oceans (see the figure). On page 284 of this issue, Barnett *et al.* (*1*) substantially strengthen the evidence that human activities are indeed warming the world's oceans.

Observations have shown that 84% of the total heating of the Earth system since the 1950s is in the oceans (*2*). This increased ocean heat content has led to thermal expansion of the ocean, contributing at least 25% of the global sea-level rise observed over the same period (*3*). Ocean warming may also lead to greater stratification of the ocean, causing a weakening of the global overturning circulation in most model projections of future climates (*4*). Furthermore, the oceans are a key element in the global carbon cycle and are estimated to be storing roughly half of the total carbon released through human activities since preindustrial times (*5*). For all these reasons, the oceans are an important place to look for changes expected due to greenhouse warming ("fingerprints").

Many of the changes observed at Earth's surface and in the free atmosphere in the 20th century can be reproduced by climate models that account for the increase in greenhouse gases, aerosols associated with pollution, changes in solar radiation, and reflection by volcanic aerosols (*6*, *7*). Fingerprint methods use detailed information about the climate response to these external influences in order to separate them from each other and from natural variability within the climate system.

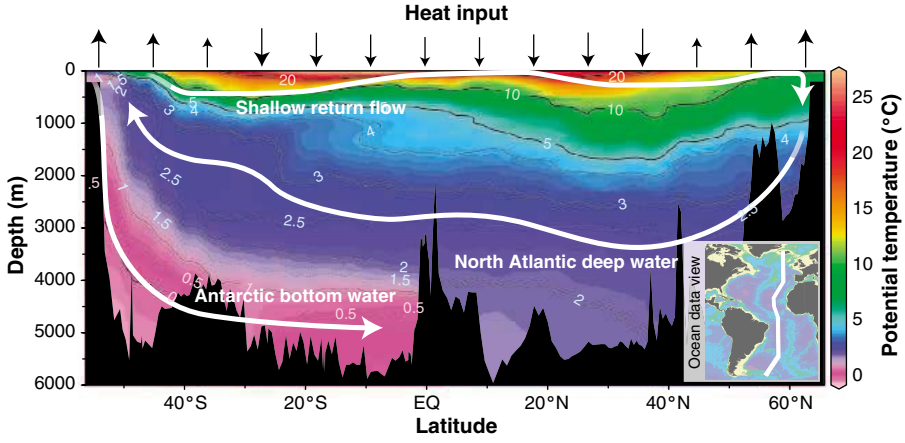

Heat transfer from atmosphere to ocean. This cross section of the Atlantic Ocean basin illustrates how atmospheric warming is transferred from the ocean surface to the ocean interior. The isolines show potential (that is, pressure-adjusted) temperature. The vertical black arrows show broadly where heat penetrates into the ocean surface layer and is then subducted into the upper ocean along surfaces of equal density. The combination of winds, sinking processes, and ocean circulation also leads to the meridional overturning circulation (and horizontal heat transport) (white arrows). Arrows pointing out of the ocean indicate net heat being transported from the oceans to the atmosphere. (**Inset**) Location of the cross section. [Adapted from (*9*)]

G. C. Hegerl is in the Nicholas School of the Environment and Earth Sciences, Duke University, Durham, NC 27708, USA. E-mail: hegerl@duke.edu N. L. Bindoff is at IASOS and CSIRO Marine Research, Unversity of Tasmania, Private Bag 80, Hobart 7001, Australia. E-mail: n.bindoff@utas.edu.au

Studies using such methods have shown with high confidence that much of the temperature change observed at Earth's surface and in the free atmosphere over the past 50 years has been caused by increases in greenhouse gas concentrations (*6*, *7*).

Barnett *et al*. (*1*) now apply a fingerprint method to the temperature history of the upper 700 m of each ocean basin since 1960. In this depth range, the greatest temperature changes are found (*1*, *2*); it is also where we have the best knowledge of ocean behavior. The authors compare the best available ocean observation data set to simulations using two different climate models. They find strong evidence that the anthropogenic fingerprint anticipated by the models is present in the observations. The results show that changes in solar radiation and volcanic forcing cannot explain the observed pattern of ocean changes. The fact that the findings are robust for two different climate models indicates that the results are not affected significantly by differences in model formulation.

The similar pattern of temperature change in the observations and in the simulations is strong evidence for a large-scale anthropogenic warming trend in the world's oceans. Barnett *et al*. thus add important information to the growing evidence that human-induced changes to the composition of the atmosphere are changing our climate (*7*).

Temperature changes in the oceans are important not only because they strengthen the evidence for anthropogenic climate change. They are also important for a reliable prediction of future warming at the Earth's surface. Climate feedbacks determine how strongly the atmosphere reacts to rising greenhouse gas concentrations. But the rate of warming at the Earth's surface also depends on how much of the excess energy trapped by greenhouse gases is transported into the ocean interior.

For example, if climate feedbacks are weak and little heat penetrates into the ocean, this would in the short term result in a surface climate change similar to one in which climate feedbacks are strong and a lot of heat penetrates into the ocean (*8*). However, as the ocean slowly comes into equilibrium with the atmosphere, these scenarios would diverge sharply, because stronger feedbacks would cause much stronger future warming. Therefore, the demonstration by Barnett *et al.* (*1*) that their two climate simulations are in quantitative agreement with the observed ocean warming improves our confidence in the simulated rate of ocean heat uptake and thus in projections of future climate.

The historical ocean data cover a relatively short time span (~50 years) and their spatial coverage is inhomogeneous, particularly in the less accessible Arctic and Southern Oceans. Therefore, it is still a challenge to validate more complex details of ocean physics in climate models than was done in (*1*). Further work is needed to determine more accurately and in more spatial detail how temperature and surface salinity changes penetrate into the ocean. We also need to better understand the ocean's major modes of climate variability, particularly on time scales of a decade or longer, and to quantify the likelihood of sudden ocean change [such as a collapse of the thermohaline circulation (*4*)]. Another question is how ocean biogeochemistry and ecosystems, and thus the global carbon cycle, will respond to global warming. Therefore, it is important that we keep probing the world's oceans.

References and Notes

1. T. P. Barnett *et al*., *Science* **309**, 284 (2005); published online 2 June 2005 (10.1126/science.1112418).
2. S. Levitus, J. I. Antonov, T. P. Boyer, *Geophys. Res. Lett.* **32**, L02604 (2005).
3. J. I. Antonov, S. Levitus, T. P. Boyer, *Geophys. Res. Lett.* **32**, L12602 (2005).
4. U. Cubasch *et al*., in *Climate Change 2001: The Scientific Basis. Contribution of Working Group I to the Third Assessment Report of the Intergovernmental Panel on Climate Change*, J. T. Houghton *et al*., Eds. (Cambridge Univ. Press, New York, 2001), pp. 525–582.
5. C. L. Sabine *et al*., *Science* **305**, 367 (2004).
6. J. F. B. Mitchell *et al*., in *Climate Change 2001: The Scientific Basis. Contribution of Working Group I to the Third Assessment Report of the Intergovernmental Panel on Climate Change*, J. T. Houghton *et al*., Eds. (Cambridge Univ. Press, New York, 2001), pp. 695–738.
7. The International Ad Hoc Detection and Attribution Group, *J. Climate* **18**, 1291 (2005).
8. C. E. Forest *et al*., *Science* **295**, 113 (2002).
9. R. Schlitzer, eWoce–Electronic Atlas of WOCE Hydrographic and Tracer Data, www.ewoce.org (2003).

10. G.C.H. is supported by the NSF, NOAA, and the DOE's Office of Biological and Environmental Research. N.L.B. is supported by the Australian Government's Cooperative Research Programme through the Antarctic Climate and Ecosystems Cooperative Research Centre (ACE CRC).

10.1126/science.1114456

ANTHROPOLOGY

The Remaking of Australia's Ecology

Christopher N. Johnson

What was the impact of early human populations on pristine ecosystems? Studies of this question have focused on the possibility that humans caused extinctions of large mammals. For example, the arrival of modern humans in the Americas ~11,000 years ago coincided with the disappearance of mammoths, ground sloths, and many other large mammals (*1*). However, the role of humans is difficult to determine in this case because the climate was also changing rapidly as the last ice age came to an end; climate change, not human impact, may have caused the extinctions.

Modern humans reached Australia much earlier. Just when they did is still debated, but occupation was widespread by 45,000 years ago and may have begun several thousand years earlier (*2*)—well before the climatic upheavals at the end of the last glacial cycle. Australia should therefore provide a clear view of the ecological impacts of human arrival. But environmental changes following human arrival in Australia have been difficult to resolve, because very few precisely dated environmental records extend through the middle of the last glacial cycle. On page 287 of this issue, Miller *et al*. (*3*) provide such a record based on diet reconstructions of the continent's two largest bird species. The results indicate that human arrival resulted in a profound environmental shift.

Miller *et al*. studied past diets of the emu (*Dromaius novaehollandiae*) and an even larger flightless herbivorous bird, the extinct *Genyornis newtoni* (see the first figure), in the arid and semi-arid regions of the south Australian interior. By analyzing carbon isotopes in individually dated eggshells, they were able to compare the contributions of plants that use the C4 photosynthetic pathway (mainly tropical and arid-adapted grasses) and those that use the C3 pathway (most shrubs, trees, and nongrass herbs) to the diet of the birds that laid the eggs. Their collection of eggshells covers the past 140,000 years, encompassing the whole of the last glacial cycle.

Miller *et al.* found a sudden change in emu diet between 50,000 and 45,000 years ago. Before 50,000 years ago, emus had variable diets, with a strong contribution from C4 plants; after 45,000 years ago, they ate mostly C3 plants. *Genyornis* eggshells were common before 50,000 years ago, but they abruptly disappeared at the same time as the diet of the emu changed. Before then, *Genyornis* also ate a mixture of C3 and C4 plants, but its diet was much less variable than that of the emu through the same

The author is in the School of Tropical Biology, James Cook University, Townsville, Queensland 4811, Australia. E-mail: christopher.johnson@jcu.edu.au

period, which suggests that it was a more specialized feeder.

These results point to a major change in vegetation. Perhaps woodland mosaics, with plenty of grass, were converted into monotonous shrubland, or nutritious grasses were replaced by poor-quality species, forcing emus to increase their feeding on non-grass species. Miller *et al.* also measured carbon isotopes in wombat teeth, showing that they changed in the same way at the same time. Nowadays, wombats are mainly grazers; the switch in their diet from C4 grass to C3 shrubs in the middle of the last glacial period can only be explained by a huge change in vegetation.

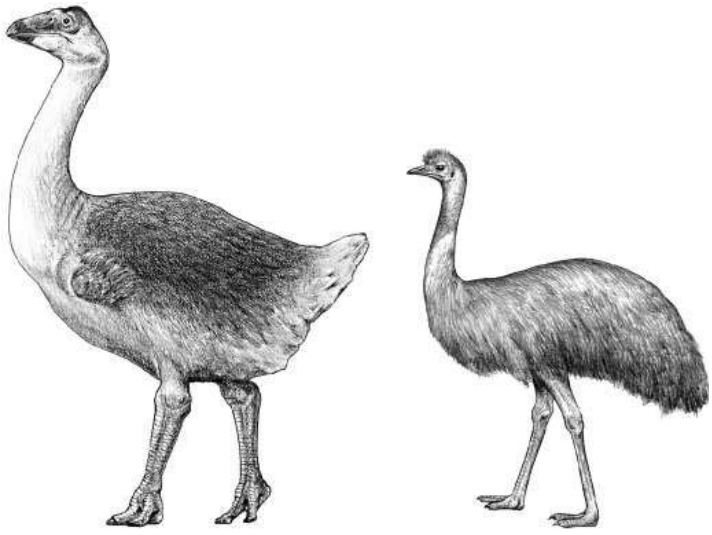

The emu (right) and the extinct *Genyornis newtoni* (left).

Human impact is the only factor that can account for this change. When humans arrived, the climate was moderate and stable. Furthermore, the diets of the emu and *Genyornis* were insensitive to climate swings (*1*). Between 140,000 and 50,000 years ago, the climate changed from cool and arid at the end of the penultimate ice age, to warm and wet during the last interglacial, and back to cool and dry with the onset of the last glacial (see the second figure). Emus and *Genyornis* were continuously present in the study area of Miller *et al.* throughout this period, and their diets did not change. Similarly, after 45,000 years ago, the diet of the emu remained constant through the deep aridity of the Last Glacial Maximum and the transition to the present interglacial.

The fact that the distributions and feeding habits of both species changed so little in response to climate extremes, but so much when people arrived, tells us that the impact of human arrival far exceeded the effects of any of the climate changes of the past 140,000 years. Human impact probably also included the extinction of up to 50 species of giant marsupials. The date of extinction of Australia's giant marsupials remains controversial, but recent evidence points to between 50,000 and 45,000 years ago (*4*, *5*).

We thus have strong evidence that human arrival caused vegetation change and megafauna extinction in Australia. The big question is, how? Miller *et al.* speculate that humans caused vegetation change, which in turn caused megafauna extinction. If fires lit by humans destroyed an original mosaic of woodlands and grasslands and replaced it with fire-adapted shrubs and spinifex (a fire-promoting grass of low palatability), this might have destroyed the habitat of specialized herbivores such as *Genyornis* and other large browsers. If this happened, there should have been an increase in charcoal between 50,000 and 45,000 years ago. No charcoal records exist for the region studied by Miller *et al.* But sediment cores elsewhere in Australia have fewer charcoal peaks between 70,000 and 40,000 years ago than before or after this interval (*6*).

Alternatively, humans may have caused megafauna extinction, which in turn caused vegetation change. Many members of the extinct marsupial megafauna were browsers (*7*), and the biggest of them weighed several tons. In Africa, such megaherbivores have huge impacts on vegetation and suppress the development of scrub and woodland (*8*). A sudden disappearance of large browsers in Australia as a result of overhunting might have triggered an expansion of shrublands and scrub, with a reduction of grass. Perhaps this is the change that caused the diet shifts in wombats and emus.

To untangle the mechanisms behind the sudden ecosystem transformation that followed human arrival in Australia, researchers must determine which plant species contributed to the vegetation changes indicated by the results of Miller *et al.* Modeling studies may help to show how those plants might have responded to changes in fire or browsing pressure. But regardless of where the story goes from here, we now have a stronger case than ever that the arrival of humans had a larger impact than the last glacial cycle on ecological change in Australia.

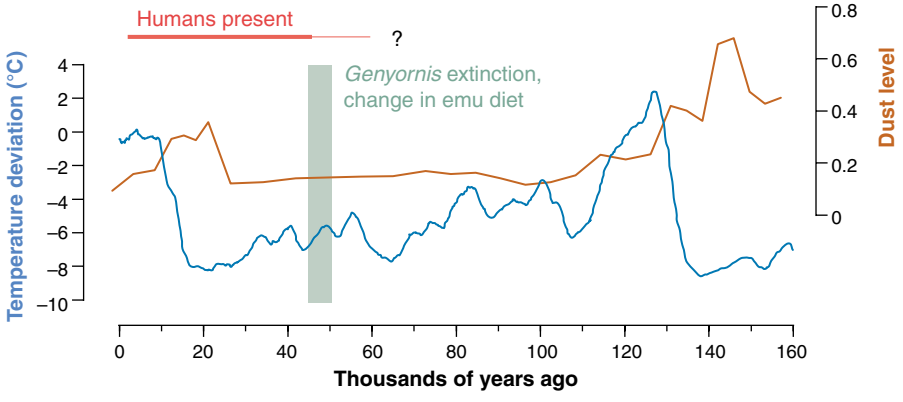

Climate change, human arrival, and ecosystem change in Australia. Two climate indicators—differences in atmospheric temperature from today [deduced from the isotopic composition of Antarctic ice (*9*)] and dust in marine sediments off the northwest coast of Australia (*10*)—suggest that between 50,000 and 45,000 years ago, the climate was relatively stable. During this time, human occupation became widespread (thick horizontal line; evidence of earlier human presence is disputed), *Genyornis* went extinct, and the emu's diet changed (vertical bar).

References

1. A. D. Barnosky, P. L. Koch, R. S. Feranec, S. L. Wing, A. B. Shabel, *Science* **306**, 70 (2004).
2. J. F. O'Connell, J. Allen, *J. Archaeol. Sci.* **31**, 835 (2004).
3. G. H. Miller *et al.*, *Science* **309**, 287 (2005).
4. R. G. Roberts *et al.*, *Science* **292**, 1888 (2001).
5. F. D. Pate, M. C. McDowell, R. T. Wells, A. M. Smith, *Austral. Archaeol.* **54**, 53 (2002).
6. A. P. Kershaw, J. S. Clark, A. M. Gill, D. M. D'Costa, in *Flammable Australia: The Fire Regimes and Biodiversity of a Continent*, R. A. Bradstock, J. E. Williams, A. M. Gill, Eds. (Cambridge Univ. Press, Cambridge, 2002), pp. 3–25.
7. C. N. Johnson, G. J. Prideaux, *Austral. Ecol.* **29**, 553 (2004).
8. R. N. Owen-Smith, *Megaherbivores: The Influence of Very Large Body Size on Ecology* (Cambridge Univ. Press, Cambridge, 1988).
9. J. R. Petit *et al.*, *Nature* **399**, 429 (1999).
10. P. P. Hesse, G. H. McTainsh, *Quat. Sci. Rev.* **22**, 2007 (2003).

10.1126/science.1113957

Complexity in Strongly Correlated Electronic Systems

Elbio Dagotto

A wide variety of experimental results and theoretical investigations in recent years have convincingly demonstrated that several transition metal oxides and other materials have dominant states that are not spatially homogeneous. This occurs in cases in which several physical interactions—spin, charge, lattice, and/or orbital—are simultaneously active. This phenomenon causes interesting effects, such as colossal magnetoresistance, and it also appears crucial to understand the high-temperature superconductors. The spontaneous emergence of electronic nanometer-scale structures in transition metal oxides, and the existence of many competing states, are properties often associated with complex matter where nonlinearities dominate, such as soft materials and biological systems. This electronic complexity could have potential consequences for applications of correlated electronic materials, because not only charge (semiconducting electronic), or charge and spin (spintronics) are of relevance, but in addition the lattice and orbital degrees of freedom are active, leading to giant responses to small perturbations. Moreover, several metallic and insulating phases compete, increasing the potential for novel behavior.

Materials in which the electrons are strongly correlated display a broad range of interesting phenomena, including colossal magnetoresistance (CMR), where enormous variations in resistance are produced by small magnetic field changes, and high-temperature superconductivity (HTSC). An important characteristic of these materials is the existence of several competing states, as exemplified by the complicated phase diagrams that transition metal oxides (TMOs) present (Fig. 1). The understanding of these oxides has dramatically challenged our view of solids. In fact, after one of the largest research efforts ever in physics, involving hundreds of scientists, even basic properties of the HTSC cuprates, such as the pairing mechanism, linear resistivity, and pseudogap phase, are still only poorly understood. In the early days of HTSC, it was expected that suitably modified theories of ordinary metals would explain the unusual properties of the cuprate's normal state. However, important experimental results gathered in recent years have revealed an unexpected property of oxides: Many TMOs are inhomogeneous at the nanoscale (and sometimes at even longer length scales). This explains why the early theories based on homogeneous systems were not successful and raises hopes that a novel avenue for progress has opened.

Department of Physics, University of Tennessee (UT), Knoxville, TN 37996–1200, USA. Condensed Matter Sciences Division, Oak Ridge National Laboratory, Oak Ridge, TN 37831–6393, USA.

What are the implications of these and other results reviewed below? It will be argued that the current status of correlated electrons investigations must be considered in the broader context of complexity. In his pioneering article (*1*), Anderson wrote that "the ability to reduce everything to simple fundamental laws does not imply the ability to start from those laws and reconstruct the universe." In complex systems (*2*), the properties of a few particles are not sufficient to understand large aggregates when these particles strongly interact. Rather, in such systems, which are not merely complicated, one expects emergence, namely the generation of properties that do not preexist in a system's constituents. This concept is contrary to the philosophy of reductionism, the traditional physics hallmark. Complex systems spontaneously tend to form structures (self-organization), and these structures vary widely in size and scales. Exceptional events are important, as when the last metallic link completes a percolative network. The average behavior is of no relevance for this phenomenon, and often only a few rare events dominate. Evidence is accumulating that TMOs and related materials have properties similar to standard complex systems, and several results must be reexamined in this broader framework.

Nanostructures in Manganites and Cuprates

Manganites. The Mn oxides called manganites (*3*–*9*), especially those displaying the CMR effect, are an important oxide family in which the presence of inhomogeneous states is widely accepted. A remarkable cross-fertilization between theory and experiments has led to considerable progress in unraveling the role of these inhomogeneities. Theoretical investigations (*4*) predicted that, in a broad region of parameter space, the ground state is actually a nanoscale mixture of phases, particularly in the presence of quenched disorder (*10*–*12*), namely, when random "frozen" deviations from the perfectly uniform system are incorporated in the study. Many experimental results are indeed in agreement with the basic notion that the relevant phases are not homogeneous; these results also provide information crucial to understanding the CMR effect (*4*, *5*, *13*, *14*). Some of the general theoretical ideas are summarized in the schematic phase diagram (Fig. 2A) (*10*), which has been experimentally confirmed (*15*, *16*) (Fig. 2B).

In the clean limit without quenched disorder, the two key competing states in manganites, ferromagnetic (FM) metallic and antiferromagnetic (AF) insulating (AFI), are known to be separated by a first-order transition (*4*, *5*). However, once the inevitable quenched disorder is included in the calculation, arising, for example, from the lattice-distorting chemical doping procedure, nonstatistical fluctuations of dopant density or strain fields, the region in which the two states are nearly degenerate (that is, they can coexist) is dramatically modified. In this regime, there is still a local tendency toward either FM or AFI short-distance correlations. However, globally neither of the two states dominates (Fig. 2C). A mixed glassy region is generated between the true critical temperatures, the Curie or Néel temperatures in this case, and a remnant of the clean-limit transition, T^*. In this regime, perturbations such as small magnetic fields can have dramatic consequences, because they only need to align the randomly oriented magnetic moments of preformed nanosize FM clusters to render the system globally ferromagnetic. A concomitant percolation induces metallicity in the compounds. The fragility of the state shown in Fig. 2C implies that several perturbations besides magnetic fields should induce dramatic changes, including pressure, strain, and electric fields (*4*, *5*). Moreover, the discussion centered on Fig. 2, A to C, is independent of the details of the competing states and should be valid for the AFI versus

superconducting (SC) state competition in cuprates (*17*) and many other cases (*18*).

Calculations that incorporate the effects of phase competition and quenched disorder have been able to reproduce the huge magnetoresistance observed experimentally (*10*, *11*); this suggests that the CMR effect would not occur without either competing states or quenched disorder and interactions necessary to nucleate clusters. This is in agreement with experiments for $Re_{0.5}Ba_{0.5}MnO_3$ (where Re is a rare earth element) (*16*), which can be prepared both in ordered and disordered forms for the Re-Ba distribution. Remarkably, only the latter was found to exhibit CMR (Fig. 2D). This suggests that when phases compete, the effect of (typically small amounts of) quenched disorder results in dramatic properties that are very different from those of a slightly impure material (*10*, *11*, *19*, *20*). Disorder in the regime of phase competition is not a mere perturbation; it alters qualitatively the properties of the material.

How strong should the disorder be to induce the inhomogeneous patterns discussed here? Are there other alternatives? Studies incorporating long-range effects, such as Coulombic forces (*21*) or cooperative oxygen octahedra distortions (*11*), suggest that very weak disorder, even infinitesimal disorder (*21*, *22*), may be sufficient to do the job. Calculations without explicit disorder incorporating strain effects (*9*), or within a phenomenological Ginzburg-Landau theory, also lead to inhomogeneous patterns (*23*). Although the discussion on the details of the origin of the inhomogeneities is still fluid, their crucial relevance to understanding the manganites, as originally predicted by theory (*4*, *5*), is by now widely accepted.

Cuprates. In the HTSC context, the $La_{2-x}Sr_xCuO_4$ (LSCO) phase diagram is usually considered the universal diagram for cuprates. However, some investigations suggest otherwise (*17*, *24*). For example, only

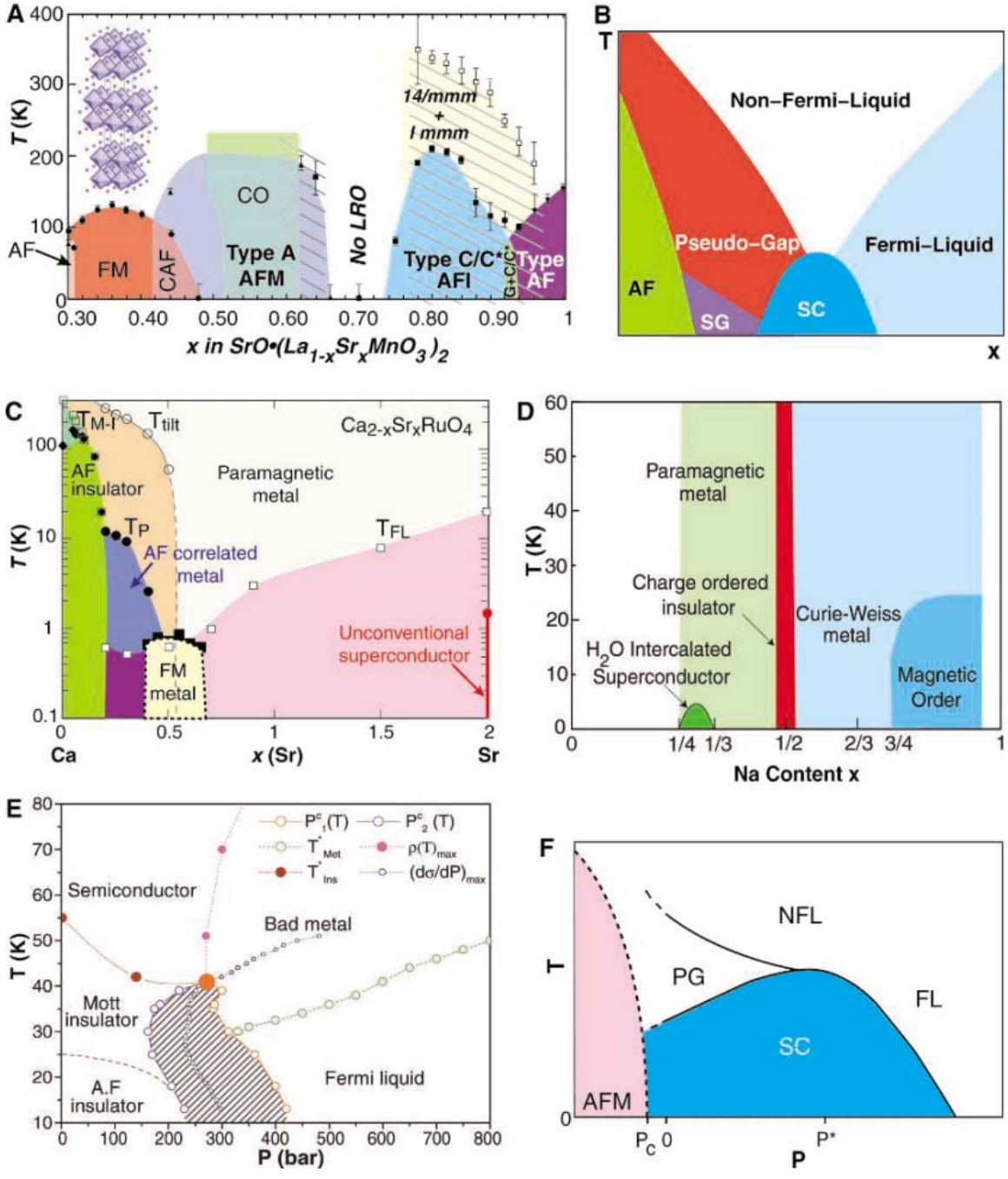

Fig. 1. Phase diagrams of representative materials of the strongly correlated electron family (notations are standard and details can be found in the original references). (**A**) Temperature versus hole density phase diagram of bilayer manganites (*74*), including several types of antiferromagnetic (AF) phases, a ferromagnetic (FM) phase, and even a globally disordered region at $x = 0.75$. (**B**) Generic phase diagram for HTSC. SG stands for spin glass. (**C**) Phase diagram of single layered ruthenates (*75*, *76*), evolving from a superconducting (SC) state at $x = 2$ to an AF insulator at $x = 0$ (x controls the bandwidth rather than the carrier density). Ruthenates are believed to be clean metals at least at large x, thus providing a family of oxides where competition and complexity can be studied with less quenched disorder than in Mn oxides. (**D**) Phase diagram of Co oxides (*77*), with SC, charge-ordered (CO), and magnetic regimes. (**E**) Phase diagram of the organic κ-(BEDT-TTF)$_2$Cu[N(CN)$_2$]Cl salt (*57*). The hatched region denotes the coexistence of metal and insulator phases. (**F**) Schematic phase diagram of the Ce-based heavy fermion materials (*51*).

after Ca is added to $YBa_2Cu_3O_{6+\delta}$ (where δ is the excess of oxygen, and it ranges between 0 and 1) does its phase diagram resemble that of LSCO (*25*, *26*). Moreover, organic superconductors do not have a glassy phase between the AFI and superconducting states, and they are believed to be cleaner than the cuprates (*27*). This suggests that quenched disorder (or strain, etc.) in cuprates may play a role as important as that in the manganites, and the exotic underdoped regime and T^* may emerge as a consequence of its influence (*17*). If so, then it is not sufficient to consider phase diagrams involving only temperature and hole-doping x. A disorder strength axis should be incorporated into the phase diagram of these materials as well.

Considerable discussion concerning the existence of inhomogeneous states in cuprates started several years ago when stripes were reported in studies carried out with neutron-scattering techniques (*28*). These states had been predicted theoretically (*29*, *30*). The nontrivial real-space structure of stripes emerges from Hamiltonians that do not break translational invariance, which is a remarkable result. However, because approximations were made in the calculations, it is still controversial whether stripes do exist in Hubbard Hamiltonians (*31*–*34*). Experimentally, the presence of stripes is also a matter of debate. Recent neutron studies of HTSC materials have been interpreted as caused by a phase that contains stripes separated by two-leg ladders (Fig. 3A) (*35*, *36*), with spin-gapped properties that could be important for pairing (*37*). In addition, doped Ni oxides and Nd-doped LSCOs are widely believed to have stripes (*29*).

While the stripe debate continues, scanning tunneling microscopy (STM) investigations have recently provided additional important information on the cuprates, unveiling a variety of other inhomogeneous states. Figure 3B shows a real-space distribution of d-wave SC gaps in $Bi_2Sr_2CaCu_2O_{8+\delta}$ (Bi-2212). The many colors illustrate the inhomogeneous nature of the state (*38*) with randomly distributed nanoscale patches. These patterns could be caused by phase competition or by a random oxygen distribution. Other recently synthesized cuprate-based compounds also have inhomogeneous states (*39*), and additionally, a new charge-ordered "checkerboard" state has been observed (Fig. 3C) (*40*). This state also exists in Bi-2212 (*41*) and appears to compete with superconductivity. Understanding these novel states remains a challenge, but for our purposes two issues are crucial: (i) When scrutinized with powerful microscopic techniques, doped HTSC systems reveal inhomogeneous states. Supporting this statement, a novel scaling law for the cuprates was interpreted as produced by a Bardeen, Cooper, and Schrieffer system in the dirty limit (*42*, *43*). (ii) The intermediate states between the AFI and SC states do not seem universal (they could have stripes, a

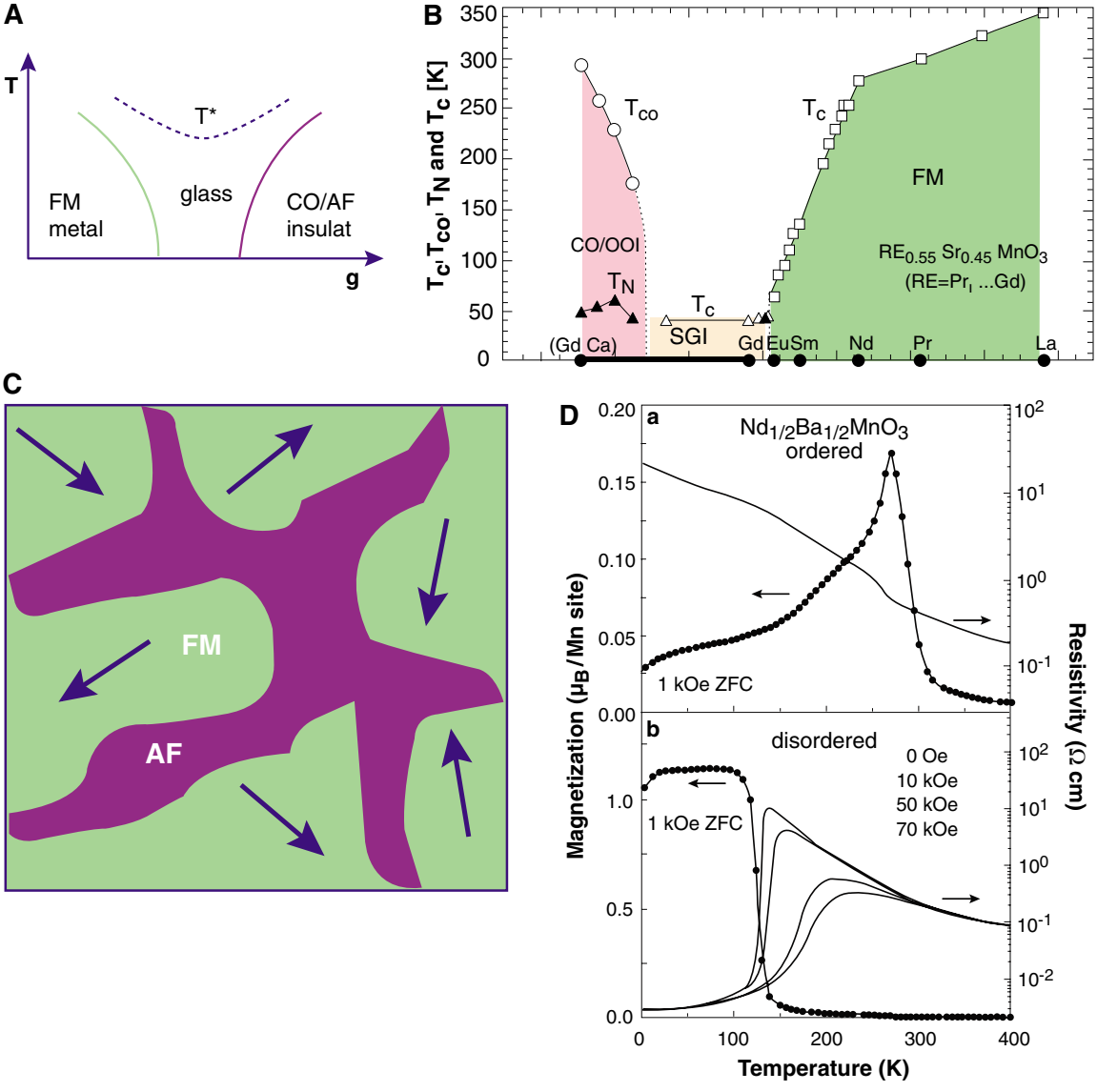

Fig. 2. (**A**) Generic phase diagram of two competing states [here FM metal versus charge-ordered antiferromagnetic (CO/AF) insulator] in the presence of quenched disorder (*4*, *5*). g is a generic variable to move from one phase to the other (e.g., electronic density or bandwidth). A glassy mixed-phase state is created and a T^* scale appears. (**B**) Experimental phase diagram of manganites with large disorder (*15*, *16*). Note the disorder-induced suppression of the ordering temperatures and the appearance of a glass state, as predicted by theory (A). Details and the phase diagram with weak disorder can be found in (*15*). (**C**) Sketch of the proposed CMR state for the manganites containing FM clusters with randomly oriented moments separated by regions where a competing CO/AF phase is stabilized (*4*, *5*, *13*). (**D**) Resistivity and magnetization versus temperature for the ordered and disordered structures of $Nd_{0.5}Ba_{0.5}MnO_3$ (*16*). Only the disordered crystal has the CMR effect (*16*).

charge checkerboard, or glassy patterns). All these characteristics are hallmarks of complex systems, showing sensitivity to details as they occur in nonlinear chaotic systems.

Some additional issues should be remarked upon: (i) Although the most complex behavior in cuprates appears in the underdoped regime, dynamic electronic inhomogeneity and competition among the many degrees of freedom could also underlie the superconductivity even at optimal doping. Are the inhomogeneities and complexity at the root of the superconducting phase, or are they unrelated? The discussion continues. (ii) Interactions can also generate inhomogeneous patterns (*17*, *29*, *44*), and the combination of these interactions with quenched disorder may be at the heart of the complexity in cuprates.

Another unexpected property of the cuprates is the giant proximity effect. This phenomenon has a long story, but recently it has been very carefully studied by using atomically smooth films made of HTSC compounds in S-N-S trilayer junctions (S is for superconductor and N equals normal metal) (*45*). The big paradox here is that the trilayer behaves as a Josephson junction for N barriers a hundred times thicker that the coherence length, ξ. Then, the normal state cannot be featureless, it must already contain a tendency toward superconductivity, which could be in the form of nanoscale SC islands (*17*) or phase-fluctuating homogeneous states (*46*). This proposal leads to an exciting prediction: Under the proper perturbation, the state with preformed SC clusters should present a gigantic susceptibility toward superconductivity (*17*). This is the analog of CMR in Mn oxides but translated into Cu-oxide language. In general, theory predicts that giant responses to external perturbations should be far more common than previously anticipated.

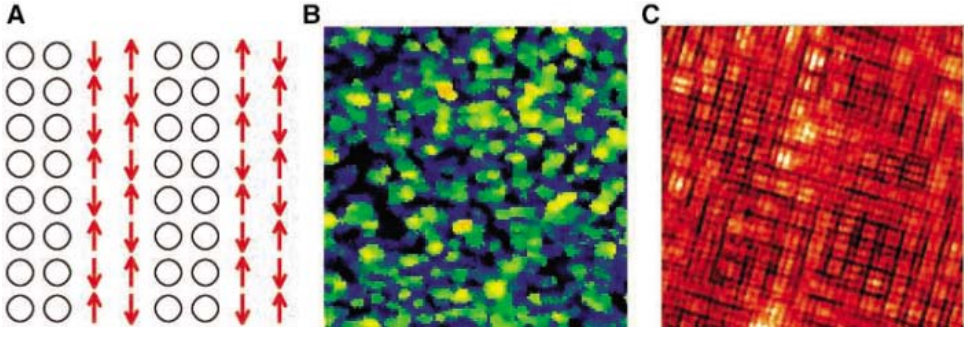

Fig. 3. Examples of inhomogeneous states in HTSC materials. (**A**) Schematic perfect stripes (*35*) (circles are holes; arrows, spins). Real systems may present more dynamical stripes (*29*). (**B**) *d*-wave SC gap real-space distribution obtained by using STM techniques (*37*). Inhomogeneities at the nanoscale are observed (patches). The entire frame is 560 Å by 560 Å. (**C**) Recently unveiled charge-order state (checkerboard) in Na-doped cuprates (*40*, *41*).

The Case for Complexity in Correlated Electron Systems

Are TMOs examples of complex matter? Considering the general properties of complexity briefly reviewed in the introduction as well as the oxide results discussed in the previous section, it is natural to wonder whether these systems can be considered as special cases of complex matter. Although complexity is natural when associated with soft matter (literally soft, for example, polymers and liquid crystals), it seems out of place in the context of hard materials. But the several simultaneously active degrees of freedom may conspire to provide a soft electronic component to transition metal oxide compounds, soft not in the physical hardness sense but denoting the existence of a multiplicity of nearly degenerate conformations of the electronic component that can be easily modified by external perturbations. Conventional soft matter is classical [$(^{h}/_{2\pi}) = 0$], but in the electronic systems described here quantum effects are important.

TMOs are soft in the sense described above as already proposed in the HTSC context (*44*). They are also complex, because several effects become simultaneously important and prevent a simple physical description. More specifically, consider one of the popular definitions of complexity recently discussed in (*47*): "… randomness and determinism are both relevant to the system's overall behavior. Such [complex] systems exist on the edge of chaos—they may exhibit almost regular behavior, but also can change dramatically and stochastically in time and/or space as a result of small changes in conditions." This definition is satisfied by manganites, in which a small magnetic field produces a drastic change in transport properties, and it may apply to underdoped cuprates as well (*17*, *45*). When phases compete, general arguments suggest that large responses to weak perturbations should be far more common than previously believed (*4*, *5*, *17*). Although the basic rules for electrons (i.e., the Hamiltonians) are deceptively simple (nearest-neighbor carrier hopping, Coulomb or phononic interactions, etc.), the outcomes are highly nontrivial when phases compete and percolative physics, as when only a narrow channel exists for electrical conductivity through a material, is at work.

Another argument can be found in the known properties of traditional soft condensed matter, which is a phase of matter between a simple fluid and a regular solid crystal. In soft matter, large groups of atoms form regular patterns as in a solid, but when several of these large groups are considered together a complex fluid behavior emerges. Typical examples are polymers: in each large molecule there is atomic regularity, but an ensemble of them has a variety of fluid phases (*48*). This variable behavior is also present in some TMOs: in manganites, several experimental investigations have found evidence for Jahn-Teller ordered small regions (i.e., with a particular form of lattice distortions) in the state above the FM ordering temperature (*4*, *5*). As a system, these small Jahn-Teller clusters, along with the magnetic clusters present in the same phase region, generate a collective behavior that is different from the behavior of the system's individual parts, and in this temperature range colossal magnetoresistance occurs (*4*, *5*). Also cuprates may behave as electron liquid crystals, intermediate between electron liquid and electron crystal (*44*). Softness in the manganite context has also been recently discussed (*23*). Once these concepts are accepted, then the long history of soft-matter investigations suggests that it is natural to expect new kinds of organized behavior. In complex systems, randomness and determinism are simultaneously relevant, and these are ideas compatible with recent correlated electrons investigations (*10*, *11*, *15*, *19*, *20*).

Each complex situation in correlated electrons may lead to a unique state. Some materials may have stripes, others may have patches, some may have phase separation at nanoscales, and others may have mesoscale phase separation; the number of states in competition and their nature can lead to enormous possibilities. This is exciting for applications but frustrating for those with a reductionist soul. What is likely is that new general concepts and paradigms will emerge as guiding qualitative principles in the study of complex oxides. It will be difficult to predict the precise shape of the nanopatterns and the phases in competition unless detailed calculations are performed. But the existence of some patterns, as well as giant responses to selected external perturbations, will be predictable. Certainly the highest degree of complexity is expected when many degrees of freedom are active simultaneously and when many phases with different properties are in competition.

Theory, phenomenology, computer simulations. How can we make further progress in this context? Investigations involving the

fundamental Hubbard and *t-J* models are reaching the limits of our current many-body techniques. It appears unlikely that the large length scales needed to fully capture the complex behavior of oxides, where percolation is probably very relevant, will be reached via this path, and we must focus on the right level of description. As Laughlin and Pines (*49*) wrote, ''Deduction from microscopics has not explained, and probably cannot explain as a matter of principle, the wealth of crossover behavior discovered in the normal state of the underdoped cuprates.'' It is still reasonable that key issues such as the pairing mechanism and short-distance nature of the dominant states can still be analyzed in the context of Hubbard-based approaches, perhaps supplemented by long-range Coulomb and/or electron-lattice interactions. However, the complexity of the resulting states, with emerging self-organization and giant responses, can only be addressed with simpler phenomenological models that assume competition between a few selected states and analyze its consequences. For example, the famous linear resistivity and puzzling underdoped behavior of the cuprates and the CMR effect in the manganites may only be explainable with use of this coarse-grain approach.

The logical chain starts with ab initio calculations to evaluate the main parameters and couplings, followed by Hubbard modeling to obtain the dominant short-distance correlations, and ends with the use of more phenomenological models (*17*) to handle the long length scales of relevance in an electronic complex fluid. The inclusion of both symmetry and spontaneous symmetry breaking will be important to achieving these objectives, as will the inclusion of the effects of disorder and lattice distortions. Essential for the success of the present flurry of research in complex systems is the ability to use high-speed computers to perform unbiased calculations. By simulating a system made of many small units, the behavior of the whole ensemble can be understood and manipulated much better than with other techniques, providing new ways of learning and visualizing in this context.

Other systems with similar complex behavior. There are many other materials that behave similarly as the TMOs emphasized in this review. For example, in the area of heavy fermions (metals where the effective mass of electrons is much larger than the bare mass) the presence of ''electronic Griffiths phases,'' inhomogeneous states at zero temperature, has been described (*50*), and strong similarities with the cuprate's phase diagram were unveiled (*51*) (Fig. 1F). In general, glassy behavior is expected near a metal-insulator transition at low temperatures (*50*, *52*, *53*), establishing an interesting connection with the area of investigations known as ''quantum critical phenomena'' (*54*). Glassy dynamics is also observed in other two-dimensional electronic systems (*55*). Cobalt oxides (*56*), organic materials (*57*, *58*) (Fig. 1E), and Ca-doped ruthenates (Fig. 1D) are other examples. Materials where charge density waves and superconductivity compete provide other cases of complex behavior (*59*). The area of complexity in correlated electrons is far wider than the two TMOs chosen in this article to focus on.

Complexity in pure states. The emphasis of this review has been on self-organization and the complexity in the electronic sector associated with the existence of several competing states. This corresponds to the physics of the HTSC cuprates in the underdoped regime and the manganites in the CMR regime. However, complexity in strongly correlated electrons also exists in the fascinating ground states observed in the clean limit or far from the region of phase competition if quenched disorder is present. For example, superconducting ground states with zero electrical resistance, a Meissner effect, and unconventional properties [*d* wave in the cuprates or spin-triplet pairing in the ruthenates (*60*)] emerge from simple interactions among electrons and lattice vibrations. In the manganites, a CE phase exists with simultaneous spin, lattice, orbital, and charge order (*4*). The list of exotic phases observed in the clean limit is enormous, and they all represent emergent phenomena in the sense that their properties cannot be predicted easily from the Hamiltonian. The collective behavior of electrons in these phases is relatively simple, and it can be described with a handful of concepts and parameters. The emergence of simplicity is part of the complex behavior of electrons (*49*). Whereas in the case of Mn oxides the inhomogeneities are crucial to understanding the CMR effect and in cuprates the analogous inhomogeneities are important to rationalize the curious underdoped regime, they do not provide an obvious means to comprehend the origin of all the many exotic ground states. Thus, with or without quenched disorder, in homogeneous or inhomogeneous forms, it is clear that systems of strongly correlated electrons are surprising and that the list of their many possible ground states is far from fully classified. Research producing highly pure samples is as important as those focusing on the region of inhomogeneities and pattern formations, leading to complementary insight. Clearly, these compounds are complex in more than one sense.

Applications? It is too early to decide if the complex properties of correlated oxides could be important for applications, but several results already provide interesting clues. To name a few, the resistance of some oxide films was unexpectedly found to switch between low and high values upon the application of voltage pulses (*61*, *62*). Also, gigantic magnetoelectric effects were reported (*63*), interfaces of magnetic oxides have been engineered (*64*), manganites with sharp magnetization steps exist (*65*), and manganite nanotubes were prepared (*66*, *67*). Creating ultra-smooth thin films and artificial superstructures is part of the avenue toward applications. Because complexity appears to be the reason behind the CMR effect, complex behavior is conducive to functionality. Relaxor ferroelectrics are also oxides with nanodomains with potential applications (*68*). Field-effect transistors made from TMOs are another exciting area of research (*69*): correlated electron materials could present phase transitions in the presence of electric fields because these fields can alter the carrier concentration. It is the diversity of behavior, namely the many possible metallic, insulating, magnetic, superconducting, and ferroelectric phases of strongly correlated systems, that makes these types of investigations so exciting.

Conclusions

TMOs are certainly not as simple as standard metals. The many active degrees of freedom—spin, charge, lattice, and orbital—interact in a nonlinear, synergetic manner, leading to an intrinsic complexity. STM, neutron and x-ray scattering, and other microscopic techniques are crucial to unveiling the subtle nanoscale phase separation tendencies that induce a variety of real-space patterns. Charge transport in oxides is quite different from the free flow in simple metals: an isolated charge strongly perturbs its environment, inducing a polaron, which often attracts other polarons to form larger structures. To capture this physics, it is important to incorporate several ingredients, including powerful nonperturbative many-body techniques, phenomenological approaches, and the effects of lattice distortions, strain, and quenched disorder. All these ingredients appear equally important. Phase competition rules the behavior of these compounds: Although the energies characterizing each phase (such as gaps) can be fairly large, at particular carrier densities or bandwidths the energetic proximity of two phases introduces a lower hidden energy scale and small perturbations cause huge responses, not via the melting of the analyzed state but by its replacement by a very different one.

Establishing electronic complexity in hard materials as a fundamental area of research will create scientific relations with other popular fields of investigations. For instance, the existence of complexity in biological systems is clear, and analogies between proteins and spin glasses, both of which have a distribution of barrier heights among competing nearly degenerate states, have often been remarked on (*70*). In fact, most correlated electronic systems exhibit exotic glassy behavior with notoriously slow dynamics (*71*, *72*), establishing one of the prime connections between traditional biological or soft systems and the complex states described here. Biological physics is one of the

major frontiers for physics in the new millennium and complexity certainly arises in macromolecules and complex fluids. A common language can also be established with other broad fields: for instance, in nuclear matter the self-generation of structures is under much discussion as well (*73*).

A novel paradigm involving "complexity in correlated electron materials" will help to focus on the right level of description, on the expected emergence of patterns, and on separating the physics of the individual phases from properties that arise from phase competition. Controlling the spontaneous tendencies toward complex pattern formation may open the way to achieving emergent functionalities in correlated electrons systems. The enormous diversity of phases in oxides provides a wide range of combinations to explore. Complexity and functionality are rapidly developing into the most exciting frontiers in the active area of strongly correlated electrons.

References and Notes

1. P. W. Anderson, *Science* **177**, 393 (1972).
2. N. Goldenfeld, L. Kadanoff, *Science* **284**, 87 (1999), and related articles in the same issue.
3. A. Moreo, S. Yunoki, E. Dagotto, *Science* **283**, 2034 (1999).
4. E. Dagotto, T. Hotta, A. Moreo, *Phys. Rep.* **344**, 1 (2001).
5. E. Dagotto, *Nanoscale Phase Separation and Colossal Magnetoresistance* (Springer-Verlag, Berlin, 2002).
6. Y. Tokura, N. Nagaosa, *Science* **288**, 462 (2000).
7. M. Salamon, M. Jaime, *Rev. Mod. Phys.* **73**, 583 (2001).
8. N. Mathur, P. Littlewood, *Phys. Today* **56**, 26 (2003).
9. K. H. Ahn, T. Lookman, A. R. Bishop, *Nature* **428**, 401 (2004).
10. J. Burgy *et al.*, *Phys. Rev. Lett.* **87**, 277202 (2001).
11. J. Burgy, A. Moreo, E. Dagotto, *Phys. Rev. Lett.* **92**, 097202 (2004).
12. S. Yunoki *et al.*, *Phys. Rev. Lett.* **80**, 845 (1998).
13. M. Uehara, S. Mori, C. H. Chen, S.-W. Cheong, *Nature* **399**, 560 (1999).
14. D. Louca, T. Egami, E. L. Brosha, H. Roder, A. R. Bishop, *Phys. Rev. B* **56**, R8475 (1997).
15. Y. Tomioka, Y. Tokura, *Phys. Rev. B* **70**, 014432 (2004).
16. D. Akahoshi *et al.*, *Phys. Rev. Lett.* **90**, 177203 (2003).
17. G. Alvarez *et al.*, *Phys. Rev. B* **71**, 014514 (2005).
18. H. Rho *et al.*, *Phys. Rev. Lett.* **88**, 127401 (2002).
19. Y. Motome, N. Furukawa, N. Nagaosa, *Phys. Rev. Lett.* **91**, 167204 (2003).
20. H. Aliaga *et al.*, *Phys. Rev. B* **68**, 104405 (2003).
21. J. Schmalian, P. Wolynes, *Phys. Rev. Lett.* **85**, 836 (2000).
22. J. Schmalian, P. Wolynes, *MRS Bull.* **30**, 433 (2005).
23. G. C. Milward, M. J. Calderon, P. B. Littlewood, *Nature* **433**, 607 (2005).
24. S.-C. Zhang, *Science* **275**, 1089 (1997).
25. S. Sanna, G. Allodi, G. Concas, A. H. Hillier, R. De Renzi; available online at http://arxiv.org/abs/cond-mat/0403608.
26. S. Sanna *et al.*, *Phys. Rev. Lett.* **93**, 207001 (2004).
27. See, for example, fig. 4 of T. Sasaki *et al.*, *Phys. Rev. B* **65**, 060505 (2002).
28. J. Tranquada *et al.*, *Nature* **375**, 561 (1995).
29. V. J. Emery, S. A. Kivelson, J. M. Tranquada, *Proc. Natl. Acad. Sci. U.S.A.* **96**, 8814 (1999).
30. J. Zaanen, *Nature* **404**, 714 (2000), and references therein.
31. S. R. White, D. Scalapino, *Phys. Rev. Lett.* **80**, 1272 (1998).
32. B. Stojkovíc *et al.*, *Phys. Rev. Lett.* **82**, 4679 (1999).
33. J.-X. Zhu *et al.*, *Phys. Rev. Lett.* **91**, 057004 (2003).
34. S. Sorella *et al.*, *Phys. Rev. Lett.* **88**, 117002 (2002).
35. J. M. Tranquada *et al.*, *Nature* **429**, 534 (2004).
36. S. M. Hayden *et al.*, *Nature* **429**, 531 (2004).
37. E. Dagotto, T. M. Rice, *Science* **271**, 618 (1996).
38. K. M. Lang *et al.*, *Nature* **415**, 412 (2002).
39. Y. Kohsaka *et al.*, *Phys. Rev. Lett.* **93**, 097004 (2004).
40. T. Hanaguri *et al.*, *Nature* **430**, 1001 (2004).
41. M. Vershinin *et al.*, *Science* **303**, 1995 (2004); published online 12 February 2004 (10.1126/science.1093384).
42. C. C. Homes *et al.*, *Nature* **430**, 539 (2004).
43. C. C. Homes, S. V. Dordevic, T. Valla, M. Strongin; available online at http://arxiv.org/abs/cond-mat/0410719.
44. S. A. Kivelson, E. Fradkin, V. J. Emery, *Nature* **393**, 550 (1998).
45. I. Bozovic *et al.*, *Phys. Rev. Lett.* **93**, 157002 (2004).
46. V. Emery, S. Kivelson, *Nature* **374**, 434 (1995).
47. T. Vicsek, *Nature* **418**, 131 (2002).
48. T. Witten, *Rev. Mod. Phys.* **71**, S367 (1999).
49. R. B. Laughlin, D. Pines, *Proc. Natl. Acad. Sci. U.S.A.* **97**, 28 (2000).
50. E. Miranda and V. Dobrosavljevic, *Rep. Prog. Phys.*, in press; preprint available online at http://arxiv.org/abs/cond-mat/cond-mat/0504411.
51. V. Sidorov *et al.*, *Phys. Rev. Lett.* **89**, 157004 (2002).
52. V. Dobrosavljevic, D. Tanaskovic, A. A. Pastor, *Phys. Rev. Lett.* **90**, 016402 (2003).
53. K. Byczuk, W. Hofstetter, D. Vollhardt, *Phys. Rev. Lett.* **94**, 056404 (2005).
54. S. Sachdev, *Quantum Phase Transitions* (Cambridge Univ. Press, Cambridge, 1999).
55. S. Bogdanovich, D. Popovic, *Phys. Rev. Lett.* **88**, 236401 (2002).
56. P. L. Kuhns *et al.*, *Phys. Rev. Lett.* **91**, 127202 (2003).
57. P. Limelette *et al.*, *Phys. Rev. Lett.* **91**, 016401 (2003).
58. K. Miyagawa, A. Kawamoto, K. Kanoda, *Phys. Rev. Lett.* **89**, 017003 (2002).
59. G. Gruner, *Density Waves in Solids* (Addison-Wesley, Boston, 1994).
60. A. P. Mackenzie, Y. Maeno, *Rev. Mod. Phys.* **75**, 657 (2003).
61. S. Q. Liu, N. J. Wu, A. Ignatiev, *Appl. Phys. Lett.* **76**, 2749 (2000).
62. M. Rozenberg, I. H. Inoue, M. J. Sanchez, *Phys. Rev. Lett.* **92**, 178302 (2004).
63. T. Kimura *et al.*, *Nature* **426**, 55 (2003).
64. H. Yamada *et al.*, *Science* **305**, 646 (2004).
65. R. Mahendiran *et al.*, *Phys. Rev. Lett.* **89**, 286602 (2002).
66. P. Levy, A. G. Leyva, H. E. Troiani, R. D. Sanchez, *Appl. Phys. Lett.* **83**, 5247 (2003).
67. L. Hueso, N. Mathur, *Nature* **427**, 301 (2004).
68. R. Blinc *et al.*, *Phys. Rev. Lett.* **83**, 424 (1999), and references therein.
69. C. H. Ahn, J.-M. Triscone, J. Mannhart, *Nature* **424**, 1015 (2003).
70. H. Frauenfelder, P. G. Wolynes, R. H. Austin, *Rev. Mod. Phys.* **71**, S419 (1999).
71. I. Deac, J. Mitchell, P. Schiffer, *Phys. Rev. B* **63**, 172408 (2001).
72. J. Sacanell, F. Parisi, P. Levy, L. Ghivelder, *Physica B* **354**, 43 (2004); also available online at http://arxiv.org/abs/cond-mat/0412499.
73. C. J. Horowitz, M. A. Perez-Garcia, J. Piekarewicz, *Phys. Rev. C* **69**, 045804 (2004), and references therein.
74. J. F. Mitchell *et al.*, *J. Phys. Chem. B* **105**, 10731 (2001).
75. S. Nakatsuji, Y. Maeno, *Phys. Rev. Lett.* **84**, 2666 (2000).
76. S. Nakatsuji *et al.*, *Phys. Rev. Lett.* **93**, 146401 (2004).
77. M.-L. Foo *et al.*, *Phys. Rev. Lett.* **92**, 247001 (2004).

78. This work was supported by NSF grant DMR-0443144 and the Laboratory Directed Research and Development program of ORNL, which is managed by UT-Battelle, Limited Liability Corporation for the U.S. Department of Energy under contract no. DE-AC05-00OR22725. The author is thankful to C. Ahn, G. Alvarez, L. Balicas, A. Bishop, I. Bozovic, R. Cava, S. L. Cooper, P. Dai, J. C. S. Davis, V. Dobrosavljevic, T. Egami, E. Fradkin, N. Goldenfeld, Y. Maeno, D. Mandrus, J. Mannhart, J. Mitchell, A. Moreo, N. Nagaosa, S. Nakatsuji, M. Rozenberg, P. Schiffer, Y. Tokura, J. Tranquada, J-M. Triscone, S. Uchida, P. Wolynes, A. Yazdani, and S. C. Zhang, for their important comments.

10.1126/science.1107559

Bioluminescent and Red-Fluorescent Lures in a Deep-Sea Siphonophore

Steven H. D. Haddock,[1]* Casey W. Dunn,[2] Philip R. Pugh,[3] Christine E. Schnitzler[1]

Examples of bioluminescent lures in the sea are quite rare, posited only for a few fish and cephalopods (*1*). In many marine organisms, including siphonophores, luminescence is thought to serve defensive purposes. Siphonophores are colonial hydrozoans (phylum Cnidaria) that are dominant predators in the ocean, some reaching tens of meters in length. Nearly all members of this group are luminous (*2*), but because of their fragility, they are rarely observed alive.

Using a submersible at depths between 1600 m and 2300 m (*3*), we collected three specimens of an undescribed species in the genus *Erenna* (Fig. 1A and movie S1). Unlike most siphonophores, *Erenna* do not feed on crustaceans but prey instead upon fish (*4*), remnants of which were found inside two of our specimens. At great depths where chance encounters with vertebrates are rare, it is unclear how they obtain prey. Here we show that the nonvisual *Erenna* sp. we captured possesses red-emitting bioluminescent appendages that may act as lures for fish prey.

Erenna tentacles have numerous side branches (tentilla), each consisting of a large cnidoband (an array of ~3000 stinging cells) attached to a central stalk (Fig. 1, B and C). The transparent stalk terminates in a bulb containing white spots, historically called "ocelli" (*4*). We found that, when ruptured in $CaCl_2$, these spots produced luminescence, indicating that they are in fact photophores filled with Ca^{2+}-regulated photoproteins. Unlike typical cnidarian photocytes, these terminal photophores did not readily flash upon direct stimulation.

Photophores of young tentilla (Fig. 1B) contained only bioluminescent tissue, but when mature, they were surrounded by red fluorescent material (Fig. 1C). This substance produced a multimodal fluorescence emission, spanning yellow to red (583, 620, and 680 nm) (Fig. 1, D and E). These mature tentilla also displayed a unique rhythmic flicking behavior (movie S1).

We observed blue-green (immature) and orange-red (mature) in vivo emission by eye, but we were unable to record bioluminescence emission spectra because of the scarcity of specimens and the small size of the photophores. We expect bioluminescence spectra to be similar to fluorescence emissions, as is the case in other cnidarians (*2*).

Among all marine organisms, only the rare scaleless dragonfishes (Stomiidae) have been known to produce red luminescence (*1*), but red fluorescent substances have been noted in several marine phyla (*5*–*7*). The fluorescent material of *Erenna* does not appear to belong to the green fluorescent protein family (*5*), nor does it resemble the biliproteins of the siphonophore *Physalia* (*6*). On the basis of emission and absorption spectra, with a Soret band at 406 nm and secondary Q bands at 570 and 583 nm (Fig. 1, F and G), the main constituents are most similar to porphyrins found in medusae and fish (*7*).

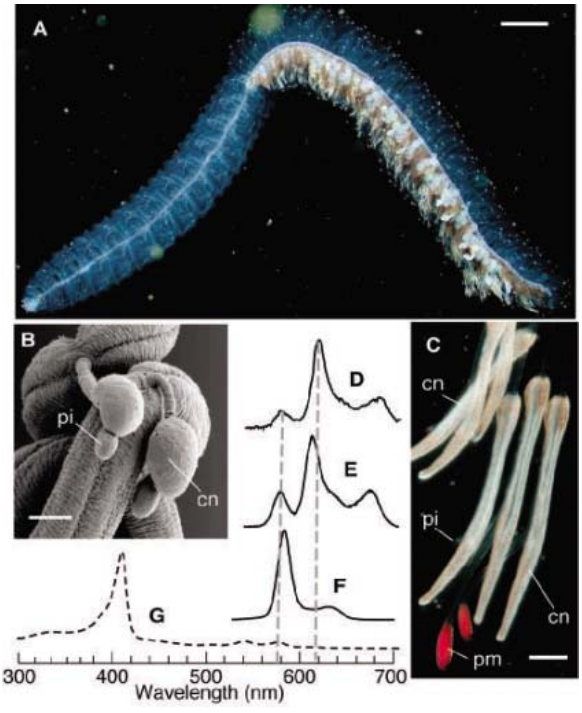

Fig. 1. (**A**) *Erenna* sp. at 1662 m. Scale bar, 2 cm. (**B**) Scanning electron micrograph of immature photophore (pi) and cnidoband (cn). Scale bar, 200 μm. (**C**) Live tentilla with mature photophores (pm). Scale bar, 1 mm. (**D** to **F**) Fluorescence emission spectra of (D) a live mature photophore (excitation wavelength λ_{ex} = 410 nm), (E) unpurified extract (λ_{ex} = 473 nm), and (F) purified extract (λ_{ex} = 410 nm). Dashed vertical lines show primary conserved emission peaks. (**G**) The absorbance spectrum of purified photophore extract.

Given the characteristic flicking of the bioluminescent and fluorescent filaments, we concluded that the siphonophore *Erenna* uses them as lures to attract fish. Fluorescent structures may serve as lures in a diverse assemblage of nonluminous taxa, from cnidarians to crustaceans, and we have found examples of putative lures in several other siphonophores and medusae. In shallow waters, fluorescence could be excited by ambient blue light rather than by bioluminescence as in deep-dwelling *Erenna*.

The assertion that red light acts as an attractant is at odds with the prevailing view that deep-living creatures cannot detect long wavelengths; however, our knowledge of deep-sea visual abilities is limited. For example, the eyes of *Cyclothone*, an abundant deep-sea fish, have not yet been studied, and evidence for red sensitivity in a deep myctophid fish has been presented only recently (*8*). Our findings suggest that the role of long-wavelength light in marine visual ecology merits a closer look.

References and Notes

1. P. J. Herring, *Symp. Zool. Soc. Lond.* **38**, 127 (1977).
2. S. H. D. Haddock, J. F. Case, *Mar. Biol.* **133**, 571 (1999).
3. Materials and methods are available as supporting material on *Science* Online.
4. P. R. Pugh, *Bull. Nat. Hist. Mus. (Zool. Ser.)* **67**, 169 (2001).
5. D. A. Shagin *et al.*, *Mol. Biol. Evol.* **21**, 841 (2004).
6. P. J. Herring, *Comp. Biochem. Physiol.* **39B**, 739 (1971).
7. R. Bonnett, E. J. Head, P. J. Herring, *J. Mar. Biol. Assoc. U.K.* **59**, 565 (1979).
8. R. H. Douglas, J. K. Bowmaker, C. W. Mullineaux, in *Bioluminescence and Chemiluminescence*, P. E. Stanley, L. J. Kricka, Eds. (World Science Publications, Singapore, 2002), pp. 391–394.
9. We thank J. Krupp, L. Christianson, L. Lundsten, G. Wagner, A. Haffa, D. Klimov, K. Johnson, and B. Robison and the crews of the *Western Flyer* and *Tiburon*. Supported by the Packard Foundation and NSF.

Supporting Online Material
www.sciencemag.org/cgi/content/full/309/5732/263/DC1
Materials and Methods
Movie S1

31 January 2005; accepted 18 April 2005
10.1126/science.1110441

[1]Monterey Bay Aquarium Research Institute, 7700 Sandholdt Road, Moss Landing, CA 95039, USA. [2]Ecology and Evolutionary Biology, Yale University, New Haven, CT 06520, USA. [3]National Oceanography Centre, Southampton, SO14 3ZH, UK.

*To whom correspondence should be addressed. E-mail: haddock@mbari.org

Professional Antigen-Presentation Function by Human γδ T Cells

Marlène Brandes, Katharina Willimann, Bernhard Moser*

Human γδ T cells are considered to play a vital role in protective immunity through cytokine secretion and cytotoxic activity. We report that cells expressing the Vγ2Vδ2$^+$–T cell receptor (Vδ2$^+$ T cells) also display principal characteristics of professional antigen-presenting cells such as dendritic cells. Thus, when activated, these cells efficiently processed and displayed antigens and provided co-stimulatory signals sufficient for strong induction of naïve αβ T cell proliferation and differentiation. We suggest that, upon microbial activation, Vδ2$^+$ T cells participate in the induction of adaptive immune responses and that these cells may be a useful tool in vaccine development and immunotherapy.

γδ T cells represent a distinct subset of T cells characterized by T cell receptors (TCRs) that possess unique structural and antigen-binding characteristics (*1*–*4*). In normal human peripheral blood, these T cells make up 2 to 10% of the total T cell pool, with the majority (>80%) expressing the Vγ2Vδ2$^+$ TCR (hereafter referred to as Vδ2$^+$ T cells) (*5*, *6*). Vδ2$^+$ T cells specifically recognize small nonpeptide antigens, derived mostly from microbes or necrotic host cells (*5*, *6*). In clear contrast to recognition of antigen by αβ T cells, Vδ2$^+$ T cell–specific antigens do not need to be processed by professional antigen-presenting cells (APCs) such as dendritic cells (DCs) and do not require binding and presentation by classical major histocompatibility complex (MHC) molecules (*5*, *6*). Vδ2$^+$ T cells are also unique to higher primates, and their absence in other mammals suggests that they may have evolved to provide protection against distinct, species-specific microbes (*3*, *4*, *7*). Vδ2$^+$ T cells display a range of innate effector functions including the rapid secretion of chemokines and cytokines and target cell lysis, as well as contribution to adaptive immunity, for example through B cell help, DC maturation, and provision of memory γδ T cell function (*8*–*11*).

Activated Vδ2$^+$ T cells display phenotypic characteristics of professional APCs. We recently showed that TCR-triggering in human Vδ2$^+$ T cells leads to rapid and transient expression of the lymph node (LN)–homing receptor CCR7 (*8*, *12*). Furthermore, Vδ2$^+$ T cells have been shown to be present in LNs draining mucosal tissues, suggesting that they might directly interact with adaptive immune cells. We hypothesized that γδ T cells might play a role in processing and presenting antigens. To explore whether γδ T cells display any feature of professional APCs, we examined tonsillar γδ T cells. We observed signs of preactivation (cell surface CD69 expression) on these cells, which is in line with LN-homing properties present in in vitro stimulated rather than in resting γδ T cells (*8*, *12*). Moreover, the antigen-presenting MHC-II molecule (human leukocyte antigen D locus-related protein) HLA-DR was also substantially up-regulated on these cells, along with a wide array of T cell co-stimulation and adhesion molecules (Fig. 1A and table S1). To investigate how these antigen-presenting features might be regulated, we stimulated freshly isolated resting blood Vδ2$^+$ T cells with the prototype Vγ2Vδ2-TCR ligand, isopentenyl pyrophosphate (IPP), to selectively expand Vδ2$^+$ T cells (*5*, *6*, *13*). As with fresh tonsillar γδ T cells IPP-stimulated but not resting, Vδ2$^+$ T cells expressed a repertoire of antigen-presentation and co-stimulation molecules that was almost indistinguishable from lipopolysaccharide (LPS)-matured, monocyte-derived DCs (Fig. 1B and table S2). Other natural Vδ2$^+$ T cell stimuli also strongly induced similar APC features, for example, *Escherichia coli* KM20 lysate and 4-hydroxy-3-methyl-but-2-enyl-pyrophosphate (HMBPP), which is produced during microbial isoprenoid synthesis (*5*, *6*) (Fig. 1C). Surface, versus intracellular, staining revealed de novo production of MHC-II during Vδ2$^+$ T cells activation and contrasted with the cell surface relocation of preformed intracellular MHC-II in maturating DCs (Fig. 1E) (*14*, *15*). Most of the activation-induced surface molecules were maintained at high concentrations during the proliferation of Vδ2$^+$ T cells (fig. S1). In contrast, peripheral blood αβ T cells displayed a relatively modest and clearly delayed expression of MHC-II and co-stimulation molecules during stimulation (Fig. 1, B and D). Abundant adhesion molecules on IPP-stimulated Vδ2$^+$ T cells may explain their clustering observed with naive αβ T cells, resembling early steps in T cell activation by DCs (fig. S2) (*16*, *17*).

To illustrate cellular distribution of MHC II and morphologic changes, we performed confocal and digital interference contrast (DIC) image analyses with resting and IPP-stimulated Vδ2$^+$ T cells (Fig. 2A). Resting Vδ2$^+$ T cells express high amounts of cell surface γδ-TCRs but lack cell surface and intracellular HLA-DR, in agreement with flow cytometry analysis (Fig. 1E). The late endosomal-lysosomal marker Lamp-1/CD107a is found in intracellular compartments. Cytospin sections document the de novo expression of HLA-DR during short-term Vδ2$^+$ T cell stimulation. The cultures were heterogeneous, i.e., contained partially and fully activated Vδ2$^+$ T cells, as evidenced by intermediate or low concentrations of γδ-TCR and inverse concentrations of HLA-DR. LAMP-1 appears to cluster intracellularly in activated γδ-TCR^{low}HLA-DR^{high} Vδ2$^+$ T cells. Control staining with immature and mature DC revealed the expected stainings, including cell surface relocation of preformed HLA-DR and Lamp-1 clustering during DC maturation (*10*, *15*). Of note, activated Vδ2$^+$ T cells carry numerous dendrite-like cell protrusions (Fig. 2A) and feature an ''amoeboid''-like cell morphology (Fig. 2B).

Activated Vδ2$^+$ T cells induce proliferation and differentiation in naïve CD4$^+$ αβ T cells. The APC-like phenotype suggested that activated but not resting Vδ2$^+$ T cells perform APC functions. This was tested by measuring the ability of IPP-stimulated Vδ2$^+$ T cells to induce primary CD4$^+$ αβ T cell responses to MHC alloantigens in mixed leukocyte reactions (MLRs) (*13*). Proliferation was readily observed in response to distinct alloantigens present on heterologous Vδ2$^+$ T cells (Fig. 3A), and was similar to that obtained with the use of LPS-matured DCs, at APC-responder ratios of up to 1:100. In contrast, very limited responses were obtained with the use of superantigen-stimulated αβ T cells as APCs (Fig. 3A).

The relative contribution of co-stimulation to the efficiency of antigen presentation function of Vδ2$^+$ T cells was next tested. To measure this, we used the superantigen, toxic shock syndrome toxin 1 (TSST-1). Because TSST-1 binds directly to MHC-II molecules on the surface of APCs, it does not require uptake and processing as required for conventional protein antigens. Furthermore, TSST-1 is selective for αβ-TCRs containing the Vβ2 chain, which make up 4 to 10% of peripheral blood CD3$^+$ T cells, allowing responder cells

Institute of Cell Biology, University of Bern, CH-3012, Switzerland.

*To whom correspondence should be addressed. E-mail: bernhard.moser@izb.unibe.ch

to be readily detected (*18*). IPP-stimulated Vδ2$^+$ T cells pulsed with 10 ng/ml TSST-1 induced a strong expansion of naïve autologous Vβ2$^+$ αβ T cells, corresponding well with the response obtained with the use of TSST-1–loaded DCs (Fig. 3B) (*19*). In contrast, activated αβ T cells and freshly isolated monocytes did not induce substantial proliferation. TSST-1 titration experiments revealed the high potency of TSST-1–presenting Vδ2$^+$ T cells, exceeding by 100-fold the responses obtained with αβ T cells or monocytes (Fig. 3C). At high TSST-1 loading concentrations, Vδ2$^+$ T cells were consistently more effective than DCs in induction of primary T cell proliferation, whereas the reverse was observed at lower TSST-1 concentrations (Fig. 3C).

During primary immune responses, naïve CD4$^+$ αβ T cells differentiate into subsets of polarized effector T helper cells: Th1, Th2, or Th0 with the capacity to produce type 1 [interferon γ (IFN-γ)], type 2 [interleukin 4 (IL-4)], or both cytokines, respectively (*20*, *21*). We thus examined whether any differentiation in CD4$^+$ T cells occurred after proliferation in response to TSST-1–presenting Vδ2$^+$ T cells. At an initial APC:responder cell ratio of 1:5, the majority of responder cells displayed a polarized response, with an equal representation of all three T helper subsets (Th1, Th2, and Th0) (Fig. 3D). At higher Vδ2$^+$ T cell concentration, the polarization response shifted to Th1, similar to the results obtained with TSST-1–loaded DCs at an APC:responder cell ratio of 1:5. Also, the percentage of Th1 cells increased (at constant APC:responder cell ratio) with increasing TSST-1 loading concentration (fig. S3A). TSST-1–presenting Vδ2$^+$ T cells had no obvious inhibitory effects, that is, did not induce abortive proliferation or secretion of anti-inflammatory cytokines in αβ T cells (Fig. 3D and fig. S3B) (*22*–*26*).

Activated Vδ2$^+$ T cells process and present soluble protein antigen. To test the ability of Vδ2$^+$ T cells to take up, process, and present soluble antigens to αβ T cells (*14*, *23*, *25*, *26*), we used two different types of protein antigens: the single-chain protein tetanus toxoid (TT) and the highly complex protein mixture *Mycobacterium tuberculosis*–purified protein derivative (PPD). Proliferation of autologous, TT- or PPD-specific CD4$^+$ αβ T cell lines, which respond to less stringent activation regimens (*27*), was readily detected (fig. S4). Processing of these two model antigens was further examined by using freshly isolated blood CD4$^+$ αβ T cells as responder cells together with PPD-presenting and TT-presenting Vδ2$^+$ T cells, respectively, leading to strong proliferation in both cases (Fig. 4A). Chloroquine, an inhibitor of endosomal and lysosomal acidification required for efficient MHC class II antigen presentation, prevented responder cell proliferation, demonstrating that intracellular processing of PPD and TT is essential for triggering antigen-specific responses. These responses also could be blocked completely with a neutralizing antibody to HLA-DR, emphasizing

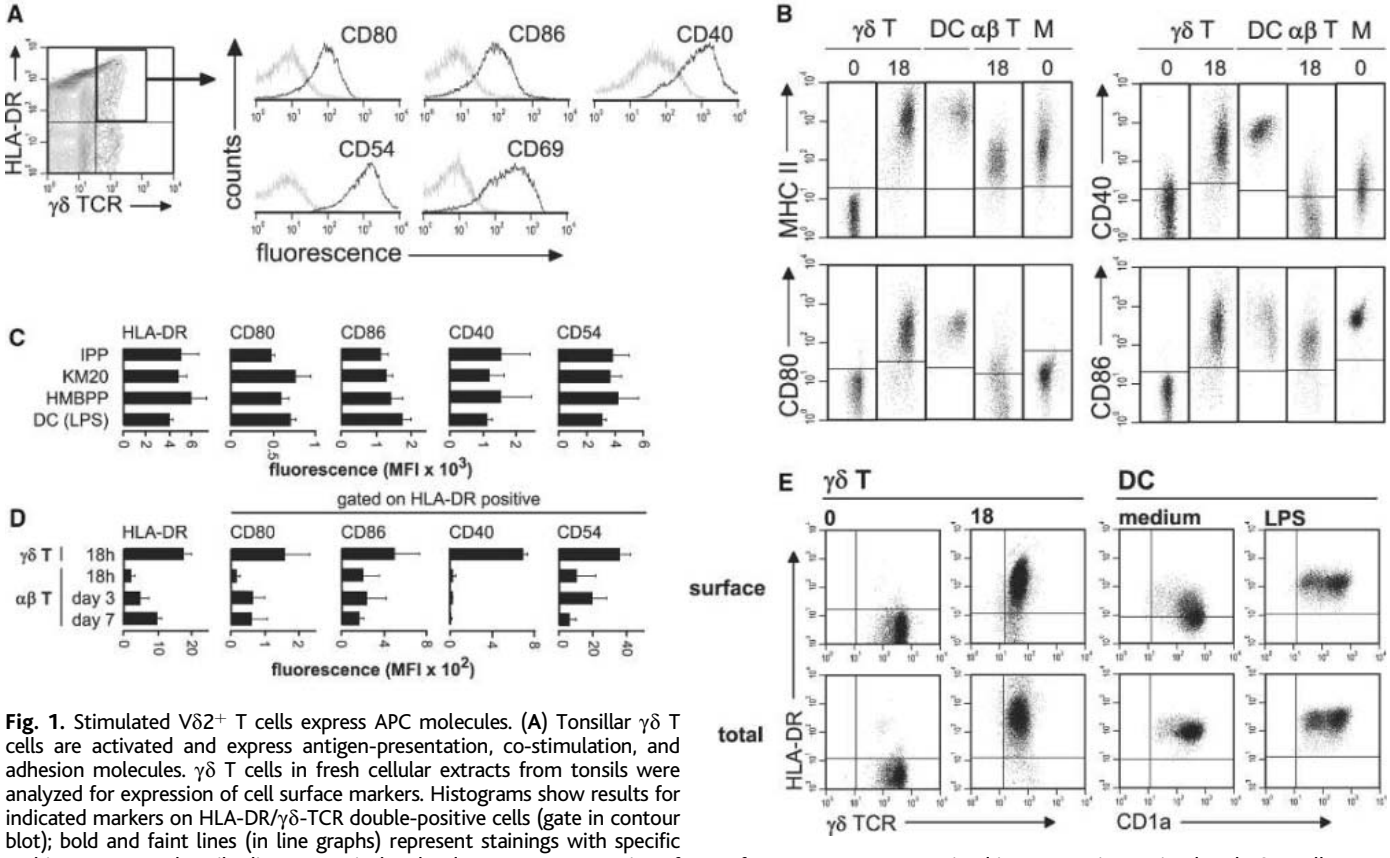

Fig. 1. Stimulated Vδ2$^+$ T cells express APC molecules. (**A**) Tonsillar γδ T cells are activated and express antigen-presentation, co-stimulation, and adhesion molecules. γδ T cells in fresh cellular extracts from tonsils were analyzed for expression of cell surface markers. Histograms show results for indicated markers on HLA-DR/γδ-TCR double-positive cells (gate in contour blot); bold and faint lines (in line graphs) represent stainings with specific and isotype control antibodies, respectively. The data are representative of three independent experiments. (**B**) Cell surface markers were determined on freshly isolated γδ T cells (γδ T), 18-hour IPP-stimulated Vδ2$^+$ T cells, monocyte-derived LPS-matured DCs (DC), 18-hour superantigen-stimulated αβ T cells (αβ T), and freshly isolated monocytes (M) (representative for six experiments). Numbers refer to the time of in vitro culture: 0, freshly isolated; 18, 18 hours. (**C**) Induction of antigen-presentation features upon treatment of Vδ2$^+$ T cells for 36 hours with *E. coli* KM20 lysate at 1:1000 dilution (KM20) with 0.5 μM HMBPP and with 50 μM IPP, in comparison with 48-hour LPS-matured monocyte-derived DCs [DC(LPS)]. Mean fluorescence intensities (MFI) ± SD; n = 2. (**D**) Moderate and delayed expression of APC molecules on superantigen-stimulated αβ T cells. Cell surface HLA-DR was examined in superantigen-stimulated αβ T cells at 18 hours, 3 days, or 7 days of culture. HLA-DR-positive αβ T cells were further analyzed for coexpression of APC markers as indicated. Vβ2$^+$ or CD4$^+$ αβ T cells were stimulated by LPS-DCs presenting TSST-1 or a superantigen cocktail [TSST-1, staphylococcal enterotoxin serotypes A (SEA) and B (SEB)] each at 100 ng/ml. Data combine results obtained with three donors. 18-hour IPP-Vδ2$^+$ T cells from the same donors were included as controls. (**E**) De novo synthesis or potential intracellular stores of preformed HLA-DR were evaluated by staining intact and permeabilized Vδ2$^+$ T cells, either freshly isolated [γδ T (0)] or 18h IPP-stimulated [γδ T (18)]. As controls, immature [DC(medium)] and 44-hour LPS-maturated DCs [DC(LPS)] were used. Expression was analyzed by flow cytometry.

the importance of MHC class II in antigen presentation (Fig. 4A). DCs stand out from all other APCs by their unparalleled efficiency in antigen uptake, processing, and presentation (*15*, *28*). Competence of activated Vδ2$^+$ T cells in these processes was examined by correlating proliferation responses in freshly isolated peripheral blood CD4$^+$ αβ T cells to various concentrations of PPD previously added during the generation of APCs (Fig. 4B). In these experiments using PPD between 0.01 and 10 μg/ml, Vδ2$^+$ T cells were at least as efficient as DCs. Vδ2$^+$ T cell–induced αβ T cell responses depended on physical contact as evidenced by lack of proliferation in the absence of direct contact with TT- or TSST-1–presenting Vδ2$^+$ T cells, excluding soluble mediators as main contributors to these responses (Fig. 4C).

Activated Vδ2$^+$ T cells induced naive CD8$^+$ αβ T cell proliferation and differentiation into cytotoxic T lymphocytes (CTLs). To determine whether Vδ2$^+$ T cells can also act as APCs in the induction of primary CD8$^+$ T cell responses, we set up naïve CD8$^+$ αβ T cells in proliferation assays with heterologous (MHC-mismatched), IPP-stimulated Vδ2$^+$ T cells, mature DCs, or superantigen-stimulated αβ T cells as APCs. Vδ2$^+$ T cells equaled or exceeded DCs in their capability to induce CD8$^+$ T cell proliferation, whereas αβ T cells proved to be greatly inferior APCs (Fig. 5A). CD8$^+$ effector cells (CTLs) taken from day 14 MLR cultures displayed alloreactive cytotoxic activity (Fig. 5B) (*13*). CTLs generated with the use of Vδ2$^+$ APCs were indistinguishable from those generated with the use of DCs with respect to perforin expression, IFN-γ production, specific cytotoxicity, and migration reprogramming, evidenced by loss of the LN receptor CCR7 in the majority of CTLs (Fig. 5B and fig. S5).

Conclusions. Our findings lead us to propose an additional and unexpected role for Vδ2$^+$ T cells in the initiation of adaptive immune processes. Human blood Vδ2$^+$ T cells rapidly and substantially expand in response to microbial infections, and in vivo this would most likely occur via the recognition of common nonpeptide antigens (*3*–*7*). Such microbial metabolites are a frequent target for responder γδ T cells (*1*, *2*, *7*) and induce highly efficient responses that may be due to superior signaling by γδ-TCR as compared with αβ-TCR (*29*, *30*). Rapid and local γδ T cell responses result in innate effector functions (cytokine and chemokine secretion and target cell lysis) (*3*–*5*, *7*) as well as induction of the LN-homing receptor CCR7 (*8*, *12*). Our in vitro findings predict that contact of Vδ2$^+$ T cells with microbes could also result in induction of a professional APC function that would serve to initiate strong adaptive responses by CD4$^+$ and CD8$^+$ αβ T cells. We suggest a scenario in which TCR-activated Vδ2$^+$ T cells take up and process microbial antigens and, after their relocation to draining LNs, induce antimicrobial responses in αβ T cells. Central to this model is the observation that Vδ2$^+$ T cells rapidly but transiently up-regulate CCR7 upon γδ-TCR–triggering (*8*, *12*), resembling induction of LN homing properties in DCs when exposed to inflammatory stimuli (*31*–*33*). We show here that αβ T cell responses generated in vitro by activated Vδ2$^+$ T cells match those obtained with mature DCs, at least in vitro. Of note, APC functions in Vδ2$^+$ T cells are expected to be restricted to infectious (inflammatory) settings, because resting Vδ2$^+$ T cells (equivalent to those not responding to infection in vivo) completely lack these features. This absence of APC function in resting Vδ2$^+$ T cells also indicates that these cells are unlikely to substitute for DCs in their other role of controlling of self-tolerance and immune regulation (*14*, *23*–*26*). Consistent with this, activated Vδ2$^+$ T cells also appear to lack anti-inflammatory effects on αβ T cells under the conditions used in our experiments, sug-

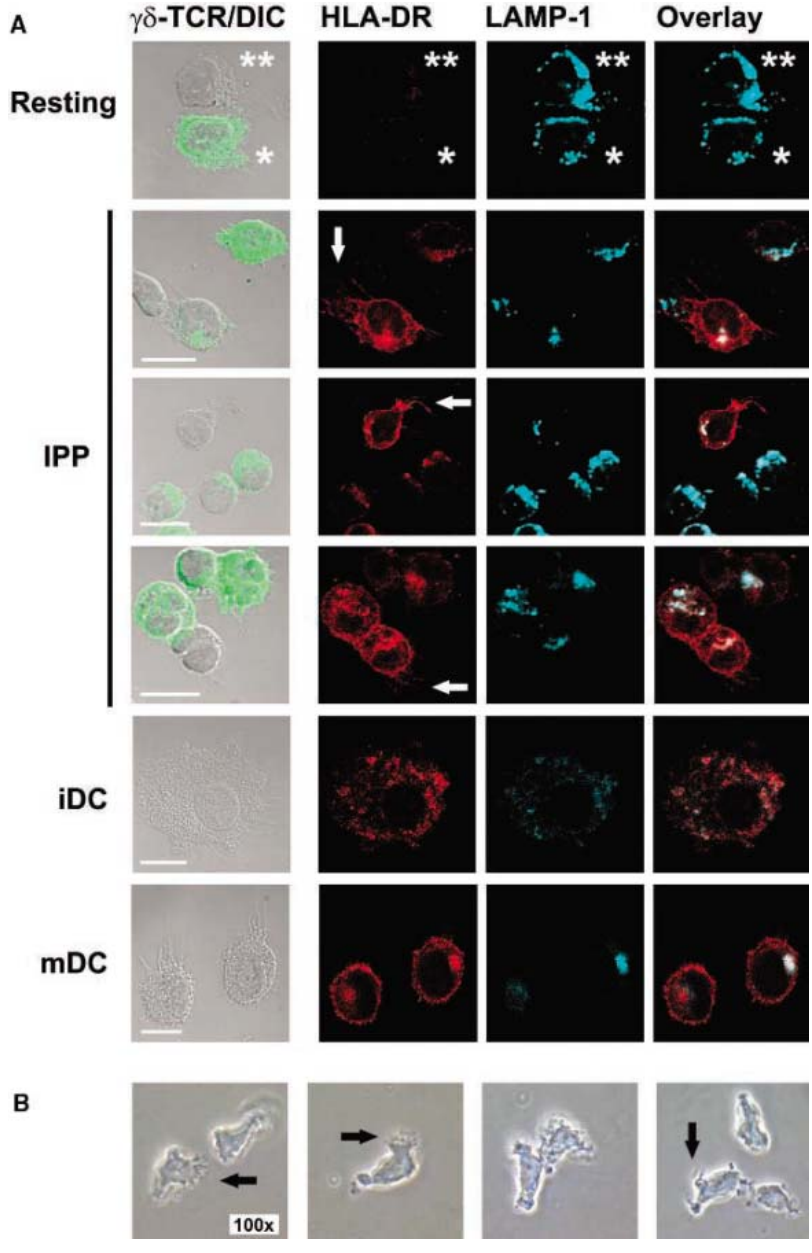

Fig. 2. HLA-DR expression and morphologic changes during Vδ2$^+$ T cells activation. (**A**) Marker expression and distribution analysis by confocal microscopy in cytospin preparations containing freshly isolated (resting) and 18-hour IPP-stimulated (IPP) Vδ2$^+$ T cells. As control for HLA-DR and Lamp-1 but not γδ-TCR expression, immature (iDC) and mature (mDC) DCs were used. Scale bars correspond to 10 μm; single and double stars denote a Vδ2$^+$ T cell and an unrelated mononuclear cell; white arrows point at filamentous cell protrusions. (**B**) Phase contrast images of cultured Vδ2$^+$ T cells after 48 hours of IPP stimulation. Black arrows point at amoeboid cell extensions.

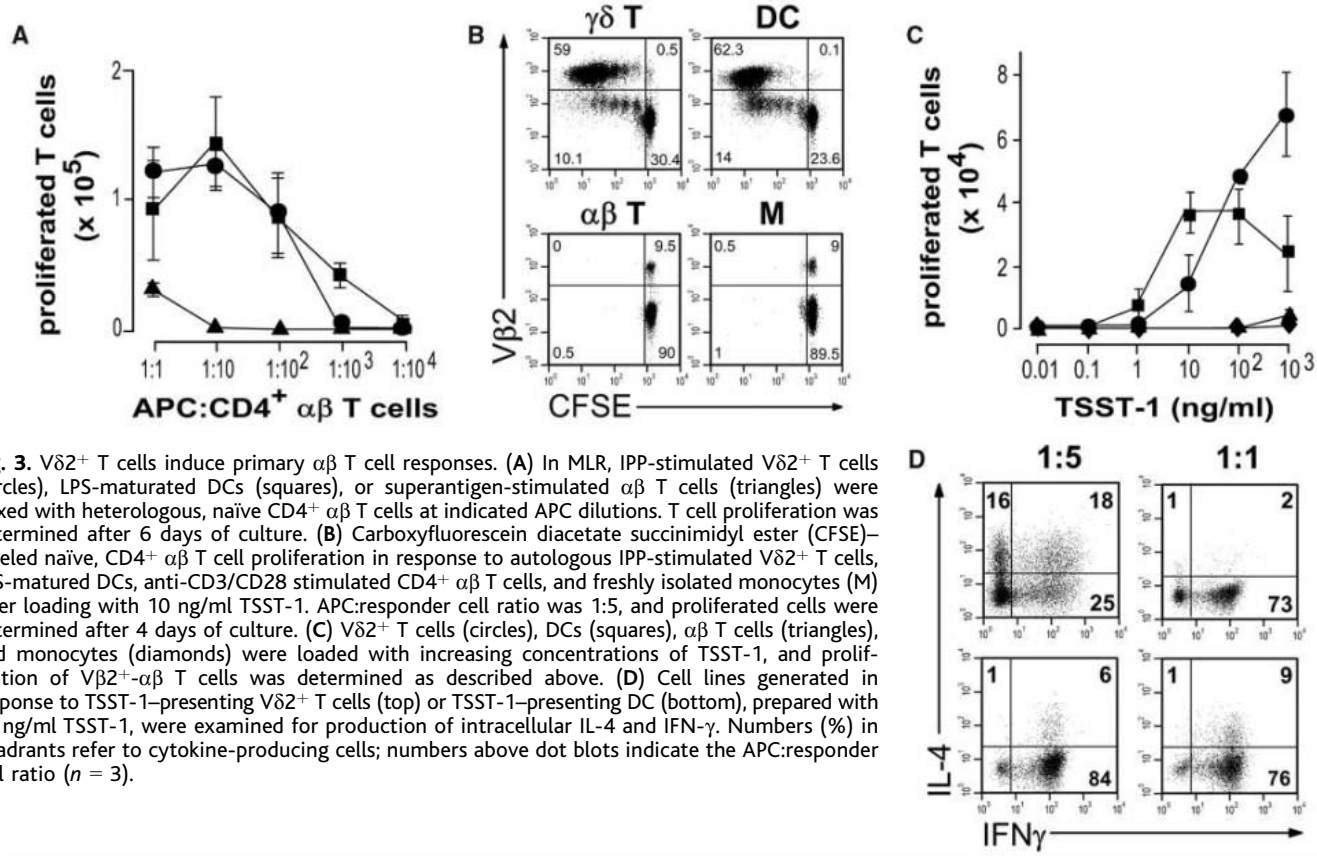

Fig. 3. Vδ2$^+$ T cells induce primary αβ T cell responses. (**A**) In MLR, IPP-stimulated Vδ2$^+$ T cells (circles), LPS-maturated DCs (squares), or superantigen-stimulated αβ T cells (triangles) were mixed with heterologous, naïve CD4$^+$ αβ T cells at indicated APC dilutions. T cell proliferation was determined after 6 days of culture. (**B**) Carboxyfluorescein diacetate succinimidyl ester (CFSE)–labeled naïve, CD4$^+$ αβ T cell proliferation in response to autologous IPP-stimulated Vδ2$^+$ T cells, LPS-matured DCs, anti-CD3/CD28 stimulated CD4$^+$ αβ T cells, and freshly isolated monocytes (M) after loading with 10 ng/ml TSST-1. APC:responder cell ratio was 1:5, and proliferated cells were determined after 4 days of culture. (**C**) Vδ2$^+$ T cells (circles), DCs (squares), αβ T cells (triangles), and monocytes (diamonds) were loaded with increasing concentrations of TSST-1, and proliferation of Vβ2$^+$-αβ T cells was determined as described above. (**D**) Cell lines generated in response to TSST-1–presenting Vδ2$^+$ T cells (top) or TSST-1–presenting DC (bottom), prepared with 10 ng/ml TSST-1, were examined for production of intracellular IL-4 and IFN-γ. Numbers (%) in quadrants refer to cytokine-producing cells; numbers above dot blots indicate the APC:responder cell ratio (n = 3).

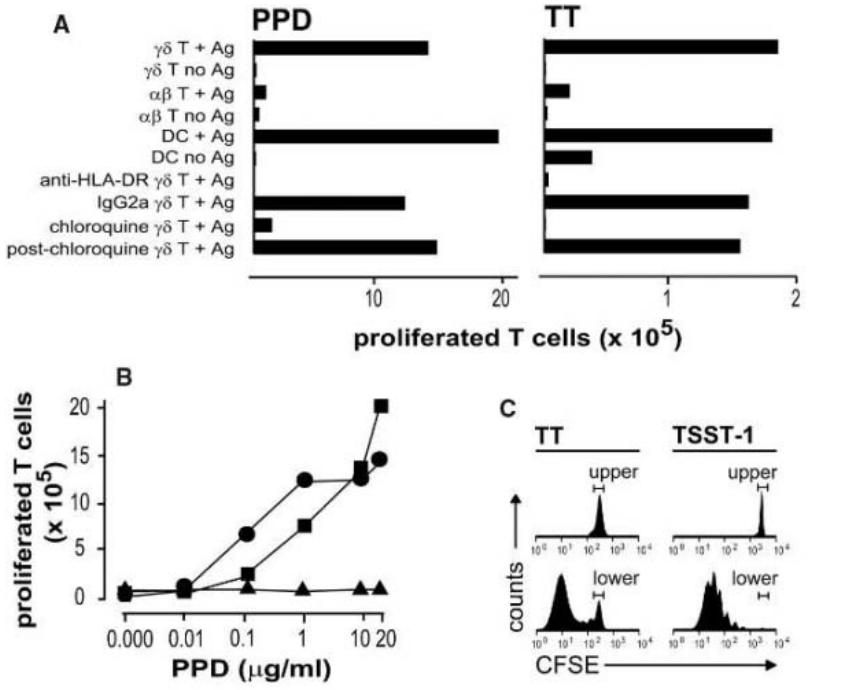

Fig. 4. Antigen processing and presentation by Vδ2$^+$ T cells. (**A**) Proliferation of fresh peripheral blood CD4$^+$ αβ T cells in response to PPD-presenting (PPD) or TT-presenting (TT) Vδ2$^+$ T cells. As control, Vδ2$^+$ T cells without antigen or antigen-presenting DCs and αβ T cells were used, and proliferation responses were determined at day 6 (PPD) or 14 (TT) of culture. Chloroquine treatment of Vδ2$^+$ T cells included treatment before and during antigen addition and treatment after antigen processing for 2 hours (post-chloroquine) followed by washing. HLA-DR or control antibodies were added to TT- or PPD-presenting Vδ2$^+$ T cells before mixing with responder cells (n = 2). (**B**) Efficiency of APC function in Vδ2$^+$ T cells evaluated by concentration-dependent proliferation of bulk primary CD4$^+$ αβ T cells. Responses to PPD-presenting Vδ2$^+$ T cells (circles) were compared with those obtained by using antigen-presenting DC (squares) or αβ T cells (triangles) after 6 days (n = 2). (**C**) Proliferation of αβ T cells is dependent on contact with TT- or TSST-1–presenting Vδ2$^+$ T cells. In a two-chamber system, the upper chambers contained either CFSE-labeled TT-specific (TT) cultured CD4$^+$ αβ T or naive CD4$^+$ αβ T (TSST-1) responder cells alone, and the lower chambers contained these responder cells together with TT- or TSST-1–presenting Vδ2$^+$ T cells at an APC:responder cell ratio of 1:5. Proliferation (reduction in CFSE fluorescence) was determined after 5 days of culture; undivided responder cells are indicated by bars.

gesting a specific role for these novel APCs in the initiation of pro-inflammatory immune responses. Early but transient CCR7 expression further predicts that the APC functions in activated Vδ2$^+$ T cells would be most effective in the early stage of antimicrobial immune processes. The physiological importance of the findings reported here now need to be explored and expanded within in vivo settings of human antimicrobial immunity. Considering the ease of Vδ2$^+$ T cell isolation and ex vivo manipulation as compared with that for DCs, it is possible that Vδ2$^+$ T cells may be useful targets for manipulation in vaccine research and immunotherapy (*24*, *25*, *34*–*36*).

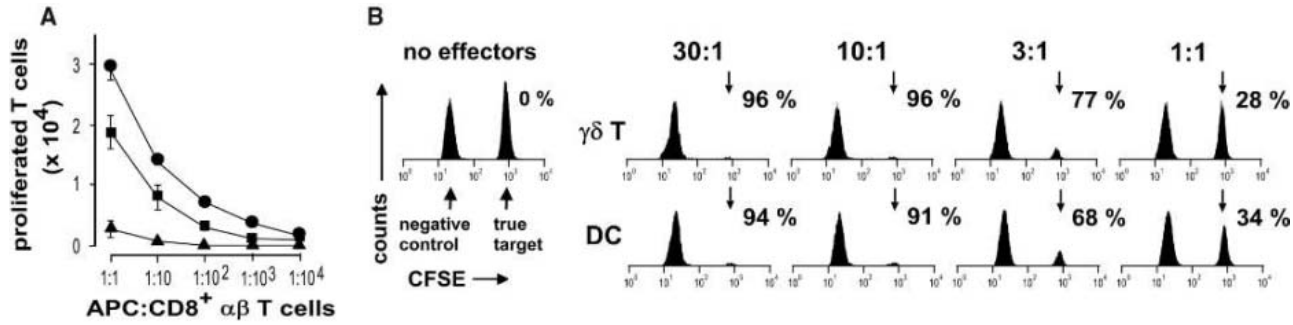

Fig. 5. Vδ2$^+$ T cells induce primary CD8$^+$ T cell responses. (**A**) MLR with naïve, CD8$^+$ αβ T cells and heterologous IPP-stimulated Vδ2$^+$ T cells (circles), LPS-matured DCs (squares), or superantigen-stimulated αβ T cells (triangles) at decreasing APC:responder cell ratios (n = 6). (**B**) CD8$^+$ T cells generated in response to heterologous Vδ2$^+$ T cells (top) or DCs (bottom) at 14 days MLR culture were examined for cytolytic activity with the use of a mixture of heterologous (true targets) and autologous (negative control) CD4$^+$ T cells that were labeled with high and low dose of CFSE, respectively. Loss in CFSE^{high} events (arrows) corresponds to percent (%) target cell killing (n = 3).

References and Notes

1. S. Shin *et al.*, *Science* **308**, 252 (2005).
2. E. J. Adams, Y.-H. Chien, K. C. Garcia, *Science* **308**, 227 (2005).
3. A. C. Hayday, *Annu. Rev. Immunol.* **18**, 975 (2000).
4. S. R. Carding, P. J. Egan, *Nat. Rev. Immunol.* **2**, 336 (2002).
5. C. T. Morita, R. A. Mariuzza, M. B. Brenner, *Springer Semin. Immunopathol.* **22**, 191 (2000).
6. M. Eberl *et al.*, *FEBS Lett.* **544**, 4 (2003).
7. Z. W. Chen, N. L. Letvin, *Trends Immunol.* **24**, 213 (2003).
8. M. Brandes *et al.*, *Blood* **102**, 3693 (2003).
9. D. S. Leslie *et al.*, *J. Exp. Med.* **196**, 1575 (2002).
10. M. S. Vincent *et al.*, *Nat. Immunol.* **3**, 1163 (2002).
11. Y. Shen *et al.*, *Science* **295**, 2255 (2002).
12. B. Moser, M. Wolf, A. Walz, P. Loetscher, *Trends Immunol.* **25**, 75 (2004).
13. Materials and methods are available as supporting material on *Science* Online.
14. J. Banchereau *et al.*, *Annu. Rev. Immunol.* **18**, 767 (2000).
15. E. S. Trombetta, I. Mellman, *Annu. Rev. Immunol.* **23**, 975 (2005).
16. K. Inaba, N. Romani, R. M. Steinman, *J. Exp. Med.* **170**, 527 (1989).
17. C. G. Figdor, Y. Van Kooyk, G. J. Adema, *Nat. Rev. Immunol.* **2**, 77 (2002).
18. Y. W. Choi *et al.*, *Proc. Natl. Acad. Sci. U.S.A.* **86**, 8941 (1989).
19. A. Langenkamp *et al.*, *Eur. J. Immunol.* **32**, 2046 (2002).
20. A. K. Abbas, K. M. Murphy, A. Sher, *Nature* **383**, 787 (1996).
21. J. Sprent, C. D. Surh, *Annu. Rev. Immunol.* **20**, 551 (2002).
22. M. P. Wymann *et al.*, *J. Biol. Chem.* **265**, 619 (1990).
23. K. Shortman, Y. J. Liu, *Nat. Rev. Immunol.* **2**, 151 (2002).
24. M. Moser, *Immunity* **19**, 5 (2003).
25. R. M. Steinman, D. Hawiger, M. C. Nussenzweig, *Annu. Rev. Immunol.* **21**, 685 (2003).
26. J. Banchereau, V. Pascual, A. K. Palucka, *Immunity* **20**, 539 (2004).
27. A. Lanzavecchia, G. Iezzi, A. Viola, *Cell* **96**, 1 (1999).
28. R. M. Steinman, *Annu. Rev. Immunol.* **9**, 271 (1991).
29. S. M. Hayes, P. E. Love, *Immunity* **16**, 827 (2002).
30. T. R. Petersen *et al.*, *Int. Immunol.* **16**, 889 (2004).
31. F. Sallusto, A. Lanzavecchia, *Immunol. Rev.* **177**, 134 (2000).
32. A. A. Itano *et al.*, *Immunity* **19**, 47 (2003).
33. R. N. Germain, M. K. Jenkins, *Curr. Opin. Immunol.* **16**, 120 (2004).
34. G. Schuler, B. Schuler-Thurner, R. M. Steinman, *Curr. Opin. Immunol.* **15**, 138 (2003).
35. C. G. Figdor, I. J. de Vries, W. J. Lesterhuis, C. J. Melief, *Nat. Med.* **10**, 475 (2004).
36. J. Banchereau, A. K. Palucka, *Nat. Rev. Immunol.* **5**, 296 (2005).

37. We thank M. Caversaccio, S. Kuchen, M. Liebi, A. Gruber, C.T. Morita, R. Pardi, and P. Schaerli for blood donations, reagents, and helpful discussions. This work was supported by grant 31-103687 from the Swiss National Science Foundation and grants 99.0471-5 and 03.0441-2 from the Staatssekretariat für Bildung und Forschung.

Supporting Online Material

www.sciencemag.org/cgi/content/full/1110267/DC1
Material and Methods
SOM Text
Figs. S1 to S5
Tables S1 and S2

26 January 2005; accepted 20 May 2005
Published online 2 June 2005;
10.1126/science.1110267
Include this information when citing this paper.

REPORTS

Single-Electron Delocalization in Hybrid Vertical-Lateral Double Quantum Dots

T. Hatano,[1] M. Stopa,[1,2] S. Tarucha[1,3]

We used a hybrid vertical-lateral double-dot device, consisting of laterally coupled vertical quantum dots, to measure the interdot tunnel coupling. By using nonlinear transport measurements of "Coulomb diamonds," we showed that an inherent asymmetry in the capacitances of the component dots influences the diamond slopes, thereby allowing for the determination of the dot through which the electron has passed. We used this technique to prepare a delocalized one-electron state and Heitler-London (HL) two-electron state, and we showed that the interdot tunnel coupling, which determines whether HL is the ground state, is tunable. This implies that our device may be useful for implementing two-electron spin entanglement.

Manipulation and verification of the state of an individual electron are at the heart of many nanoelectronic and spintronic applications, including those seeking to implement quantum computing in systems of semiconductor quantum dots. Double quantum dots (*1*–*11*) are particularly important device structures for entangled quantum bit (qubit) operations, such as that of the "exclusive or" (XOR) (*12*). Electron spin is a natural two-level system and can be used for implementing spin qubits with quantum dots (*12*). Entanglement of spin qubits is realized by manipulating the spin-spin (i. e., exchange) interaction between electrons localized on each of the two dots (*13*). The two-electron states can be represented by a Heitler-London (HL) model (*14*). The exchange interaction, which is equivalent to a splitting between the singlet and the triplet two-electron states, depends critically on tunnel coupling, which mediates the splitting of the symmetric and antisymmetric (SAS) delocalized one-electron

[1]Quantum Spin Information Project, International Cooperative Research Project, Japan Science and Technology Agency, Morinosato Wakamiya 3-1, Atsugi-shi, Kanagawa, 243-0198, Japan. [2]Center for Nanoscale Systems, Harvard University, Cambridge, MA 02138, USA. [3]Department of Applied Physics, University of Tokyo, Hongo, Bunkyo-ku, Tokyo, 113-0033, Japan.

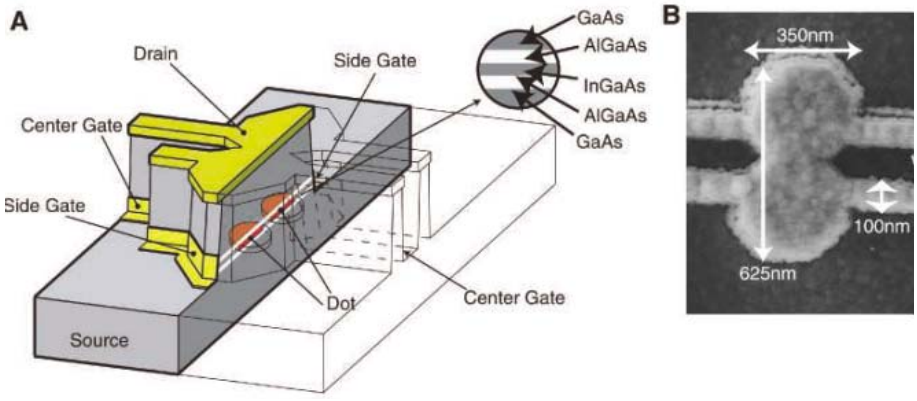

Fig. 1. (**A**) Schematic of hybrid vertical-lateral double-dot device. The two dots are vertically confined in the quantum well, which is made from the AlGaAs (7 nm)/InGaAs (12 nm)/AlGaAs (7 nm) heterostructure, and they are laterally confined by the harmonic potential, which is made of the depletion layer. The two dots are designed as octagonal shapes by electron-beam lithography. (**B**) Scanning electron micrograph of the device. The double quantum dot is located inside the 350 × 625 nm^2 mesa.

states (*15*). This coupling has been studied, for example, with microwave spectroscopy (*16*, *17*) and integrated quantum point contacts (*18*). Tuning the SAS splitting with a coupling gate between the dots thereby modulates the exchange interaction and provides a handle on entanglement of the two spins.

The hybrid vertical-lateral double-dot structure used in this experiment allows us to evaluate the filling pattern of the one-electron and two-electron states. From measurements of stability diagrams in the plane of two side-gate voltages and nonlinear conductance characteristics, we derived important parameters such as the inter- and intradot Coulomb energies and the tunnel coupling energy, which influence the electronic configurations in the double-dot structure. Thus, we confirmed the filling of the HL two-electron state, with one electron localized in each dot in the weak tunnel-coupling regime.

Our device (Fig. 1A) consists of two laterally coupled vertical dots (*19*) with four split gates. Two of the gates (side gates) are used to tune the electron numbers in the adjacent dots. The other two gates (center gates) pinch the barrier between the two dots, and modulating them principally changes the interdot barrier height. Current flows vertically from a conductive substrate through the parallel double dot to a common metal contact on the top surface. In the scanning electron micrograph of the device (Fig. 1B), four line mesas emerge from the double-dot mesa, which serve to split the Schottky gate metal, allowing the four aforementioned gates to be independently biased (*20*). In addition, the four line mesas support the metal contact to the top of the device, obviating the need for an air bridge. The mesas are sufficiently narrow (100 nm) that current only flows through the metal on the top, and not through the semiconductor. The dots are denoted L and R (left and right), and we measured the addition energies E_c^L = 1.8 meV and E_c^R = 1.4 meV, respectively, as determined by nonlinear transport measurements. The measurements described here were all carried out in a dilution refrigerator with a base temperature of 30 mK.

In the small source-drain bias (V_{sd}) limit, or "linear" regime, the conductance in parallel through the double-dot structure exhibits a series of Coulomb oscillations in the plane of the two side-gate voltages V_{sL} and V_{sR} (*21*). Crossing Coulomb oscillations parallel to V_{sL} adds an electron to a well-defined quantum state in dot L (and similarly for dot R in sweeps parallel to V_{sR}). The combined Coulomb and quantum-mechanical tunnel coupling between the dots inhibits the simultaneous addition of electrons to both dots, thereby opening up diagonal gaps, or so-called anticrossings, at the Coulomb oscillation vertices, resulting in the characteristic hexagonal or honeycomb stability diagram (Fig. 2A) (*21*). Each honeycomb cell represents a region where a given pair of electron numbers of the two dots are stable; e.g., (N_L, N_R). At cell boundaries, the total energies $E(N_L, N_R)$ of neighboring charge states are degenerate. We estimate the electron numbers in each dot to be ≤10 (and level spacings are much greater than k_BT, where k_B is Boltzmann's constant and T is temperature). The diagonal vertex lines (DVLs) in Fig. 2A mark the boundaries where a single electron tunnels from one dot to the other, i.e., $E(N_L + 1, N_R) = E(N_L, N_R + 1)$.

In the nonlinear transport regime, Coulomb diamonds (*19*) are obtained that show conductance as a function of both gate voltage and source-drain bias (Fig. 2, B to D). In the double-dot case, the gate voltage is swept along any chosen path in the V_{sL}-V_{sR} plane. Diamond regions where conductance (G) = 0 have stable electron numbers N_L and N_R. Point borders along V_{sd} = 0 between stable regions are Coulomb oscillations where the total electron number $N_L + N_R$ increases by one. Depending on the chosen gate voltage path, two electrons are added (predominantly) to dot R and then dot L (path a-b in Fig. 2A), to dot L and then dot R (path e-f), or half an electron to each dot two times (path c-d). Here, and in our analysis below, we are supposing that the region in Fig. 2A (or Fig. 2E) marked (N_L, N_R) corresponds to a filled "core," indicated by two empty states, and we concentrate on the filling of these two states at the Fermi surface (*22*). The slopes of the Coulomb diamonds reveal the reciprocal of the "lever arms" $\alpha_i \equiv C_{si}/C_{ii}$, where i = L or R, and C_{si} and C_{ii} are the side-gate capacitance and self-capacitance, respectively, of dot i (*19*). In Fig. 2B, the intersections at the two Coulomb oscillations (the X shapes) occur with two different slopes, giving the Coulomb diamond the appearance of a kite. The two different slopes indicate that the two dots have, by chance, somewhat different lever arms whereby we can distinguish into which dot a given Coulomb oscillation places an electron. In Fig. 2D, as we expect, the order in which the electrons enter the two dots is reversed from that of Fig. 2B. We plot the measured slopes of the Coulomb diamonds, changing solely $\Delta \equiv V_{sL} - V_{sR}$ (perpendicular to a-b, c-d, and e-f, see Fig. 2A) in Fig. 3A. The black dots indicate $V_a/\Delta V$ and the red dots indicate $V_b/\Delta V$, where V_a, V_b, and ΔV are defined by the schematic Coulomb diamond (inset in Fig. 3A). If the electron is fractionally added to the two dots, as it is along c-d, the slopes of the Coulomb diamonds (at the X shapes) become composites of the two lever arms and are given by

$$\tilde{\alpha}_{L(R)} = \alpha_{R(L)}(1 - \eta) + \alpha_{L(R)}\eta \qquad (1)$$

where η is the fraction of an electron added to L.

The manner in which the two electrons fill the double dot can be described by two limiting cases, which we term the HL case and the noninteracting (NI) case. In both cases, the first electron enters the lowest single-particle state [recall that we are treating the other electrons as an inert core (*22*)]. This state is a symmetric combination of states localized on the left and on the right, $\phi_S = \phi_L \sin^2\theta + \phi_R \cos^2\theta$, where ϕ_S is the symmetric state function and $\theta = \tan^{-1}\left[(\Delta/2t) + \sqrt{1 + (\Delta/2t)^2}\right]$. Here, t is the tunnel coupling of the two states. Exactly on the DVL, $\Delta = 0$ and $\theta = \pi/4$. As $\theta \to 0$, $\phi_S \to \phi_R$ and as $\theta \to \pi/2$, $\phi_S \to \phi_L$. Thus, for the first electron, $\eta = \sin^2\theta$. In the noninteracting limit, the second electron occupies the opposite spin state of the same spatial state, and the two-particle state (suppressing the spin part) is simply $\phi_S(\mathbf{r}_1)\phi_S(\mathbf{r}_2)$, where $\mathbf{r}_1$ and $\mathbf{r}_2$ are the coordinates of two electrons, respectively. Note that ϕ_S, despite the name "symmetric", does not have equal probability in dots L and R except at $\Delta = 0$. The correlated HL limit, on the other hand, takes the (spatial symmetrized) two-electron state as $[\phi_L(\mathbf{r}_1)\phi_R(\mathbf{r}_2) + \phi_R(\mathbf{r}_1)\phi_L(\mathbf{r}_2)]$, which

has identically one electron in each dot, independent of Δ. In the HL limit, the final state is always (N_L + 1, N_R + 1). This implies that for the second (primed) electron, $\eta' = 1 - \eta = \cos^2\theta$. We assume here that the second electron forces the creation of two localized states and that it pushes the first electron into one and occupies the other; i.e., the HL limit (Fig. 2E). In that case, Eq. 1 can be plotted simply as a function of Δ for $\eta = \sin^2\theta$ and $\eta' = 1 - \eta = \cos^2\theta$, given a knowledge of t. Figure 3A shows a fit of the measured (inverse) lever arms (black and red circles) from the diamond slopes (several additional sweeps parallel to those in Fig. 2A have been performed) that yield the following values of t, which differ slightly for the first and second electron: t = 0.079 and 0.084 meV, respectively. We calculated η and 1 –η using Fig. 3A and Eq. 1, and the results are plotted in Fig. 3B. The functions are well reproduced by calculations of $\sin^2\theta$ and $\cos^2\theta$. As Δ becomes large, an electron initially localized in dot R becomes delocalized in the symmetric state, and then localized again but in dot L (Fig. 2E).

An additional check of the extracted value of t is provided for this anticrossing by measuring the dependence of the magnetic field B on the anticrossing gap size (converted to energy with the dot capacitances) (Fig. 4). Assuming that we are in the correlated HL regime, the distance along the DVL between the Coulomb oscillations can be written as $\Delta V = V_{inter} + 2t$, where V_{inter} is the interdot Coulomb interaction. (*21*). As B increases, the tunnel coupling is expected to become negligibly small because of the contraction of the wave functions localized in the two dots. However, V_{inter} should be practically independent of the wave function extent and therefore roughly independent of B. The stability diagram at B = 2 T is shown in the upper inset of Fig. 4. The corresponding ΔV is enclosed by a yellow circle. It is confirmed that the anticrossing ΔV becomes small and is a sharp form like the classical honeycomb diagram. We conclude that at high B, the saturation value of ΔV is given simply by $V_{inter} \approx$ 0.175 meV, and therefore the variation of ΔV between B = 0 T and the saturation limit is a measure of $2t$. The value of the tunneling coefficient extracted in this way is t = 0.075 meV, which is in reasonable agreement with that obtained from the Coulomb diamond asymmetry.

We now discuss the correlating influence of the second added electron and our assumption of the HL state. First we estimate the energy necessary to add two electrons to the same spatial state (NI model). If we denote a typical intradot Coulomb matrix element for dot L or R as V^L_{intra} or V^R_{intra}, respectively, and a typical interdot matrix element as V_{inter}, and if we ignore exchange and other higher-order interaction terms (*23*), then the NI addition energy to go from 0 to 2 electrons, proportional to the length of the diagonal lines

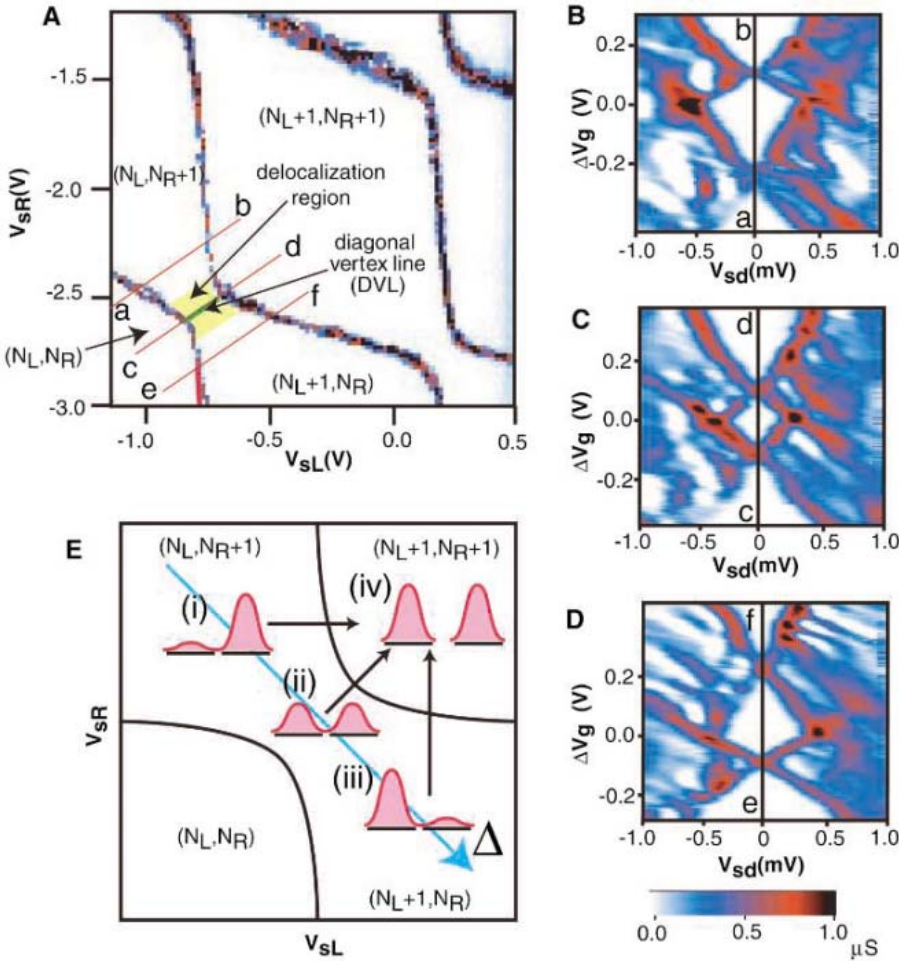

Fig. 2. (**A**) Charging diagram in parallel through the double dot as functions of the two side-gate voltages V_{sL} and V_{sR}. The center-gate voltage is fixed at V_c = –2.4 V and source-drain voltage V_{sd} = 8 μV. (**B** to **D**) Differential conductance dI_{sd}/dV_{sd} by sweeping both the gate voltage and the source-drain bias. The gate voltages V_{sL} and V_{sR} of (B) to (D) are swept along the red lines a-b, c-d, and e-f in (A), respectively. In (B) and (D), the diamonds for the double dot are clearly asymmetric. In (C), on the other hand, the Coulomb diamond is very symmetrical, like that of a single dot, and the slopes are intermediate between the slopes characterizing the two dots independently. This implies that the highest filled state is delocalized across the two dots. (**E**) Schematic of a single anticrossing. This shows evolution along the diagonal from the state localized in dot R, to a single electron delocalized across both dots, to a state localized in dot L. The second electron will occupy one dot while forcing the first electron to occupy the other. This is the strongly correlated state, the HL limit (*14*).

such as a-b, c-d, and e-f in Fig. 2A or, alternatively, to the spacing between Coulomb oscillations, is $E_C(\mathrm{NI}) = \eta^2 V^L_{intra} + (1 - \eta)^2 V^R_{intra} + 2\eta(1 - \eta)V_{inter}$. The HL state, by contrast, has a constant Coulomb energy of V_{inter}, so that its addition energy is $E_C(\mathrm{HL}) = V_{inter} + E_A - E_S$, where the energy of the antisymmetric state $E_A = (\varepsilon_L + \varepsilon_R)/2 + \sqrt{[t^2 + (\Delta/2)^2]}$ and the energy of the symmetric state $E_S = (\varepsilon_L + \varepsilon_R)/2 - \sqrt{[t^2 + (\Delta/2)^2]}$, where ε_L and ε_R are the single-particle levels in each dot. The Δ dependence of the HL energy is entirely contained in the single-particle energies, whereas for the NI model, η depends on Δ, and so the Coulomb energy varies as we move away from the DVL.

The expressions for E_C(NI) and E_C(HL) depend on the intradot Coulomb matrix elements, which are approximately given by the charging energies of the two dots (1.8 and 1.4 meV). As noted above, the high B saturation of the anticrossing provides a value of V_{inter} = 0.175 meV. Then, using t = 0.08 meV, we plot the functions E_C (NI) and E_C(HL) versus Δ, as shown in the lower inset of Fig. 4. We have also plotted the spacing (ΔV) between Coulomb oscillations weighted by the average lever arms (blue triangles in Fig. 4). For small |Δ|, the HL addition energy is far below the NI energy, justifying our assumption of its validity in this regime. For sufficiently large |Δ|, the gap between E_S and E_A exceeds the Coulomb cost of double occupancy, and the NI state becomes lower in energy. The experimental data of the spacing between measured Coulomb oscillations nearly agrees

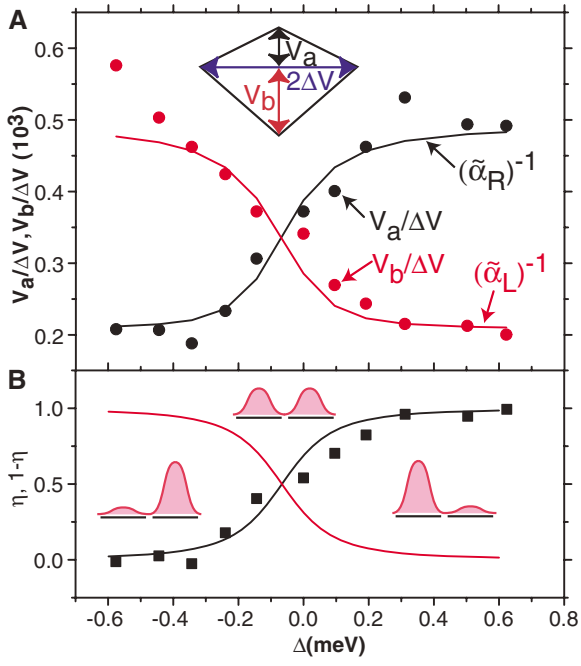

Fig. 3. (**A**) Δ dependence of the slope of Coulomb kites. We performed several additional gate-voltage sweeps parallel to the three illustrated in Fig. 2A. The black dots indicate $V_a/\Delta V$ and the red dots indicate $V_b/\Delta V$. V_a, V_b, and ΔV are defined by the schematic Coulomb diamond (inset). The black ($\tilde{\alpha}_R$) and red ($\tilde{\alpha}_L$) curves are plotted along with a fit of the data to Eq. 1. The two curves yield values of t that differ slightly, $t = 0.079$ and 0.084 meV. (**B**) Δ dependence of the fractions η and 1 − η of an electron added to dot L and dot R. The black squares indicate the average of the values η calculated from both data of $V_a/\Delta V$ and $V_b/\Delta V$ using Eq. 1. The black and red curves are calculations of $\eta = \sin^2\theta$ and $1 - \eta = \cos^2\theta$ with a parameter $t = 0.082 = (0.079 + 0.084)/2$ meV.

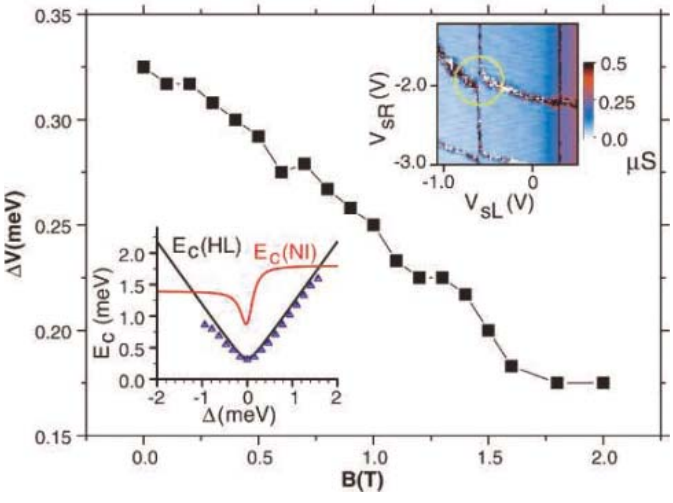

Fig. 4. *B* dependence of the anticrossing gap size (Δ*V*) converted to energy with the dot capacitances. The variation of Δ*V* between $B = 0$ and the saturation limit is a measure of $2t = 0.15$ meV. (Upper inset) Stability diagram at $B = 2$ T. (Lower inset) Charging energies E_C(HL) and E_C(NI) for the HL (black line) and NI (red line) addition of two electrons, using $V^L_{intra} = 1.8$ meV, $V^R_{intra} = 1.4$ meV, $V_{inter} = 0.175$ meV, and $t = 0.08$ meV. The spacing (Δ*V*) between measured Coulomb oscillations, weighted by the average lever arms, is shown as blue triangles.

with E_C(HL). Thus our two-electron state is HL up to around the borders of the honeycomb cell. We are able to estimate an exchange coupling energy $J = 4t^2/(V_{intra} - V_{inter}) = 0.021$ meV, using $t = 0.08$ meV, $V_{intra} = 1.4$ meV, and $V_{inter} = 0.175$ meV. The J is much smaller than $2t$, V_{inter}, and V_{intra}, indicating that the HL model is a good approximation.

Finally, we discuss the relevance of our coupled dot device for implementing a quantum gate and quantum entanglement. In our device, the exchange coupling J between two electron spins in two dots is tunable with magnetic field and cente-gate voltage (*11*). The temporal control of J between $J = 0$ and $\neq 0$ enables the swapping of two spins (*12*) by applying a pulsed voltage to the center gate between the dots. The operation time τ_{swap} is, for example, $\tau_{swap} \approx 100$ ps for $J = 0.02$ meV, which we estimated for $t = 0.08$ meV in our experiments. This J can be too small to perform reliable quantum gate operations, and the τ_{swap} is not short enough as compared to the decoherence time. We have very recently obtained $J \geq 0.1$ meV in a similar but smaller double-dot device and also by carefully tuning the center-gate voltage. Thus, the estimated $\tau_{swap} < 20$ ps is much shorter than the decoherence time and electrically accessible to change the t value as a function of center-gate voltage.

One way to test quantum spin entanglement is to measure Aharonov-Bohm (AB) oscillations when an HL state is present in the double-dot device. Theory predicts that the HL state undergoes a transition from a two-electron singlet state to the triplet state with increasing magnetic field. The singlet is an entangled state, and the transition is signified by a π shift in the AB oscillations (*24*, *25*). In addition, XOR is realized by combining the swap operation and the single spin rotation (*12*). Particularly for the spin rotation, it will be necessary to modify our device design to implement, for example, pulsed local electron spin resonance.

References and Notes

1. C. Livermore, C. H. Crouch, R. M. Westervelt, K. L. Campman, A. C. Gossard, *Science* **274**, 1332 (1996).
2. J. M. Golden, B. I. Halperin, *Phys. Rev. B* **53**, 3893 (1996).
3. K. A. Matveev, L. I. Glazman, H. U. Baranger, *Phys. Rev. B* **54**, 5637 (1996).
4. R. H. Blick, D. Pfannkuche, R. J. Haug, K. v. Klitzing, K. Eberl, *Phys. Rev. Lett.* **80**, 4032 (1998).
5. M. Brodsky, N. B. Zhitenev, R. C. Ashoori, L. N. Pfeiffer, K. W. West, *Phys. Rev. Lett.* **85**, 2356 (2000).
6. M. Rontani, F. Troiani, U. Hohenester, E. Molinari, *Solid State Comm.* **119**, 309 (2001).
7. A. W. Holleitner, R. H. Blick, A. K. Küttel, K. Eberl, J. P. Kotthaus, *Science* **297**, 70 (2002).
8. J. M. Elzerman *et al.*, *Phys. Rev. B* **67**, 161308 (2003).
9. M. Pioro-Ladrière *et al.*, *Phys. Rev. Lett.* **91**, 026803 (2003).
10. I. H. Chan *et al.*, *Nanotechnology* **15**, 609 (2004).
11. T. Hatano *et al.*, *Phys. Rev. Lett.* **93**, 066806 (2004).
12. D. Loss, D. P. DiVincenzo, *Phys. Rev. A.* **57**, 120 (1998).
13. G. Burkard, D. Loss, D. P. DiVincenzo, *Phys. Rev. B* **59**, 2070 (1999).
14. P. Fulde, *Electron Correlations in Molecules and Solids* (Springer, Berlin, 1995).
15. S. Amaha *et al.*, *Solid States Commun.* **119**, 183 (2001).
16. T. H. Oosterkamp *et al.*, *Nature* **395**, 873 (1998).
17. H. Qin, A. W. Holleitner, K. Eberl, R. H. Blick, *Phys. Rev. B* **64**, 241302 (2001).
18. L. DiCarlo *et al.*, *Phys. Rev. Lett.* **92**, 226801 (2004).
19. S. Tarucha, D. G. Austing, T. Honda, R. J. van der Hage, L. P. Kouvenhoven, *Phys. Rev. Lett.* **77**, 3613 (1996).
20. D. G. Austing, T. Honda, S. Tarucha, *Semicond. Sci. Technol.* **12**, 631 (1997).
21. W. G. van der Wiel *et al.*, *Rev. Mod. Phys.* **75**, 1 (2003).
22. Qualitatively, the core electrons make this double-dot system different in two ways from the Hund-Mulliken model, where a single electron occupies the lowest level of each dot. First, the core provides screening of all the Coulomb matrix elements. Second, the states at the Fermi surface must be orthogonal to all the core states. The only case where such features will undermine our analysis is where level degeneracy occurs at the Fermi surface, a case that we expect to be rare.
23. HL is the limiting case of the Hund-Milliken method, where double occupancy is ignored. It is this double occupancy in the Hund-Milliken method that lowers the energy of the singlet so that it becomes the ground state, as compared to the triplet, even though the exchange energy favors spin alignment (i.e., the triplet). In our treatment, we have ignored both the delocalization energy and the exchange, which we find are only small perturbations on our results.
24. D. Loss, E. V. Sukhorukov, *Phys. Rev. Lett.* **84**, 1035 (2000).
25. We previously used a similar device to observe AB oscillations but not related to HL states (*26*).
26. T. Hatano *et al.*, *Physica E (Amsterdam)* **22**, 534 (2004).
27. We thank T. Yamaguchi, T. Ota, K. Yamada, T. Sato, S. Teraoka, T. Inoshita, W. Izumida, A. Shibatomi, T. Maruyama, K. Ono, S. Amaha, Y. Nishi, S. Sasaki, and D. G. Austing for experimental help and useful discussions. Part of this work is financially supported by the Grant-in-Aid for Scientific Research A (no. 40302799) by Core Research for Evolutional Science and Technology–Japan Science and Technology Agency; by the Focused Research and Development Project for the Realization of the World's Most Advanced Information Technology (IT) Nation; IT Program-Ministry of Education, Culture, Sports, Science, and Technology; and by the Defense Advanced Research Projects Agency–Quantum Information Science and Technology program (grant DAAD19-01-1-0659).

17 February 2005; accepted 23 May 2005
10.1126/science.1111205

Tunable Supercurrent Through Semiconductor Nanowires

Yong-Joo Doh,[1]* Jorden A. van Dam,[1]* Aarnoud L. Roest,[1,2]
Erik P. A. M. Bakkers,[2] Leo P. Kouwenhoven,[1]
Silvano De Franceschi[1]†

Nanoscale superconductor/semiconductor hybrid devices are assembled from indium arsenide semiconductor nanowires individually contacted by aluminum-based superconductor electrodes. Below 1 kelvin, the high transparency of the contacts gives rise to proximity-induced superconductivity. The nanowires form superconducting weak links operating as mesoscopic Josephson junctions with electrically tunable coupling. The supercurrent can be switched on/off by a gate voltage acting on the electron density in the nanowire. A variation in gate voltage induces universal fluctuations in the normal-state conductance, which are clearly correlated to critical current fluctuations. The alternating-current Josephson effect gives rise to Shapiro steps in the voltage-current characteristic under microwave irradiation.

The recent interest in chemically grown semiconductor nanowires arises from their versatility, which translates into a wide range of potential applications. Many important proofs of concept have already been provided, such as field-effect transistors, elementary logic circuits, resonant tunneling diodes, light-emitting diodes, lasers, and biochemical sensors (*1*–*3*). These achievements, together with the recent advance in the monolithic integration of III-V nanowires with standard Si technology (*4*, *5*), hold great promise for the development of next-generation (opto)electronics. Simultaneously, the high degree of freedom in nanowire growth and device engineering creates new opportunities for the fabrication of controlled one-dimensional systems for low-temperature applications and fundamental science. Quantum confinement and single-electron control have been achieved in a variety of single-nanowire devices (*6*–*8*). In these experiments, the transport properties were dominated by Coulomb interactions among conduction electrons because of the presence of high-resistance barriers either at the interface with the metal leads or within the nanowire itself.

Here we describe an entirely different regime, in which the nanowires are contacted by superconducting electrodes with deliberately low contact resistance. While Coulomb blockade effects are suppressed, the semiconductor nanowires acquire superconducting properties because of the proximity effect, a well-known phenomenon that can be described as the leakage of Cooper pairs of electrons from a superconductor (S) into a normal-type conductor (N) (*9*). The proximity effect takes place only if the S-N interface is highly transparent to electrons. This requirement is particularly hard to meet when the N element is a semiconductor, the major obstacle being posed in most cases by the unavoidable presence of a Schottky barrier. In this respect, indium arsenide (InAs) is an exceptional semiconductor because it can form Schottky barrier–free contacts with metals (*10*). This motivated our choice of this material in the present work.

The InAs nanowires are grown via a catalytic process based on a vapor-liquid-solid mechanism (*11*). The nanowires are monocrystalline, with diameters ranging from 40 to 130 nm and lengths of 3 to 10 μm. From field-effect electrical measurements (discussed below), we find *n*-type conductivity, with an average electron density n_s = (2 to 10) × 10^{18} cm^{-3}, and an electron mobility μ = 200 to 2000 $cm^2/V{\cdot}s$. These values correspond to a mean free path, l = 10 to 100 nm. Right after growth, the nanowires are transferred to a p^+ silicon substrate with a 250-nm-thick SiO_2 overlayer. The conductive substrate is used as a back gate to vary the electron density in the nanowires. Custom metal electrodes are defined by e-beam lithography followed by e-beam evaporation of Ti (10 nm)/Al (120 nm). Before metal deposition, the nanowire surface is deoxidized by a 6-s wet etching in buffered hydrofluoric acid. No thermal annealing is performed, in order to minimize interdiffusion at the contacts. The spacing, L, between the source and drain electrodes is varied between 100 and 450 nm. To perform four-point measurements, both source and drain electrodes are split in two branches (Fig. 1A). A representative single-nanowire device is shown in Fig. 1B.

The nanowire devices exhibit ohmic behavior with a normal state resistance, R_N, in the range from 0.4 to 4.5 kilohms. R_N is virtually insensitive to temperature all the way down to the superconducting transition temperature of the Al-based electrodes, T_C = 1.1 K. Below T_C, the proximity effect manifests itself through the appearance of a dissipationless supercurrent, which can be viewed as a

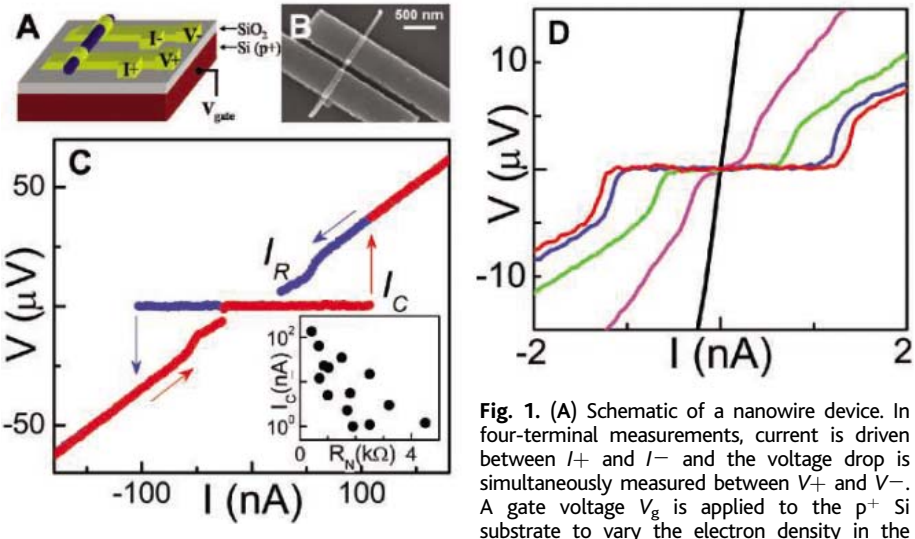

Fig. 1. (**A**) Schematic of a nanowire device. In four-terminal measurements, current is driven between $I+$ and $I-$ and the voltage drop is simultaneously measured between $V+$ and $V-$. A gate voltage V_g is applied to the p^+ Si substrate to vary the electron density in the nanowire. (**B**) Scanning electron micrograph of a nanowire device. The nanowire diameter is determined by the size of the gold catalytic particle, which is visible at the upper end of the nanowire. (**C**) $V(I)$ characteristics for device no. 1 measured in a four-terminal configuration at T = 40 mK for both increasing (red) and decreasing (blue) current bias. (Inset) Correlation between I_C and R_N (the data points correspond to different devices and V_g = 0). (**D**) $V(I)$ characteristics of device no. 2 at T = 40 mK for V_g = 0 (red), –10 (blue), –50 (green), –60 (purple), and –71 V (black). When V_g is made more negative, the critical current is progressively reduced all the way to zero. When the supercurrent vanishes, the zero-bias resistance of the device is 70 kilohms. The characteristic parameters at V_g = 0 are I_C = 1.2 nA and R_N = 4.5 kilohms.

[1]Kavli Institute of Nanoscience, Delft University of Technology, Post Office Box 5046, 2600 GA Delft, Netherlands. [2]Philips Research Laboratories, Professor Holstlaan 4, 5656 AA Eindhoven, Netherlands.

*These authors contributed equally to this work
†Present address: Laboratorio Nazionale TASC-INFM, I-34012 Trieste, Italy.

consequence of the diffusion of Cooper pairs throughout the entire length of the nanowire section between the two superconducting electrodes. (This requires the phase-coherence length for electron propagation in the nanowire to be longer or at least comparable to the distance between source and drain contacts.) To investigate this superconductivity regime, we performed four-terminal dc measurements, in which the voltage across the nanowire, V, is measured while sweeping the bias current, I. In Fig. 1C we show a representative measurement taken at base temperature T = 40 mK. The $V(I)$ characteristic exhibits a clear supercurrent branch (that is, a region of zero resistance) as well as a dissipative quasiparticle branch with a dependence on the sweeping direction of the source-drain current. The switching from superconductive to dissipative conduction occurs when I approaches a critical current, I_C, leading to the abrupt appearance of a finite voltage. The reversed switching, from resistive to superconductive regime, occurs at a lower current level I_R. The observed $V(I)$ characteristics, as well as their hysteretic behavior, are typically found in capacitively shunted Josephson junctions (*12*). (In our devices, the shunting capacitors are formed between the source-drain electrodes and the conductive Si substrate.)

The presence of a supercurrent has been assessed in 14 devices (90% yield) with critical currents ranging from a few nA to 135 nA at 40 mK (see fig. 2S for the temperature dependence). On average, I_C decreases with R_N (inset in Fig. 1C), and the I_CR_N product, a typical figure of merit for Josephson junctions, varies between 2 and 60 μV. The highest value is comparable to the expectation for an ideal S-N-S junction embedding a short and diffusive ($l < L$) normal conductor; that is, $I_CR_N \sim \Delta_0/e$, where Δ_0 = 100 to 120 μeV is the superconducting energy gap of the contact electrodes obtained from finite-voltage measurements discussed below. The semiconductor nature of the nanowires allows the magnitude of the critical current to be controlled by a voltage, V_g, applied to the back-gate electrode (*13–17*). Because of their n-type character, a negative V_g results in a reduction of the electron concentration in the nanowires, leading to a higher R_N and hence a lower I_C. Thus, the nanowires can operate as tunable superconducting weak links. For sufficiently negative gate voltages, I_C is entirely suppressed (Fig. 1D), where the "off" state (I_C = 0) is reached for $V_g \approx -70$ V. This large voltage is due to the weak capacitive coupling between the nanowire conducting channel and the back gate. The use of alternative gating geometries, such as local top gates or gate-around configurations, would provide a much stronger coupling and, at the same time, the possibility of individually controlling different nanowires on the same chip. This would allow a bottom-up assembly of superconducting integrated circuits based on independently addressable S-N-S elements.

To gain more insight into the Josephson behavior of the nanowire S-N-S junction, we investigated the effect of an external microwave field. Because of phase locking between the microwave angular frequency ω_{rf} and the voltage-dependent Josephson frequency (*18*) $\omega_J = 2eV/\hbar$, the $V(I)$ characteristic exhibits voltage plateaus at $V_n = n\hbar\omega_{rf}/2e$, the Shapiro steps (*12*) (here $\hbar$ is Planck's constant, e is the electron charge, and n = 0,±1,±2,…). A representative set of plateaus (up to $|n|$ = 4) is shown in Fig. 2A in the case of 4-GHz radiation. A $V(I)$ curve for the same device in the absence of the microwave field is also shown for direct comparison. We varied the microwave frequencies in the 2- to 10-GHz range in order to verify the proportionality relation between the step height ΔV and ω_{rf}. As shown in the inset in Fig. 2A, the experimental values fall on top of the expected linear dependence $\Delta V = (\hbar/2e)\omega_{rf}$. By increasing the microwave field proportionally to the square root of the externally applied microwave power P_{rf}, higher-order steps become progressively visible and their step width, ΔI_n, exhibits quasi-periodic oscillations. This behavior emerges clearly in a plot of differential resistance, dV/dI, as a function of $P_{rf}^{1/2}$ and source-drain current. In Fig. 2B we show an example of such plots corresponding to the same microwave frequency (4 GHz). The Shapiro steps appear as dark regions (dV/dI = 0) separated by bright (high-dV/dI) lines corresponding to the sharp boundary between consecutive steps. The wiggling behavior of these lines reflects the quasi-periodic oscillations in ΔI_n. These oscillations are quantitatively shown in Fig. 2C for n = 0 to 4. We find good agreement with the theoretical expectation $\Delta I_n = 2I_C|J_n(2ev_{rf}/\hbar\omega_{rf})|$ (*12*), where J_n is the n-th order Bessel function and v_{rf} is the amplitude of rf voltage across the nanowire junction. I_C and a scaling factor, α, for the horizontal axis ($v_{rf} = \alpha P_{rf}^{1/2}$) are the only fitting parameters for all of the five theoretical curves. The observed Shapiro steps represent clear evidence of genuine Josephson coupling through the nanowire.

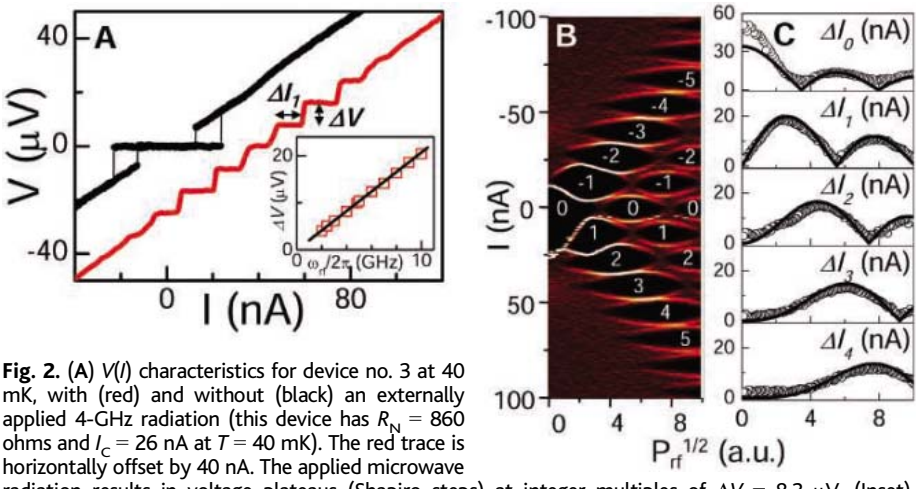

Fig. 2. (**A**) $V(I)$ characteristics for device no. 3 at 40 mK, with (red) and without (black) an externally applied 4-GHz radiation (this device has R_N = 860 ohms and I_C = 26 nA at T = 40 mK). The red trace is horizontally offset by 40 nA. The applied microwave radiation results in voltage plateaus (Shapiro steps) at integer multiples of ΔV = 8.3 μV. (Inset) Measured voltage spacing ΔV (symbol) as a function of microwave angular frequency ω_{rf}. The solid line (theory) shows the agreement with the ac Josephson relation $\Delta V = \hbar\omega_{rf}/2e$. (**B**) dV/dI plotted on a color scale as a function of the bias current I and the square root of the microwave excitation power P_{rf}. In this plot, the microwave frequency is fixed at 4 GHz. The voltage plateaus at $V_n = n\hbar\omega_{rf}/2e$ appear as black regions (dV/dI = 0) labeled by the corresponding integer index n. These regions are delimited by bright lines (high dV/dI) corresponding to the sharp increase of the V between consecutive plateaus. At lower frequencies, we have also observed half-integer steps, such as n = ±1/2, ±3/2,… (fig. S3). (**C**) Current width ΔI_n of the n-th Shapiro steps (n = 0,1,2,3,4) versus $P_{rf}^{1/2}$ as extracted from (**B**). The five solid lines are Bessel-type functions obtained from a single two-parameter fit.

We now discuss in more detail the basic properties of the S-N-S nanowire devices and elucidate their mesoscopic nature. At the onset of the quasi-particle branch (just above I_C), the device conductance is found to be higher than the normal-state value $G_N = 1/R_N$. This is apparent from the slope of the wide-range $I(V)$ characteristic shown in the inset of Fig. 3A (red trace). Only for $V > 0.3$ mV does the slope change to the normal-state value, as becomes clear by a comparison with an $I(V)$ trace taken at 100 mT (black trace), a magnetic field high enough to suppress superconductivity in the electrodes. Evidently, the high-bias linear $I(V)$ at zero field does not extrapolate to the origin, as in the normal state, but to a finite excess current I_{exc} = 0.23 μA. The enhanced conductance at low bias and the consequent excess current provide a clear indication of strong Andreev reflection (*19*): An electron above the Fermi energy coming from the N region is reflected at the S-N interface as a phase-conjugated hole (that is,

the lack of an electron below the Fermi energy) while at the same time creating a Cooper pair in the S region. Andreev reflection at the S-N interface and phase-coherent electron propagation in the normal conductor can be viewed as the microscopic origin of the proximity effect (*10*, *20*). Being a two-particle process, Andreev reflection requires high interface transparency. Under this condition, it enables electrical conduction at subgap voltages, $eV < 2\Delta_0$, where the factor 2 accounts for the presence of two S-N interfaces in series. A subgap conductance, G_{AR}, larger than the normal-state value (up to 2 G_N) can be observed in the case of almost ideal interfaces having a transmission coefficient, T_{int}, close to unity. Shown in Fig. 3A is a plot of the differential conductance dI/dV versus V for the same nanowire device. We find $G_{AR}/G_N \approx 1.4$, and from the value of I_{exc} we estimate $T_{int} \approx 0.75$ (*21*). Similar values are consistently obtained for most of the devices (fig. S4). This high transparency is in line with the best results ever achieved for micrometer-scale superconductor/semiconductor interfaces (*22*). Besides an overall conductance enhancement, the subgap regime is characterized by a series of peaks in dI/dV occurring at $V = 2\Delta_0/me$ (and m = 1, 2, 3) and denoted by vertical arrows. These peaks are due to multiple Andreev processes (*23*–*25*). Between two consecutive Andreev reflections the motion of electron-like (or hole-like) quasiparticles between the two S-N interfaces is diffusive ($l < L$) but phase-coherent.

This mesoscopic character of the nanowire S-N-S junctions emerges clearly from a detailed analysis of the V_g dependence. I_C exhibits reproducible and time-independent fluctuations. In a color plot of dV/dI versus (V_g,I), shown in Fig. 3B, these appear as irregular variations in the I width of the zero-dV/dI supercurrent branch (black region). The superimposed white trace illustrates the evolution of the corresponding normal-state conductance G_N over the same V_g range. Interestingly, $I_C(V_g)$ and $G_N(V_g)$ fluctuations exhibit a clear correlation, which indicates a common physical origin. We interpret these $G_N(V_g)$ oscillations as universal conductance fluctuations (UCFs) (*26*) associated with the phase-coherent diffusive motion along the nanowire. Similar $G_N(V_g)$ fluctuations are also found in the other nanowire devices. The corresponding root mean square (RMS) amplitudes, δG_N, are reported in Fig. 3C. We find an average value of 0.55 e^2/h, which is very close to the expectation for UCF in a phase-coherent quasi–one-dimensional conductor ($\delta G_N = 0.7\ e^2/h$). I_C fluctuations arising from the diffusive motion of electrons in a disordered weak link have been theoretically addressed for two distinct conditions: $\Delta_0 \ll E_{Th}$ (*27*) and $\Delta_0 \gg E_{Th}$ (*28*), where $E_{Th} = \hbar D/L^2$ is the Thouless energy in the normal conductor and D is the diffusion coefficient. In the first case, which is the most pertinent to the present study (Fig. 3C), a universal limit of $\delta I_C \sim e\Delta_0/\hbar$ is expected for the RMS amplitude of the I_C fluctuations, in analogy with universal conductance fluctuations in the normal state. Experimentally, we find δI_C = 0.2 to 3 nA, which is much smaller than the expected value (~25 nA). This discrepancy could be due to non-ideal interface transparency or to an incomplete screening from the electromagnetic environment.

Finally, we would like to comment on the reproducibility of the results presented above as well as on the prospects for nanowire-based S-N structures. About 90% of the devices fabricated in this work have a normal-state resistance below a few kilohms and exhibit a supercurrent branch at low temperature. This indicates reproducibly low contact resistances, an important requirement for successful scaling up to even small superconducting circuits incorporating multiple nanowire devices. The functionalities of these circuits could be integrated with conventional silicon technology or with solid-state quantum computer architectures currently under study. For instance, electrically tunable Josephson nanojunctions may be used as building blocks for superconducting quantum interference devices, in which the circulating supercurrent can be switched on and off by a control voltage. Such devices may serve as switchable coupling elements between superconducting qubits (*29*, *30*). Several important issues still need to be addressed, such as the local gating of individual nanowires and the replacement of Al with wider-gap superconductors allowing for higher operation temperatures. We believe, however, that InAs-based semiconductor nanowires can already provide a convenient basis for the development of more complex hybrid nanostructures, which may enable the investigation of exotic and so-far elusive phenomena resulting from the interplay between size quantization and different types of electron-electron correlations such as superconductivity, Coulomb interactions, and Kondo-type correlations.

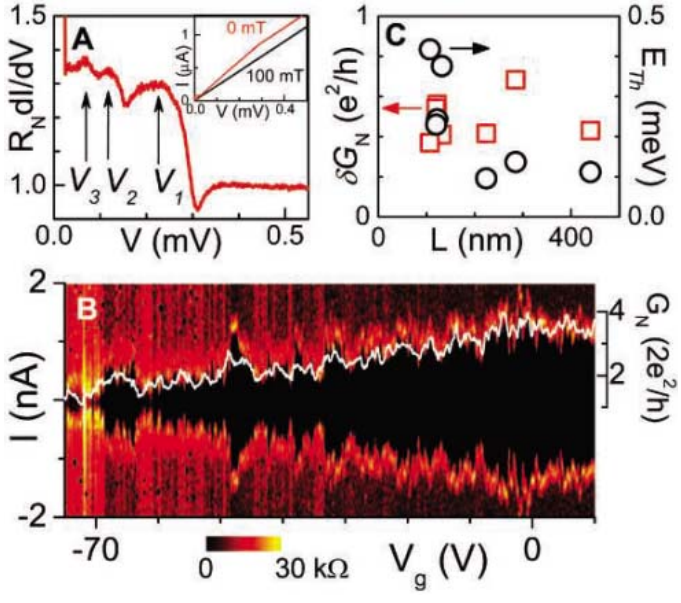

Fig. 3. (**A**) V dependence of dI/dV, normalized to the normal-state value R_N^{-1} for device no. 1. The vertical arrows indicate three dI/dV maxima at $V_m = 2\Delta_0/me$ (m = 1, 2, 3), due to multiple Andreev reflection. (Inset) $I(V)$ characteristics at 40 mK for zero magnetic field (red trace) and for a 100-mT field perpendicular to the substrate (black trace). The supercurrent branch at zero field is not clearly visible in this large bias range. (**B**) dV/dI versus I and V_g for device no. 2. As V_g is varied from 0 to negative values, the supercurrent branch (black region) shrinks and simultaneously exhibits reproducible fluctuations. These fluctuations correlate with those of the normal-state conductance $G_N(V_g)$, as is shown by the comparison with the superimposed plot (white line) sharing the same horizontal scale. [In practice, $G_N(V_g)$ is obtained by measuring dV/dI at $V > 2\Delta_0/e$.] (**C**) The Thouless energy E_{Th} and the RMS value δG_N of the $G_N(V_g)$ fluctuations are plotted as a function of the distance L between source and drain contacts. $E_{Th} = \hbar D/L^2$, where $D = l\ v_F/d$ is the diffusion coefficient for a d-dimensional conductor expressed in terms of the mean free path l and the Fermi velocity v_F. l and v_F are extracted from the mobility, and the carrier density is obtained from the pinch-off $G_N(V_g)$ characteristics (*6*). Because l is typically comparable to the nanowire diameter, we take d = 3 instead of d = 1. Even with this conservative assumption, $E_{Th} \geq \Delta_0$.

References and Notes

1. C. M. Lieber, *Mat. Res. Soc. Bull.* **28**, 486 (2003).
2. P. Yang, *Mat. Res. Soc. Bull.* **30**, 85 (2005).
3. L. Samuelson *et al.*, *Phys. E (Amsterdam)* **25**, 313 (2004).
4. E. P. A. M. Bakkers *et al.*, *Nat. Mater.* **3**, 769 (2004).
5. T. Mårtensson *et al.*, *Nano Lett.* **4**, 1987 (2004).
6. S. De Franceschi *et al.*, *Appl. Phys. Lett.* **83**, 344 (2003).
7. M. T. Björk *et al.*, *Nano Lett.* **4**, 1621 (2004).
8. Z. Zhong, Y. Fang, W. Lu, C. M. Lieber, *Nano Lett.* **5**, 1143 (2005).
9. P. G. de Gennes, *Rev. Mod. Phys.* **36**, 216 (1964).
10. B. J. van Wees, *Phys. World* **9**, 41 (1996).
11. Materials and methods are available as supporting material on *Science* Online.
12. M. Tinkham, *Introduction to Superconductivity* (McGraw-Hill, Singapore, ed. 2, 1996).
13. T. D. Clark, R. J. Prance, A. D. C. Grassie, *J. Appl. Phys.* **51**, 2736 (1980).

14. T. Nishino, M. Miyake, Y. Harada, U. Kawabe, *IEEE Electron Device Lett.* **EDL-6**, 297 (1985).
15. H. Takayanagi, T. Kawakami, *Phys. Rev. Lett.* **54**, 2449 (1985).
16. A. W. Kleinsasser *et al.*, *Appl. Phys. Lett.* **55**, 1909 (1989).
17. C. Nguyen, J. Werking, H. Kroemer, E. L. Hu, *Appl. Phys. Lett.* **57**, 87 (1990).
18. B. D. Josephson, *Phys. Lett.* **1**, 251 (1962).
19. A. F. Andreev, *Zh. Eksp. Theor. Fiz.* **46**, 1823 (1964) [*Sov. Phys. JETP* **19**, 1228 (1964)].
20. B. Pannetier, H. Courtois, *J. Low Temp. Phys.* **118**, 599 (2000).
21. K. Flensberg, J. B. Hansen, M. Octavio, *Phys. Rev. B* **38**, 8707 (1988).
22. A. Chrestin, U. Merkt, *Appl. Phys. Lett.* **70**, 3149 (1997).
23. M. Octavio, M. Tinkham, G. E. Blonder, T. M. Klapwijk, *Phys. Rev. B* **27**, 6739 (1983).
24. E. Scheer *et al.*, *Phys. Rev. Lett.* **86**, 284 (2001).
25. M. R. Buitelaar *et al.*, *Phys. Rev. Lett.* **91**, 057005 (2003).
26. P. A. Lee, A. D. Stone, *Phys. Rev. Lett.* **55**, 1622 (1985).
27. C. W. J. Beenakker, *Phys. Rev. Lett.* **67**, 3836 (1991).
28. B. L. Al'tshuler, B. Z. Spivak, *Zh. Eksp. Theor. Fiz.* **92**, 609 (1987) [*Sov. Phys. JETP* **65**, 343 (1987)].
29. Y. Makhlin, G. Schön, A. Shnirman, *Rev. Mod. Phys.* **73**, 357 (2001).
30. M. J. Storcz, F. K. Wilhelm, *Appl. Phys. Lett.* **83**, 2387 (2003).
31. We thank J. Eroms, R. Schouten, C. Harmans, P. Hadley, Yu. Nazarov, C. Beenakker, T. Klapwijk, B. van Wees, and F. Giazotto. Financial support was obtained from the Dutch Fundamenteel Onderzoek der Materie, the Japanese Solution Oriented Research for Science and Technology program, and the Korean Science and Engineering Foundation.

Supporting Online Material
www.sciencemag.org/cgi/content/full/309/5732/272/DC1
Materials and Methods
Figs. S1 to S4
References

13 April 2005; accepted 25 May 2005
10.1126/science.1113523

Skeleton of *Euplectella* sp.: Structural Hierarchy from the Nanoscale to the Macroscale

Joanna Aizenberg,[1]* James C. Weaver,[2] Monica S. Thanawala,[1] Vikram C. Sundar,[1] Daniel E. Morse,[2] Peter Fratzl[3]

Structural materials in nature exhibit remarkable designs with building blocks, often hierarchically arranged from the nanometer to the macroscopic length scales. We report on the structural properties of biosilica observed in the hexactinellid sponge *Euplectella* sp. Consolidated, nanometer-scaled silica spheres are arranged in well-defined microscopic concentric rings glued together by organic matrix to form laminated spicules. The assembly of these spicules into bundles, effected by the laminated silica-based cement, results in the formation of a macroscopic cylindrical square-lattice cagelike structure reinforced by diagonal ridges. The ensuing design overcomes the brittleness of its constituent material, glass, and shows outstanding mechanical rigidity and stability. The mechanical benefits of each of seven identified hierarchical levels and their comparison with common mechanical engineering strategies are discussed.

Nature fascinates scientists and engineers with numerous examples of exceptionally strong building materials. These materials often show complex hierarchical organization from the nanometer to the macroscopic scale (*1*–*7*). Every structural level contributes to the mechanical stability and toughness of the resulting design. For instance, the subtle interplay between the lattice structure, fibril structure, and cellulose is responsible for the remarkable properties of wood. In particular, it consists of parallel hollow tubes, the wood cells, which are reinforced by nanometer-thick cellulose fibrils wound helically around the cell to adjust the material as needed (*8*). Deformation occurs by shearing of a matrix rich in hemicelluloses and lignin, "gluing" neighboring fibrils, and allowing a stick-slip movement of the fibrils (*9*). Wood is an example that shows the wide range of mechanical performance achievable by constructing with fibers. Bone is another example of a hierarchically assembled fibrous material. Its strength critically depends on the interplay between different structural levels—from the molecular/nanoscale interaction between crystallites of calcium phosphate and an organic framework, through the micrometer-scale assembly of collagen fibrils, to the millimeter-level organization of lamellar bone (*4*, *10*–*12*). Whereas wood is fully organic material, bone is a composite, with about half organic and half mineral components tightly interconnected at the nanoscale. However, nature has also evolved almost pure mineral structures, which—despite the inherent brittleness of most minerals—are tough enough to serve as protection for the organism. In mollusk nacre, for example, the toughening effect is due to well-defined nanolayers of organics at the interfaces between microtablets of calcium carbonate (*5*, *6*). In such structures, the stiff components (usually mineral) absorb the bulk of the externally applied loads. The organic layers, in turn, provide toughness, prevent the spread of the cracks into the interior of the structure, and even confer a remarkable capacity for recovery after deformation (*13*).

Glass is widely used as a building material in the biological world, despite its fragility (*14*–*20*). Organisms have evolved means to effectively reinforce this inherently brittle material. It has been shown that spicules in siliceous sponges exhibit exceptional flexibility and toughness compared with brittle synthetic glass rods of similar length scales (*15*, *20*). The mechanical protection of diatom cells was suggested to arise from the increased strength of their silica frustules (*16*). We have recently described the structural and optical properties of individual spicules of the glass sponge *Euplectella* sp., a deep-sea, sediment-dwelling sponge from the Western Pacific (*21*, *22*). Not only do these spicules have optical properties similar to manufactured optical fibers, but they are also structurally resistant. The individual spicules are, however, just one structural level in a highly sophisticated, nearly purely mineral skeleton of this siliceous sponge (*23*). Here, we discuss the structural hierarchy of the entire skeleton of *Euplectella* sp. from the nanoscale to the macroscale. We show that the assembly of a macroscopic, mechanically resistant cylindrical glass cage is possible in a modular, bottom-up fashion comprising at least seven hierarchical levels, all contributing to mechanical performance. These include silica nanospheres that are arranged into concentric layers separated from one another by alternating organic layers to yield lamellar fibers. The fibers are in turn bundled and organized within a silica matrix to produce flexurally rigid composite beams at the micron scale. The macroscopic arrangement of these beams in a rectangular lattice with ancillary crossbeams is ideal for resisting tensile and shearing stresses. Finally, we identify various structural motifs that provide additional structural benefits to this unique glass skeletal system.

Figure 1A is a photograph of the entire skeleton of *Euplectella* sp., showing the intricate, cylindrical cagelike structure (20 to 25 cm long, 2 to 4 cm in diameter) with lateral ("oscular") openings (1 to 3 mm in diameter). The diameter of the cylinder and the size of the oscular openings gradually increase from the bottom to the top of the structure. The basal segment of *Euplectella* sp. is anchored into the soft sediments of the sea floor and is loosely connected to the rigid cage structure, which is

[1]Bell Laboratories/Lucent Technologies, Murray Hill, NJ 07974, USA. [2]Institute for Collaborative Biotechnologies and Materials Research Laboratory, University of California, Santa Barbara, CA 93106, USA. [3]Max Planck Institute of Colloids and Interfaces, D-14424 Potsdam, Germany.

*To whom correspondence should be addressed. E-mail: jaizenberg@lucent.com

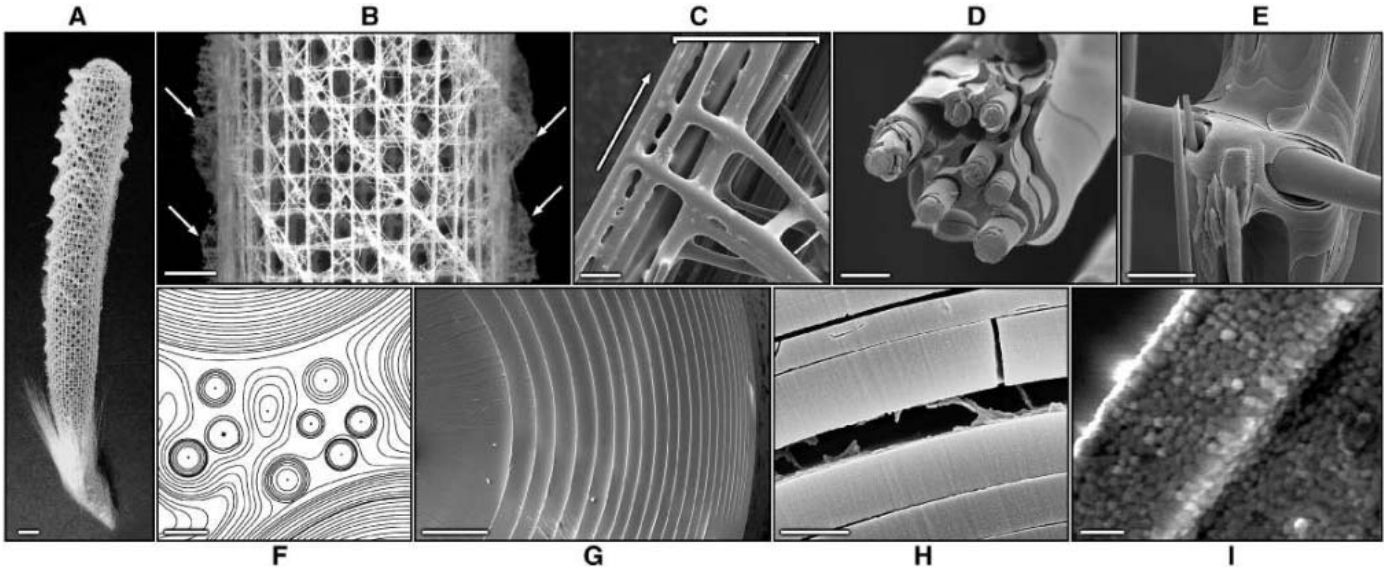

Fig. 1. Structural analysis of the mineralized skeletal system of *Euplectella* sp. (**A**) Photograph of the entire skeleton, showing cylindrical glass cage. Scale bar, 1 cm. (**B**) Fragment of the cage structure showing the square-grid lattice of vertical and horizontal struts with diagonal elements arranged in a chessboard manner. Orthogonal ridges on the cylinder surface are indicated by arrows. Scale bar, 5 mm. (**C**) Scanning electron micrograph (SEM) showing that each strut (enclosed by a bracket) is composed of bundled multiple spicules (the arrow indicates the long axis of the skeletal lattice). Scale bar, 100 μm. (**D**) SEM of a fractured and partially HF-etched (*25*) single beam revealing its ceramic fiber-composite structure. Scale bar, 20 μm. (**E**) SEM of the HF-etched (*25*) junction area showing that the lattice is cemented with laminated silica layers. Scale bar, 25 μm. (**F**) Contrast-enhanced SEM image of a cross section through one of the spicular struts, revealing that they are composed of a wide range of different-sized spicules surrounded by a laminated silica matrix. Scale bar, 10 μm. (**G**) SEM of a cross section through a typical spicule in a strut, showing its characteristic laminated architecture. Scale bar, 5 μm. (**H**) SEM of a fractured spicule, revealing an organic interlayer. Scale bar, 1 μm. (**I**) Bleaching of biosilica surface revealing its consolidated nanoparticulate nature (*25*). Scale bar, 500 nm.

exposed to ocean currents and supports the living portion of the sponge responsible for filtering and metabolite trapping (*23*, *24*). The characteristic sizes and construction mechanisms of the *Euplectella* sp. skeletal system are expected to be fine-tuned for these functions.

At the macroscale, the cylindrical structure is reinforced by external ridges that extend perpendicular to the surface of the cylinder and spiral the cage at an angle of 45° (shown by arrows in Fig. 1B). The pitch of the external ridges decreases from the basal to the top portion of the cage. The surface of the cylinder consists of a regular square lattice composed of a series of cemented vertical and horizontal struts (Fig. 1B), each consisting of bundled spicules aligned parallel to one another (Fig. 1C), with diagonal elements positioned in every second square cell (Fig. 1B). Cross-sectional analyses of these beams at the micron scale reveal that they are composed of collections of silica spicules (5 to 50 μm in diameter) embedded in a layered silica matrix (Fig. 1, D to F). The higher solubility of the cement when treated with hydrofluoric acid (HF) (*25*), compared with the underlying spicules, suggests that the cement is composed of more hydrated silica (Fig. 1, D and E). The constituent spicules have a concentric lamellar structure, with the layer thickness decreasing from ~1.5 μm at the center of the spicule to ~0.2 μm at the spicule periphery (Fig. 1G). These layers are arranged in a cylindrical fashion around a central proteinaceous filament and are separated from one another by organic interlayers (Fig. 1H). Etching of spicule layers and the surrounding cement showed that at the nanoscale the fundamental construction unit consists of consolidated hydrated silica nanoparticles (50 to 200 nm in diameter) (Fig. 1I) (*17*–*19*, *22*). The different levels of structural complexity are schematically shown in Fig. 2. In the following discussion, each hierarchical level is examined from the mechanical perspective.

The first level is biologically produced glass composed of consolidated silica nanospheres formed around a protein filament (Fig. 2A). Glass as a building material suffers primarily from its brittleness. This means that its strength is limited mostly by surface defects where the applied stresses concentrate. A scratch in the surface of glass readily induces fracture. If we consider that surface defects in the biosilica may be induced by external point loads, either biologically or otherwise applied, a scratched plain glass spicule would lose most of its strength and would fracture when subsequently loaded in tension or bending. This can be expressed quantitatively by the well-known Griffith law, which relates the strength σ_f to the size of the largest defect, h, for $h \geq h^*$, as

$$\sigma_f = \frac{K_{1C}}{\sqrt{\pi h}} \approx \sigma_f^{th}\sqrt{\frac{h^*}{h}} \qquad \text{(Eq. 1)}$$

where K_{1C} is the fracture toughness of the glass, σ_f^{th} is the theoretical strength of the defect-free material, and h^* is a characteristic length (for typical ceramic materials, this length is on the order of 10 to 30 nm) (*26*). For defects smaller than h^*, there is no stress concentration at the defect, and the strength of the material is equal to its defect-free value (*26*). Because the mineral particles in bone, for example, are thinner than this value, these particles should be insensitive to defects and therefore flaw tolerant. This argument does not apply, however, to biologically produced glass, because individual silica nanospheres range from 50 nm to 200 nm in diameter and thus are larger than h^*.

The intrinsically low strength of the glass is balanced at the next structural level. The spicule as a whole can be regarded as a laminated composite (*27*) in which the organic interlayers act as crack stoppers (Fig. 2B). If a point load is applied to the surface, one may expect that the damage will be restricted to the outermost layers (*28*). A larger number of individual glass layers should protect the spicule more effectively from this type of damage. Thin organic interlayers seem also to be important to prevent cracks from propagating to inner layers under the influence of indentation (*28*). The observed decrease of the silica layer thickness from the spicule core to the periphery is likely to provide an additional reinforcement to the spicules. Thicker inner layers help enhance mechanical rigidity of the

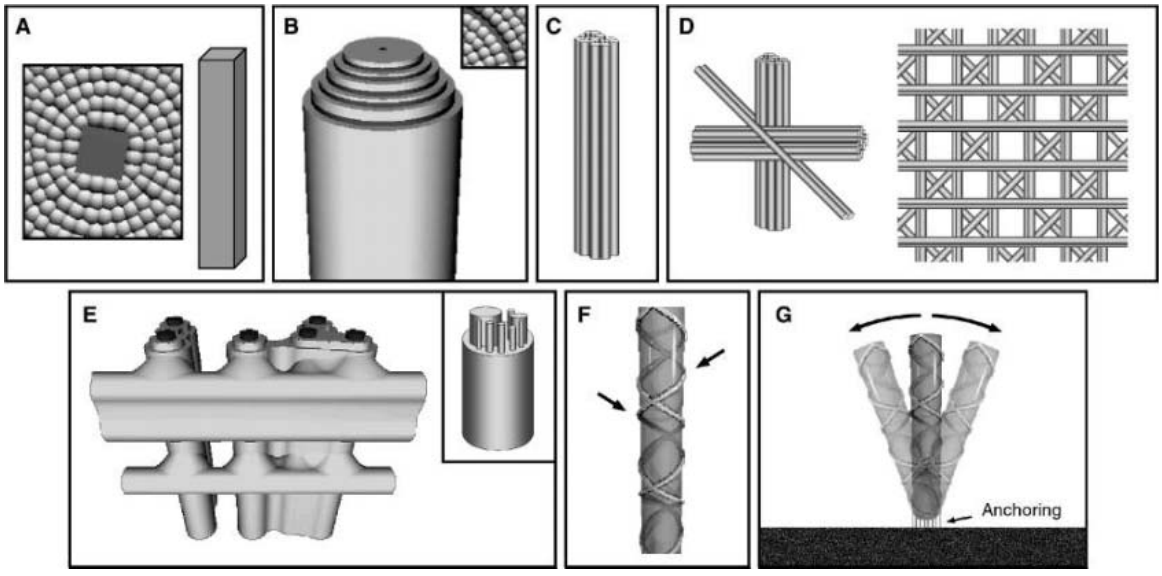

Fig. 2. Proposed scheme summarizing the seven levels of structural hierarchy in the skeletal system of *Euplectella* sp. (**A**) Consolidated silica nanoparticles deposited around a preformed organic axial filament (shown on the right). (**B**) Lamellar structure of spicule made of alternating organic and silica layers. Inset depicts the organically glued interlayer region. (**C**) Bundling of spicules. (**D**) (Right) Vertical and horizontal ordering of bundled spicules forming a square-lattice cylindrical cage with every second cell reinforced by diagonal elements (see Eq. 2). (Left) The node structure. (**E**) Cementation of nodes and spicules in the skeletal lattice with layered silica matrix. (Inset) Fiber-reinforced composite of an individual beam in the strut. (**F**) Surface ridges protect against ovalization of the skeleton tube. (**G**) Flexural anchoring of the rigid cage into the soft sediments of the sea floor.

spicule, whereas the thinner outer layers effectively limit the depth of crack penetration. The crack deviation by organic interlayers in laminated spicules can be clearly seen in Fig. 3.

In a further level of hierarchy, spicules are joined into parallel bundles (Fig. 2C), a well-known construction principle in ceramic materials (*29*). Generally, a bundle of fibers with slightly different strength will have a much larger defect tolerance (and, therefore, strength) than each of the individual fibers. Indeed, if one fiber fails (e.g., under tension), neighboring ones still hold, and the crack in the first fiber will be deflected at the interface to its neighbors (or at the interface between the fiber and cement). A weak lateral bonding between fibers (or between fiber and matrix) is essential for this toughening mechanism to work (*30*).

The bundled spicules are arranged horizontally and vertically into a square-grid cylindrical cage reinforced by ancillary diagonal fibers running in both directions (Fig. 2D). Theoretical analyses of strut structures have shown that when the number of struts per node, Z, exceeds a certain value, the structure is stable even if the nodes can rotate freely. Deshpande *et al*. (*31*) have given the stability limit as

$$Z \geq 6\ (D - 1) \qquad \text{(Eq. 2)}$$

for grids in $D = 2$ or in $D = 3$ dimensions. A simple square grid made of fibers (with $D = 2$ and $Z = 4$) is clearly unstable with respect to shear when the nodes can rotate freely. In cases where a free rotation of the nodes is not possible, the shear stability of the simple square grid is limited by the bending moments, which the nodes and struts can withstand. However, cellular structures are usually much stronger when the struts are loaded in tension rather than in bending (*32*). Hence, structures fulfilling inequality (Eq. 2), where any type of loading will result in tension and compression of the fibers only, are likely to be stronger. In the *Euplectella* skeletal system, three main spicular struts (horizontal, vertical, and one of the two possible diagonals) are joined in every node of the square grid, which means that $Z = 6$. This is just sufficient to fulfill Eq. 2 for a two-dimensional grid. Most remarkably, every second square in the skeletal lattice is left without a diagonal fiber. By adding the crossbeams in these empty squares, the number Z would jump to 8, which would be an overdesign in terms of Eq. 2, with no apparent structural advantages for the prevention of shear stresses.

Hierarchical levels shown in Fig. 2, A to D, describe the structure of the *Euplectella* skeletal system at its early stages of development [the "flexible phase" (*24*)]. During maturation, the flexible cage is rigidified into a "stiff sponge" (*24*) as a result of the use of two additional levels of structural hierarchy. All the fibers become joined at the nodes of the square grid with silica cement that effectively coats the entire skeletal lattice (Fig. 2E) and thus forms the matrix of a ceramic fiber composite. The only exception is the region where basalia (anchor spicules) emerge from the base of the composite structure. It is also noteworthy that the cement itself exhibits a laminated architecture (Fig. 1, D to F) that hinders crack propagation through this silica matrix.

The resultant rigid structure ensures that the sheet forming the cylinder is very stable

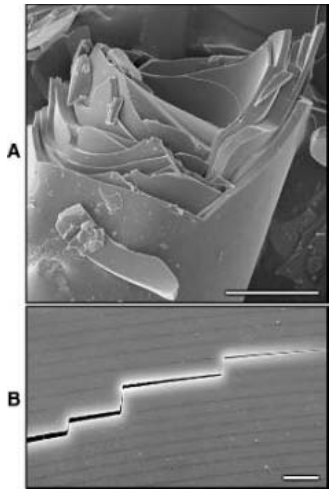

Fig. 3. Fracture surfaces in the spicules from *Euplectella* sp. (**A**) SEM of a fractured laminated spicule. (**B**) Examination of a polished cross section of the spicule from a related species clearly reveals crack deviation by the organic layers. Scale bars for both micrographs, 10 μm.

in two dimensions with a number of measures to reduce the intrinsic brittleness of glass. Finally, the cylindrical cage must also be stable in three dimensions, and the main limitation is the ovalization of the cylinder, which reduces the bending stability of the tubelike cage. In this sense, it is very likely that the helical ridges around the skeleton of *Euplectella* sp. (Fig. 2F), in conjunction with the consolidating silica matrix discussed above, serve primarily a mechanical function in preventing ovalization of the sponge skeleton. This argument is further supported by the fact that the ridges are absent in the narrow bottom portion of the tube and ap-

pear in the middle region where the sponge diameter increases beyond a specific point. To ensure the stability of the tube with the vertically growing diameter, there is a distinct increase of the surface density and thickness of the external ridges in the upper regions of the skeletal system (Fig. 1A) (*23*, *24*).

Exposed to currents, the elevated rigid sponge cage attached to the ocean floor will experience bending stresses that are concentrated at the anchor point. Two mechanical strategies may counteract the stress concentration: to stiffen the anchor point, which will withstand bending forces up to a certain limit and then break, or to make the anchor very flexible. The sponge uses the latter strategy by loosely incorporating the basalia (anchor) spicules into the vertical struts of the rigid cage (Fig. 2G). The advantage of this strategy is that there is no limiting stress from currents, and the cage swings freely in the ocean because of the inherent flexibility of the individual spicules that form the connection.

The structural complexity of the glass skeleton in the sponge *Euplectella* sp. is an example of nature's ability to improve inherently poor building materials. The exceptional mechanical stability of the skeleton arises from the successive hierarchical assembly of the constituent glass from the nanometer to the macroscopic scale. The resultant structure might be regarded as a textbook example in mechanical engineering, because the seven hierarchical levels in the sponge skeleton represent major fundamental construction strategies such as laminated structures, fiber-reinforced composites, bundled beams, and diagonally reinforced square-grid cells, to name a few (*33*). We conclude that the *Euplectella* sp. skeletal system is designed to provide structural stability at minimum cost, a common theme in biological systems where critical resources are often limited. We believe that the study of the structural complexity of unique biological materials and the underlying mechanisms of their synthesis will help us understand how organisms evolved their sophisticated structures for survival and adaptation and ultimately will offer new materials concepts and design solutions.

References and Notes

1. S. A. Wainwright, W. D. Biggs, J. D. Currey, J. M. Gosline, *Mechanical Design in Organisms* (Wiley, New York, 1976).
2. J. D. Currey, *J. Exp. Biol.* **202**, 3285 (1999).
3. H. A. Lowenstam, S. Weiner, *On Biomineralization* (Oxford Univ. Press, Oxford, 1989).
4. S. Weiner, H. D. Wagner, *Annu. Rev. Mater. Sci.* **28**, 271 (1998).
5. S. Kamat, X. Su, R. Ballarini, A. H. Heuer, *Nature* **405**, 1036 (2000).
6. A. G. Evans *et al.*, *J. Mater. Res.* **16**, 2475 (2001).
7. G. Mayer, M. Sarikaya, *Exp. Mech.* **42**, 395 (2002).
8. H. Lichtenegger, A. Reiterer, S. E. Stanzl-Tschegg, P. Fratzl, *J. Struct. Biol.* **128**, 257 (1999).
9. J. Keckes *et al.*, *Nat. Mater.* **2**, 810 (2003).
10. P. Fratzl, H. S. Gupta, E. P. Paschalis, P. Roschger, *J. Mater. Chem.* **14**, 2115 (2004).
11. A. E. Porter, L. W. Hobbs, V. B. Rosen, M. Spector, *Biomaterials* **23**, 725 (2002).
12. T. Hassenkam *et al.*, *Bone* **35**, 4 (2004).
13. B. L. Smith *et al.*, *Nature* **399**, 761 (1999).
14. C. C. Perry, T. Keeling-Tucker, *J. Biol. Inorg. Chem.* **5**, 537 (2000).
15. C. Levi, J. L. Barton, C. Guillemet, E. Le Bras, P. Lehuede, *J. Mater. Sci. Lett.* **8**, 337 (1989).
16. C. E. Hamm *et al.*, *Nature* **421**, 841 (2003).
17. J. N. Cha *et al.*, *Proc. Natl. Acad. Sci. U.S.A.* **96**, 361 (1999).
18. N. Kroger, S. Lorenz, E. Brunner, M. Sumper, *Science* **298**, 584 (2002).
19. J. C. Weaver *et al.*, *J. Struct. Biol.* **144**, 271 (2003).
20. M. Sarikaya *et al.*, *J. Mater. Res.* **16**, 1420 (2001).
21. V. C. Sundar, A. D. Yablon, J. L. Grazul, M. Ilan, J. Aizenberg, *Nature* **424**, 899 (2003).
22. J. Aizenberg, V. C. Sundar, A. D. Yablon, J. C. Weaver, G. Chen, *Proc. Natl. Acad. Sci. U.S.A.* **101**, 3358 (2004).
23. F. E. Schulze, *Report on the Hexactinellida Collected by H. M. S. Challenger During the Years 1873-1876*, vol. XXI (Berlin, 1887).
24. T. Saito, I. Uchida, M. Takeda, *J. Zool.* **258**, 521 (2002).
25. HF treatment and bleaching experiments: Small sections (2 cm by 2 cm) of the *Euplectella* sp. skeletal lattice were soaked for 10 min in 5 M NH_4F:2.5 M HF or 2.5% NaOCl solution, respectively. The remaining skeletal material was removed, rinsed with water and 95% ethanol, dried, and prepared for examination by scanning electron microscope.
26. H. J. Gao, B. H. Ji, I. L. Jager, E. Arzt, P. Fratzl, *Proc. Natl. Acad. Sci. U.S.A.* **100**, 5597 (2003).
27. M. Seshadri, S. J. Bennison, A. Jagota, S. Saigal, *Acta Mater.* **50**, 4477 (2002).
28. H. Chai, B. R. Lawn, *Acta Materialia* **50**, 2613 (2002).
29. W. J. Clegg, K. Kendall, N. M. Alford, T. W. Button, J. D. Birchall, *Nature* **347**, 455 (1990).
30. K. T. Faber, *Annu. Rev. Mater. Sci.* **27**, 499 (1997).
31. V. S. Deshpande, M. F. Ashby, N. A. Fleck, *Acta Materialia* **49**, 1035 (2001).
32. L. J. Gibson, M. F. Ashby, *Cellular Solids: Structure and Properties* (Cambridge University Press, ed. 2, 1999).
33. G. Mayer, *Ceram. Bull.* **83**, 9305 (2004).

34. We thank M. Ilan, G. E. Fantner, D. Kisailus, and M. J. Porter for their help. J.C.W. and D.E.M. were supported by grants from NASA (NAG1-01-003 and NCC-1-02037), the Institute for Collaborative Biotechnologies through grant DAAD19-03D-0004 from the Army Research Office, and the NOAA National Sea Grant College Program, U.S. Department of Commerce (NA36RG0537, Project R/MP-92) through the California Sea Grant College System.

14 March 2005; accepted 4 May 2005
10.1126/science.1112255

Isolation of Two Seven-Membered Ring C_{58} Fullerene Derivatives: $C_{58}F_{17}CF_3$ and $C_{58}F_{18}$

Pavel A. Troshin,[1] Anthony G. Avent,[2] Adam D. Darwish,[2] Natalia Martsinovich,[2] Ala'a K. Abdul-Sada,[2] Joan M. Street,[3] Roger Taylor[2]*

Fluorination of C_{60} at 550°C leads to milligram quantities of two stable fullerene derivatives with 58-carbon cage structures: $C_{58}F_{18}$ and $C_{58}F_{17}CF_3$. The compounds were characterized by mass spectrometry and fluorine nuclear magnetic resonance spectroscopy, and the data support a heptagonal ring in the framework. The resulting strain, which has hindered past attempts to prepare these smaller quasi-fullerenes, is mitigated here by hybridization change of some of the carbons in the pentagons from sp^2 to sp^3 because of fluorine addition. The loss of carbon from C_{60} is believed to occur via sequential fluorine addition to a C–C single bond and an adjacent C=C bond, followed by loss of a $:CF_2$ carbene.

Numerous papers describe the structure and properties of fullerenes larger than C_{60} and C_{70} and their derivatives (*1*). The stability of these compounds has been explained by the low strain inherent in a framework of pentagonal carbon rings surrounded by hexagons. By contrast, smaller fullerenes violate this nonadjacent pentagon rule and accordingly have been hard to prepare. Examples comprise the recent isolation of $C_{50}Cl_{10}$ (*2*) and a controversial report of C_{36} (*3*, *4*).

The possibility of fullerenes having seven- as well as five- and six-membered rings (quasi-fullerenes) was first proposed in 1992 (*5*). The structure of C_{58} requires a seven-membered ring produced by removal from C_{60} of a 6:5 bond, that is, one shared by a pentagon and a hexagon (*6*, *7*). The resultant C_{58} structure violates the strain-based nonadjacent pentagon rule (*8*), but a C_{58} derivative will be less strained because of the presence of sp^3 carbons and isolation ought to be feasible (*6*). Both phenylated and methylated C_{58} fragment ions have been observed in electron impact (EI) mass spectrometry of corresponding C_{60} precursors, together with C_{58}/C_{60} ion intensity ratios of up to 76% (*9*–*13*). A C_{58}

[1]Institute of Problems of Chemical Physics of Russian Academy of Sciences, Chernogolovka 142432, Russia. [2]Chemistry Department, Sussex University, Brighton BN1 9QJ, UK. [3]School of Chemistry, University of Southampton, Southampton SO17 1BJ, UK.

*To whom correspondence should be addressed. E-mail: R.Taylor@sussex.ac.uk

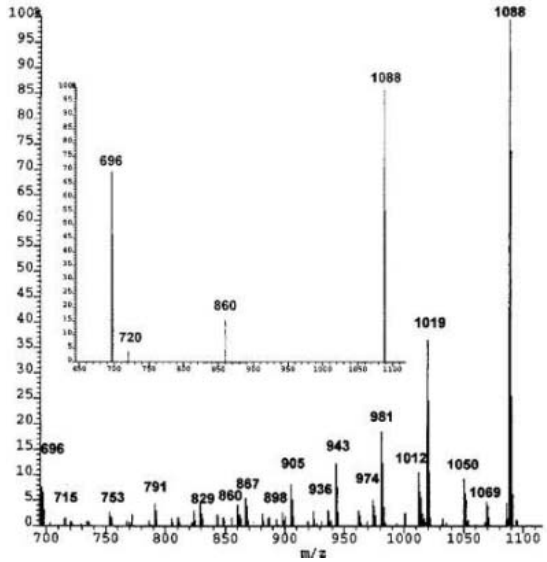

Fig. 1. (**Left**) EI mass spectrum (70 eV) of $C_{58}F_{17}CF_3$ (**1**, 1088 amu). (**Inset**) A spectrum of a second sample.

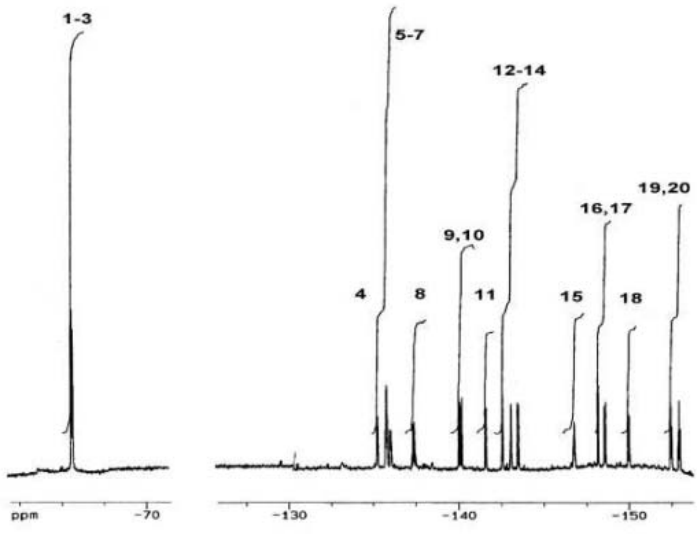

Fig. 2. (**Right**) ^{19}F NMR spectrum (376 MHz) of $C_{58}F_{17}CF_3$ (**1**).

fragment ion intensity equal to that of C_{60} has been observed in the mass spectrum of a fullerene dimer (*14*). Very recently the EI dissociation and ionization of C_{60} was reported to produce nanogram quantities of C_{58} itself (*15*). Our strategy was to stabilize C_{58} by fluorination. Here, we report isolation and characterization of milligram quantities of two C_{58} compounds: $C_{58}F_{17}CF_3$ (**1**) and $C_{58}F_{18}$ (**2**).

Reaction of C_{60} with either transition metal fluorides or fluorine gas gives only fluorinated C_{60} derivatives (*16*). Binary fluorides behave similarly, but those containing cesium showed anomalies attributed to their hygroscopic nature that resulted in the incorporation of oxygen, and this was explored further. Oxyfluorides, $Cs_xPbO_yF_z$ [x equals 2, 3, or 4; y from 0.2 to 0.5; and $z = (4 + x) - 2y$], were prepared by partial fluorination (1:9 F_2/N_2, 500°C, 2 to 4 hours) of appropriate molar ratios of CsCl and PbO_2. A finely ground mixture of these fluorinating reagents (6.5 g) and [60]fullerene (300 mg) was heated in vacuum (3 to 9 mBar; the pressure changes as fluorine is released) at 550°C for 7 hours. Volatile fluorinated products were collected in a cold zone of the apparatus (*17*); cosublimation of inorganic fluorides was sometimes observed. These products were purified by extraction into an equal-volume mixture of CCl_4 and hexane and by subsequent chromatography of the dark red solution (30 to 75 μm silica gel, 1:1 CCl_4–toluene by volume eluent). The major fraction (50 to 80 mg) contained predominantly $C_{60}F_{18}$ together with circa (ca.) 15 mg of fluorinated C_{58} species.

A toluene solution of the crude product was further purified by HPLC (high pressure liquid chromatography) with the use of a Cosmosil Buckyprep (Nacalai Tesque Incorporated, Kyoto, Japan) column (20 mm by 250 mm, toluene eluent at 18.7 ml min^{-1}). Two fractions were collected from this run. The later fraction (55 to 105 min) was processed again on a Cosmosil 5 PYE column (10 mm by 250 mm, toluene eluent at 4.7 ml min^{-1}) to yield 1 mg of $C_{58}F_{18}$ (eluted at 87 min). The earlier fraction (45 to 55 min) was also purified further with use of the 5 PYE column. A $C_{60}F_{18}O$ by-product (57.5-min elution) separated at this stage, whereas a mixture eluted at 48.5 min was subjected to a third purification using a Buckyprep column (10 mm by 250 mm, toluene eluent at 4.7 ml min^{-1}) to yield 4 mg of $C_{58}F_{17}CF_3$, which eluted at 50 min.

The EI mass spectrum (70 eV, direct chemical ionization probe) of $C_{58}F_{17}CF_3$ (**1**) (Fig. 1) shows the 1088–atomic mass unit (amu) parent ion, with two fragmentation paths: The main one involves initial loss of CF_3 (69 amu) followed by eight F_2 (38 amu) and one F (19 amu); in the minor path, initial loss of six F_2 is followed by loss of CF_3 then F_2 and F. The Fig. 1 inset shows a lower concentration sample that fragmented directly to C_{58} (696 amu); the 860 amu fragmentation ion is due to $C_{58}F_5CF_3$, and the trivial peak at 720 amu arises from residual traces of $C_{60}F_{18}O$. The data establish the existence of a C_{58} compound containing a CF_3 group and 17 fluorine atoms.

This assignment is confirmed by the ^{19}F nuclear magnetic resonance (NMR) spectrum (376 MHz) of **1** (Fig. 2), which shows one CF_3 group and 17 fluorines (*18*). The peak assignments were established as detailed below.

Two-dimensional ^{19}F correlation spectroscopy showed the following couplings (fluorine numbers as in Fig. 2): CF_3 to 8 (29 Hz), 15 (16 Hz), 13 (5 Hz); 20-12,7,6 (all 1,2); 12-7, 7-6 (both 1,3); 19-13,5,4 (all 1,2); 13-5, 9-8, 5-4 (all 1,3); 18-17, 16-12, 15-13, 14-9, 11-10 (all 1,2); 16-7 (1,4-conjugated), 14-11 (1,6-conjugated), 18-14, 18-8 (long range).

The composition of $C_{58}F_{18}$ (**2**) was established by its EI mass spectrum (1038 amu) (Fig. 3) and nine-peak ^{19}F NMR spectrum (*19*). Thus, $C_{58}F_{18}$ has a plane of symmetry and no fluorines on the symmetry plane. This result was the key to solving the structure of both **2** and **1**.

It seemed probable that the $C_{58}F_{17}CF_3$ structure was related to $C_{60}F_{18}$ (*20*, *21*). Derivatives of $C_{60}F_{18}$ characteristically show three upfield multiplets having three strong couplings; these multiplets are due to fluorine attached to carbon that has three C-F neighbors. In each quartet of coupled fluorines, one always appears in the most downfield region (128 to 134 parts per million) of the spectrum, because it is attached to carbon having two sp^2-hybridized carbons. However, the spectrum of $C_{58}F_{17}CF_3$ differs in having only two such upfield multiplets (F-19 coupled to F-4,5,13 and F-20 coupled to F-6,7,12).

There are seven ways to remove a 6:5 C–C bond from $C_{60}F_{18}$ (options a through g in Fig. 4A), but only one (bond g) is consistent with the ^{19}F NMR spectrum of **1**. Removal of bond g disrupts the aromatic ring, but the resultant framework (Fig. 3B) is much less strained than the alternatives: Density functional theory (DFT) favors this isomer over the alternatives by 32 to 73 kcal mol^{-1} on the basis of calculated heats of formation. DFT calculations used the AIMPRO program (*22*) as described previously (*23*).

The two quartets of fluorine (19-13,5,4; 20-12,7,6) were located by analogy with the $C_{60}F_{18}$ structure; the position of F-16 followed from its 1,2-coupling with F-12 and 1,4-coupling with F-7, and that of the CF_3 group followed from its 1,2-coupling with F-8 and F-15, and the 1,3-coupling with F-13. The CF_3 group occupies a position analogous to that found in the minor

isomer of $C_{60}F_{17}CF_3$ (*24*) and is able to freely rotate (revealed by variable-temperature NMR), confirming that it does not have three fluorine neighbors that would restrict rotation. The major isomer (CF_3 at site y in Fig. 4A) would not conveniently rearrange to the observed product for reasons detailed below.

Fluorines 9, 10, 11, 14, 17, and 18 could not be located without knowing whether the C_1 symmetry arose from the overall fluorine framework or from asymmetric location of the CF_3 group. The similar chemical shifts for the ca. 27-Hz coupled pairs, F-17,18 and F-10,11, indicated a symmetrical location for the fluorines in each pair, whereas the substantially differing chemical shifts for F-9,14 suggested that these fluorines have an unsymmetrical location. Comparison of the NMR spectra of **1** and **2** (Fig. 5) showed that for every resonance for **2**, there are two for **1** (except in group b, where there are only seven instead of eight because one is replaced by CF_3). In each molecule, there are only two upfield multiplets (F-19,20 in **1** and 2 times F-9 in **2**). Because of the symmetry in **2**, only one 27-Hz coupling remains (F-4,6 ≡ F-9,14 for **1**), confirming that F-10,11 and F-17,18 are in a pseudosymmetrical position in **1**. The onplane fluorine pair in $C_{60}F_{18}$ has migrated in $C_{58}F_{18}$ and straddles the symmetry plane.

Together the data support the structures in Fig. 6. The location of F-10,11 compared with F-17,18 has its basis in the much more downfield location of the chemical shifts for the former, consistent with the fluorines having two sp^2 neighbors in F-10,11 and only one in F-17,18. Fluorines F-10,11 could in principle be located across two other bonds that straddle the pseudosymmetry plane, but then either two or six pentagons acquire double bonds, giving very unstable structures.

The migration of the onplane fluorines to positions F-10,11 (in **1**) and F-3 (in **2**) can be accomplished by a series of 1,3-fluorine shifts; such shifts in fluorofullerenes have been documented by time-lapse ^{19}F NMR (*25*). However, DFT calculations give similar heats of formation for the isomer before (Fig. 4B) and after the shift. The driving force for the rearrangement is unclear but evidently there is one, because we failed to detect a derivative analogous to the main isomer of $C_{60}F_{17}CF_3$; here, the CF_3 group is located at one of the sites from which migration is required, and CF_3 groups migrate poorly, if at all. Compound **1** is evidently formed from $C_{60}F_{17}CF_3$; otherwise insertion of the $:CF_2$ group known to produce trifluoromethyl compounds from fluorofullerenes (*24*) could take place at other positions after the rearrangement. This mechanism is supported by our isolation of the fluorinated C_{59} intermediates $C_{59}F_{19}CF_2CF_3$ and $C_{59}F_{19}CF_3$ (characterized provisionally by mass spectroscopy and ^{19}F NMR), which likely form by C_2 elimination from $C_{60}F_{17}CF_3$ via successive steps of fluorination and difluorocarbene loss.

We considered but dismissed two alternative scenarios. One involved loss of onplane C_2, but this created two very strained four-membered rings and would require strong coupling between (adjacent) F-8,9. The other involved Stone-Wales rearrangement (*26*) of the onplane C–C bond whereby the adjacent pentagons become hexagons (and vice versa), and the C–C bond group then straddles the symmetry plane. However, the resultant structure is calculated to have higher energy, most probably from the high strain arising from the presence of three fused pentagons.

The main bands in the CF stretch region of the infrared spectrum of **1** are at 1281 (CF_3) 1197, 1133, and 1098 cm^{-1} (with some unresolved shoulders); minor bands are at 942, 922, 829, 685, and 614 cm^{-1}. The spectrum shows some band coincidences (±1 to 2 cm^{-1}) with that for $C_{60}F_{17}CF_3$. A weak band at 1718 cm^{-1} is insufficiently intense to be carbonyl (confirmed by the mass spectrum) but further supports the proposed structure because C=C bonds exocyclic to pentagonal rings show frequencies in the 1700 to 1780 cm^{-1} region (*27*).

Lastly, both **1** and **2** appear to be as stable as their C_{60} counterparts, suggesting that further chemistry of C_{58} ([58]quasi-fullerene) is in prospect. The HPLC retention times of these C_{58} compounds are ca. twice those for the corresponding C_{60} compounds (under conditions detailed above), which may help in identifying further C_{58} derivatives.

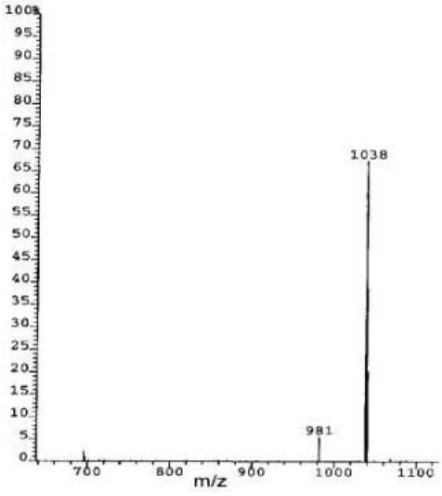

Fig. 3. EI mass spectrum (70 eV) of $C_{58}F_{18}$ (**2**, 1038 amu).

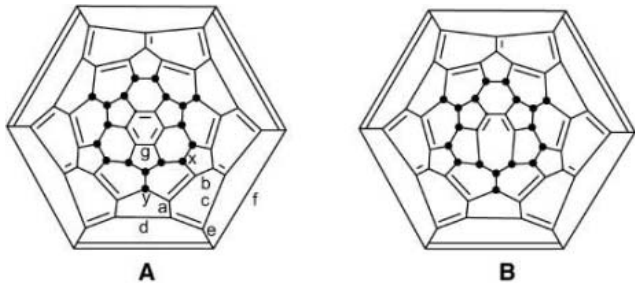

Fig. 4. Schlegel diagram for $C_{60}F_{18}$ (• = F) showing (**A**) options (a to g) for formation of $C_{58}F_{18}$ by 6:5 C–C bond removal from $C_{60}F_{18}$ and (**B**) a structure resulting from removal of g; x and y are the location sites for CF_3 in $C_{60}F_{17}CF_3$.

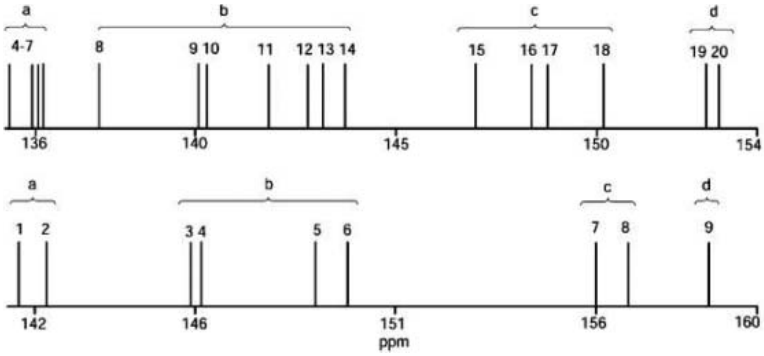

Fig. 5. (**Left**) Comparison of the chemical shifts for $C_{58}F_{17}CF_3$ (**top**) and $C_{58}F_{18}$ (**bottom**).

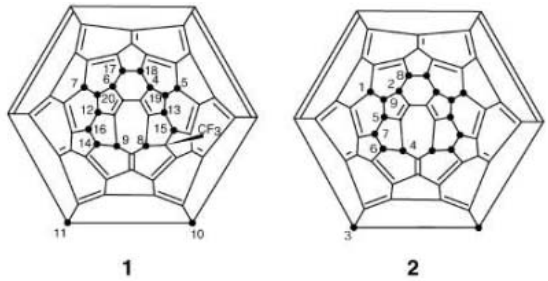

Fig. 6. (**Right**) Schlegel diagrams for the structures of $C_{60}F_{17}CF_3$ (**1**) and $C_{60}F_{18}$ (**2**).

References and Notes

1. A. K. Abdul-Sada *et al.*, *J. Chem. Soc. Perkin Trans. 2* **1999**, 2659 (1999), and references therein.
2. S.-Y. Xie *et al.*, *Science* **304**, 699 (2004).
3. C. Piskotl, J. Yarger, A. Zettl, *Nature* **393**, 771 (1998).
4. P. W. Fowler, T. Heine, *J. Chem. Soc. Perkin Trans. 2* **2001**, 487 (2001).
5. R. Taylor, *Interdiscip. Sci. Rev.* **17**, 161 (1992).
6. R. Taylor, *Lecture Notes on Fullerene Chemistry* (Imperial College Press, London, 1999), pp. 126–127.
7. Y.-H. Hu, E. Ruckenstein, *J. Chem. Phys.* **119**, 10073 (2003).
8. H. W. Kroto, *Nature* **329**, 529 (1987).
9. A. D. Darwish *et al.*, *Fullerene Sci. Technol.* **5**, 705 (1997).
10. H. Al-Matar, P. B. Hitchcock, A. G. Avent, R. Taylor, *Chem. Commun.* **2000**, 1071 (2000).
11. A. D. Darwish *et al.*, *J. Chem. Soc. Perkin Trans. 2* **2001**, 1038 (2001).
12. H. Al-Matar, A. K. Abdul-Sada, A. G. Avent, R. Taylor, *Org. Lett.* **3**, 1669 (2001).
13. H. Al-Matar *et al.*, *J. Chem. Soc. Perkin Trans. 2* **2002**, 53 (2002).
14. A. G. Avent, A. K. Abdul-Sada, R. Taylor, in *Recent Advances in the Chemistry and Physics of Fullerenes and Related Materials*, P. V. Kamat, D. M. Guldi, F. D'Souza, S. Fukuzumi, Eds. (The Electrochemical Society, Pennington, NJ, 2004) vol. 14, p. 249.
15. A. Böttcher, P. Weis, A. Bihlmeier, M. M. Kappes, *Phys. Chem. Chem. Phys.* **6**, 5213 (2004).
16. R. Taylor, *Chem. Eur. J.* **7**, 4074 (2001).
17. For a description of the apparatus, see O. V. Boltalina *et al.*, *Recent Advances in the Chemistry and Physics of Fullerenes and Related Materials*, K. M. Kadish, R. S. Ruoff, Eds. (The Electrochemical Society, Pennington, NJ, 1997), vol. 14, p. 257.
18. Spectroscopy details were as follows: δ –65.79, (3 F, qd, 29 Hz, 16 Hz, 5 Hz, F-1,2,3, CF_3), –135.45 (1 F, d, 16 Hz, F-4), –135.95 (1 F, d, 25 Hz, F-5), –136.02 (1 F, d, 19 Hz, F-6), –136.04 (1 F, d, 22 Hz, F-7), –137.6 (1 F, q, 29 Hz, F-8), –140.23 (1 F, d 27 Hz, F-9), –140.35 (1 F, d, 28 Hz, F-10), –141.77 (1 F, d, 27 Hz, F-11), –142.77 (1 F, bs, F-12), –143.26 (1 F, bs, F-13), –143.68 (1 F, d, 28 Hz, F-14), –147.0 (1 F, m, F-15), –148.39 (1 F, m, ca. 4-6 Hz, F-16), –148.80 (1 F, d, 26 Hz, F-17), –150.19 (1 F, d, 26 Hz, F-18), –152.67 (1 F, m, F-19), –153.14 (1 F, m, F-20).
19. Spectroscopy details were as follows: δ –134.5 (2 F, m, F-1), –135.3 (2 F, m, F-2), –138.95 (2 F, s, F-3), –139.1 (2 F, d, 27 Hz, F-4), –142.0 (2 F, s, F-5), –142.8 (2 F, d, 28 Hz, F-6), –149.0 (2 F, 3, F-7), –149.8 (2 F, s, F-8), –151.9 (2 F, m, F-9).
20. O. V. Boltalina, V. Yu. Markov, R. Taylor, M. P. Waugh, *Chem. Commun.* **1996**, 2549 (1996).
21. I. S. Neretin *et al.*, *Angew. Chem. Int. Ed.* **39**, 3273 (2000).
22. R. Jones, P. R. Briddon, in *Identification of Defects in Semiconductors*, M. Stavola, Ed., vol. 51A of *Semiconductors and Semimetals*, R. K. Willardson, A. C. Beer, E. R. Weber, Eds. (Academic Press, Boston, 1998), pp. 287–334.
23. P. B. Hitchcock, A. G. Avent, N. Martsinovich, P. A. Troshin, R. Taylor, *Org. Lett.* **7**, 1875 (2005).
24. O. V. Boltalina, P. B. Hitchcock, P. A. Troshin, J. M. Street, R. Taylor, *J. Chem. Soc. Perkin Trans. 2* **2000**, 2410 (2000).
25. A. G. Avent, R. Taylor, *Chem. Commun.* **2002**, 2726 (2002).
26. A. J. Stone, D. J. Wales, *Chem. Phys. Lett.* **128**, 501 (1986).
27. L. J. Bellamy, *The Infra-red Spectra of Complex Molecules* (Methuen, London, ed. 3, 1975), pp. 39–48.

28. We thank N. V. Polyakova and R. N. Lyubovskaya for making equipment available for reagent synthesis and C_{60} fluorination and O. V. Boltalina for assistance with a preliminary investigation. P.A.T. acknowledges partial financial support from (grant 04-03-32870).

7 March 2005; accepted 28 April 2005
10.1126/science.1111904

Resonating Valence-Bond Ground State in a Phenalenyl-Based Neutral Radical Conductor

S. K. Pal,[1] M. E. Itkis,[1] F. S. Tham,[1] R. W. Reed,[2] R. T. Oakley,[2] R. C. Haddon[1]*

An organic material composed of neutral free radicals based on the spirobiphenalenyl system exhibits a room temperature conductivity of 0.3 siemens per centimeter and a high-symmetry crystal structure. It displays the temperature-independent Pauli paramagnetism characteristic of a metal with a magnetic susceptibility that implies a density of states at the Fermi level of 15.5 states per electron volt per mole. Extended Hückel calculations indicate that the solid is a three-dimensional organic metal with a band width of ~0.5 electron volts. However, the compound shows activated conductivity (activation energy, 0.054 electron volts) and an optical energy gap of 0.34 electron volts. We argue that these apparently contradictory properties are best resolved in terms of the resonating valence-bond ground state originally suggested by Pauling, but with the modifications introduced by Anderson.

The familiar properties of inorganic metals, such as the inverse temperature dependence of their conductivity, are well understood in terms of band theory, in which valence electrons populate delocalized states that extend throughout a solid. The localized models of the electronic structure of metals, such as the resonating valence bond (RVB) theory put forward by Pauling (*1*), attempted to explain the bonding and conductivity in terms of alternating valence structures, in much the same way that the resonance structures that describe the bonding in molecules such as benzene are an alternative to the molecular orbital description. Although the RVB model was not useful in describing ordinary metals, it was revisited by Anderson, who explored the implications of a state in which valence bonds could move freely between pairs of atoms in a solid (*2*). The most characteristic feature of the RVB state is the presence of many resonance structures that lead to high-symmetry structures rather than forming the Peierls distorted structures that are characteristic of charge density wave states. Anderson argued that the state that is described only as a superposition of valence bonds cannot conduct electricity at absolute zero, because there will be an energy gap to any state that has long-range charge fluctuations, according to the standard arguments that apply to the Mott insulator (*2*); thus, any conductivity would be activated. Anderson's version of RVB theory has been applied to antiferromagnets (*3*–*5*) and superconductors (*6*, *7*), but a definitive answer to the questions posed by Anderson regarding the RVB state is lacking (*2*).

In recent years, we have reported a series of compounds **1** to **4** with largely unexplained electronic structures and properties (*8*–*11*), which have large intermolecular separations in their lattices, Curie susceptibility, and conductivities that are higher than those of other neutral organic solids. We now describe a compound **5** that shares many of these characteristics but exhibits features that we can best rationalize under the RVB rubric (Scheme 1).

We synthesized the phenalenyl ligand by a previously reported method (*11*). Subsequent steps yielded the chloride salt ($\mathbf{5}^+$, Cl^-), the tetraphenylborate salt ($\mathbf{5}^+$, BPh_4^-), and finally the neutral radical **5** (*12*). Black needle-like crystals of **5** were obtained after 10 days by chemical reduction of a solution of $\mathbf{5}^+$, BPh_4^- with bis-(pentamethylcyclopentadienyl)nickel in acetonitrile in an invertable H cell fitted

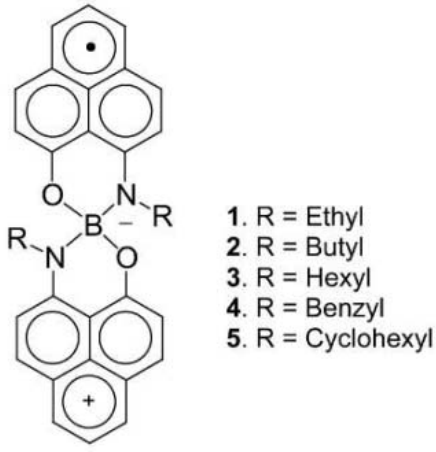

1. R = Ethyl
2. R = Butyl
3. R = Hexyl
4. R = Benzyl
5. R = Cyclohexyl

Scheme 1.

[1]Departments of Chemistry and Chemical and Environmental Engineering, University of California, Riverside, CA 92521–0403, USA. [2]Department of Chemistry, University of Waterloo, Waterloo, Ontario N2L 3G1, Canada.

*To whom correspondence should be addressed. E-mail: haddon@ucr.edu

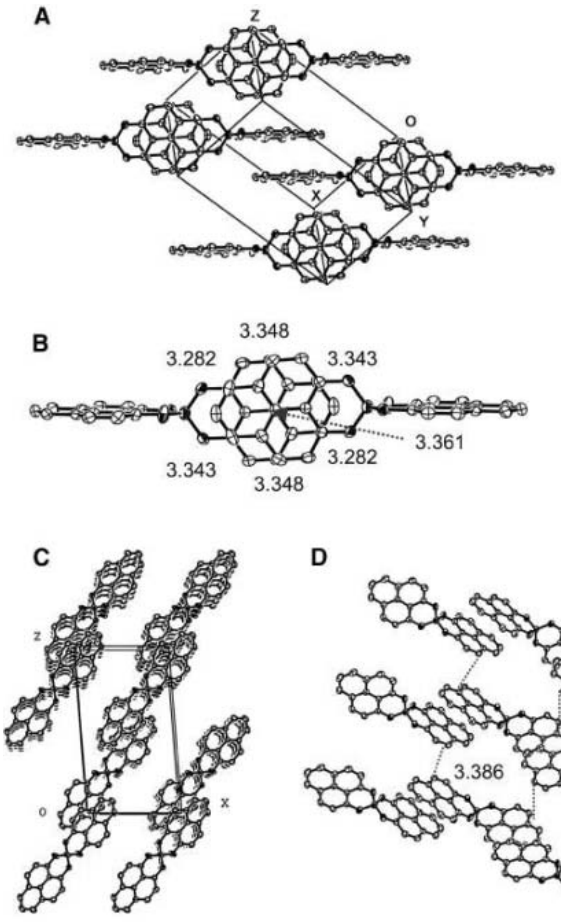

Fig. 1. (**A**) Unit cell of crystalline **5**, showing the packing in the *xz* plane viewed normal to one of the phenalenyl planes. o, origin. (**B**) Overlap and atomic separations (in Å) between pairs of radicals **5** (the dotted line is used to indicate the separation between central carbon atoms of the phenalenyl rings); this mode of overlap is repeated along the spiro-conjugated one-dimensional chain that runs along [1 0 1]. (**C** and **D**) Packing of **5** along the *y* axis: (C) Viewed along the *y* axis, and (D) showing the close contact along the *y* axis.

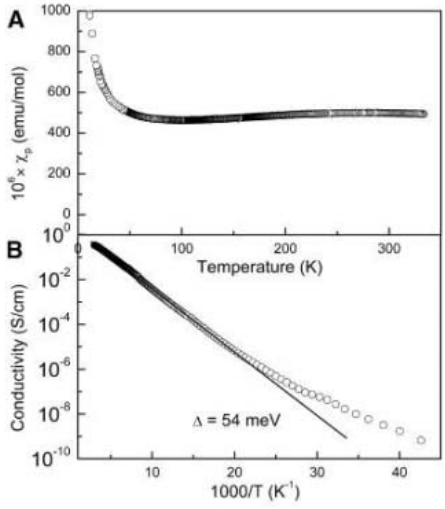

Fig. 2. (**A**) Magnetic susceptibility and (**B**) single-crystal conductivity of radical **5** as a function of the reciprocal temperature. *T*, temperature.

with a medium porosity frit (*8*). Radical **5** crystallizes in a simple and closely packed monoclinic unit cell (Fig. 1) containing two molecules within the *P2/n* space group. The asymmetric unit is half of the molecule and is almost planar; the molecule is located on a twofold rotational axis parallel to the *y* axis, and the phenalenyl rings are parallel in the *x* and *z* directions (Fig. 1).

The pattern of overlap shown in Fig. 1A leads to a spiro-conjugated chain along the [1 0 1] direction, and within this chain the C…C distances between repeating π-dimers are in the range 3.282 to 3.361 Å (Fig. 1B). Thus, all of the interradical distances are shorter than the sum of the van der Waals radii (3.4 Å) at the spin-bearing carbon atoms along this chain. The molecules are almost perfectly superimposed at the spin-bearing carbon positions, so the overlap between molecules is very effective (see the band structure discussion below) (*13*–*17*), and the interplanar separation between the molecules is 3.28 Å. The packing in the *y* direction is quite different from the packing in the *x* and *z* directions; the molecules form a stack along the *y* axis (Fig. 1C). Each of the phenalenyl rings interacts with the neighboring chain through a pair of spin-bearing carbon atoms (separated by 3.386 Å), in a similar manner to the π-step structure seen in **4** (Fig. 1D) (*11*).

Single-crystal resistivity measurements were made along the needle axis down to 20 K. The measured room-temperature conductivity (σ_{RT}) was 0.3 S/cm, compared with $\sigma_{RT} = 1.4 \times 10^{-3}$ S/cm for compound **4**. The conductivity shows a semiconducting temperature dependence with a small activation energy (transport energy gap Δ) Δ of 54 meV (Fig. 2). The static paramagnetic susceptibility (χ_p) of crystalline **5** shows temperature-independent behavior in the range from 50 to 333 K, and the value of $\chi_p = 5.0 \times 10^{-4}$ electromagnetic units (emu) mol^{-1} is consistent with Pauli paramagnetism (Fig. 2); its magnitude is typical of the values obtained for other molecular metals and superconductors (*18*, *19*) and suggests metallic character. The Curie tail observed below 50 K corresponds to the presence of residual paramagnetic centers (defects) at a concentration of 0.5% in the crystal lattice, typical of other materials in this series (*11*). The room temperature electron paramagnetic resonance spectrum of **5** shows a single line centered at gyromagnetic $g = 2.0029$, close to the free electron value of 2.0023.

Transmission spectroscopy of a single crystal of **5** shows an optical energy gap E_g(optical) of 0.34 eV. The spectrum remains opaque past 10,000 cm^{-1} because of very strong bandlike excitations that extend throughout this region of the spectrum (Fig. 3A); for an intrinsic semiconductor, E_g(optical) is related to the transport energy gap (Δ) by the relationship E_g(optical) = 2Δ (0.11 eV). The solution near-infrared spectrum of **5** (Fig. 3B) shows a feature at 0.54 eV, and there are clear differences between the spectra in the solid and solution states of this compound. The solution-phase absorption arises from an excitation from the singly occupied molecular orbital (SOMO) to the lowest unoccupied molecular orbital (LUMO). This pair of orbitals (SOMO and LUMO) results from the spiro-interaction between the symmetrical and antisymmetrical combinations of the 1,9-disubstituted-phenalenyl nonbonded molecular orbitals (*20*). The difference in the absorption features in the solid and solution states suggests that the absorption spectrum of the solution state is due to molecular transitions, whereas the association of the molecules in the crystal lattice strongly modifies the electronic structure governing these excitations.

Figure 3C shows the results obtained from extended Hückel theory (EHT) band structure and density of state (DOS) calculations carried out on the lattice found in the x-ray crystal structure of **5**. The four bands shown in Fig. 3C are derived from the two LUMOs of the cation, for each of the two molecules of **5** in the unit cell. Basically, these consist of the symmetric and antisymmetric combinations of the 1,9-disubstituted phenalenyl LUMO (*20*); alternatively, they can be viewed as arising from the nonbonding molecular orbitals of each of the four phenalenyl units in the unit cell. In this picture, these four orbitals now accommodate a total of two electrons, leading to a quarter-filled band complex and a finite DOS at the Fermi level (a metallic character). There are substantial band dispersions along the principal directions in reciprocal space in **5** (Fig. 3C) and even greater dispersions along

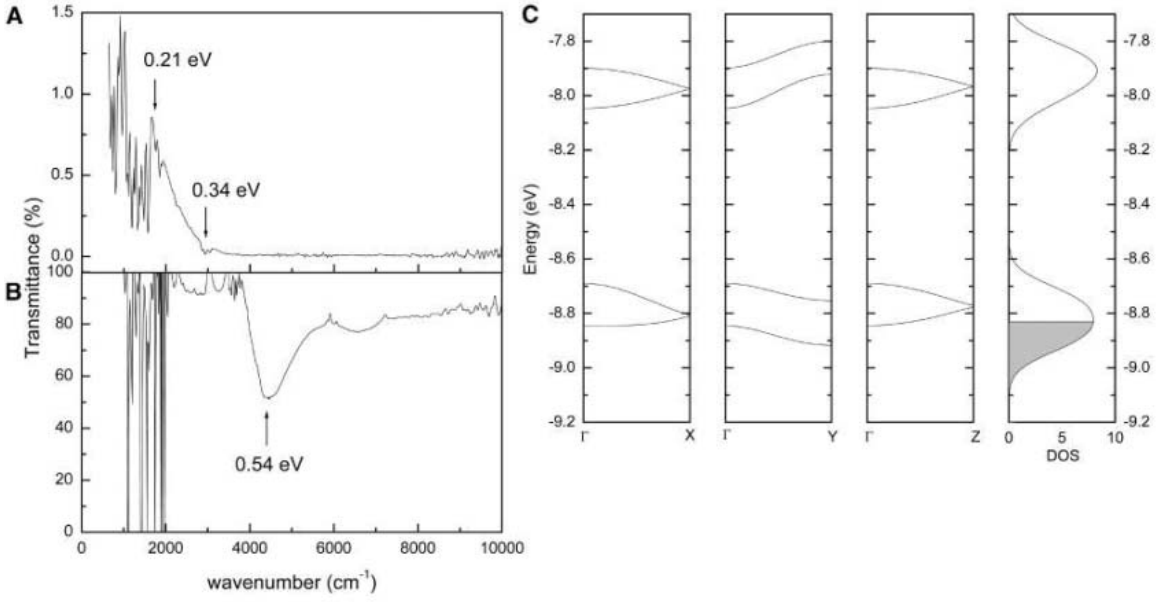

Fig. 3. (**A** and **B**) Near- and mid-infrared transmission spectra of (A) a single crystal of the cyclohexyl radical **5** and (B) a solution of **5** in dichloromethane. (**C**) The EHT band structure and DOS calculated for the experimental structure of crystalline **5** (Γ = 0, 0, 0; $x = \frac{1}{2}$, 0, 0; y = 0, $\frac{1}{2}$, 0; and z = 0, 0, $\frac{1}{2}$, where the coordinates are given in units of the reciprocal lattice vectors). The shaded region indicates the occupied states.

some of the diagonal directions (*12*), whereas the dispersions in **4** are 0.05 eV at (0, 0, $\frac{1}{2}$), 0.37 eV at (0, $\frac{1}{2}$, 0), and 0.05 eV at (0, 0, $\frac{1}{2}$) (*11*).

There is a clear structural difference between radical **4** (one-dimensional) and radical **5** (three-dimensional) that is captured by the EHT band structure calculations; however, the common feature between the two compounds is the large bandwidth of ~0.5 eV and the metallic ground state that is to be expected from their highly symmetric, periodic structures. The high-symmetry structures found for these two compounds contrast with the Peierls distorted structures characteristic of charge density wave states. Based on Pauli paramagnetism, it is possible to estimate a DOS at the Fermi level of $N(E_f)$ = 15.5 states per eV per mol^{-1}, that may be compared to the value from the EHT calculations, $N(E_f)$ = 8.0 states per eV per mol^{-1}. The enhanced susceptibility implied by $N(E_f)$ is characteristic of other organic metals and superconductors and is usually attributed to strong electron-electron correlations (*18*).

In order to rationalize these contradictory properties, we turn to the RVB theory. In his original paper, Pauling (*1*, p. 1019) argued that

> *For example, in lithium each atom has one valence electron, permitting the formation of an electron-pair bond for each pair of atoms. These bonds resonate among alternative positions, mainly the eight positions between each atom and its eight nearest ligands. If each atom were required to remain neutral by retaining its valence electron, the stabilization through the permitted synchronized bond resonance* [Fig. 4A]*, analogous to that in the benzene molecule, would be relatively small. Much greater stabilization results from unsynchronized resonance such as* [Fig. 4B]*, involving the use of an additional orbital on the atom receiving an extra bond. The electronic conductivity and other characteristic properties of metals may be described in terms of the transfer of the positive and negative charges from atom to atom accompanying the resonance of the valence bonds.*

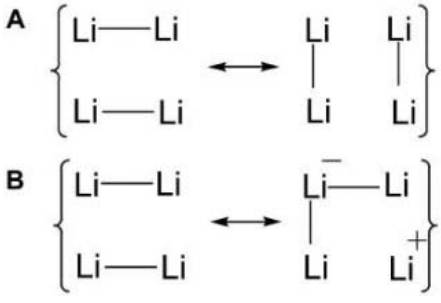

Fig. 4. Lithium resonance structures as given by Pauling (*1*). (**A**) Covalent (synchronized). (**B**) Ionic (unsynchronized).

Referring to the resonance structures in Fig. 4A, Anderson (*2*, p. 153) went on to pose the question: "…is a state in which valence bonds move around freely between pairs of atoms a metal in fact? Does it conduct electricity in the characteristic metallic way? More fundamentally, does it exist?"

A representation of the spiro-conjugated one-dimensional chain in **5** initially shows the resonance of the unpaired electron between each phenalenyl unit in the molecules (Fig. 5A) (*20*). However, the intermolecular distances are within the van der Waals radii of carbon, and it is therefore appropriate to couple the spins into electron pair bonds (Fig. 5B). Such π-dimers

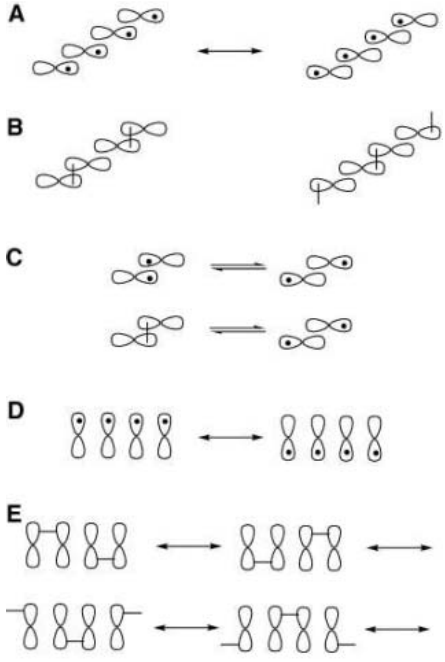

Fig. 5. Lewis free radical resonance structures for (**A**) **5**, (**C**) **1** and **2**, and (**D**) **4**, and the corresponding covalent RVB resonance structures for (**B**) **5**, (C) **1** and **2**, and (**E**) **4**. The spirobiphenalenyl structure (Scheme 1) is simplified to a figure eight for convenience.

are often diamagnetic (*13*). Compounds **1** and **2** also exist as π-dimers and adopt the electronic structure in Fig. 5C in different temperature regimes, as shown by the existence of their high-temperature paramagnetic, transparent, and low-electrical conductivity states (Fig. 5C, right) and their low-temperature diamagnetic, opaque, and high-electrical conductivity states (Fig. 5C, left) (*9*, *10*).

The most characteristic feature of the RVB ground state is a symmetrical structure stabi-

lized by resonance, such as occurs in benzene. The structures shown in Fig. 5B would normally be found in charge density wave ground states, but instead they are equally contributing resonance structures. Particularly in one dimension, the energy of delocalized systems is usually lowered by distortions. We recently reported the preparation and solid-state characterization of radical **4**, although we were unable to rationalize its electronic structure and properties (*11*). Compound **4** crystallizes as a highly one-dimensional but uniformly spaced π-step structure, and the magnetism may be fit to the antiferromagnetic Heisenberg $S = \frac{1}{2}$ linear chain model (Fig. 5D). Despite its relatively large bandwidth, the absence of a superlattice, and its uniform stacking, compound **4** has σ_{RT} of 1.4×10^{-3} S/cm, and the electronic structure of this compound is best rationalized by the one-dimensional RVB ground state (Fig. 5E). The primary mode of interaction in **5** consists of a linear chain of almost perfectly superimposed π-dimers, in which all of the spin-bearing carbon atoms are in registry. The structure of **4** places neighboring molecules in the stack such that they can only interact through the overlap of one pair of active (spin-bearing) carbon atoms per phenalenyl unit, leading to the π-step structure in which the remaining four active carbon atoms per phenalenyl unit do not interact with their nearest neighbor molecules. In fact, a form of the π-step mode of interaction is also present in **5** (Fig. 1D) and gives rise to the three-dimensional electronic structure of this compound. Nevertheless, in common with lithium (Fig. 4A), in which a number of different interatom electron-pair bonds are possible, compounds **4** and **5** both allow resonance among many pairs of intermolecular (carbon-carbon) bonds.

The structure and properties of compounds **4** and **5** allow us to answer the questions posed by Anderson (*2*). The RVB ground state exists in one (**4**) and three (**5**) dimensions; it is stabilized by resonance and prefers a high-symmetry structure; it conducts electricity but is not a metal; and the excitation spectrum is complex: In the case of **5**, the (band) structure, magnetic susceptibility, conductivity, and electronic spectrum imply different energy gaps (0, 0, 0.11, and 0.34 eV, respectively).

References and Notes

1. L. Pauling, *Nature* **161**, 1019 (1948).
2. P. W. Anderson, *Mater. Res. Bull.* **8**, 153 (1973).
3. P. Fazekas, P. W. Anderson, *Philos. Mag.* **30**, 423 (1974).
4. K. Hirakawa, H. Kadowaki, K. Ubukoshi, *J. Phys. Soc. Jpn.* **54**, 3526 (1985).
5. I. Yamada, K. Ubukoshi, K. Hirakawa, *J. Phys. Soc. Jpn.* **54**, 3571 (1985).
6. P. W. Anderson, *Science* **235**, 1196 (1987).
7. B. J. Powell, R. H. McKenzie, *Phys. Rev. Lett.* **94**, 047004 (2005).
8. X. Chi *et al.*, *J. Am. Chem. Soc.* **121**, 10395 (1999).
9. X. Chi *et al.*, *J. Am. Chem. Soc.* **123**, 4041 (2001).
10. M. E. Itkis, X. Chi, A. W. Cordes, R. C. Haddon, *Science* **296**, 1443 (2002).
11. S. K. Pal *et al.*, *J. Am. Chem. Soc.* **126**, 1478 (2004).
12. Methods and materials are available as supporting material on *Science* Online.
13. K. Goto *et al.*, *J. Am. Chem. Soc.* **121**, 1619 (1999).
14. J. Huang, M. Kertesz, *J. Am. Chem. Soc.* **125**, 13334 (2003).
15. V. Ganesan, S. V. Rosokha, J. K. Kochi, *J. Am. Chem. Soc.* **125**, 2559 (2003).
16. J. Lu, S. V. Rosokha, J. K. Kochi, *J. Am. Chem. Soc.* **125**, 12161 (2003).
17. D. Small *et al.*, *J. Am. Chem. Soc.* **126**, 13850 (2004).
18. R. C. Haddon, A. P. Ramirez, S. H. Glarum, *Adv. Mater.* **6**, 316 (1994).
19. T. Murata *et al.*, *Angew. Chem. Int. Ed. Engl.* **43**, 6343 (2004).
20. R. C. Haddon, S. V. Chichester, J. H. Marshall, *Tetrahedron* **42**, 6293 (1986).

21. Supported by the Office of Basic Energy Sciences, U.S. Department of Energy, under grant no. DE-FG02-04ER46138, and by the U.S. Department of Defense, Defense Advanced Research Projects Agency, Defense Microelectronics Activity under grant no. H94003-04-2-0404.

Supporting Online Material
www.sciencemag.org/cgi/content/full/309/5732/281/DC1
Materials and Methods
Figs. S1 and S2
Tables S1 to S6

18 March 2005; accepted 24 May 2005
10.1126/science.1112446

Penetration of Human-Induced Warming into the World's Oceans

Tim P. Barnett,[1]* David W. Pierce,[1] Krishna M. AchutaRao,[2] Peter J. Gleckler,[2] Benjamin D. Santer,[2] Jonathan M. Gregory,[3] Warren M. Washington[4]

A warming signal has penetrated into the world's oceans over the past 40 years. The signal is complex, with a vertical structure that varies widely by ocean; it cannot be explained by natural internal climate variability or solar and volcanic forcing, but is well simulated by two anthropogenically forced climate models. We conclude that it is of human origin, a conclusion robust to observational sampling and model differences. Changes in advection combine with surface forcing to give the overall warming pattern. The implications of this study suggest that society needs to seriously consider model predictions of future climate change.

Wide-ranging evidence shows that Earth has been warming in recent decades (*1*). Observations show that ~84% of the total heating of the Earth system (oceans, atmosphere, continents, and cryosphere) over the last 40 years has gone into warming the oceans (*2*). Therefore, if one wishes to understand and explain this warming, the oceans are clearly the place to look.

There have been only a few studies that have tried to both detect (i.e., differentiate from expected natural variability) and attribute (i.e., ascribe a cause to) the observed ocean warming signal (*3*–*8*). All used the equivalent of a single ocean-basin temperature measure and tracked its change with time. This approach neglects information on how the warming penetrates vertically into the ocean, and variations of the penetration from basin to basin. The studies all suggest human impacts on the oceans, but some did not consider the possibility that the observed warming was due to natural external forcing such as solar variability or volcanic activity.

Here we investigate the warming since 1960 on an ocean-by-ocean basis and focus on how the signal penetrates down into the ocean. We use a recently upgraded and much expanded observed ocean data set (*2*), which provides the best available description of the ocean's warming signal and its evolution through time. In addition to examining these observational data, we compare them to simulations from two independent climate models, the Parallel Climate Model (PCM) (*9*) and the Hadley Centre model (HadCM3) (*10*). We then use the results of numerical experiments with these models to attribute the causes of the observed warming. The models allow gross heat budgets to be constructed by basin; these show that changes in net surface heat flux combine with advection at depth to give the observed signal.

We first define a model-based "fingerprint" describing the warming signal at each vertical level using the geographical and temporal variability of ocean temperature (*11*). The observations, projected onto this fingerprint at each level, show that the strength of the warming signal varies from ocean to ocean (*11*) (Fig. 1). The warming extends to depths of

[1]Climate Research Division, Scripps Institution of Oceanography, 0224, La Jolla, CA 92037, USA. [2]Program for Climate Model Diagnoses and Intercomparison/Lawrence Livermore National Laboratory, Post Office Box 808, Livermore, CA 94550, USA. [3]UK Met Office Hadley Centre and University of Reading, Reading RG6 6BB, UK. [4]National Center for Atmospheric Research, Post Office Box 3000, Boulder, CO 80307, USA.

*To whom correspondence should be addressed. E-mail: tbarnett@ucsd.edu

700 m or more in both the North and South Atlantic oceans, but is largely confined to the upper 100 m of the northern Pacific and northern Indian oceans. The northern Indian Ocean is particularly unusual in that it has a subsurface maximum. Both the northern and southern Pacific Ocean show a sign reversal in the warming signals, indicating a cooling at ~150-m depth. These differences between oceans constitute the spatial structure of the warming fingerprint. The final dimension of the signal is the temporal evolution of the differences. Because we are interested in low-frequency variations, we use decadal time averages to describe this time evolution.

Our purpose is to understand the origin of this complex time- and space-dependent signal. We explore three possible causes: natural variability internal to the coupled ocean-atmosphere system; external natural variability, such as solar or volcanic forcing; and forcing arising from human activity [emission of greenhouse gases (GHGs) and sulfate aerosols].

The likelihood that natural internal climate variability is the cause of the observed warming signal can be examined by analyzing a long control run of the PCM; i.e., how well did natural internal variability in the control run project onto the warming fingerprint (*11*)? This approach was used in earlier work (*3*) and is a variant of standard detection and attribution analysis (*12–15*). It has the advantage of having a simple geometric explanation while being rigorous in a statistical sense (*11*).

The strength of the warming signal in the control run (sampled in the same places as the observations) is shown in Fig. 2 for each ocean. This gives some indication of the fluctuations in signal strength that one might expect due to natural internal variability alone. Because we had multiple realizations of the 40-year time period in the control runs, we can show the 90% confidence limits of the natural variability by the hatched region. Also shown is the signal strength in the observations (red dots) from Fig. 1. The illustration demonstrates that the warming signal is far stronger than would be expected from natural internal variability, as estimated by the model. To assess whether the model's estimate of natural variability is reasonable, we compared the levels of variance in the control run at decadal time scales to those observed and found that they matched reasonably well (*16*) (supporting online text). Therefore, the control run variations are a reasonable representation of natural internal variability, at least on the decadal time scales of interest here.

Another possible candidate for the warming signal is natural variability external to the ocean-atmosphere system, such as solar variability or volcanic eruptions ("SV" forcing). We explored this possibility by analyzing PCM runs forced by estimates of observed solar variability and volcanic aerosol loadings (*17*). The results of four such runs were combined and the warming signal strength estimated in the SV data set. The results (Fig. 2) show that in none of the oceans can the SV forcing (green triangles) replicate the observed warming. Indeed, at these space and time scales, the SV forcing produces signal strengths indistinguishable from those expected from natural internal variability (hatched region).

The final candidate for explaining the signal is anthropogenic factors, such as well-mixed GHGs and sulfate aerosol particles. We examined this possibility in an ensemble of

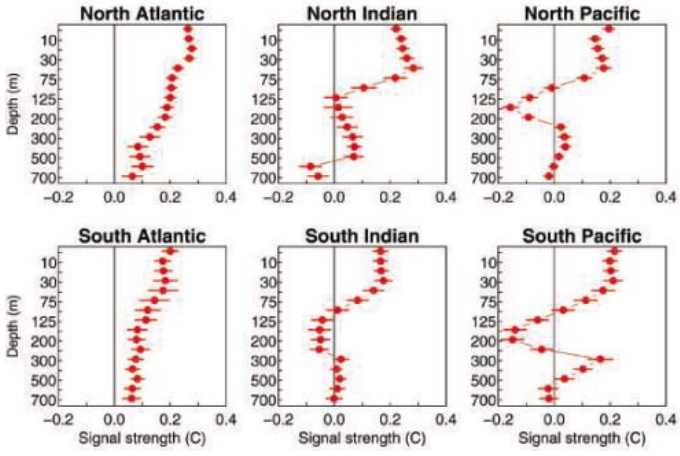

Fig. 1. Warming signal strength by ocean and depth. The dots represent the projection of the observed temperature changes onto the model-based pattern of warming. They show substantial basin-to-basin differences in how the oceans have warmed over the past 40 years, although all oceans have experienced net warming over that interval. The horizontal bars represent the ±2SD limits associated with sampling uncertainty.

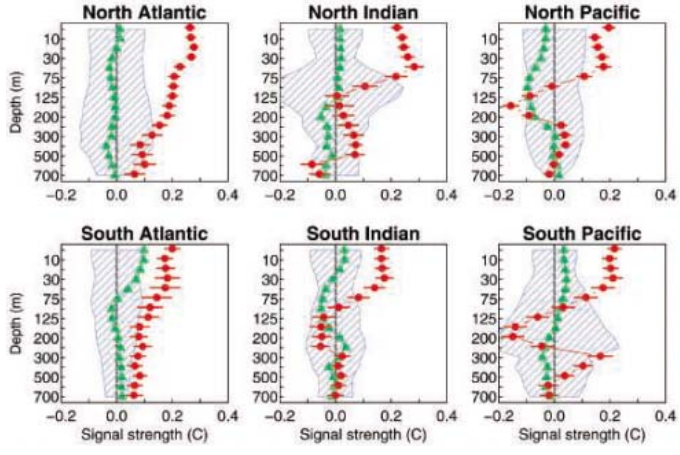

Fig. 2. Multiple realizations from the PCM control run allowed estimation of the probability distribution of signal strength associated with natural internal variability. The hatched region represents the 90% confidence limits of the natural internal variability signal strength. The observed signal strength (red dots) bears little resemblance to that expected from natural internal variability. The ensemble-averaged strength of the warming signal in four runs forced by observed solar and volcanic variability (green triangles) is also shown. There is no agreement between the two. The solar plus volcanic signals are generally indistinguishable from those expected from natural internal variability alone on the time and space scales used in this study.

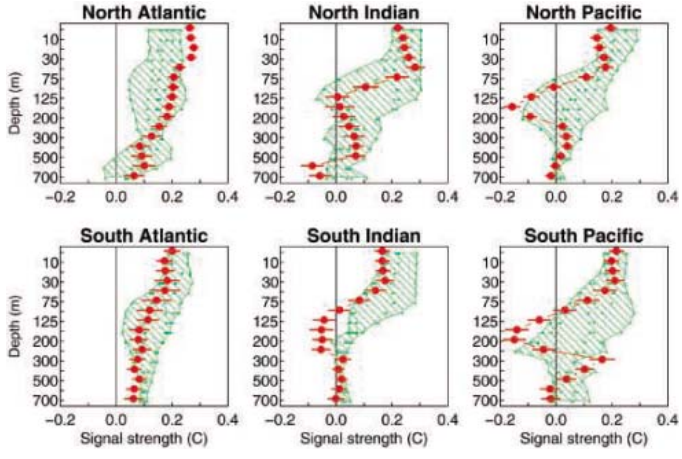

Fig. 3. Anthropogenic forcing signal strength (green hatched region) compared to that obtained from the observations (red dots). There is excellent agreement at most depths in all oceans. The hatched region shows the range of the signal strength estimates from five different realizations of identically forced simulation with the PCM, whereas the smaller green dots within the region are the individual realizations.

five PCM runs with such forcing (*17*, *18*). The results (Fig. 3) show the range of the signal strength in five scenario runs by ocean and depth (hatched area) in comparison with the observations (red dots). An ocean-by-ocean and depth-by-depth comparison shows that the agreement is compelling. The immediate conclusion is that human influences are largely responsible for the warming signal. This level of agreement could not have been tuned into the models, because the fingerprint is too complex in space and time. Further, about half of the observations used in this study were not available when the computer simulations were run.

The different response of individual oceans to GHG forcing is an interesting finding. The physical reasons for this are fairly well known, with one major surprise. For instance, it is well known that deep convection is characteristic of both the North and South Atlantic oceans (*19*). That explains why the warming signal penetrates relatively deeply in these oceans. In contrast, the northern Pacific Ocean is characterized by a rather shallow meridional overturning circulation (*20*) that tends to isolate the surface layers from the deeper ocean. It is also true that no deep water is formed in the northern Pacific. Both physical properties act to confine the signal to the upper ocean. The same situation is thought to hold over much of the southern Indian Ocean.

One notable feature from the observed and modeled signal strength (Figs. 1 and 3) is the negative lobe at 150- to 200-m depth in the Pacific. The simulation that captured this signal showed that it is associated with a thinning of the western Pacific warm pool associated with shoaling of the deeper isotherms, which has also been observed in the Pacific since the 1970s (*20*).

The major surprise is the northern Indian Ocean, which has rather shallow signal penetration and a subsurface maximum in signal strength. The heat budget for this region (Fig. 4) shows that it is the only basin where the ensemble variability includes zero for the net surface heat flux, and where advective warming is the dominant cause of the basin temperature change over the last 60 years in PCM. This result is likely due to the cancellation of GHG warming by sulfate aerosol cooling, a result recently found from direct observations (*21*). Further simulations have shown that carbon aerosols also play a role in this effect (*22*), but are not included in the simulations of this paper. Hence the warming of this ocean over the past 60 years in the simulation was largely due to changes in advection. Recent observations show a slowing of the shallow meridional circulation cell in the Indian Ocean such that advection from northern to southern Indian Ocean is reduced, leading to a net warming of the northern Indian Ocean (*23*), a result in accord with the model predictions. Indeed, inspection of the partition of net surface air/sea heat exchange and advection for the various oceans (Fig. 4) shows that in several basins, changes in advection of heat by ocean currents redistribute the heat gained from the anthropogenic forcing, and so are important to determining the structure and evolution of the warming signal in the oceans [compare (*7*)].

The normalization by surface area used in Fig. 4 removes the geometric impact of ocean size on our results. It also makes clear that the southern oceans are absorbing more heat per unit area than are the northern oceans. We suggest that this is again due to the smaller aerosol concentrations over the southern oceans. They do not have the same near-canceling effects observed in the more polluted Northern Hemisphere (*21*, *22*).

Is PCM unique in being able to capture the complex observed signal? To address this question, we repeated the analysis with HadCM3, which was developed at the Hadley Centre independently of PCM. The four realizations from this model were the "All" forcings runs, which combined a variety of forcings [GHG, solar, volcanic, aerosols, etc. (*24*)]. HadCM3's warming fingerprint (not shown) is little different from PCM's, but we use exclusively PCM's fingerprint here for consistency. The results from HadCM3 are compared to observations in Fig. 5. Using the HadCM3 fingerprint gives even better agreement (not shown), as one would expect. In any event, Figs. 3 and 5 show that PCM and HadCM3 both reflect reasonably well the evolution and spatial characteristics of the warming signal.

An interesting feature of the above result is that the PCM and HadCM3 are very different models. In the simulations used here, their forcings are also rather different. How could they give very similar evolutions of ocean temperature? Whatever the combinations of forcing used by the two modeling groups, the net forcing at the surface of the ocean had to be essentially the same. Inspection of each model's surface heat flux fields, in so far as possible, shows this to be the case. The details of the atmospheric forcing and climate feedbacks that go into producing that net value do not affect the overall oceanic response. The story may be different in the atmosphere.

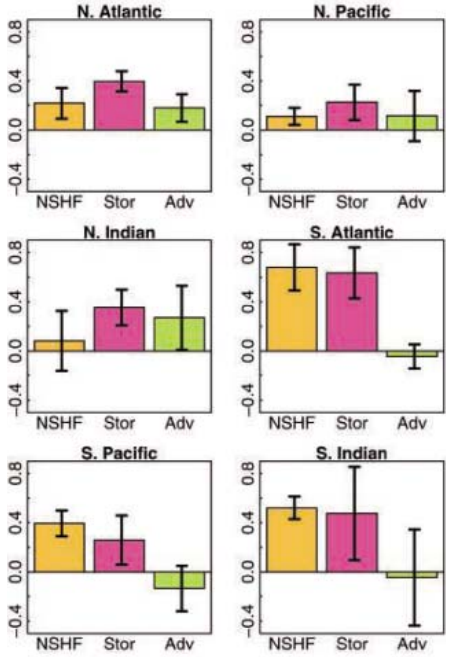

Fig. 4. Gross heat budget by ocean showing the important role that heat advection by ocean currents plays in the anthropogenic warming of the world's oceans. The PCM's net ocean surface heat flux averaged over 1940 to 1999 is shown by the "NSHF" bars, the modeled changes in ocean basin heat storage by the "Stor" bars, and the advection of heat by ocean currents needed to close the heat budget by the "Adv" bars. The latter was obtained as a residual from the first two estimates. The uncertainty bars indicate ±1SD based on the ensemble spread. The actual energy change (joules) over the time period has been normalized by surface area of respective oceans to give the average heating rate in W/m^2. This normalization makes it appear that the net advection over the globe is nonzero, a condition that vanishes using the area-weighted fluxes.

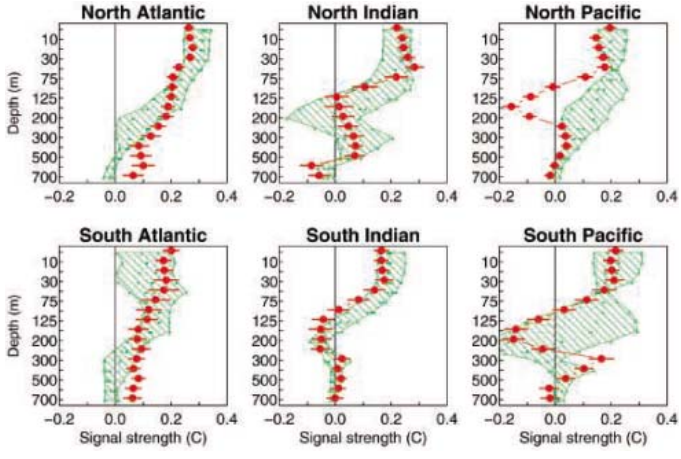

Fig. 5. Comparison of the model-predicted anthropogenic signals between HadCM3 and observations for the oceans. The format is described in Fig. 3. Comparison of Figs. 3 and 5 shows that both models capture the main structure of the signal in the observations. These figures were derived by using the warming signal defined by PCM as the basis set to allow a consistent comparison.

It is also important to investigate the influence of the upgraded data set (*2*), sampling, and model uncertainties on our conclusions. In all our results, we use a sampling strategy that compares model and observations only where observations exist; we do not use the infilled or interpolated data set (*11*). As a test, however, we repeated the analysis using the infilled data and found that it made no difference to the conclusions. More details on these sampling issues are found in (*16*). We also estimated the impact that model errors might have on the results. Multiple models run with the same GHG forcing (*25*) show a factor of 2 difference in ocean basin heat content after 80 years of integration (*26*, *27*). We estimated the effect that this had in the detection scheme and still found robust detection results above the level of natural variability (*16*). Therefore, the conclusion that the observed ocean warming is due to human influences is robust to major perturbations of both the observed data set and model error.

The implications of our results go far beyond identifying the reasons for ocean warming. First, they show that uncertainties in the models used here are too small to affect the conclusion attributing the historic ocean warming signal to anthropogenic forcings, at least for the temperature-driven part of the signal. Second, taking these new results with those obtained in the last few years [e.g., (*1*, *28*–*30*); see earlier detection studies cited above] leaves little doubt that there is a human-induced signal in the environment. Third, because the historical changes have been well simulated, future changes predicted by these global models are apt to be reasonably good, at least out to, say, 20 to 30 years into the future. How to respond to the serious problems posed by these predictions is a question that society must decide.

References and Notes

1. IPCC, "WG1 Third Assessment Report," J. T. Houghton *et al.* Eds. (2001).
2. S. Levitus, J. Antonov, T. Boyer, *Geophys. Res. Lett.* **32**, L02604, doi:10.1029/2004GL021592 (2005).
3. T. P. Barnett, D. W. Pierce, R. Schnur, *Science* **292**, 270 (2001).
4. S. Levitus *et al.*, *Science* **292**, 267 (2001).
5. B. K. Reichert, R. Schnur, L. Bengtsson, *Geophys. Res. Lett.* **29**, 1525 (2002).
6. J. Hansen *et al.*, *J. Geophys. Res.* **107** (D18), 4347 (2002).
7. J. M. Gregory, H. T. Banks, P. A. Stott, J. A. Lowe, M. D. Palmer, *Geophys. Res. Lett.* **31**, L15312 (2004).
8. P. R. Gent, G. Danabasoglu, *J. Clim.* **17**, 4058 (2004).
9. W. M. Washington *et al.*, *Clim. Dyn.* **16**, 755 (2000).
10. C. Gordon *et al.*, *Clim. Dyn.* **16**, 147 (2000).
11. Methods are available as supporting material on *Science* Online.
12. G. C. Hegerl *et al.*, *J. Clim.* **9**, 2281 (1996).
13. G. C. Hegerl *et al.*, *Clim. Dyn.* **13**, 613 (1997).
14. M. R. Allen, S. F. B. Tett, *Clim. Dyn.* **15**, 419 (1999).
15. K. Hasselmann, *Clim. Dyn.* **13**, 601 (1997).
16. D. W. Pierce *et al.*, in preparation.
17. G. A. Meehl, W. M. Washington, T. M. L. Wigley, J. M. Arblaster, A. Dai, *J. Clim.* **16**, 426 (2003).
18. A. Dai, W. M. Washington, G. A. Meehl, T. W. Bettge, W. G. Strand, *Clim. Change* **62**, 29 (2004).
19. G. Neumann, W. J. Pierson, *Principles of Physical Oceanography* (Prentice-Hall, NJ, 1966).
20. M. J. McPhaden, D. Zhang, *Nature* **415**, 603 (2002).
21. V. Ramanathan *et al.*, *J. Geophys. Res.* **106**, 28,371 (2001).
22. V. Ramanathan *et al.*, in preparation.
23. T. Lee, *Geophys. Res. Lett.* **31**, L18305 (2004).
24. S. F. B. Tett, P. A. Stott, M. R. Allen, W. J. Ingram, J. F. B. Mitchell, *Nature* **399**, 569 (1999).
25. CMIP2+ runs are available at http://www-pcmdi.llnl.gov.
26. A. P. Sokolov, C. E. Forest, P. H. Stone, *J. Clim.* **16**, 1573 (2003).
27. K. M. AchutaRao *et al.*, in preparation.
28. B. D. Santer *et al.*, *Science* **301**, 479 (2003).
29. B. D. Santer *et al.*, *J. Geophys. Res.* **109**, D21104 (2004).
30. B. D. Santer, J. E. Penner, P. W. Thorne, in *Temperature Trends in the Lower Atmosphere: Steps for Understanding and Reconciling Differences* (Report by the U.S. Climate Change Science Plan and the Subcommittee on Global Change Research, Washington, DC, in press).

31. This work is a contribution from the International Detection and Attribution Group funded by the National Oceanic and Atmospheric Association (NOAA) and the U.S. Department of Energy (DOE) through NOAA's CCDD program. We gratefully acknowledge DOE support through grants DE-FG03-01ER63255 to the Scripps Institute of Oceanography and DOE-W-7405-ENG-48 to the Program for Climate Model Diagnoses and Intercomparison at Lawrence Livermore National Labatory. Work at the Hadley Centre was supported by the UK Department for Environment, Food and Rural Affairs under contract PECD 7/12/37 and by the Government Meteorological Research and Development Programme. We especially thank S. Levitus for making his new ocean data set available and colleagues at NCAR and the Hadley Centre for performing and making available the model runs used in this work. Computer time for the PCM simulations was provided by the National Center for Atmospheric Research Scientific Computing Division, the DOE National Energy Research Scientific Computing Center, Oak Ridge National Laboratory, and the Los Alamos National Laboratory's Advanced Computing Laboratory. Discussions with L. Talley and R. Davis were helpful in several aspects of the study.

Supporting Online Material

www.sciencemag.org/cgi/content/full/1112418/DC1
Materials and Methods
SOM Text
Figs. S1 and S2
References and Notes

17 March 2005; accepted 12 May 2005
Published online 2 June 2005;
10.1126/science.1112418
Include this information when citing this paper.

Ecosystem Collapse in Pleistocene Australia and a Human Role in Megafaunal Extinction

Gifford H. Miller,[1] Marilyn L. Fogel,[2] John W. Magee,[3] Michael K. Gagan,[4] Simon J. Clarke,[5] Beverly J. Johnson[6]

Most of Australia's largest mammals became extinct 50,000 to 45,000 years ago, shortly after humans colonized the continent. Without exceptional climate change at that time, a human cause is inferred, but a mechanism remains elusive. A 140,000-year record of dietary $\delta^{13}C$ documents a permanent reduction in food sources available to the Australian emu, beginning about the time of human colonization; a change replicated at three widely separated sites and in the marsupial wombat. We speculate that human firing of landscapes rapidly converted a drought-adapted mosaic of trees, shrubs, and nutritious grasslands to the modern fire-adapted desert scrub. Animals that could adapt survived; those that could not, became extinct.

Humans are thought to have colonized Australia between 55 and 45 thousand years ago (ka) (*1*–*5*), and most of its large animals became extinct between 50 and 45 ka (*6*, *7*). The 60 taxa known to have become extinct include all large browsers, whereas large grazing forms, such as red and gray kangaroos, were less affected. The selective loss of large browse-dependent taxa suggests that ecosystem change may have been important, although animal size may have played a role (*8*). Inferential evidence of vegetation reorganization and a changed fire regime beginning 45 ka is recorded in terrestrial (*9*, *10*) and marine (*11*, *12*) sediment cores. But no records of ecosystem status through this time interval are available from the vast semiarid zone. We used isotopic tracers of diet preserved in avian eggshells and marsupial teeth (*13*, *14*) to monitor ecosystems before and after human colonization. These dietary reconstructions document ecosystem collapse across the semiarid zone between 50 and 45 ka.

We recovered eggshells of the Australian emu *Dromaius novaehollandiae* and the extinct giant flightless bird *Genyornis newtoni* from longitudinal desert dunes and shoreline-

[1]INSTAAR and Geological Sciences, University of Colorado, Boulder, CO 80309–0450 USA. [2]Geophysical Laboratory, Carnegie Institution of Washington, 1051 Broad Branch Road, Washington, DC 20015, USA. [3]Department of Earth and Marine Sciences, [4]Research School of Earth Sciences, Australian National University, Canberra, ACT 0200, Australia. [5]Charles Sturt University, Locked Bag 588, Wagga Wagga, NSW 2678, Australia. [6]Department of Geology, Bates College, Lewiston, ME 04240–6028, USA.

marginal dunes around Lake Eyre (LE), the terminal playa of a large interior basin in central Australia (Fig. 1). These collections were supplemented by eggshell remains collected near Port Augusta (PA) and the Darling-Murray lakes (DM) (Fig. 1). Because the eggshells are fragmented, we grouped most shells into collections taken from locations separated by 100 m or more to avoid analyzing multiple fragments from the same egg. Temporal constraints are based on ^{14}C dates on eggshell (LE, n = 111 samples; PA and DM, n = 60), luminescence ages on sand grains enclosing eggshells found in eolian deposits >40,000 years old (n = 28, table S5), and amino acid racemization (AAR) in eggshell organic matter for all eggshells in which we measured isotopic ratios (LE, n = 893; PA, n = 276; DM, n = 220). AAR measurements were converted to calendar ages using an age model derived from ^{14}C and luminescence dates; of 191 LE *Dromaius* eggshells <45,000 years old, 84 were dated by ^{14}C analyses. All ^{14}C-dated *Genyornis* eggshells (n = 18) are beyond the reliable age of radiocarbon dating; for LE, they were plotted against calibrated AAR ages.

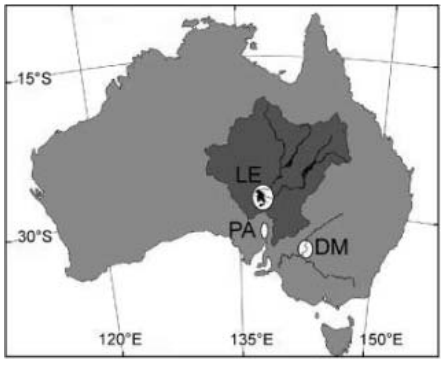

Fig. 1. Map of Australia, showing the Lake Eyre Basin (dark gray) and primary collecting localities around Lake Eyre (LE, black), Port Augusta (PA), and the Darling-Murray Lakes (DM), which include the Minindee, Annabranch, and Willandra Lakes; the Perry Sand Hills; and Lake Victoria.

We reconstructed paleodiets for *Dromaius* and *Genyornis* based on the carbon isotopic composition ($\delta^{13}C$) of their eggshells (tables S1 to S3). Bird eggshells are a calcite biomineral containing 3% organic matter, most of which is sequestered within the calcite crystals of the eggshell, where it is stable in the geological environment for >10^6 years (*15*). The isotopic composition of carbon in eggshell organic residues ($\delta^{13}C_{org}$) and in the calcite matrix ($\delta^{13}C_{carb}$) is determined by the $\delta^{13}C$ of the birds' diet, offset by systematic biochemical fractionation (*16*, *17*). Most plants use either the C_3 or C_4 photosynthetic pathways, which around LE yield average $\delta^{13}C$ values of –26.3 ± 2.1 per mil (‰) and –13.7 ± 0.7‰ (table S6). Crassulacean acid metabolism plants rarely contribute to *Dromaius* diet. The offset between eggshell $\delta^{13}C_{org}$ and the $\delta^{13}C$ values of food sources is 3‰ (*18*), which is similar to that observed in controlled feeding experiments (*17*). The average offset between $\delta^{13}C_{carb}$ and $\delta^{13}C_{org}$ in *Dromaius* eggshell is 10.4 ± 2.0‰ (n = 269), whereas the offset is 11.1 ± 1.5‰ (n = 127) for *Genyornis*, after adjusting for biases due to apparent summer breeding (*18*). Each eggshell records conditions during a single season. Calcite carbon, derived from blood, reflects food sources in the days to weeks before egg-laying (*16*). In contrast, eggshell organic residues are derived from protein sources and reflect both recent and potentially older protein reserves, integrating dietary intake over several months.

Dromaius lives across the Australian mainland, nesting in the austral winter throughout its range. Our 140,000-year dietary reconstruction for *Dromaius* from LE is based on $\delta^{13}C_{org}$

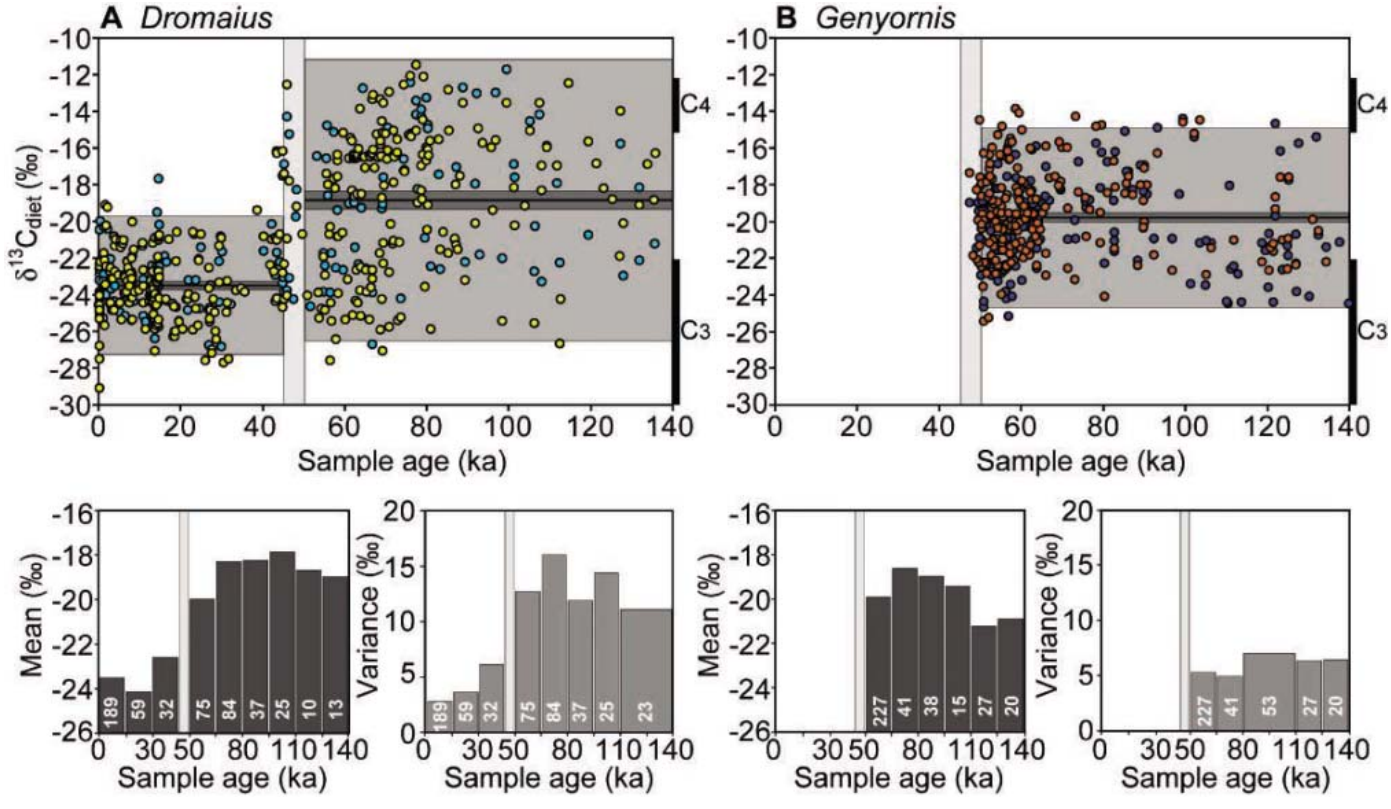

Fig. 2. Time series of *Dromaius* (**A**) and *Genyornis* (**B**) dietary $\delta^{13}C$ reconstructed from $\delta^{13}C_{carb}$ (light colors) and $\delta^{13}C_{org}$ (dark colors) of individually dated eggshells from the LE region (Fig. 1). The vertical bars (50 to 45 ka) define the megafaunal extinction window, with its estimated uncertainty. Measured $\delta^{13}C_{org}$ and $\delta^{13}C_{carb}$ values were converted to dietary $\delta^{13}C$ by applying biochemical fractionation factors (tables S1 to S3). End-member dietary $\delta^{13}C$ values corresponding to 100% C_3 and 100% C_4 diets (±2σ) are shown on the right. Differences in dietary $\delta^{13}C$ values for the preextinction and postextinction windows are shown by the mean (black line), standard error of the mean (dark gray, 95% confidence), and standard deviation (±2σ, light gray). Bar graphs below each time series show the mean and variance calculated for 15,000-year intervals to test whether climate influenced these statistics significantly. White numbers in each bar denote the number of samples (n) in each interval. Because variance is highly dependent on sample size, we have combined adjacent time windows when n < 20.

(n = 181) and $\delta^{13}C_{carb}$ (n = 344) values in individually dated eggshells (Fig. 2). Between 50 and 45 ka, mean dietary $\delta^{13}C$ decreased by at least 3.4‰ (95% confidence level), accompanied by an even larger decrease in dietary variance, from 14.8 to 3.8‰ (Fig. 2). Before 50 ka, *Dromaius* ate a wide range of food sources, ranging from a nearly pure C_4 diet to a nearly pure C_3 diet, with almost any combination of intermediate feeding strategies. This $\delta^{13}C$ distribution is consistent with an opportunistic feeder that lived in an environment with high interannual moisture variability. The isotopic data imply that *Dromaius* utilized abundant nutritious grasslands in wet years (C_4), relying more on shrubs and trees in drier years (C_3). After 45 ka, *Dromaius* utilized a restricted range of food sources, dominated by C_3 plants.

Frequency histograms of *Dromaius* dietary $\delta^{13}C$ (Fig. 3) provide clues about the nature of past ecosystems around LE. Before 50 ka, $\delta^{13}C$ dietary tracers reflect a weakly bimodal pattern, with a broad dominance of C_4 dietary sources and a subsidiary peak dominated by C_3 plants. Two-thirds of both dietary tracers reflect >50% C_4 plant sources, suggesting common nutritious grasslands. In contrast, *Dromaius* living after 45 ka utilized dominantly C_3 dietary sources, always with <50% C_4 plants. Although our dietary reconstructions document increased reliance on C_3 plants by *Dromaius* after 45 ka, the landscape around LE included abundant spinifex and cane grass, C_4 grasses that are largely inedible and low in nutrition and hence a minor component of recent *Dromaius* diets.

To evaluate the possible role of climate in the observed dietary shift, we subdivided the data into 15,000-year intervals back to 140 ka, which includes contrasting climates of the Holocene (15 to 0 ka), the last glacial maximum (30 to 15 ka), and the last interglaciation (125 to 110 ka). The mean and variance of each interval (Fig. 2) are not statistically different from the mean and variance of their larger groupings (>50 and <45 ka), suggesting that climate is not the dominant control on dietary $\delta^{13}C$. The restricted, C_3-dominated dietary range for *Dromaius* after 45 ka persists through the cold, dry, last glacial maximum and the Holocene, when temperatures rose and rainfall increased (*14*, *19*).

The $\delta^{13}C$ values in eggshells of *Genyornis* living around LE between 140 and 50 ka ($\delta^{13}C_{org}$ n = 161; $\delta^{13}C_{carb}$ n = 207; Fig. 2) allow us to compare feeding strategies between a taxon that became extinct and one that survived to the present. *Genyornis* consumed a more restricted diet, exhibiting only 40% of the isotopic variance observed in contemporary *Dromaius*. Frequency histograms of *Genyornis* diet (Fig. 3) are symmetrically distributed and always include some C_4 dietary sources, unlike *Dromaius*, which tolerates a pure C_3 diet. There are no large differences in average dietary $\delta^{13}C$ or in its variance at 15,000-year intervals (Fig. 2), despite large changes in climate (*20*). We conclude that *Genyornis* was a more specialized feeder than *Dromaius*, targeting a specific set of food resources, and that these resources were frequently available through the range of climates between 140 and 50 ka.

To test the inferences derived from the LE data sets, we developed dietary reconstructions using eggshells from two other regions, PA and DM (Fig. 1); both are cooler and wetter than LE. Although both data sets are large, insufficient samples are available to produce time series spanning the past 140,000 years. Luminescence, ^{14}C, and calibrated AAR dates at both sites demonstrate that *Genyornis* extinction and ecosystem change occurred 50 to 45 ka. The lack of any time dependence in the mean or variance in $\delta^{13}C$ for either taxon from LE (Fig. 2) allows firm comparisons between the diets of *Dromaius* and *Genyornis* in age clusters >50 ka and <45 ka for all three regions, without concerns about biasing the statistics by an overrepresentation or absence of data in certain time intervals.

Dietary $\delta^{13}C$ values for *Dromaius* eggshells <45,000 years old from PA and DM reflect almost exclusively C_3 food sources, whereas eggshells >50,000 years old exhibit a greater range in $\delta^{13}C$ values and a higher proportion of C_4 dietary sources (Fig. 3). *Genyornis* dietary $\delta^{13}C$ values exhibit less variance than those of contemporary *Dromaius* and always include some C_4 plants, although in lower proportions (27 to 39%) than at LE (46%). *Genyornis* eggshell $\delta^{13}C$ values show a strong central tendency in both tracers, whereas diets of coexisting *Dromaius* lack a clear central tendency and have greater variance. The results for all three localities are consistent with a substantial reduction in food sources for *Dromaius* 50 to 45 ka and a more specialized feeding strategy for *Genyornis*.

The coeval dietary retraction recorded by *Dromaius* eggshells from three regions widely separated by geography and climate reflects a major disruption in the range of food sources available to the birds about the time of human colonization. If these changes represent a reorganization of vegetation communities across the Australian semiarid zone, we expect to find similar responses in other animal groups. To test this prediction, we measured $\delta^{13}C$ values in hydroxyapatite extracted from wombat tooth enamel from the PA and DM regions (table S4). Wombats are strict herbivores, relying almost exclusively on grasses and reeds. They live, and often die, in sandy deposits used by *Dromaius* and *Genyornis* as breeding sites, and their association with eggshells of known age can date their remains (*18*). Teeth from wombats that lived >50 ka exhibit a wider range of $\delta^{13}C$ values and a much larger proportion of C_4 plants than do teeth of wombats that lived <45 ka (Fig. 3). This difference

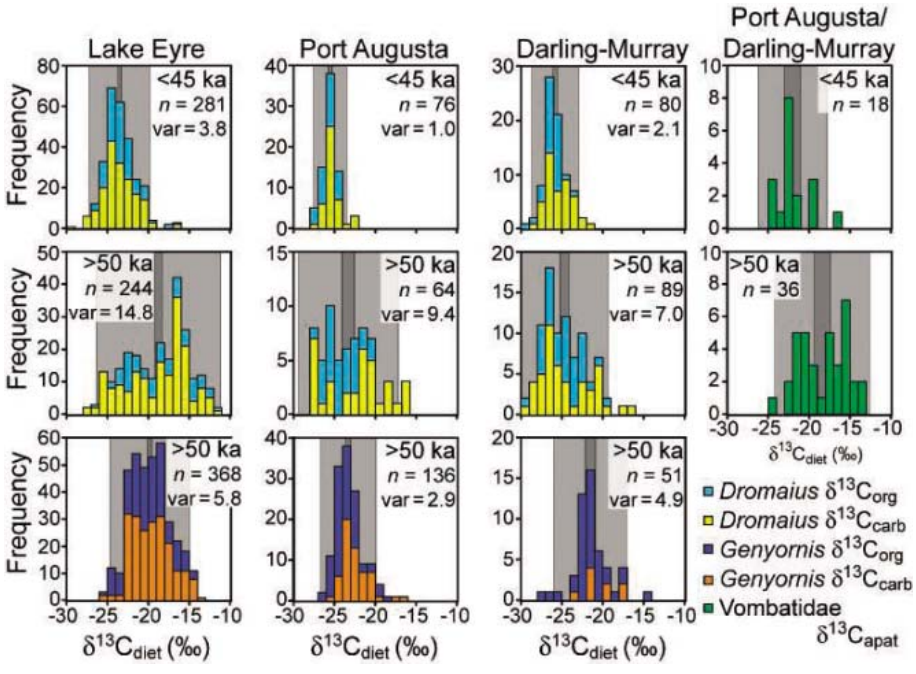

Fig. 3. Frequency histograms of dietary $\delta^{13}C$ for *Dromaius* (middle and top rows) and *Genyornis* (bottom row) from LE, PA, and DM. All sites reveal a shift toward lower mean dietary $\delta^{13}C$ values (95% confidence, dark gray) and reduced spread [$\pm 2\sigma$ (light gray) and variance (var)] after 45 ka. A similar trend is apparent in Vombatidae tooth enamel from PA and DM. *Genyornis* dietary $\delta^{13}C$ always shows less spread and a more consistent proportion of C_4 food sources than does that of coexisting *Dromaius*. Dietary $\delta^{13}C$ is derived from measured $\delta^{13}C_{org}$, $\delta^{13}C_{carb}$, and $\delta^{13}C_{apat}$ (apat, hydroxyapatite) (tables S1 to S4). The number of analyses (n) is shown.

suggests that before 50 ka, C_4 plants made up 40 to 100% of the wombat's dietary intake, whereas after 45 ka, their diet was dominated by C_3 plants, supporting the conclusions derived from *Dromaius* eggshells.

Our eggshell and tooth $\delta^{13}C$ data provide firm evidence for an abrupt ecological shift around the time of human colonization and megafaunal extinction in Australia, about 50 to 45 ka. Climate forcing of the observed vegetation change is unlikely, given that earlier dramatic climate shifts did not result in such a large biotic response and that climate change between 60 and 40 ka was not large, consistent, or sustained. During this interval, the DM region experienced somewhat greater effective moisture, whereas modest drying occurred around LE (*2*, *19*, *20*). A persistently weak Australian monsoon after 45 ka may explain the lack of abundant nutritious C_4 grasses around LE (*14*).

A changed fire regime is another plausible mechanism for ecosystem reorganization. Early human colonizers may have altered the timing and frequency of biomass burning. Humans burn landscapes for many purposes, from clearing passageways and hunting along the fire front, to signaling distant bands and promoting the growth of preferred plants. We speculate that systematic burning practiced by the earliest human colonizers may have converted a drought-adapted mosaic of trees and shrubs intermixed with palatable nutrient-rich grasslands to the modern fire-adapted grasslands and chenopod/desert scrub. Nutrient-poor soils (*21*) may have facilitated the replacement of nutritious C_4 grasses by spinifex, a fire-promoting C_4 grass that is well adapted to low soil nutrient concentrations. A range of C_3 plants may have been lost at the same time, but the isotopic dietary proxy lacks sensitivity to such a loss.

Neither overhunting nor human-introduced diseases, the two most widely cited alternative agents for a human-caused extinction event in Australia, would result in the dramatic changes at the base of the food web documented by our data sets. The reduction of plant diversity apparent in our data, however it came about, would have led to the extinction of specialized herbivores and indirectly to the extinction of their large nonhuman predators. Dietary specialization, rather than feeding strategy (browsing versus grazing), may be the critical extinction predictor. Animals such as *Dromaius*, with wide dietary tolerances, survived the extinction event, whereas more specialized feeders, such as *Genyornis*, became extinct.

References and Notes

1. R. G. Roberts, R. Jones, M. A. Smith, *Nature* **345**, 153 (1990).
2. J. M. Bowler *et al.*, *Nature* **421**, 837 (2003).
3. R. Roberts *et al.*, *Nature* **393**, 358 (1998).
4. C. S. M. Turney *et al.*, *Quat. Geochronol.* **55**, 3 (2001).
5. J. F. O'Connell, J. Allen, *Archaeol. Sci.* **31**, 835 (2004).
6. G. H. Miller *et al.*, *Science* **283**, 205 (1999).
7. R. G. Roberts *et al.*, *Science* **292**, 1888 (2001).
8. C. N. Johnson, G. J. Prideaux, *Austral Ecol.* **29**, 553 (2004).
9. A. P. Kershaw, *Nature* **322**, 47 (1986).
10. C. S. M. Turney *et al.*, *J. Quat. Sci.* **16**, 767 (2001).
11. A. P. Kershaw, P. Moss, S. van der Kaars, *Freshw. Biol.* **48**, 1274 (2003).
12. S. van der Kaars, P. De Deckker, *Rev. Palaeobot. Palynol.* **120**, 17 (2002).
13. P. L. Koch, M. L. Fogel, N. Tuross, in *Stable Isotopes in Ecology and Environmental Science*, K. Lajtha, R. H. Michener, Eds. (Blackwell Scientific, London, 1994), pp. 63–92.
14. B. J. Johnson *et al.*, *Science* **284**, 1150 (1999).
15. G. H. Miller, C. P. Hart, E. B. Roark, B. J. Johnson, in *Perspectives in Amino Acid and Protein Geochemistry*, G. A. Goodfriend, M. J. Collins, M. L. Fogel, S. A. Macko, J. F. Wehmiller, Eds. (Oxford Univ. Press, New York, 2000), pp. 161–181.
16. K. A. Hobson, *Condor* **97**, 752 (1995).
17. B. J. Johnson, M. L. Fogel, G. H. Miller, *Geochim. Cosmochim. Acta* **62**, 2451 (1998).
18. Methods are available as supporting material on *Science* Online.
19. P. P. Hesse, J. W. Magee, S. van der Kaars, *Quat. Int.* **118-119**, 87 (2004).
20. J. W. Magee, G. H. Miller, N. A. Spooner, D. Questiaux, *Geology* **32**, 885 (2004).
21. D. J. Barrett, *Global Biogeochem. Cycles* **16**, 1108 (2002).

22. We thank S. DeVogel, H. Scott-Gagan, N. Spooner, M. Cupper, J. Duncan, and C. Ostertag-Henning for analytical assistance. G.H.M. is responsible for AAR data, M.L.F. and S.J.C. for $\delta^{13}C_{org}$ data, M.K.G. for $\delta^{13}C_{carb}$ data, J.W.M. for site selection, and B.J.J. for eggshell isotope-diet relations. Fieldwork was supported by the U.S. NSF (NSF-ESH) and the Australian Research Council (ARC), and was done with the permission and assistance of local landowners. Analyses were supported by NSF, ARC, and the Australian National University. Assistance in the field provided by P. Clark, S. Webb, G. Atkin, O. Miller, and H. Johnston is gratefully appreciated.

Supporting Online Material

www.sciencemag.org/cgi/content/full/309/5732/287/DC1
Methods
Figs. S1 to S3
Tables S1 to S6
References

22 February 2005; accepted 9 May 2005
10.1126/science.1111288

Stomatal Patterning and Differentiation by Synergistic Interactions of Receptor Kinases

Elena D. Shpak,[1,2]* Jessica Messmer McAbee,[1,2]* Lynn Jo Pillitteri,[1] Keiko U. Torii[1,2]†

Coordinated spacing and patterning of stomata allow efficient gas exchange between plants and the atmosphere. Here we report that three ERECTA (ER)–family leucine-rich repeat–receptor-like kinases (LRR-RLKs) together control stomatal patterning, with specific family members regulating the specification of stomatal stem cell fate and the differentiation of guard cells. Loss-of-function mutations in all three *ER*-family genes cause stomatal clustering. Genetic interactions with a known stomatal patterning mutant *too many mouths* (*tmm*) revealed stoichiometric epistasis and combination-specific neomorphism. Our findings suggest that the negative regulation of ER-family RLKs by TMM, which is an LRR receptor–like protein, is critical for proper stomatal differentiation.

The growth and development of multicellular organisms require both proliferative and asymmetric cell division, the latter of which generates two daughter cells with distinct cell fates. During epidermal development in higher plants, protodermal cells undergo proliferative division to form pavement cells, which protect tissue layers underneath and prevent

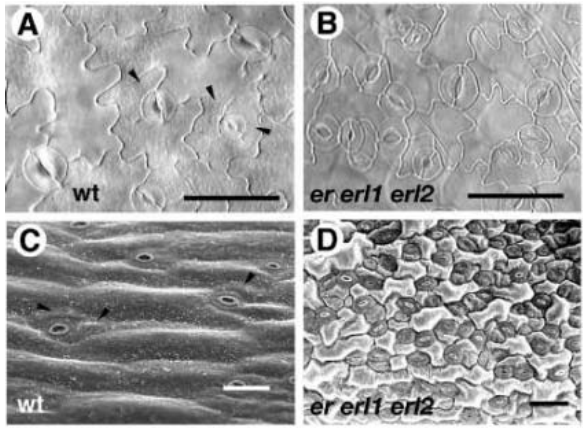

Fig. 1. *ER*-family genes act together in regulating stomatal density and clustering. (**A** and **B**) Cleared differential interference contrast images of abaxial epidermis of a mature rosette leaf of wild type (wt) (A) and *er erl1 erl2* triple mutant (B) leaves. (**C** and **D**) Scanning electron microscopy images of silique epidermis of wild-type (C) and *er erl1 erl2* triple mutant (D) leaves. Overproliferation of stomata and formation of high-density stomatal clusters are evident in the triple mutant. Arrowheads indicate SLGCs. Scale bars in (A) and (B), 50 μm; in (C) and (D), 20 μm.

water loss (*1*). In contrast, differentiation of stomatal complexes initiates with asymmetric divisions in a subset of protodermal cells called meristemoid mother cells, which give rise to small triangular meristemoids (*2*). All derivatives of the meristemoids are defined as stomatal-lineage cells. In *Arabidopsis*, meristemoids typically undergo one to three rounds of asymmetric division. After each division, the smaller daughter cell maintains the stem cell activity of a meristemoid. The meristemoid eventually differentiates into a round guard mother cell, which divides symmetrically to generate a pair of guard cells (*2*). The larger daughter cells generated by asymmetric division of the meristemoids will be defined here as stomatal-lineage ground cells (SLGCs). Although *Arabidopsis* SLGCs would eventually adopt some pavement cell–like characteristics (*2*), they can be clearly distinguished by their small size and shape as well as by their expression of stomatal-lineage markers (Figs. 1 to 3). Some SLGCs may further divide asymmetrically to generate satellite stomatal complexes. The orientation of asymmetric division is regulated by preexisting stomata, so that guard cells are very rarely found adjacent to each other (one-cell spacing rule) (Fig. 1, A and C). The coordinated spacing of stomata indicates that cell-cell signaling is likely very important in stomatal patterning (*2*–*5*).

[1]Department of Biology, University of Washington, Seattle, WA 98195, USA. [2]Core Research for Evolutional Science and Technology, Japan Science and Technology Agency, Saitama, 332-0012, Japan.

*These authors contributed equally to this work.
†To whom correspondence should be addressed. E-mail: ktorii@u.washington.edu

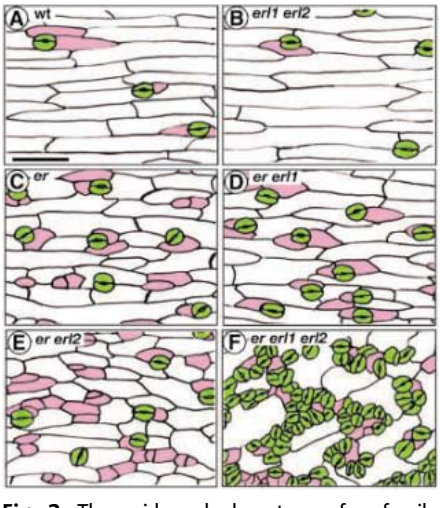

Fig. 2. The epidermal phenotype of *er*-family mutants. Line drawings of mature epidermis of wild-type (wt) (**A**), *erl1 erl2* (**B**), *er* (**C**), *er erl1* (**D**), *er erl2* (**E**), and *er erl1 erl2* (**F**) pedicels [stage 17 (*22*)] are shown. Guard cells and SLGCs are false colored in green and pink, respectively. Scale bar, 50 μm.

A single loss-of-function mutation in *Arabidopsis STOMATAL DENSITY AND DISTRIBUTION1* (*SDD1*), *TOO MANY MOUTHS* (*TMM*), or *YODA* (*YDA*) genes confers increased stomatal density and clusters (*6*–*8*). *SDD1*, *TMM*, and *YDA* encode a putative subtilicin-like extracytoplasmic protease, a transmembrane leucine-rich repeat (LRR) receptor-like protein, and a mitogen-activated protein kinase kinase (MAPKK) kinase, respectively (*7*–*9*). Based on genetic analyses, a model has been proposed in which SDD1 modifies a ligand for TMM, and the activated receptor signals to downstream MAPK cascades via YDA to repress stomata formation (*8*, *10*, *11*). Because TMM lacks any recognizable intracellular domain, signal transduction is thought to occur via interaction with its coreceptor kinase, which has not yet been identified (*9*).

Arabidopsis ER and its functional paralogues *ERL1* and *ERL2* show synergistic interaction in promoting above-ground organ growth (*12*, *13*). These three genes encode members of the large family of plant LRR receptor-like kinases (RLKs) (*13*, *14*). In the cortex, the three ER-family proteins act together to coordinate proliferative cell division (*13*). We investigated the roles of ER-family proteins in epidermal cell patterning to gain insight into their function in tissues that give rise to distinct cell types by asymmetric division. Complete loss of function of all three *ER*-family genes led to the generation of high-density stomatal clusters (Fig. 1, B and D, and fig. S1) and a 50 to 200% increase in the stomatal index (table S1). Together, the ER-family LRR-RLKs act as negative regulators of stomatal development.

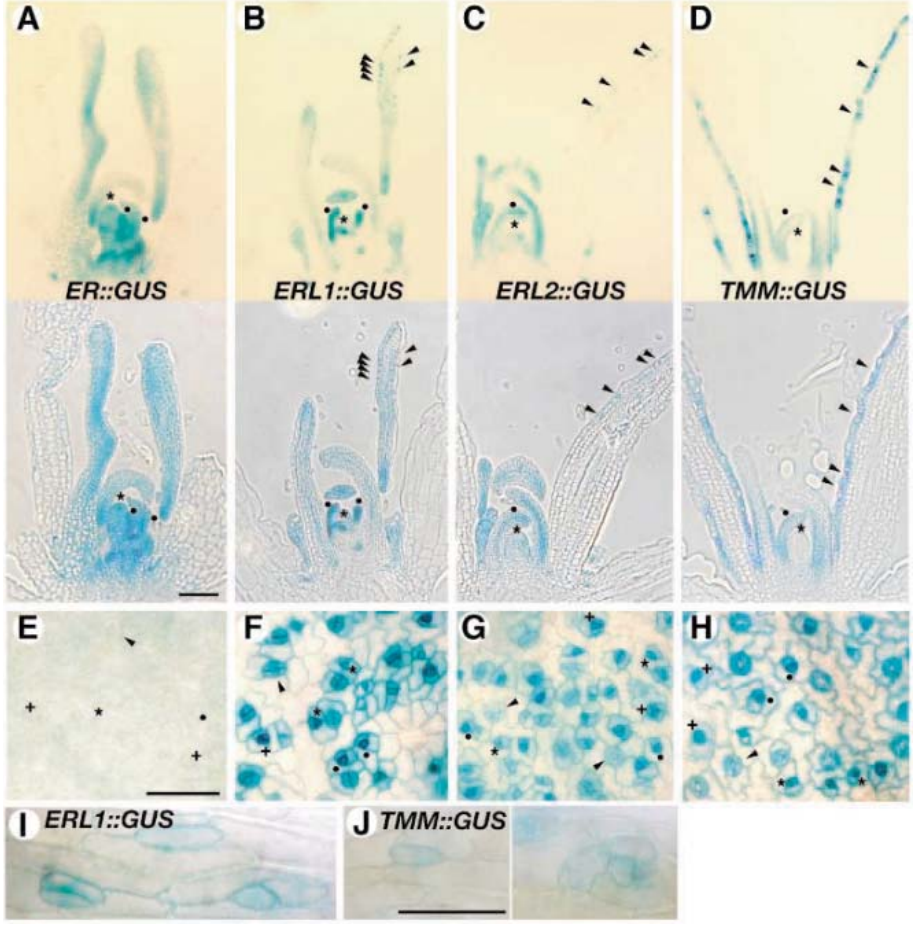

Fig. 3. *ER*, *ERL1*, *ERL2*, and *TMM* promoter activity. (**A** to **D**) Longitudinal sections of the shoot apex of 2-week-old, wild-type seedlings expressing *ER::GUS* (A), *ERL1::GUS* (B), *ERL2::GUS* (C), and *TMM::GUS* (D). The promoters of *ER*-family genes are active in the meristem (marked with asterisks) and entire leaf primordia (marked with black circles), whereas additional stomatal-lineage–specific signal can be seen in the leaf epidermis expressing *ERL1::GUS* and *ERL2::GUS* (arrowheads). *TMM::GUS* marks the protodermal-layer and stomatal-lineage cells. The images of the lower panels were taken with phase-contrast microscopy to show the tissues. Scale bar, 100 μm. (**E** to **H**) Adaxial surface of a developing rosette leaf expressing *ER::GUS* (E), *ERL1::GUS* (F), *ERL2::GUS* (G), and *TMM::GUS* (H). *ERL1*, *ERL2*, and *TMM* promoters are highly active in meristemoids (asterisks), guard mother cells (black circles), and immature guard cells (plus signs); somewhat active in SLGCs and mature guard cells (arrowheads); and not active in pavement cells. Scale bar, 50 μm. (**I** and **J**) SLGCs in *er* pedicel epidermis express moderate levels of stomatal-lineage markers *ERL1::GUS* (I) and *TMM::GUS* (J). Scale bar, 25 μm.

To dissect specific roles for each ER-family protein during stomatal complex formation, we examined epidermal patterning in three single *er*-family mutants, three combinations of double mutants, and a triple mutant (Fig. 2). The phenotypes of *er*-family mutations were uniform in all epidermal tissues that normally produce stomatal complexes, including cotyledons, leaves, stems, pedicels, and siliques (Fig. 2; figs. S1, S2, S4; and S5, and table S1).

The growth phenotypes of *erl1* and *erl2* single-mutant plants, as well as those of *erl1 erl2* double-mutant plants, did not differ from those of the wild type (*12*, *13*). These mutants conferred a reduction in the number of SLGCs. Consequently, many stomata were unaccompanied by SLGCs (Fig. 2B and fig. S1). *ERL1* and *ERL2* may prevent precocious differentiation of meristemoids into guard mother cells or promote continued asymmetric division of the meristemoid to produce a stomatal complex that includes adequate SLGCs.

In contrast, the *er* single mutation conferred an increased number of SLGCs that failed to differentiate into stomata (Fig. 2C and figs. S1 and S2). This failure led to characteristic patches of two or three small cells surrounded by larger pavement cells (Fig. 2C and fig. S1). If each patch of SLGCs is derived from a series of asymmetric divisions of a mersitemoid, then the *er* epidermis must produce substantially more meristemoids. We analyzed the cotyledon epidermis at different developmental time points and observed that *er* undergoes excessive asymmetric division and meristemoid formation (fig. S2). An additional *erl1* or *erl2* mutation had different effects on *er* (Fig. 2, D and E). With an additional *erl1* mutation, guard mother cell differentiation resumed in all of the more numerous stomatal complexes seen in *er* (Fig. 2D), so that the stomatal index was elevated in *er erl1* double mutants (table S1). In contrast, an additional *erl2* mutation enhanced the number of SLGCs seen in *er* (Fig. 2E). The presence of any functional *ER*-family gene was sufficient to enforce the one-cell spacing rule, because stochastic stomatal cluster formation occurred only in the *er erl1 erl2* triple mutant (Figs. 1, B and D; and 2F; and fig S1).

Promoter activity of *ER*, *ERL1*, and *ERL2* in the epidermis of wild-type developing leaves was analyzed to determine whether the timing and location of expression corresponded to the proposed site of function. Initially, all three promoters were uniformly active in the protoderm of wild-type leaf primordia (Fig. 3, A to C). The expression of *ER::GUS* (β-glucuronidase) diminished to below detectable levels before epidermal cells differentiated (Fig. 3, A and E). Meanwhile, *ERL1::GUS* and *ERL2::GUS* showed strong expression in stomatal-lineage cells in developing leaves: high activity in meristemoids, guard mother cells, and immature guard cells; reduced activity in mature guard cells and SLGCs; and no activity in pavement cells (Fig. 3, B, C, F, and G). These expression patterns were very similar to *TMM::GUS* expression (Fig. 3, D and H), so they were used as molecular stomatal-lineage markers to characterize the patches of SLGCs (those small and irregular cells that appear to derive from asymmetric division) seen in the *er* epidermis (Fig. 2C). Indeed, these cells expressed moderate levels of *ERL1::GUS* and *TMM::GUS*, supporting their molecular identity as stomatal-lineage cells (Fig. 3, I and J).

ER-family RLKs regulate two critical steps during stomatal development (fig. S3). First, *ER*, *ERL1*, and *ERL2* together govern the initial decision of protodermal cells to enter proliferative division to produce pavement cells or asymmetric division to generate stomatal complexes. Second, *ERL1* and, to a lesser extent, *ERL2* are important for maintaining stomatal stem cell activity and preventing terminal differentiation of the meristemoid into the guard mother cell.

The identification of three LRR-RLKs involved in stomatal patterning facilitates further understanding of cell-cell signaling in this process. Among known players in stomatal patterning, TMM LRR-receptor–like protein is thought to associate with a coreceptor kinase. *TMM* has contrasting effects in different organs: *tmm* leaves and siliques develop stomatal clusters, whereas *tmm* stems produce no stomata at all (*3*, *15*). We genetically tested the interaction of the *ER* family and *TMM* and discovered the *ER*-family–dependent basis for *TMM* function in different organs. Like *tmm*, *tmm er* and *tmm erl2* formed no stomatal-lineage cells in the stems, indicating that *TMM* is epistatic to *ER* and *ERL2* (Fig. 4, A and B, and fig. S4). *TMM* is partially epistatic to *ERL1*, because *tmm erl1* led to the formation of stomata, albeit at a very low density (fig. S4). *tmm er erl1* conferred recovery of stomatal differentiation at normal density (Fig. 4C and fig. S4). Finally, the *tmm er erl1 erl2* quadruple mutant formed stomatal clusters similar to *er erl1 erl2*, indicating that together, the three *ER*-family genes are epistatic to *TMM* (Fig. 4D and fig. S4). The epistasis of *TMM* to *ER* and *ERL2* in the stem is dependent on the presence of functional *ERL1*. Therefore, *TMM* may primarily act to inhibit the activity of *ERL1* in repressing asymmetric division in the stomatal pathway. The stoichiometric dynamics of epistasis suggest that these four putative receptors act in close proximity.

In cauline leaves and siliques, where *tmm* and *er erl1 erl2* independently form clustered stomata, specific combinations of *tmm* and *er*-family mutations created a novel phenotype. Whereas *tmm* produced some clustered stomata (Fig. 4E) and *er* produced stomatal com-

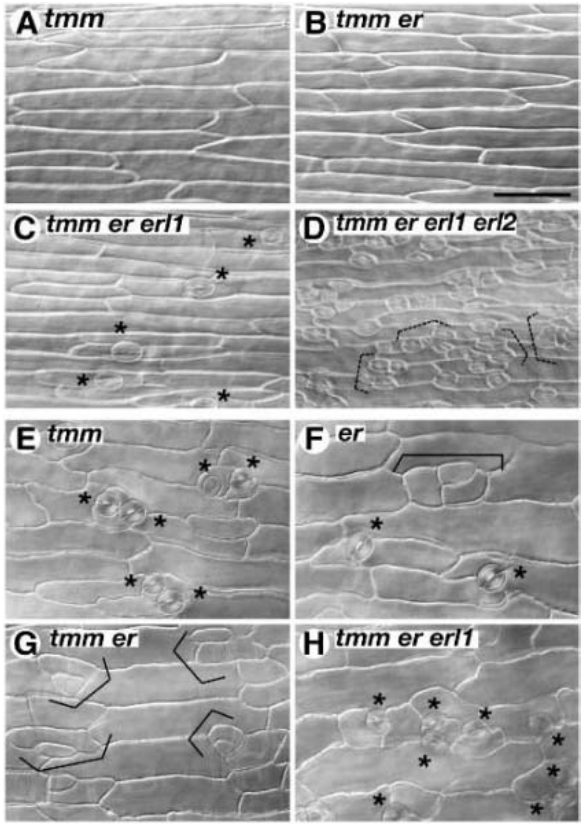

Fig. 4. Genetic interactions of ER-family RLKs and TMM. (**A** to **D**) Stoichiometric nature of epistasis between *ER*-family genes and *TMM* in stem epidermis. *tmm* (A) and *tmm er* (B) do not differentiate stomata. In contrast, *tmm er erl1* (C) confers a recovery of stomatal differentiation (asterisks). A *tmm er erl1 erl2* quadruple mutant (D) produces high-density stomatal clusters (dashed brackets). (**E** to **H**) A combination-specific neomorphism revealed by interactions of *TMM* with *ER*-family genes in silique epidermis. *tmm* (E) produces guard cells (asterisks) with a mild clustering, whereas *er* (F) confers occasional failure of guard mother cell differentiation (bracket). In *tmm er* double mutants (G), all stomatal-lineage cells adopted SLGC cell fate (brackets). Again, guard cells (asterisks) differentiate in *tmm er erl1* (H). Scale bar, 50 μm.

plexes with and without guard cells (Fig. 4F), both *tmm er* and *tmm er erl2* differentiated SLGCs but no stomata (Fig. 4G and fig. S5). However, an additional *erl1* mutation caused stomatal differentiation to resume as *tmm er erl1* formed stomata (Fig. 4H). *tmm er erl1 erl2* silique epidermis resembled *er erl1 erl2* epidermis (fig. S5). The observed neomorphism in *tmm er* and *tmm er erl2* indicates that *TMM* is conditionally required for stomata formation in the absence of *ER*. Again, *TMM* may inhibit the activity of *ERL1,* this time in repressing guard mother cell differentiation.

The complex interaction of *TMM* and *ER*-family genes suggests that their products are not simply upstream or downstream of each other but work in combination to determine stomatal-lineage cell fate. *TMM* negatively regulates specific *ER*-family members at both critical steps in stomatal differentiation, first at the initial decision of a protodermal cell to divide asymmetrically to enter the stomatal lineage and then at the later decision of a meristemoid to terminally differentiate into a guard mother cell (fig. S3). The mechanism for regulation of the ER family by TMM is unknown. One possibility is that TMM forms a receptor heterodimer with ER-family RLKs, most likely with ERL1, and prevents signaling. The lack of a signal transducer domain in TMM supports this inhibitory function. The association of an LRR-RLK with an LRR receptor–like protein has been proposed for shoot apical meristem development, in which case CLAVATA1 (CLV1) and CLV2 may form a functional heterodimer to signal (*16*, *17*). Alternatively, TMM may titrate the same ligands as the ER family, hence repressing the ER-family signaling pathway. In the absence of TMM, ER, and ERL2, remaining ERL1 could become overly active as an inhibitor of guard mother cell differentiation because of excessive ligand availability.

We have shown that three ER-family RLKs act in overlapping but unique manners during stomatal stem cell fate specification and differentiation. Landsberg *er* was isolated nearly half a century ago and has since been used as a wild type (*18*). However, the effects of *er* on epidermal patterning have not been documented until now. Using distinct combinations of *er*-family mutants, we have elucidated a specific function for TMM during stomatal development in different organs. The diverse and overlapping functions of ER-family RLKs highlight the versatile nature of this receptor subfamily and emphasize the universal theme of receptor signaling in plants and animals. In animals, key signaling components, such as bone morphogenetic protein and Wnt, act as both mitogens and morphogens in various developmental processes, and their signaling pathways are used reiteratively during development (*19*–*21*). Similarly, ER-family RLKs regulate cell proliferation and differentiation, during both plant organ growth and epidermal patterning. Now that a possible receptor partner for stomatal differentiation has been identified, we can begin to elucidate how specific functions of ER-family RLKs are manifested at the molecular and cellular level. The use of the same signaling components in different combinations for unique developmental processes has likely been a key factor in the diversification of plants.

References and Notes

1. B. J. Glover, *J. Exp. Bot.* **51**, 497 (2000).
2. J. A. Nadeau, F. D. Sack, *Stomatal Development in Arabidopsis*, in *The Arabidopsis Book*, C. Somerville, E. Meyerowitz, Eds. (American Society of Plant Biologists, Rockville, MD, 2002), available at www.aspb.org/publications/arabidopsis.
3. L. Serna, C. Fenoll, *Trends Plant Sci.* **5**, 458 (2000).
4. M. Geisler, J. Nadeau, F. D. Sack, *Plant Cell* **12**, 2075 (2000).
5. M. J. Geisler, D. O. Deppong, J. A. Nadeau, F. D. Sack, *Planta* **216**, 571 (2003).
6. M. Yang, F. D. Sack, *Plant Cell* **7**, 2227 (1995).
7. D. Berger, T. Altmann, *Genes Dev.* **14**, 1119 (2000).
8. D. C. Bergmann, W. Lukowitz, C. R. Somerville, *Science* **304**, 1494 (2004).
9. J. A. Nadeau, F. D. Sack, *Science* **296**, 1697 (2002).
10. L. Serna, *Nature* **430**, 302 (2004).
11. F. D. Sack, *Science* **304**, 1461 (2004).
12. E. D. Shpak, M. B. Lakeman, K. U. Torii, *Plant Cell* **15**, 1095 (2003).
13. E. D. Shpak, C. T. Berthiaume, E. J. Hill, K. U. Torii, *Development* **131**, 1491 (2004).
14. K. U. Torii *et al.*, *Plant Cell* **8**, 735 (1996).
15. M. Geisler, M. Yang, F. D. Sack, *Planta* **205**, 522 (1998).
16. S. Jeong, A. E. Trotochaud, S. E. Clark, *Plant Cell* **11**, 1925 (1999).
17. C. C. Carles, J. C. Fletcher, *Trends Plant Sci.* **8**, 394 (2003).
18. G. P. Rédei, *Z. Vererbungsl.* **93**, 164 (1962).
19. B. L. Hogan, *Genes Dev.* **10**, 1580 (1996).
20. K. M. Cadigan, R. Nusse, *Genes Dev.* **11**, 3286 (1997).
21. R. T. Moon, B. Bowerman, M. Boutros, N. Perrimon, *Science* **296**, 1644 (2002).
22. D. R. Smyth, J. L. Bowman, E. M. Meyerowitz, *Plant Cell* **2**, 755 (1990).

23. We thank T. Kakimoto, D. Kimelman, D. Raible, and D. Sloan for commenting on the manuscript; M. Geisler for providing detailed protocols for quantitative analysis of stomata; and the Arabidopsis Biological Resource Center for *tmm-1* seeds. Supported by the U.S. Department of Energy (grant DE-FG02-03ER15448) and by a Japan Science and Technology Agency–Core Research for Evolutional Science and Technology award to K.U.T. L.J.P. is a U.S. Department of Agriculture–National Research Initiative Competitive Grants Program postdoctoral fellow. K.U.T. was a University of Washington–ADVANCE professor.

Supporting Online Material

www.sciencemag.org/cgi/content/full/309/5732/290/DC1
Materials and Methods
Figs. S1 to S5
Table S1

12 January 2005; accepted 13 May 2005
10.1126/science.1109710

FKF1 F-Box Protein Mediates Cyclic Degradation of a Repressor of *CONSTANS* in *Arabidopsis*

Takato Imaizumi, Thomas F. Schultz, Frank G. Harmon, Lindsey A. Ho, Steve A. Kay*

The temporal control of CONSTANS (CO) expression and activity is a key mechanism in photoperiodic flowering in *Arabidopsis*. FLAVIN-BINDING, KELCH REPEAT, F-BOX 1 (FKF1) protein regulates *CO* transcription, although the molecular mechanism is unknown. We demonstrate here that FKF1 controls the stability of a Dof transcription factor, CYCLING DOF FACTOR 1 (CDF1). FKF1 physically interacts with CDF1, and CDF1 protein is more stable in *fkf1* mutants. Plants with elevated levels of CDF1 flower late and have reduced expression of *CO*. *CDF1* and *CO* are expressed in the same tissues, and CDF1 binds to the *CO* promoter. Thus, FKF1 controls daily *CO* expression in part by degrading CDF1, a repressor of *CO* transcription.

Photoperiodism manages a plant's flowering in response to changes in day length (*1*–*3*) through control of CONSTANS (CO) protein expression and activity (*4*–*7*). The protein FLAVIN-BINDING, KELCH REPEAT, F-BOX 1 (FKF1) governs the daytime expression pattern of *CO* (*6*) and is thought to be a component of a Skp1-Cullin-F-box (SCF) E3 ubiquitin ligase complex (*8*–*10*). This raises the possibility that FKF1 controls *CO* expression by degrading a regulator of *CO*. For most *Arabidopsis* F-box proteins, the C-terminal domains contain specific binding sites for substrates targeted for ubiquitination (*11*). With the use of a yeast two-hybrid screen to isolate proteins interacting with the FKF1 C-terminal kelch repeats, we identified three Dof transcription factors (*12*) (Fig. 1A). These Dof proteins also interacted with the LOV KELCH REPEAT PROTEIN 2 (LKP2) kelch repeats

Department of Cell Biology, The Scripps Research Institute, 10550 North Torrey Pines Road, La Jolla, CA 92037, USA.

*To whom correspondence should be addressed. E-mail: stevek@scripps.edu

but not with the ZEITLUPE (ZTL) kelch repeats (Fig. 1A). Because the expression levels of the three Dof transcripts oscillated in constant light conditions (Fig. 1B), we named these genes *CYCLING DOF FACTOR 1* (*CDF1*), *CDF2*, and *CDF3* (Arabidopsis Genome Initiative gene codes At5g62430, At5g39660, and At3g47500, respectively) (fig. S1). To verify the interactions detected in yeast, we carried out binding studies using recombinant glutathione *S*-transferase (GST)–FKF1 and –LKP2 kelch fusions and the three His/T7-CDF proteins. The results of the in vitro pull-down assays were similar to those of the two-hybrid assays (Fig. 1C), validating the interactions observed in yeast.

If FKF1, LKP2, or both are involved in the degradation of CDF proteins in vivo, overexpression of these CDF proteins might produce flowering phenotypes similar to those of *fkf1* and/or *lkp2* loss-of-function mutant plants. Plants overexpressing *CDF1* (*35S::CDF1* plants) (fig. S3) flowered later than wild-type plants in long-day (LD) conditions (Fig. 1D). In contrast, overexpression of either *CDF2* or *CDF3* did not change flowering time under long- or short-day (SD) conditions (*13*). The flowering phenotype of the *lkp2* mutant (fig. S2) resembled that of wild-type plants (Fig. 1D). Because the *fkf1* mutant, but not the *lkp2* mutant, exhibited a late-flowering phenotype similar to that of the *35S::CDF1* lines, this raised the possibility that FKF1 might be responsible for regulating CDF1 protein turnover in vivo.

To characterize the flowering time phenotype of the *cdf1* mutants, we used double-stranded RNA interference (RNAi) to reduce *CDF1* expression in wild-type and *fkf1* plants. *CDF1* expression in *CDF1* RNAi (*cdf1-R*) lines (wild-type and *fkf1*) was reduced to less than 15% of that observed in nontransgenic lines (fig. S3). The *cdf1-R* lines flowered earlier than wild-type plants in LD conditions (fig. S4), indicating that CDF1 may contribute to the regulation of flowering time. In *fkf1 cdf1-R* lines, reduction of *CDF1* expression also resulted in early flowering but did not completely rescue the *fkf1* late-flowering phenotype (fig. S4). This suggests that CDF1 is not the sole effector of FKF1 control over flowering time, athough the *CDF1* gain-of-function experiments indicate a genetic interaction between *FKF1* and *CDF1*.

To determine whether FKF1 regulates CDF1 protein stability in vivo, we examined the expression of CDF1 protein in the wild type and in the *fkf1* mutant. We used transgenic plants constitutively expressing hemagglutinin (HA)–tagged CDF1 (*35S::HA-CDF1*) to distinguish between transcriptional and post-transcriptional control of CDF1 protein levels. Plants harboring the *35S::HA-CDF1* construct exhibited a similar late-flowering phenotype to those with *35S::CDF1* (*13*). Although the expression of the *CDF1* transcripts was constitutively high in both LD and SD conditions, HA-CDF1 protein levels were diminished from *zeitgeber* time (ZT) 10 to ZT22 in LD and ZT7 to ZT19 in SD conditions (Fig. 2, A and B), indicating that CDF1 protein abundance is post-transcriptionally regulated. Consistent with this notion, *35S::HA-CDF1* plants treated with the proteasome inhibitor MG-132 from ZT8 to ZT16 exhibited elevated levels of HA-CDF1 proteins at ZT16 (fig. S5), demonstrating that the stability of CDF1 is controlled by the proteasome-dependent pathway. In the *fkf1* mutant background, HA-CDF1 protein was more stable between ZT10 to ZT22 in LD and ZT7 to ZT19 in SD conditions, compared to the wild type (Fig. 2, C and D, and fig. S6). These results indicate that FKF1 functions as an E3 ubiquitin ligase involved in CDF1 protein turnover.

Because the *35S::HA-CDF1* construct does not reflect the endogenous expression pattern of *CDF1*, we used an *HA-CDF1* cDNA driven by the *CDF1* promoter (*CDF1::HA-CDF1*) to analyze the native expression of CDF1. *CDF1::HA-CDF1* (*24*) and *fkf1-2/CDF1::HA-CDF1* (*29*) lines with similar *CDF1* transcript levels (fig. S3) were used in our analysis. In both lines, HA-CDF1 protein levels remained high in the morning in both LD and SD conditions. In the *CDF1::HA-CDF1* line, CDF1 protein decreased rapidly to undetectable levels between ZT7 and ZT10 in LD and between ZT4 and ZT10 in SD conditions (Fig. 2, E and F). By contrast, we observed a more gradual decrease in CDF1 protein abundance in the *fkf1-2/CDF1::HA-CDF1* line during these time periods (Fig. 2, G and H). Because FKF1 protein begins to accumulate during this part of the day, the data suggest that FKF1 mediates the acute reduction of CDF1 protein observed in the *CDF1::HA-CDF1* line.

To further verify that FKF1 is directly involved in the degradation of CDF1, we analyzed the in vivo protein stability of a CDF1 variant harboring a point mutation (K253A) that attenuates the binding to FKF1 in yeast (fig. S6). When the *CDF1 K253A* transcript was driven by the constitutive 35S promoter, the CDF1 K253A protein was more stable in transgenic lines than nonmutated CDF1 protein at ZT13 (the time of the peak expression of FKF1) (fig. S6). In addition, when the *CDF1 K253A* cDNA was introduced in plants with a *CDF1* minigene context (*CDF1::HA-CDF1 K253A* plants) (fig. S3), the expression profiles of CDF1 K253A protein resembled those of CDF1 protein expressed in *fkf1* mutants (Fig. 2, I and J). These results indicate that the physical interaction with FKF1 renders the CDF1 protein unstable in vivo. We also examined whether FKF1 controls *CDF1* transcription and determined that *CDF1* expression in *fkf1* was similar to that in wild-type plants (fig. S3), indicating that FKF1 is not likely a regulator of *CDF1* transcription. To-

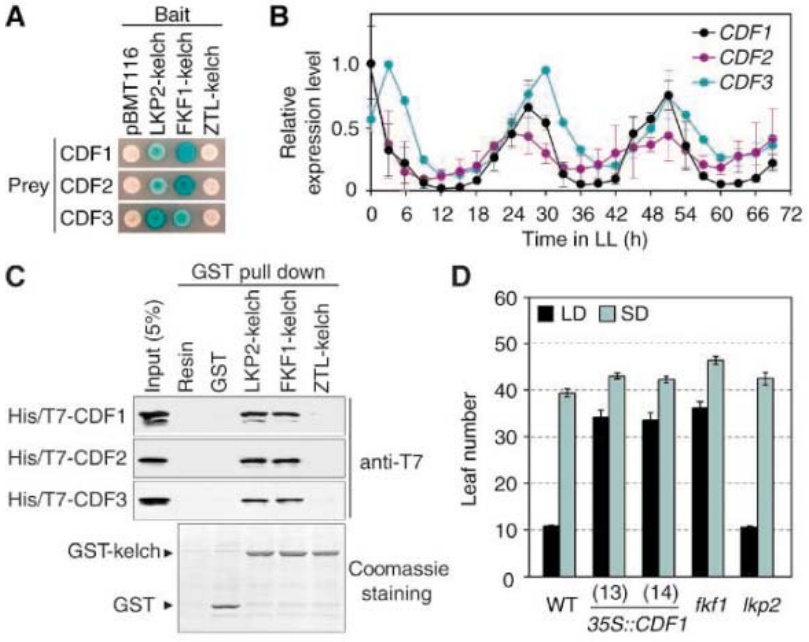

Fig. 1. FKF1 binds to the CDF1 protein, which affects flowering time. (**A**) Interaction between the FKF1, LKP2, and ZTL kelch domains and the CDF1, CDF2, and CDF3 proteins in yeast. Bait, a hybrid protein containing a DNA binding domain; prey, a hybrid protein containing an activation domain (*18*). (**B**) Expression patterns of *CDF1*, *CDF2*, and *CDF3* transcripts under constant light conditions (LL). Wild-type plants were entrained under 12 hours light and 12 hours dark conditions for 10 days and then released to the LL condition. The data show the mean ± SEM of quantified expressions of three experiments. (**C**) In vitro pull-down assay between FKF1, LKP2, and ZTL kelch domains and CDF proteins. (**D**) Flowering time phenotype of the wild type (WT), *CDF1*-overexpressing lines (*35S::CDF1*), and *fkf1* and *lkp2* mutants under LD and SD conditions. Data are mean ± SEM of 16 plants.

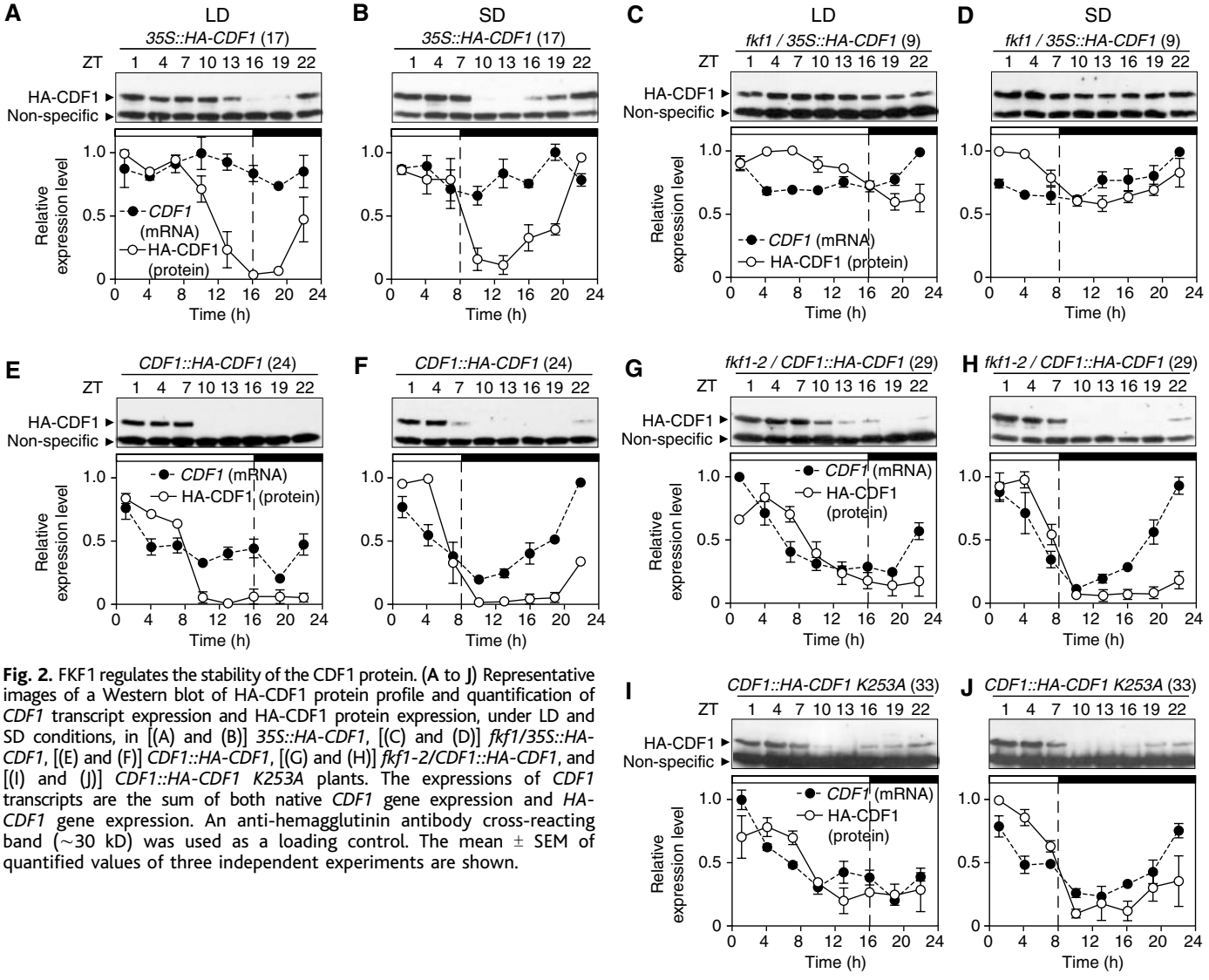

Fig. 2. FKF1 regulates the stability of the CDF1 protein. (**A** to **J**) Representative images of a Western blot of HA-CDF1 protein profile and quantification of *CDF1* transcript expression and HA-CDF1 protein expression, under LD and SD conditions, in [(A) and (B)] *35S::HA-CDF1*, [(C) and (D)] *fkf1/35S::HA-CDF1*, [(E) and (F)] *CDF1::HA-CDF1*, [(G) and (H)] *fkf1-2/CDF1::HA-CDF1*, and [(I) and (J)] *CDF1::HA-CDF1 K253A* plants. The expressions of *CDF1* transcripts are the sum of both native *CDF1* gene expression and *HA-CDF1* gene expression. An anti-hemagglutinin antibody cross-reacting band (~30 kD) was used as a loading control. The mean ± SEM of quantified values of three independent experiments are shown.

gether with the data demonstrating that FKF1 regulates HA-CDF1 protein stability, these results suggest that endogenous CDF1 abundance is higher in the *fkf1* mutant compared to the wild type, especially in late afternoon.

FKF1 is involved in the regulation of proper daytime *CO* expression (*6*), and *CO* transcripts are expressed in specific tissues (*14*, *15*). If CDF1 is a transcription factor involved in the regulation of *CO* expression, the spatial pattern of *CDF1* expression is likely to overlap with that of *CO*. To examine the subcellular localization of CDF1 protein, we generated plants expressing a CDF1–yellow fluorescence protein (YFP) fusion and determined that the protein was localized in the nucleus (Fig. 3). We then analyzed the spatial expression pattern of *CDF1* using a *CDF1* promoter–driven β-glucuronidase (*GUS*) gene construct (*CDF1::GUS*). CDF1::GUS activity was observed mainly in the vascular tissues of cotyledons, leaves, and hypocotyls, as well as in stomata, and the staining patterns were similar between LD- and SD-grown plants (Fig. 3). No GUS activity was detected in the roots under either growth condition (*13*). *FKF1::GUS* is expressed in whole leaves and strongly in stomata (*16*), whereas *CO::GUS* is expressed in vascular tissues (*14*, *15*). The overlapping expression patterns of *FKF1*, *CDF1*, and *CO* support the notion that these genes are involved in the same regulatory pathway.

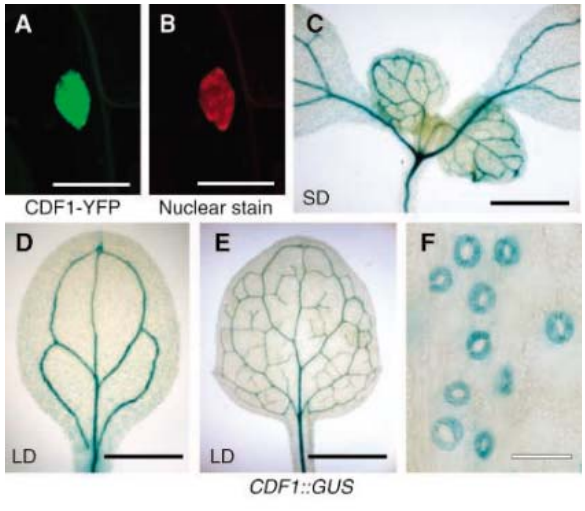

Fig. 3. CDF1 is a nuclear protein and expresses mainly in vascular tissues. (**A**) Subcellular localization of CDF1-YFP protein in root. (**B**) Nuclear staining of the same cell shown in (A). Scale bars in (A) and (B), 10 μm. (**C** to **F**) Staining of GUS activity in *CDF1::GUS* plants. *CDF1::GUS* plants were grown under LD or SD conditions. Scale bars in (C) to (E), 2 mm. Scale bar in (F), 50 μm.

Considering that CDF1 may be involved in the regulation of *CO* expression, we examined *CO* and *FLOWERING LOCUS T* (*FT*) expression in both *CDF1* gain- and loss-of-function mutants. In *35S::CDF1* plants, *CO* expression was suppressed at all ZT times under both LD and SD conditions (Fig. 4A and fig. S7), indicating that CDF1 functions as a transcriptional repressor of *CO*. *FT* transcript was not induced under either LD or SD conditions in *35S::CDF1* plants (fig. S8), which is likely due to the severely depressed *CO* levels. In *cdf1-R* lines, both the *CO* and *FT* expression patterns were unaltered (figs. S7 and S8), suggesting the existence of an additional suppressor(s) of *CO*. In *fkf1 cdf1-R* lines, we observed an increase in *CO* expression under LD conditions from ZT10 to ZT19 (Fig. 4B and fig. S7), the time period in which CDF1 protein is more abundant in the *fkf1* mutant versus wild-type plants. In addition, the slight increase in *CO* transcription in *fkf1 cdf1-R* lines under LD conditions appeared to be sufficient to elevate the peak level of *FT* expression, a sensitive readout for the level of *CO* induction (fig. S8). These results support the notion that CDF1 is a suppressor of *CO*. However, the daytime peak of *CO*, which is present in the wild type, was not observed in the *fkf1 cdf1-R* plants; thus, FKF1-mediated degradation of CDF1 is not the only mechanism by which FKF1 controls the daytime *CO* expression.

To further analyze the role of CDF1 as a suppressor of *CO*, we used *CDF1::HA-CDF1* plants with varying levels of CDF1 expression. Increasing *CDF1* dosage resulted in an incremental delay in flowering time under LD conditions (fig. S10). Because *FKF1* is expressed in these lines, it is expected that higher levels of CDF1 would be observed in the morning (Fig. 2 and fig. S9). The levels of *CO* expression in these lines were reduced in the early morning (from ZT22 to ZT1) (Fig. 4C and figs. S7 and S9). Induction of *FT* was also delayed, and the daily amount of *FT* expression was reduced (figs. S8 and S9). This alteration in *FT* expression is likely to contribute to the late-flowering phenotype observed in these lines. In the *CDF1::HA-CDF1 K253A* line, *CO* expression was reduced at all ZT time points under LD and SD conditions (Fig. 4D and fig. S7), and *FT* expression was diminished under both LD and SD conditions (fig. S8). In addition, two *CDF1::HA-CDF1 K253A* lines (expressing a stable CDF1 variant) (Fig. 2) with less than threefold overexpression of *CDF1* displayed a late-flowering phenotype (fig. S10) similar to that observed in *35S::CDF1* lines with greater than 50-fold overexpression. Thus, the removal of CDF1 protein in the afternoon by FKF1 regulates *CO* expression and subsequent flowering events.

To determine if CDF1 directly regulates *CO* expression, we analyzed the *CO* promoter for CDF1 binding sites. Twenty putative Dof binding sites (AAAG) lie within 1 kilobase pair upstream of the *CO* transcription start site. Two regions in the *CO* promoter contained clusters of three or four Dof binding sites (–397/–358 and –173/–135 regions) (Fig. 4E). CDF1 protein binds to both fragments but exhibited a 10-fold greater preference for the

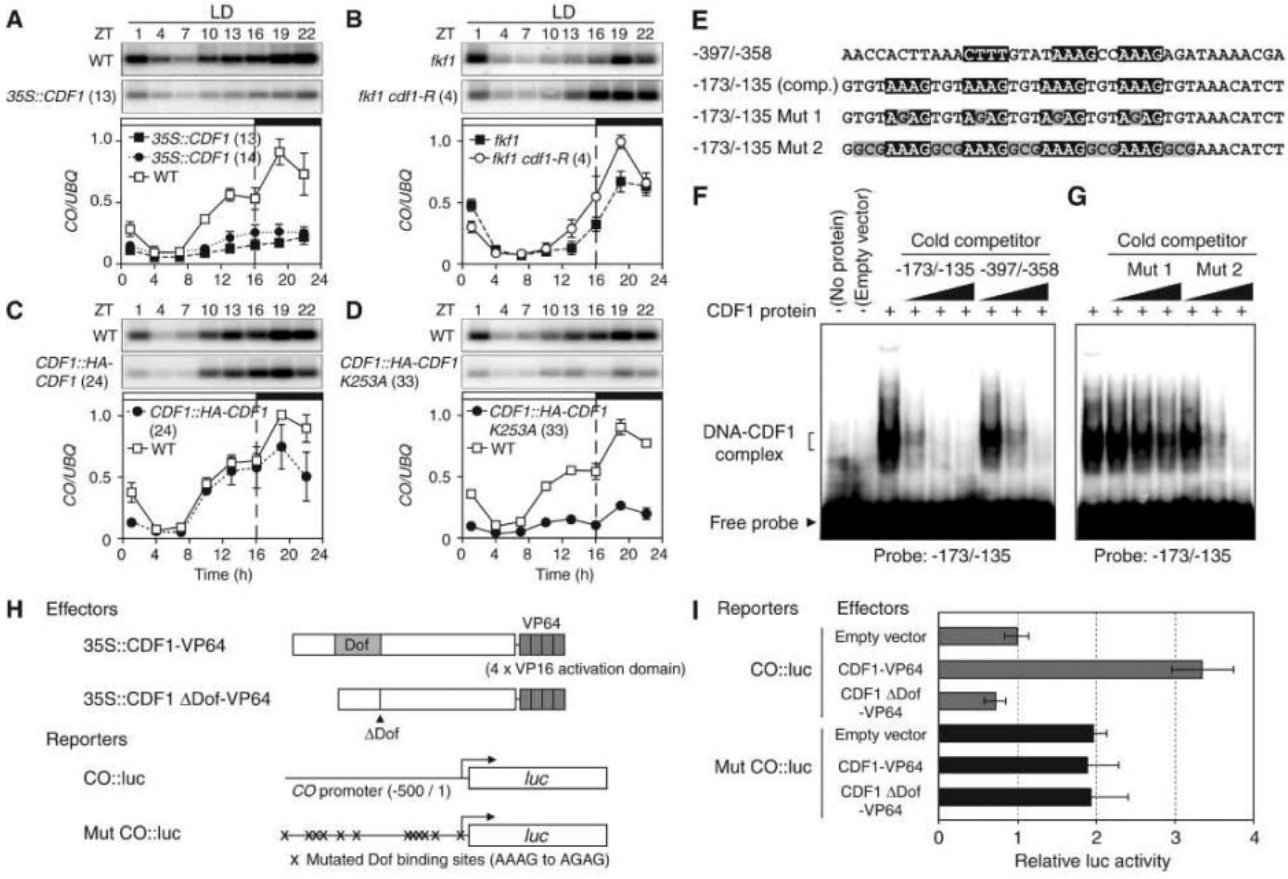

Fig. 4. CDF1 functions as a *CO* repressor and binds to specific sequences in the *CO* promoter. (**A** to **D**) *CO* expression under LD conditions in (A) wild-type and *35S::CDF1* plants, (B) *fkf1* and *fkf1 cdf-R* plants, (C) wild-type and *CDF1::HA-CDF1* plants, and (D) wild-type and *CDF1::HA-CDF1 K253A* plants. Representative blotting images of individual transgenic lines and the mean ± SEM of quantified values of blotting images derived from three independent experiments are shown in all panels. *UBQ*, ubiquitin (*4*–*6*). (**E**) The sequences of the probe and the competitors for DNA binding assay. The Dof binding motifs are shaded in black, and the nucleotide changes in the mutated fragments are shaded in gray. The sequences of the complementary strands are shown for the –173/–135 fragments. (**F** and **G**) Sequence specificity of CDF binding. We used (F) two sequences present in the *CO* promoter or (G) two mutated sequences as cold competitors. The molar ratios of probe to competitors are 1:1, 1:10, and 1:100. (**H**) Schematic drawing of effectors and reporters used in the transient assay. (**I**) The effects of CDF1-VP64 protein on the two *CO* promoter activities. The activities of the firefly luciferase (luc) were normalized by the activities of Renilla luciferase. The mean ± SEM of normalized values of four independent samples are shown.

–173/–135 fragment over the –397/–358 fragment (Fig. 4F). The sequences of these fragments differ not only in the number of the Dof binding motifs but also in the makeup of the sequences flanking the motifs (TGT versus nonconserved sequences). To assess whether the TGT flanking sequences confer specificity for CDF1 binding to the –173/–135 region, we mutated the –173/–135 fragment in both the consensus Dof binding site (Mut 1) and the flanking sequences (Mut 2) (Fig. 4E). The Mut 1 probe did not compete effectively with the nonmutated probe, and the Mut 2 probe was 10 times less effective as a competitor than the original probe (Fig. 4G). Thus, the core Dof binding sequence is necessary for CDF1 binding, whereas the flanking TGT sequence contributes to the specificity of binding.

To verify the direct binding of CDF1 to the Dof binding sites in the *CO* promoter in vivo, we performed a transient expression assay in which seedlings were bombarded with particles coated with constructs encoding CDF1 proteins and *CO* promoter–driven luciferase (*luc*) gene reporters (Fig. 4H and fig. S11). Both CDF1 and CDF1 K253A reduced the *CO* promoter activity (fig. S11). However, the reduction in *luc* expression may have been caused by physical damage due to bombardment. To avoid this complication, a translational fusion of CDF1 and the tetrameric VP16 activation domains (VP64) was constructed to convert this molecule to a transcriptional activator (*17*). The CDF1-VP64 fusion protein activated the CO (2.5 kb)::luc reporter, whereas neither CDF1 ΔDof-VP64 or VP64 alone stimulated expression of the reporter (fig. S11); thus, the Dof domain of CDF1-VP64 is required for activation. CDF1-VP64, but not CDF1 ΔDof-VP64, also induced *luc* expression driven by a smaller *CO* promoter (0.5 kb) (Fig. 4I). We then examined the ability of CDF-VP64 to activate a *CO* promoter with 11 Dof-binding site mutations (Fig. 4H). The basal level of *luc* expression of the mutated *CO* reporter was twofold higher than that of the nonmutated one (Fig. 4I), suggesting that endogenous Dof transcription factor(s) are involved in the repression of *CO* promoter activity. Importantly, CDF1-VP64 failed to induce the expression of the mutated *CO* promoter::luc reporter (Fig. 4I). Together with the findings from the in vitro DNA binding assay, these results indicate that CDF1 directly binds to the Dof binding sites in the *CO* promoter to regulate *CO* transcription.

Control of CO expression and activity is crucial in the regulation of photoperiodic flowering in *Arabidopsis* (*2*, *7*). We have determined that, in the afternoon, FKF1 F-box protein degrades the transcription factor CDF1, a suppressor of *CO*. We propose that *CO* is repressed in the morning partially because of the accumulation of CDF1 binding to the *CO* promoter. Late in the afternoon, as FKF1 levels rise, CDF1 protein is quickly degraded in an FKF1-dependent manner to reduce the suppression of *CO*. Concomitantly, FKF1 also promotes *CO* transcription by a currently unknown mechanism(s) to produce the *CO* peak during the critical time period in which CO activity is required to promote flowering.

References and Notes

1. W. W. Garner, H. A. Allard, *J. Agric. Res.* **18**, 553 (1920).
2. M. J. Yanovsky, S. A. Kay, *Nat. Rev. Mol. Cell Biol.* **4**, 265 (2003).
3. R. Hayama, G. Coupland, *Plant Physiol.* **135**, 677 (2004).
4. P. Suarez-Lopez *et al.*, *Nature* **410**, 1116 (2001).
5. M. J. Yanovsky, S. A. Kay, *Nature* **419**, 308 (2002).
6. T. Imaizumi, H. G. Tran, T. E. Swartz, W. R. Briggs, S. A. Kay, *Nature* **426**, 302 (2003).
7. F. Valverde *et al.*, *Science* **303**, 1003 (2004).
8. N. Takahashi *et al.*, *Plant Cell Physiol.* **45**, 83 (2004).
9. L. Han, M. Mason, E. P. Risseeuw, W. L. Crosby, D. E. Somers, *Plant J.* **40**, 291 (2004).
10. R. D. Vierstra, *Trends Plant Sci.* **8**, 135 (2003).
11. J. M. Gagne, B. P. Downes, S. H. Shiu, A. M. Durski, R. D. Vierstra, *Proc. Natl. Acad. Sci. U.S.A.* **99**, 11519 (2002).
12. S. Yanagisawa, *Trends Plant Sci.* **7**, 555 (2002).
13. T. Imaizumi, T. F. Schultz, S. A. Kay, unpublished data.
14. S. Takada, K. Goto, *Plant Cell* **15**, 2856 (2003).
15. H. An *et al.*, *Development* **131**, 3615 (2004).
16. D. C. Nelson, J. Lasswell, L. E. Rogg, M. A. Cohen, B. Bartel, *Cell* **101**, 331 (2000).
17. R. R. Beerli, D. J. Segal, B. Dreier, C. F. Barbas III, *Proc. Natl. Acad. Sci. U.S.A.* **95**, 14628 (1998).
18. Materials and methods are available as supporting material on *Science* Online.

19. We thank L. Pettigrew, H. Tran, S. Hazen, and E. Farre for critical reading of the manuscript; M. Yanovsky for involvement in an early stage of this work; K. Hitomi for helping to purify recombinant proteins; K. Spencer for microscopy assistance; P. Waterhouse for pHannibal; C. Barbas III for VP64 plasmid; and the Arabidopsis Biological Resource Center for the transferred DNA insertion line. Supported by an NIH grant (S.A.K.), an NSF Postdoctoral Fellowship in Biosciences Related to the Environment (T.F.S.), and a grant from Japan Society for the Promotion of Science Postdoctoral Fellowships for Research Abroad (T.I.). F.G.H. is a U.S. Department of Energy–Energy Biosciences Research Fellow of the Life Sciences Research Foundation. This is manuscript no. 16849-CB of The Scripps Research Institute.

Supporting Online Material

www.sciencemag.org/cgi/content/full/309/5732/293/DC1
Materials and Methods
Figs. S1 to S12
Table S1
References and Notes

2 February 2005; accepted 12 May 2005
10.1126/science.1110586

The Kinesin Klp2 Mediates Polarization of Interphase Microtubules in Fission Yeast

Rafael E. Carazo-Salas,[1]* Claude Antony,[2] Paul Nurse[1,3]

Fission yeast (*Schizosaccharomyces pombe*) cells grow longitudinally in a manner dependent on a polarized distribution of their interphase microtubules. We found that this distribution required sliding of microtubules toward the cell center along preexisting microtubules. This sliding was mediated by the minus end–directed kinesin motor Klp2, which helped microtubules to become properly organized with plus ends predominantly oriented toward the cell ends and minus ends toward the cell center. Thus, interphase microtubules in the fission yeast require motor activities for their proper organization.

The linear growth of fission yeast cells relies on transport from the cell center to the cell ends of "end markers" along cytoplasmic microtubules (MTs) (*1*, *2*). MTs lie parallel to the long cellular axis in bundles spanning half of the cell length and overlapping at the cell's center; these are termed interphase microtubule assemblies (IMAs) (*3*). MTs are apparently uniformly polarized within IMAs, with minus ends concentrated at the cell center and plus ends facing the cell periphery (*3*, *4*). This polarization is thought to result from central MT nucleation from interphase microtubule organizing centers and the spindle pole body (*3–6*), followed by MT plus-end growth toward the cell periphery and MT alignment parallel to the main cellular axis (*7*). However, MTs can be nucleated elsewhere in the cytoplasm (*8*).

We examined IMA turnover and dynamics in cells expressing green fluorescent protein (GFP) fused to α-tubulin (GFP-Atb2) (*9*, *10*). In a population of interphase cells (n = 89), each cell contained three or four IMAs on average (Fig. 1A) (*3–5*). This could result from each cell having a different, fixed number of IMAs. However, IMA number within each cell varied continually through time (Fig. 1B). One cause for this variation was MT nucleation both close to (0.25 events/min) and away from (0.06 events/min) the nucleus (Fig. 1C) (table

[1]Cell Cycle Laboratory, 44 Lincoln's Inn Fields, Cancer Research UK, London Research Institute, WC2A 1PX, UK. [2]European Molecular Biology Laboratory, Meyerhofstrasse 1, 69117 Heidelberg, Germany. [3]Rockefeller University, 1230 York Avenue, New York, NY 10021, USA.

*To whom correspondence should be addressed. E-mail: carazo01@cancer.org.uk

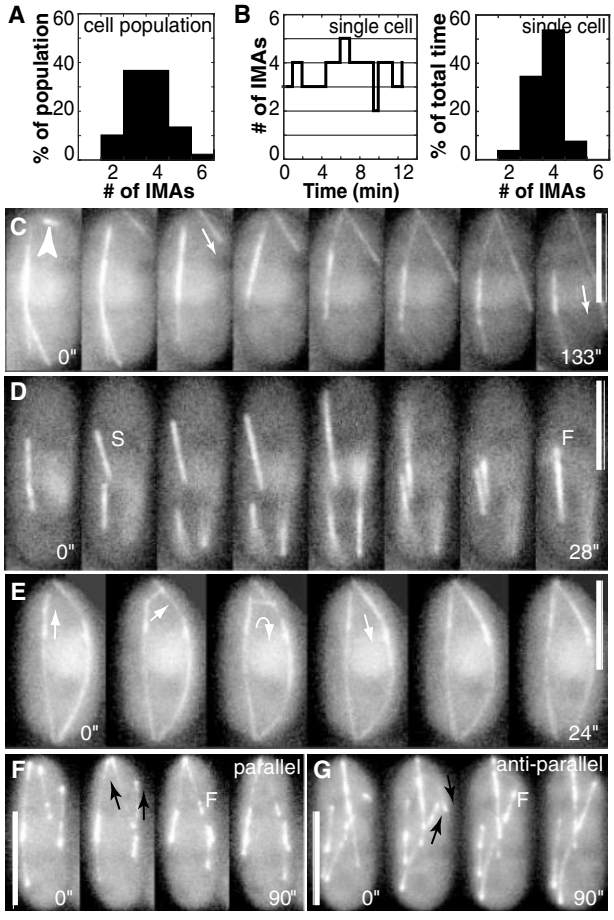

Fig. 1. Dynamics of IMA formation and maintenance. (**A**) Distribution of IMA number per cell in interphase GFP-Atb2 cells. (**B**) Variation of IMA number inside a single cell (left, IMA number as it fluctuates; right, "temporal" distribution of IMA number in the cell). (**C**) De novo IMA assembly (whole-cell projection). Arrowhead, nucleation; arrows, longitudinal alignment. (**D**) Image sequence (single focal plane) revealing IMA "separation" (S) and "fusion" (F). (**E**) Whole-cell time series showing a GFP-Atb2 structure inverting orientation as it transits from one IMA into another (white arrows). (**F** and **G**) Whole-cell image series of cells expressing GFP-Mal3 [a protein that decorates the MT lattice and accumulates at MT plus ends (*29*)] revealing parallel (F) and antiparallel (G) MT "fusion" ("F") events. Arrows denote MT orientations inferred from the GFP-Mal3 signal (stronger at plus ends). Scale bars, 5 μm.

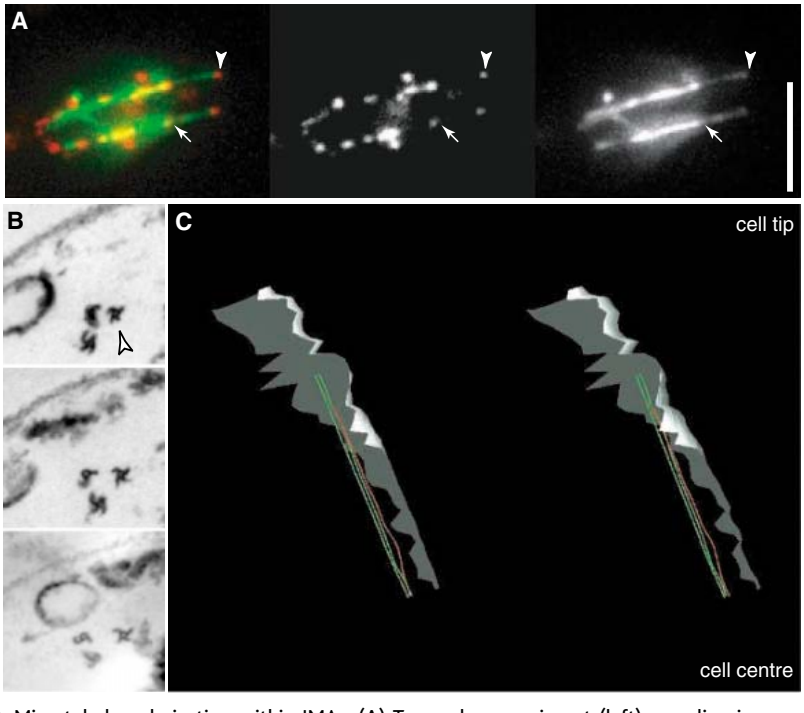

Fig. 2. Microtubule polarization within IMAs. (**A**) Two-color experiment (left) revealing incorporation of exogenous tubulin (center) onto endogenous GFP-Atb2 yeast IMAs (right). Arrowheads, IMA tips; arrows, end of overlap region. Scale bar, 5 μm. (**B**) Serial EM sections showing a bundle of three hook-decorated MTs. Arrowhead indicates MT antiparallel (with opposite hook handedness) to the other two. (**C**) Three-dimensional reconstruction stereopair of a hook-decorated MT bundle near the cell tip. Green, MT with plus end toward the cell tip; red, MT with opposite polarity; white/gray surface, cell cortex. Bundle length shown, ~1.8 μm.

S1). Another cause was the occurrence of "separation/fusion" (S/F) events, in which either a single IMA gave rise to two independent assemblies (0.06 events/min) or two IMAs fused into one (0.18 events/min) (Fig. 1D) (fig. S1, movie S1, and table S1). Fusion occurred with arbitrary direction of alignment between the two IMAs, and IMAs could be seen to invert their direction of alignment during the transit from one IMA into another (Fig. 1, E to G) (movie S2). These findings suggested that IMAs may contain MTs that are not uniformly polarized in the way conventionally thought (*3*–*5*).

To investigate this possibility, we determined MT plus-end localization in vitro in permeabilized cells. Elongation of endogenous GFP-MTs with rhodamine-labeled porcine tubulin led to the decoration of most IMA tips facing cell ends, indicating the presence there of MT plus ends (Fig. 2A). We then examined the polarity of individual MTs within IMAs by "hook decoration," a method in which preexisting MTs are decorated with hook-shaped tubulin appendages (*11*). Electron microscopic (EM) cross sections revealed cells with bundles of two to five MTs decorated by hooks; some bundles contained MTs labeled with hooks of opposite handedness, corresponding to MTs of opposite orientation (Fig. 2B) (fig. S2). Three-dimensional reconstruction from serial sections revealed that bundles of oppositely oriented MTs could be found near the cell tip (Fig. 2, B and C) (movie S3). However, the bundles contained a majority of MTs with plus ends directed toward the cell tips (Fig. 2C) (movie S3). Thus, although antiparallel MTs can coexist within IMAs, MTs within IMAs are mostly uniformly polarized, as predicted by in vivo studies (*3*–*5*).

How could a generally uniform polarization of MTs in IMAs be maintained if MTs are able to undergo random "fusion"? One way would be if random association due to fusion were only transient and followed by a reorganization of the MTs leading to uniform polarization. Such a reorganization would be revealed by corresponding variations in MT content within IMAs. Examination of GFP-Atb2 fluorescence intensity revealed that IMAs often contained multiple, brighter MT overlap regions that gradually became "focused" near the cell's midplane (average velocity 8.75 ± 1.15 μm/min, 8 events; Fig. 3A and movie S4), suggestive of MT movement within IMAs. To test this idea, we photobleached GFP-IMAs and observed their fluorescence recovery after photobleaching (FRAP) by kymograph analysis (*5*). The dark (photobleached) zones of IMAs often regained fluorescence due to outward MT polymerization (Fig. 3B) (movie S5). However, we also detected fluorescence recovery from the periphery inward (Fig. 3C) (movie S6). This was most obvious in the kymographs, where short MTs (Fig. 3D) were seen to enter and exit the photobleached re-

gions of the IMAs (only short MTs could be unequivocally tracked as single MT units). The average velocity of these MTs within IMAs (8.22 ± 1.67 μm/min, 22 events, 250 IMAs filmed) was identical to that of overlap region focusing and differed from individual MT shrinkage and growth velocities [15.45 ± 2.95 μm/min, 30 events, and 3.54 ± 0.63 μm/min, 22 events, respectively (*5*)]. Moreover, the MTs shrank, grew, or kept a constant length as they crossed the photobleached marks. For this reason, and because the velocity of movement was more than double that of MT growth, we concluded that the movement was not due to MT "treadmilling" (*12*) and was due to MT translocation ("sliding") along the IMA (*12*). Furthermore, in all cases the movement was directed inward (i.e., toward the main MT overlap region of the IMA), indicating a motion directed toward MT minus ends.

To investigate whether MT-associated motor protein(s) were involved in this sliding movement, we constructed GFP-Atb2 strains carrying deletions of one or several genes encoding fission yeast MT motors. Deletions of the genes *klp3* (*13*), *tea2/klp4* (*14*), *klp5* (*15*), *klp6* (*15*), and *klp8*, corresponding to putative plus end–directed kinesin-like proteins (KLPs), had no effect on motility (15 events, 214 IMAs filmed; Fig. 3E); sliding occurred with the same frequency, velocity, and directionality as in wild-type cells. However, in cells deleted for *dhc1* [dynein heavy chain (*9*)], *klp1/pkl1* (*16*), and *klp2* (*17*), the genes encoding three putative minus end–directed motors, sliding was abolished (0 events, 202 IMAs filmed). Sliding took place in cells singly deleted for *dhc1* and *pkl1* but was abolished in *klp2*-deleted (*klp2*Δ) cells (0 events, 110 IMAs filmed), suggesting that *klp2* mediates MT sliding.

Kymograph analysis of IMAs in *klp2*Δ cells revealed features consistent with a defect

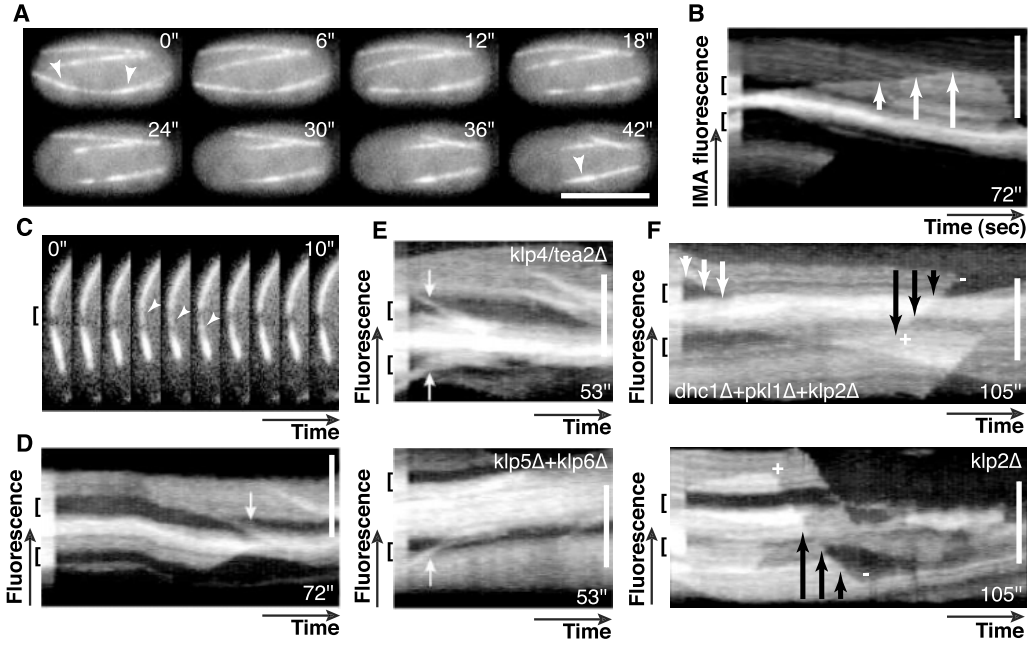

Fig. 3. Klp2-mediated sliding of microtubules within IMAs. (**A**) Whole-cell image sequence revealing overlap region focusing within a single IMA (arrowheads). (**B**) Kymograph of "outward" IMA fluorescence recovery (single focal plane). Arrows denote "outward" growing MT. (**C** and **D**) Single focal plane image sequence (C) and corresponding kymograph (D) showing "inward" IMA fluorescence recovery. Arrowheads and arrow denote "inward" sliding MT. (**E**) Kymographs of IMAs photobleached in cells lacking *klp4/tea2* (top) or *klp5* and *klp6* (bottom). Arrows denote "inward" fluorescence recovery. (**F**) Kymographs from cells lacking *dhc1*, *pkl1*, and *klp2* (top) or *klp2* (bottom). Note lack of "inward" MT sliding after photobleaching. White arrows, MT growth from the cell tip inward; black arrows, MT shrinkage until cell tip (inferred MT minus and plus end localizations marked with – and +). Brackets at left indicate photobleaching sites. Scale bars, 5 μm.

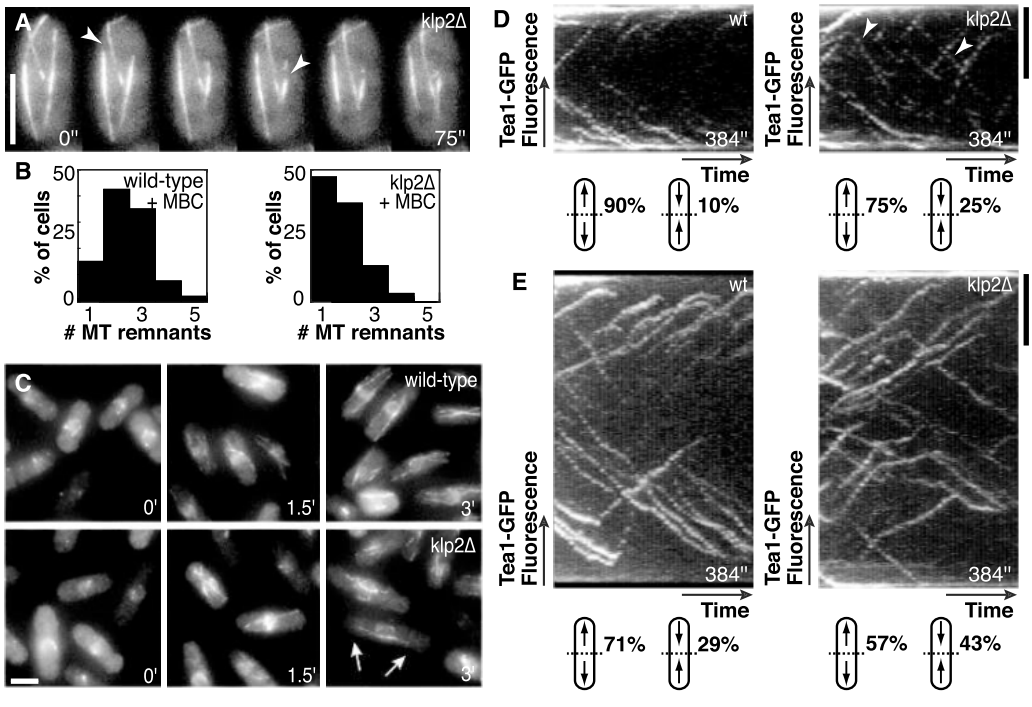

Fig. 4. Role of Klp2 in interphase microtubule stabilization and polarization. (**A**) Whole-cell sequences of a GFP-Atb2 *klp2*Δ cell showing two "separation" events (arrowheads, IMA "separation" sites). (**B**) Number of MT remnants in wild-type and *klp2*Δ cells after 15 min of treatment with MBC. (**C**) MT repolymerization during recovery from 10 min of MBC treatment (samples taken after 0, 1.5, and 3 min at 25°C). Arrows indicate an IMA failing to occupy the cell length. (**D**) Top: Whole-cell kymographs of Tea1-GFP–expressing wild-type (left) and *klp2*Δ (right) cells (average cell size, 9.5 ± 1.1 μm and 9.5 ± 0.9 μm, respectively). Each track corresponds to an individual Tea1-GFP particle. Arrowheads: "inward" moving Tea1-GFP. Bottom: Percentages of Tea1-GFP moving "outward" (left) and "inward" (right). (**E**) Tea1-GFP kymographs (top) and quantitation (bottom) using HU-elongated wild-type (left) and *klp2*Δ (right) cells (average cell size, 21.5 ± 1.7 μm and 21.7 ± 1.6 μm, respectively). Scale bars, 5 μm.

in MT (minus end) focusing at the cell center. These included lack of fusion of MT overlap regions and features indicative of MT minus-end localization at the cell periphery, such as MT growth from the cell end inward and MT depolymerization ("shrinkage") all the way to the cell tip (Fig. 3F). *klp2*Δ cells also displayed decreased IMA stability. Although the frequencies of IMA nucleation and fusion in *klp2*Δ cells were similar to those in the wild type, the frequency of IMA "separation" and catastrophe was increased by a factor of 3 in *klp2*Δ cells (0.20 events/min and 0.26 events/min, respectively; Fig. 4A) (table S1). In addition, IMAs in *klp2*Δ and wild-type cells were unstable in the presence of the MT-depolymerizing drug carbendazim (MBC) but, unlike in control cells, the number of MBC-stable MT remnants in *klp2*Δ cells decreased with time of exposure to the drug (Fig. 4B), and IMAs reassembled after drug removal frequently failed to occupy the whole cell length (Fig. 4C).

To determine whether Klp2 was involved in the generation of uniformly polarized MTs, we examined the movement of the GFP-labeled cell end marker Tea1 in wild-type and *klp2*Δ cells. Tea1 particles associate with MT plus ends and travel outward from the cell center (*1*, *14*, *18*), and so act as a marker of MT polarization. In kymographs of wild-type cells, 90% of Tea1-GFP moved outward and 10% inward (231 particles, 25 cells; Fig. 4D), indicating a factor of 9 excess of MT plus-end orientation toward the cell tips. In *klp2*Δ cells, the corresponding values were 75% outward and 25% inward (310 particles, 24 cells; Fig. 4D), indicating only a factor of 3 excess of MT plus-end orientation toward the cell tips. This difference was enhanced in elongated cells generated by treatment for 5 hours with the DNA synthesis inhibitor hydroxyurea (HU). In HU-treated wild-type cells, 71% of Tea1-GFP moved outward and 29% inward (565 particles, 29 cells; Fig. 4E and movie S7), whereas in HU-treated *klp2*Δ cells the values were 57% outward and 43% inward (695 particles; 29 cells; Fig. 4E and movie S8). These indicate, respectively, a factor of 2.5 and a factor of 1.3 excess of MT plus-end orientation toward the cell tips. A value of 1.3 is close to random (i.e., 50% outward and 50% inward), indicating that in elongated cells Klp2 is required to maintain normal MT polarization with MT plus ends oriented toward the cell tips.

Klp2 is a member of the conserved Kar3/Ncd family of minus end–directed KLPs (*19*) that generally act in mitotic and meiotic spindles. Its *Drosophila melanogaster* homolog Ncd exerts an inward force on spindle poles by cross-linking and sliding interpolar MTs (*20*), and moves along MTs at ~16 μm/min in vitro (*21*). In the fission yeast, Klp2 regulates spindle size (*17*) and localizes to MTs during interphase (*17*). We suggest that, like bipolar spindles (*22*–*27*), fission yeast interphase MTs require motor activity for their proper organization. We propose that Klp2 mediates minus end–directed sliding of cytoplasmic MTs relative to each other, which is necessary to maintain the uniform polarization of interphase microtubular arrays (fig. S3). Interestingly, interphase microtubule organizing center integrity can be lost upon disruption of minus-ended motor complexes in mammalian cells (*28*). Hence, minus end–directed MT sliding may contribute to interphase MT polarization in other eukaryotes.

References and Notes

1. J. Mata, P. Nurse, *Cell* **89**, 939 (1997).
2. J. Hayles, P. Nurse, *Nat. Rev. Mol. Cell Biol.* **2**, 647 (2001).
3. D. R. Drummond, R. A. Cross, *Curr. Biol.* **10**, 766 (2000).
4. P. T. Tran, L. Marsh, V. Doye, S. Inoue, F. Chang, *J. Cell Biol.* **153**, 397 (2001).
5. M. J. Sagolla, S. Uzawa, W. Z. Cande, *J. Cell Sci.* **116**, 4891 (2003).
6. R. Ding, R. R. West, D. M. Morphew, B. R. Oakley, J. R. McIntosh, *Mol. Biol. Cell* **8**, 1461 (1997).
7. D. Brunner, P. Nurse, *Cell* **102**, 695 (2000).
8. K. E. Sawin, P. C. Lourenco, H. A. Snaith, *Curr. Biol.* **14**, 763 (2004).
9. A. Yamamoto, R. R. West, J. R. McIntosh, Y. Hiraoka, *J. Cell Biol.* **145**, 1233 (1999).
10. See supporting data on *Science* Online.
11. S. R. Heidemann, *Methods Enzymol.* **196**, 469 (1991).
12. V. I. Rodionov, G. G. Borisy, *Science* **275**, 215 (1997).
13. S. C. Brazer, H. P. Williams, T. G. Chappell, W. Z. Cande, *Yeast* **16**, 149 (2000).
14. H. Browning, D. D. Hackney, P. Nurse, *Nat. Cell Biol.* **5**, 812 (2003).
15. R. R. West, T. Malmstrom, C. L. Troxell, J. R. McIntosh, *Mol. Biol. Cell* **12**, 3919 (2001).
16. J. L. Paluh *et al.*, *Mol. Biol. Cell* **11**, 1225 (2000).
17. C. L. Troxell *et al.*, *Mol. Biol. Cell* **12**, 3476 (2001).
18. R. Behrens, P. Nurse, *J. Cell Biol.* **157**, 783 (2002).
19. S. A. Endow, *Eur. J. Biochem.* **262**, 12 (1999).
20. D. J. Sharp, K. R. Yu, J. C. Sisson, W. Sullivan, J. M. Scholey, *Nat. Cell Biol.* **1**, 51 (1999).
21. S. A. Endow, H. Higuchi, *Nature* **406**, 913 (2000).
22. A. Dammermann, A. Desai, K. Oegema, *Curr. Biol.* **13**, R614 (2003).
23. U. S. Tulu, N. M. Rusan, P. Wadsworth, *Curr. Biol.* **13**, 1894 (2003).
24. N. M. Rusan, U. S. Tulu, C. Fagerstrom, P. Wadsworth, *J. Cell Biol.* **158**, 997 (2002).
25. T. Wittmann, A. Hyman, A. Desai, *Nat. Cell Biol.* **3**, E28 (2001).
26. T. J. Keating, G. G. Borisy, *Biol. Cell.* **91**, 321 (1999).
27. A. Hyman, E. Karsenti, *J. Cell Sci.* **111**, 2077 (1998).
28. N. J. Quintyne *et al.*, *J. Cell Biol.* **147**, 321 (1999).

29. K. E. Busch, D. Brunner, *Curr. Biol.* **14**, 548 (2004).
30. We thank E. Piddini, M. Godinho-Ferreira, H. Masuda, U. Euteneuer, T. Toda, F. Uhlmann, N. Hirokawa, T. Wittmann, J. Höög, F. Chang, J. R. McIntosh, and members of the Nurse lab for discussions; E. Karsenti, J. R. McIntosh, K. Sawin, and D. Brunner for materials; and E. Piddini, F. Uhlmann, J. Hayles, M. Pardo, S. Castagnetti, J. Zhurinsky, J. R. McIntosh, M. Godinho-Ferreira, and T. Surrey for reading the manuscript. Supported by an International Human Frontier Science Program Organization (HFSPO) postdoctoral fellowship (R.E.C.-S.), HFSPO (ST00069/2001-C/1) and EMBO (ASTF9977) fellowships (C.A.), and Cancer Research UK and Rockefeller University (P.N.). In memoriam Heidi Browning.

Supporting Online Material

www.sciencemag.org/cgi/content/full/309/5732/297/DC1
Materials and Methods
Figs. S1 to S3
Table S1
Movies S1 to S8

12 April 2005; accepted 16 May 2005
10.1126/science.1113465

A Self-Organized Vortex Array of Hydrodynamically Entrained Sperm Cells

Ingmar H. Riedel,[1]* Karsten Kruse,[2] Jonathon Howard[1]*

Many patterns in biological systems depend on the exchange of chemical signals between cells. We report a spatiotemporal pattern mediated by hydrodynamic interactions. At planar surfaces, spermatozoa self-organized into dynamic vortices resembling quantized rotating waves. These vortices formed an array with local hexagonal order. Introducing an order parameter that quantifies cooperativity, we found that the array appeared only above a critical sperm density. Using a model, we estimated the hydrodynamic interaction force between spermatozoa to be ~0.03 piconewtons. Thus, large-scale coordination of cells can be regulated hydrodynamically, and chemical signals are not required.

Eukaryotic cilia and flagella are rodlike appendages that contain a conserved motile structure called the axoneme (*1*), an example of which is the tail of many animal spermatozoa. Oscillatory waves generated by the sperm tail propel spermatozoa through fluid, usually along helical paths. If spermatozoa approach planar surfaces, they become trapped at these surfaces and follow circular swimming paths with a strongly preferred handedness (*2*) (movie S1).

We found that the spermatozoa of sea urchins (*Strongylocentrotus droebachiensis* and *S. purpuratus*) self-organize at high surface densities into an array of vortices (Fig. 1, A and B, and movies S2 and S3) (*3*). At a density of 6000 cells/mm^2, each vortex contained 10 ± 2 spermatozoa (mean ± SD) circling clockwise (observed from inside the water phase) around a common center (Fig. 1, C to F). The circular paths had a radius of R =

13.2 ± 2.8 μm, the time for one revolution was T = 0.67 ± 0.09 s, and the swimming speed was v = 125 ± 21 μm/s. The beat frequency was f = 41.7 ± 3.7 Hz. Occasionally the hopping of spermatozoa between vortices and the fusion of two vortices were observed. The vortices were densely packed and their centers moved randomly with an apparent diffusion coefficient of D = 6.2 ± 0.9 μm²/s. This apparent diffusion coefficient is much larger than the thermal diffusion coefficient D = 0.06 μm²/s of a disk similar in size to a vortex [$D = kT/\gamma$; $\gamma = (32/3) \times \eta R$ = 0.07 μN·s/m, where radius R = 13 μm and friction in water η = 1 mPa·s] (*4*). This indicates that the array is out of thermal equilibrium because of the active propulsion of the spermatozoa (*5*, *6*), and hence the pattern is an example of self-organization (*7*–*9*). Slight changes of the microscopic parameters of such self-organized systems can lead to sudden changes in the overall pattern, making these systems amenable for regulation (*10*). We therefore analyzed the unexpected vortex array of spermatozoa to understand its underlying physical cause and to determine its possible relevance for related biological processes.

The vortex array reflected two levels of order: a clustering of spermatozoa into vortices and a packing of these vortices into an array. We assessed the packing order of the vortex array by measuring various correlation functions of the vortex centers. The pair-correlation function and the triplet-distribution function (*11*) revealed a local hexagonal order with an average vortex spacing of 49 ± 9 μm (Fig. 2). Furthermore, the bond-angular correlation function (*12*) showed an exponential decay indicating the absence of long-range order. Thus, the array is liquidlike rather than hexatic or crystalline (*12*).

We asked how the spermatozoa within a vortex influence each other (Fig. 3A and movie S4). Interactions could lead to changes in the circling radius, the swimming velocity, or the beat frequency. However, within experimental errors, we found no differences in these parameters whether spermatozoa were in a vortex or isolated. Instead, we did find a particular form of synchronization of the beating patterns of spermatozoa within a vortex: We described each spermatozoon by two variables: (i) the phase of the oscillation of the head during the beat of the spermatozoon, $\varphi(t)$ [this oscillation is driven by and has the same frequency as the oscillation of the tail (Fig. 3B)] and (ii) the angular position of the head in its trajectory around the vortex, $\Phi(t)$ (Fig. 3C). No correlation in $\Phi(t)$ between any two spermatozoa in the same vortex was found. The same was true for $\varphi(t)$. Hence, spermatozoa within a vortex swim at different speeds and beat at different frequencies. However, there is a strong correlation between the differences $\Delta\varphi(t)$ and $\Delta\Phi(t)$ between pairs of spermatozoa in the same vortex (Fig. 3, D to E). This implies, for example, that if one spermatozoon swims twice as fast as another then it also beats at twice the frequency. Thus, locally the tails are beating in synchrony and a trailing spermatozoon follows in the wake of the leading one. Because the spermatozoa swim in closed circular paths, there must be an integral number of wavelengths along the circumference of the vortex. The slope, $\Delta\varphi/\Delta\Phi$, was 4.2 ± 0.2 (Fig. 3E), consistent with a wave number of 4, which is determined by the geometry of the vortex: Dividing the circumference of the swimming path ($2\pi R$, R = 11.6 ± 3.0 μm for this particular vortex) by the beat wavelength on the sperm tail (λ = 17.6 ± 1.3 μm; along the curved centerline of the flagellar waveform, not along the arc length of the tail) gives 4.1 ± 1.4. Thus, hydrodynamic coupling of the sperm tails within a vortex leads to a quantized rotating wave with wave number 4 (Fig. 3F). This rotating wave is a generalization of the synchronization of the beats of spermatozoa swimming close to one another (*13*–*15*). Furthermore, it is related to the three-dimensional (3D) metachronal waves observed on the surfaces of ciliates and ciliated epithelia, which are important for swimming motility and the movement of mucus, where hydrodynamic interactions are also thought to play an important role (*16*, *17*).

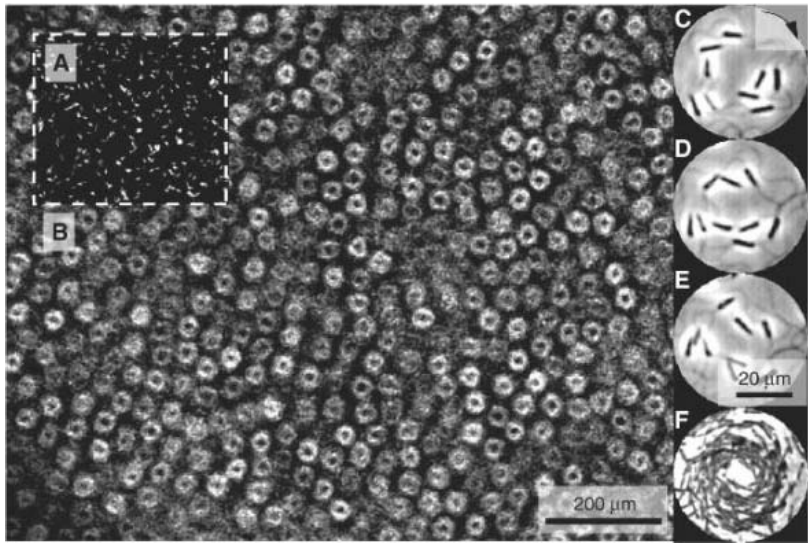

Fig. 1. Circulating spermatozoa form a 2D array of vortices. (**A**) Dark field-contrast image (single frame) showing the heads of sea urchin spermatozoa (*S. droebachiensis*) at a surface density of 6000 cells/mm². (**B**) The average intensity of 25 consecutive frames shows an arrangement of rings, each corresponding to a vortex of ~10 spermatozoa. (**C** to **E**) Successive frames of a phase-contrast movie showing nine spermatozoa swimming clockwise (arrow) within a vortex. (**F**) Average of 25 frames similar to (C) to (E) giving a magnified view of the vortices shown in (B). Frame rate, 17 frames per second (fps).

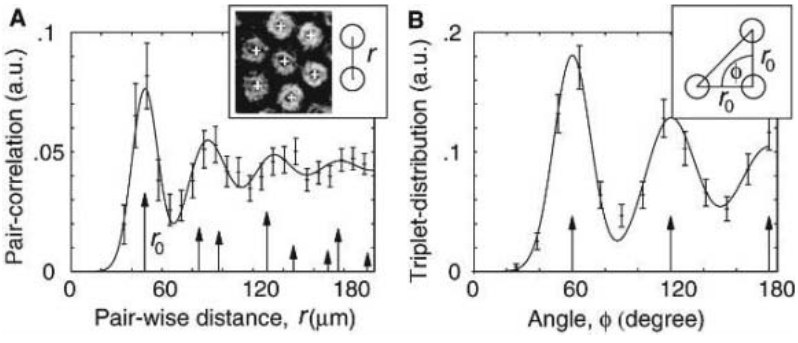

Fig. 2. The vortex array is liquidlike with local hexagonal order. (**A**) Pair-correlation function and (**B**) triplet-distribution function of the vortex centers. Insets illustrate how these functions were calculated. Arrows denote position and relative weight of the maxima for an ideal hexagonal lattice. Solid fit-lines were obtained by convoluting these maxima with Gaussians whose standard deviations increase linearly from the origin. Error bars show mean ± SEM. a.u., arbitrary units.

[1]Max Planck Institute of Molecular Cell Biology and Genetics, Pfotenhauerstrasse 108, D-01307 Dresden, Germany. [2]Max Planck Institute for the Physics of Complex Systems, Nöthnitzer Strasse 38, D-01187 Dresden, Germany.

*To whom correspondence should be addressed. E-mail: riedel@mpi-cbg.de (I.H.R.); howard@mpi-cbg.de (J.H.)

How is the vortex array formed? Because we did not observe vortex arrays at low sperm surface densities, we suspected that density might play a role in the self-organization process. To quantify the order at the different densities, we defined an order parameter χ as follows. The binary images of each movie showing only sperm heads were summed such that each pixel value in the resulting image was proportional to the number of different spermatozoa that swam over that pixel (Fig. 4A) (*3*). If the swimming paths of different spermatozoa were uncorrelated, then these pixel values would be binomially distributed. However, if spermatozoa accumulated in a vortex they would trail each other and the distribution would differ from a binomial one because low and high pixel values (corresponding to centers of the vortices and swimming trails, respectively) would be overrepresented (Fig. 4B). In this case, the variance of the measured distribution (σ_m^2) will be larger than that of the binomial distribution (σ_b^2). This motivated our definition of the order parameter $\chi = (\sigma_m^2/\sigma_b^2) - 1$, which had the expected properties: zero for a random configuration, and greater than zero if spermatozoa shared similar swimming paths. The value of χ depended on the average number of spermatozoa per vortex and how well the centers of their circular swimming paths colocalized. χ was a robust measure for the correlation among the objects and was related to the pair-correlation function [supporting online material (SOM) text]. Furthermore, χ required no labor-intensive object tracking, and hence it might be useful for quantifying order in other spatiotemporal patterns involving tracks of multiple particles or signals such as intracellular organelle transport (*18*) or ant trails (*19*).

We measured the order parameter χ for various sperm surface densities (Fig. 4C) and found a rapid change in the slope of the curve at ~2500 cells/mm² (fitting a Hill equation revealed a cooperativity factor of 5). This suggested a bifurcation separating a disordered and an ordered regime: one where the swimming paths of the spermatozoa were random and one where the correlation among the swimming paths increased, reflecting an increasingly pronounced vortex array.

To support this interpretation and to gain insight into the physical mechanisms underlying the pattern formation, we propose a simplified model. Each spermatozoon is represented by a point particle located at the

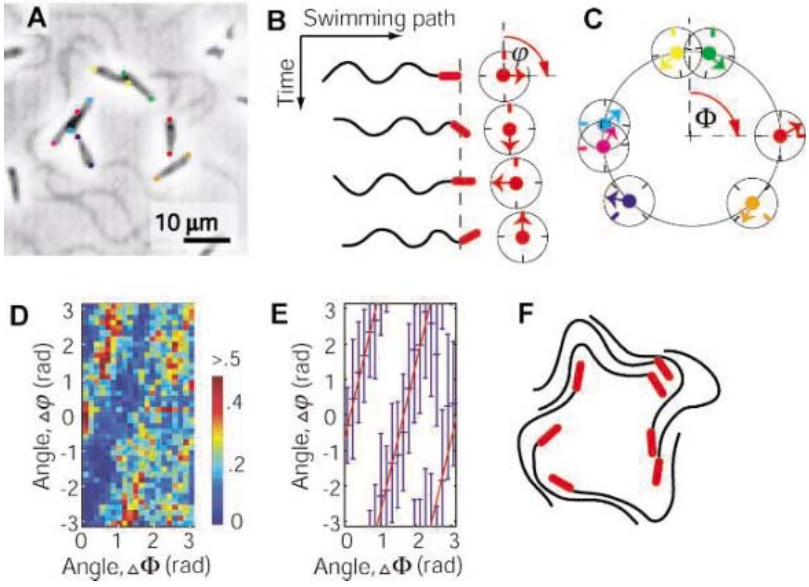

Fig. 3. Hydrodynamic coupling among spermatozoa within a vortex leads to quantized rotating waves. (**A**) Position and orientation of seven sperm heads (colored dots) within a vortex were traced. Frame rate, 250 fps. (**B**) The phases of the head oscillation were represented with circling pointers (arrow of clock, φ). (**C**) Angular positions of sperm heads within the vortex were projected onto a unit circle (center of clock, Φ; the reference frame for φ changes with Φ) (*3*). (**D**) Histogram of phase differences $\Delta\varphi$ versus $\Delta\Phi$ among any pair of spermatozoa over the observation time (color coding shows relative frequency). (**E**) In each $\Delta\Phi$ channel (D), the circular mean was obtained (errors contain 95% of the density). Linear fit (red line) $\Delta\varphi = (4.2 \pm 0.2) \times \Delta\Phi + (-0.7 \pm 0.4)$ corresponds to a quantized wave with wave number 4 (errors denote 68% confidence in fit parameters). (**F**) Illustration of the dynamics. While the spermatozoa swim around the vortex, their heads and tails oscillate. These oscillations couple hydrodynamically and form a quantized rotating wave [similar to (A)].

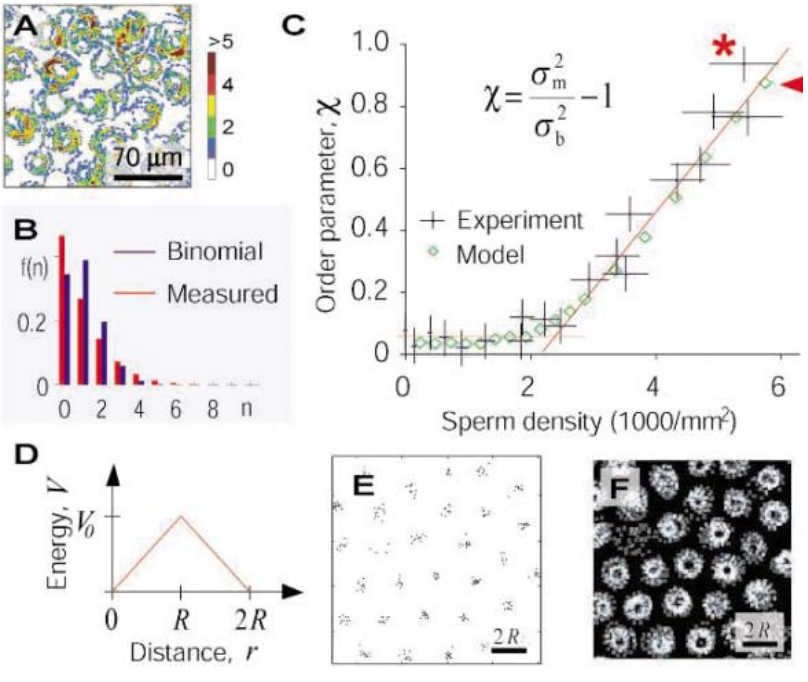

Fig. 4. The vortex array formation depends on a critical sperm density as supported by a model. (**A**) Summed-up images of a binary movie showing only sperm heads used for the calculation of the order parameter χ (*3*). Colors correspond to the number of spermatozoa that were swimming over each pixel. Frame rate, 17 fps. (**B**) Example of the expected binomial distribution (blue) versus the measured distribution (red) in (A) from which the variances σ_b^2 and σ_m^2 were obtained. (**C**) Dependence of χ on the density of spermatozoa (black crosses). The transition occurs at a sperm density of about ~2500 spermatozoa per mm² (red lines were inserted for visual guidance). χ obtained with the model is given as green diamonds. Asterisk and arrowhead denote data presented in (A) and (B) and in (E) and (F), respectively. Error bars show mean ± SD. (**D**) Sketch of the radial pair-interaction potential *V* used in the model with its repulsive and attractive components. *R* is the circling radius of the spermatozoon. (**E**) Result of a simulation with point particles (*3*). The hexagonal arrangement of clusters containing about 10 particles is apparent. (**F**) Average of a simulated movie generated from (E). It resembles Fig. 1B.

center of its circular swimming path. These particles move randomly with an apparent diffusion coefficient of $D = 9.0 \pm 2.0\ \mu m^2/s$, measured for isolated spermatozoa. A short-range pairwise attraction, arising from the hydrodynamic forces leading to the observed synchronization (*20*), and a longer range repulsion, which could be of steric or hydrodynamic origin (*21*), are assumed (Fig. 4D). Although one cannot describe circular flow by a potential (*22*), the important features of the observed pattern are captured by our model.

Stochastic simulations of this model (SOM text) also revealed two regimes: a random distribution of particles at low densities with a transition toward a hexagonal array of clusters at a critical particle density (Fig. 4E). Assigning to each particle a spermatozoon circling around that position, we generated simulated movies (*3*) mimicking the experimental observation (Fig. 4F versus Fig. 1B). Moreover, the order parameter χ computed for different simulated sperm densities agreed with the experimentally observed dependency (Fig. 4C). Our numerical results were further supported by a 1D mean-field analysis (SOM text), which indicated the existence of a supercritical pitchfork bifurcation at a critical sperm density (*23*). This critical density was proportional to the interaction strength and inversely proportional to the diffusion coefficient, the latter being associated with the noise in the system. This analysis demonstrates how the activity of biological processes can be regulated by critical points or bifurcations. For example, ciliary metachronal waves (*16*, *24*) might be switched on and off by small physiologically controlled changes of the activity of the individual cilia, thereby tuning the critical density for the onset of the metachronal wave.

The only free parameter in our model was the ratio of the maximum interaction potential to the drag coefficient, $V_0/\gamma = 5\ \mu m^2/s$, which was chosen to match the critical density (Fig. 4C). This allowed us to estimate the interaction force between two spermatozoa $F_{int} = |\mathrm{grad}(V)| = (V_0/\gamma) \times \gamma/R \sim 0.03$ pN (using $R = 13\ \mu m$ and $\gamma = 0.07\ \mu N \cdot s/m$ from above). This force is about 1% of the forward propulsion force of spermatozoa $F_{for} \sim 5$ pN (*25*). Although this hydrodynamic interaction force is smaller than typical adhesion forces involved in sperm cooperation (*26*), it is evidently large enough to coordinate the cells and to regulate large-scale pattern formation in the absence of chemical signals (*27*).

References and Notes

1. I. R. Gibbons, *J. Cell Biol.* **91**, 107*s* (1981).
2. D. M. Woolley, *Reproduction* **126**, 259 (2003).
3. Materials and methods are available as supporting material on *Science* Online.
4. H. C. Berg, *Random Walks in Biology* (Princeton Univ. Press, Princeton, NJ, 1993).
5. X. L. Wu, A. Libchaber, *Phys. Rev. Lett.* **84**, 3017 (2000).
6. N. Darnton, L. Turner, K. Breuer, H. C. Berg, *Biophys. J.* **86**, 1863 (2004).
7. A. M. Turing, *Philos. Trans. R. Soc. London Ser. B* **237**, 37 (1952).
8. I. Prigogine, G. Nicolis, *J. Chem. Phys.* **46**, 3542 (1967).
9. T. Misteli, *J. Cell Biol.* **155**, 181 (2001).
10. F. J. Nédélec, T. Surrey, A. C. Maggs, S. Leibler, *Nature* **389**, 305 (1997).
11. K. Zahn, G. Maret, C. Russ, H. H. von Grünberg, *Phys. Rev. Lett.* **91**, 115502 (2003).
12. K. Zahn, R. Lenke, G. Maret, *Phys. Rev. Lett.* **82**, 2721 (1999).
13. J. Gray, *Ciliary Movement* (Cambridge Univ. Press, New York, 1928).
14. J. Gray, G. J. Hancock, *J. Exp. Biol.* **32**, 802 (1955).
15. G. I. Taylor, *Proc. R. Soc. London Ser. A* **209**, 447 (1951).
16. K. I. Okamoto, Y. Nakaoka, *J. Exp. Biol.* **192**, 61 (1994).
17. S. Gueron, K. Levit-Gurevich, *Biophys. J.* **74**, 1658 (1998).
18. E. Nielsen, F. Severin, J. M. Backer, A. A. Hyman, M. Zerial, *Nat. Cell Biol.* **1**, 376 (1999).
19. B. Hoelldobler, E. O. Wilson, *The Ants* (Springer, Berlin, 1990).
20. L. J. Fauci, A. McDonald, *Bull. Math. Biol.* **57**, 679 (1995).
21. P. Lenz, J. F. Joanny, F. Jülicher, J. Prost, *Phys. Rev. Lett.* **91**, 108104 (2003).
22. L. D. Landau, E. M. Lifshitz, *Fluid Mechanics, Course of Theoretical Physics* (Pergamon Press, Oxford, 1987).
23. S. H. Strogatz, *Nonlinear Dynamics and Chaos* (Westview Press, Cambridge, MA, 2000).
24. M. A. Sleigh, Ed., *Cilia and Flagella* (Academic Press, London, 1974).
25. J. Howard, *Mechanics of Motor Proteins and the Cytoskeleton* (Sinauer Associates, Sunderland, MA, 2001).
26. H. Moore, K. Dvorakova, N. Jenkins, W. Breed, *Nature* **418**, 174 (2002).
27. C. Dombrowski, L. Cisneros, S. Chatkaew, R. E. Goldstein, J. O. Kessler, *Phys. Rev. Lett.* **93**, 098103 (2004).

28. We thank D. Babcock, C. Brokaw, R. Goldstein, F. Jülicher, H. Machemer, K. Müller, F. Nédélec, E. Schäffer, and members of the Howard lab and Jülicher lab for discussions and comments on the manuscript. All authors contributed ideas and discussion, and I.H.R. carried out experiments, programming, and data analysis.

Supporting Online Material

www.sciencemag.org/cgi/content/full/309/5732/300/DC1
Materials and Methods
SOM Text
Figs. S1 to S6
References
Movies S1 to S5

27 January 2005; accepted 24 May 2005
10.1126/science.1110329

Inferential Structure Determination

Wolfgang Rieping,* Michael Habeck,* Michael Nilges†

Macromolecular structures calculated from nuclear magnetic resonance data are not fully determined by experimental data but depend on subjective choices in data treatment and parameter settings. This makes it difficult to objectively judge the precision of the structures. We used Bayesian inference to derive a probability distribution that represents the unknown structure and its precision. This probability distribution also determines additional unknowns, such as theory parameters, that previously had to be chosen empirically. We implemented this approach by using Markov chain Monte Carlo techniques. Our method provides an objective figure of merit and improves structural quality.

A major difficulty in the determination of three-dimensional macromolecular structures is that experimental data are indirect. We observe physical effects that depend on the atomic geometry and use a forward model to relate the observed data to the atomic coordinates. For example in nuclear magnetic resonance (NMR), the intensity I_i of peaks in nuclear Overhauser effect spectroscopy (NOESY) data is proportional to the inverse sixth power of the distance d_i of two spins: $I_i = \gamma d_i^{-6}$ (*1*). This isolated spin pair approximation (ISPA) involves an unknown scaling factor γ. It seems straightforward to obtain the structure in the example: simply use the observed intensities to calculate sufficient distances to define the structure.

In realistic applications, this approach runs into difficulties. One problem is that the forward model is usually inherently degenerate, meaning that different conformations can lead to the same observations and therefore cannot be distinguished experimentally, and even a formally invertable forward model is practically degenerate if the data are incomplete. A further complication is that there are uncertainties in both the data and the forward model: Data are subject to experimental errors, and theories rest on approximations. Moreover, the forward model typically involves parameters that are not measurable. Algorithms for structure calculation from x-ray reflections, NMR spectra, or homology-derived restraints should account for these fundamental difficulties in some way.

Structure determination in general is an ill-posed inverse problem, meaning that going from the data to a unique structure is impossible. However, the current paradigm in structure calculation is to attempt an inversion of the forward model. Most algorithms minimize a hybrid energy $E_{hybrid} = E_{phys} +$

Unité de Bioinformatique Structurale, Institut Pasteur, CNRS URA 2185, 25-28 rue du Docteur Roux, 75724 Paris CEDEX 15, France.

*These authors contributed equally to this work.
†To whom correspondence should be addressed. E-mail: nilges@pasteur.fr

$w_{data}E_{data}$ (*2*), where a nonphysical energy E_{data} uses the forward model and a restraining function to assess the agreement between data and structure. A force field E_{phys} describes the physical properties of the macromolecule, such as bonded and nonbonded interactions between the atoms, and partially removes the degeneracy of the problem. The rationale is that minimization of the hybrid energy effectively inverts the forward model, yielding the "true" structure.

This strategy works in the case of many data of good quality. In less favorable situations, the ill-posed nature of the inverse problem becomes apparent. Specifically, it remains unclear how to choose auxiliary parameters like the weight w_{data} or theory parameters such as the scaling factor γ in the ISPA. Because the hybrid energy minimization paradigm offers no principle to settle these issues, such parameters need to be determined heuristically.

The principal difficulty in structure determination by NMR is the lack of information that is indispensible to reconstruct the structure unambiguously. By formulating an optimization problem ("search for the minimum of E_{hybrid}"), one however implicitly assumes that there is a unique answer. Repeating the optimization procedure multiple times to obtain several "unique" solutions hides but does not solve the ambiguity and makes it difficult to judge the validity and precision of NMR structures in an objective way.

We suggest that it is a misconception to use structure calculation methods that are only appropriate if the objective is to obtain a unique structure. Instead, we view structure determination as an inference problem, requiring reasoning from incomplete and uncertain information. We consider the entire conformational space and use the data only to rank the molecule's possible conformations. We assign a number P_i to every conformation X_i. If $P_i > P_j$, conformation X_i is more supported by the data than X_j. Cox (*3*) proved that such rankings are equivalent to a probability and that probability theory is the only consistent calculus to solve inference problems. The distribution of the probabilities P_i reflects the information content of the data. If all but one P_i vanish, the data determine the structure uniquely. If P_i are uniform throughout conformational space, the data are completely uninformative with respect to the structure.

Any inferential structure determination (ISD) is solved by calculating the probabilities P_i. We demand the probabilities to be objective in the sense that they only depend on data D and on relevant prior information I (such as the forward model or knowledge about physical interactions). Thus, P_i is a conditional probability, $P_i = P(X_i|D,I)$; it is not a frequency of occurence but a quantitative representation of our state of knowledge. In the case of a continuous parametrization of conformations, such as Cartesian coordinates, P_i is a density $p(X|D,I)$.

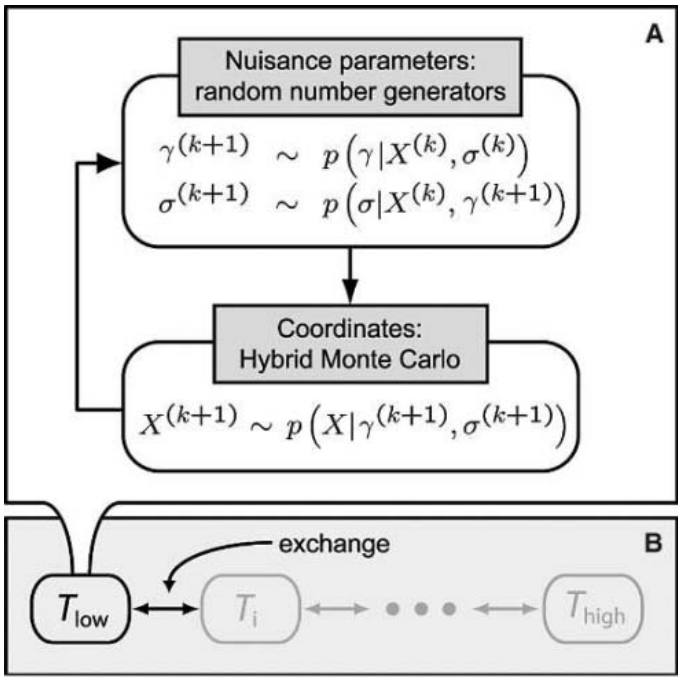

Fig. 1. Replica-exchange Monte Carlo algorithm. (**A**) We generate a stochastic sample ($X^{(k)}$, $\gamma^{(k)}$, $\sigma^{(k)}$) from the joint posterior distribution in an iterative fashion by using Gibbs sampling (*20*). The nuisance parameters γ and σ are consecutively drawn from their conditional posterior distributions, with the values of the other parameters being fixed to their previously generated values. Coordinates are updated by using the hybrid Monte Carlo method (*21*). (**B**) To overcome energy barriers, we embed this scheme in a replica-exchange strategy, which simulates a sequence of heated copies of the system. Samples of the target distribution are generated in the low-temperature copy (T_{low}) and propagate via stochastic exchanges between intermediate copies ($T_{low} < T_i < T_{high}$) to the high-temperature system (T_{high}). The temperature T_{high} is chosen such that the polypeptide chain can move freely in order to escape local modes of the probability density.

A direct consequence of probability calculus is Bayes' theorem (*4*), which formally solves our inference problem. The posterior density

$$p(X|D,I) \propto p(D|X,I)\, p(X|I) \qquad (1)$$

factorizes into two natural components: The likelihood function $p(D|X, I)$ combines a forward model and an error distribution and quantifies the likelihood of observing data D given a molecular structure X. Because we model deviations between measurements and predictions explicitly, the precision of the coordinates depends on the quality of the data and on the accuracy of the forward model. In the ideal case of a uniquely invertible model, the likelihood function is only peaked at the structure that satisfies the data (i.e., the conventional approach is contained as limiting case). The prior density $p(X|I)$ takes prior knowledge about biomolecular structures into account and is determined by the physical energy and the temperature of the system (*5*).

The error distribution and the forward model typically contain auxiliary parameters ξ that are unavailable from the data but necessary in order to describe the problem adequately. In Bayesian theory, such nuisance parameters are treated in the same way as the coordinates: They are estimated from the experimental data by replacing X with (X, ξ) in Eq. 1. Assuming independence of X and ξ, the joint posterior density for all unknown parameters is

$$p(X,\xi|D,I) \propto p(D|X,\xi,I)\, p(X|I)\, p(\xi|I) \qquad (2)$$

Equation 2 provides a unique rule to determine any quantity that is not accessible by experiment.

To demonstrate the practical feasibility of the ISD approach, we infer the molecular structure of the Fyn SH3 domain (59 amino acids length). Experimental distances between amide protons were derived from a series of NOESY spectra on a {15N, 2H} enriched protein (*6*). The data set is sparse: It comprises 154 measurements, of which on average only one per amino acid provides long-range structural information. The forward model $I_i = \gamma d_i^{-6}(X)$ defined by the ISPA does not account for experimental errors and systematic effects like spin diffusion (*1*) and internal dynamics (*7*); hence, observed intensities will deviate from theoretical predictions. A log normal distribution (*5*) describes these deviations and introduces a second nuisance parameter σ that quantifies their magnitude. Thus, we have two nuisance parameters, $\xi = (\gamma,\sigma)$.

Although given in analytically closed form (*5*), it is practically impossible to evaluate the posterior density $p(X,\gamma,\sigma|D,I)$ over all conformational space. Therefore, in our view, structure calculation comprises posterior simulation, which samples only regions that carry a considerable amount of probability mass. We have

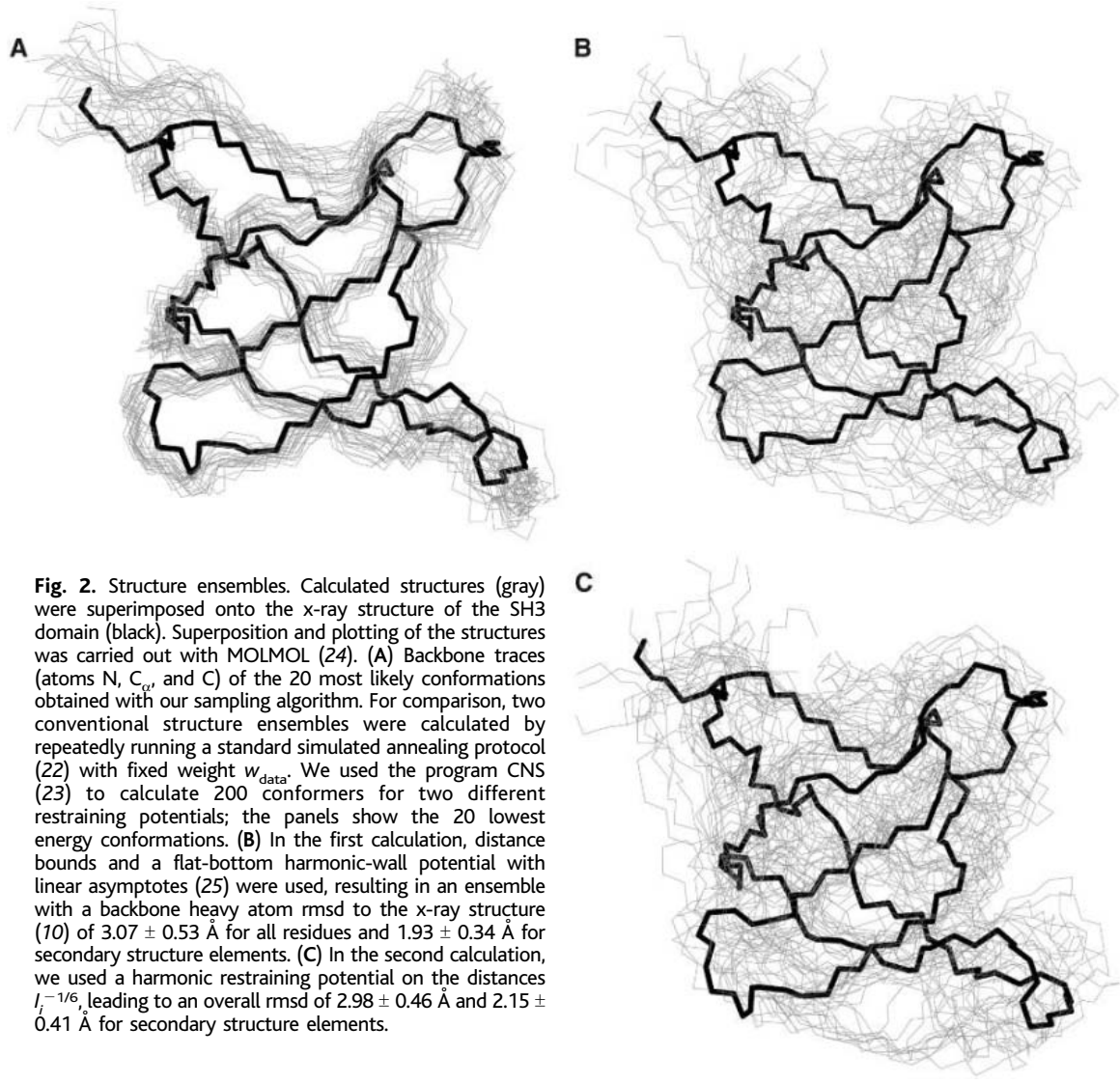

Fig. 2. Structure ensembles. Calculated structures (gray) were superimposed onto the x-ray structure of the SH3 domain (black). Superposition and plotting of the structures was carried out with MOLMOL (*24*). (**A**) Backbone traces (atoms N, C_α, and C) of the 20 most likely conformations obtained with our sampling algorithm. For comparison, two conventional structure ensembles were calculated by repeatedly running a standard simulated annealing protocol (*22*) with fixed weight w_{data}. We used the program CNS (*23*) to calculate 200 conformers for two different restraining potentials; the panels show the 20 lowest energy conformations. (**B**) In the first calculation, distance bounds and a flat-bottom harmonic-wall potential with linear asymptotes (*25*) were used, resulting in an ensemble with a backbone heavy atom rmsd to the x-ray structure (*10*) of 3.07 ± 0.53 Å for all residues and 1.93 ± 0.34 Å for secondary structure elements. (**C**) In the second calculation, we used a harmonic restraining potential on the distances $I_i^{-1/6}$, leading to an overall rmsd of 2.98 ± 0.46 Å and 2.15 ± 0.41 Å for secondary structure elements.

developed a Markov chain Monte Carlo (MCMC) algorithm based on the replica-exchange method (*8*) to simulate the joint posterior density of a structure determination problem (*5*, *9*) (Fig. 1 and fig. S1).

The most pronounced features of the posterior density can be represented in a set of conformational samples. Although this looks at first glance like a conventional structure ensemble, the rationale behind our approach to obtain conformational samples is very different. The uncertainty of atomic positions is directly influenced by the uncertainty of nuisance parameters and by the quality of the data. Effects not described in the ISPA, such as protein dynamics, tend to increase the deviations between predicted and measured peak intensities. This is reflected in an increase of the error σ and consequently leads to a loss in structural precision. However, unless the forward model incorporates experimental information on protein dynamics, we cannot discriminate motion from imprecisions due to experimental errors or lack of data.

Compared with conventional structure ensembles, our conformational samples are much better defined and systematically closer to the structure obtained with x-ray crystallography (*10*) (Fig. 2). A comparison of the 20 most probable conformations with the x-ray structure yields a backbone heavy atom rmsd (root mean square deviation) of 1.84 ± 0.20 Å for all residues and 1.36 ± 0.19 Å for the secondary structural elements. This is a considerable improvement over conventional techniques used in (*6*), where an ensemble with an overall rmsd of 2.86 ± 0.33Å and an rmsd of 2.01 ± 0.28 Å for secondary structure elements was obtained. This improvement originates in the calculation of structures by random sampling, which searches conformational space more exhaustively and suppresses topologically unlikely conformations. Misfolds such as mirror images can only be realized in a small number of ways; thus, they are entropically suppressed and do not show up in a statistical ensemble. Discriminating such conformations on the basis of the hybrid energy is more difficult, in particular if the data are sparse.

A probabilistic structure ensemble is exclusively determined by the data and the working hypotheses that enter the analysis (which are in the presented example the ISPA, the log-normal error distribution, and our choice of the force field). Modifications will, of course, lead to changes in the structures. The atom positions, for example, are sensitive to the parameters and the functional form of the force field used in the conformational prior density. This also holds for conventional approaches, which are based on analogous assumptions. However, in addition, conventional methods require empirical rules to treat nuisance parameters, because they cannot be determined from the hybrid energy alone. Cross-validation (*11*, *12*) and maximum likelihood methods (*13*), for example, have successfully been applied in NMR and crystallographic refinement to determine certain nuisance parameters such as the weight w_{data}. The ISD approach goes

beyond these techniques. Once the working hypotheses are made, Eq. 2 provides definite rules to determine any nuisance parameter, including its uncertainty, directly from the data (Fig. 3). Therefore heuristics and other subjective elements are superfluous.

Because conventional structure ensembles depend on user-specific parameter settings and on the minimization protocol, it is difficult if not impossible to assign statistically meaningful error bars to atomic coordinates. In contrast, stochastic samples drawn from the joint posterior density $p(X, \gamma, \sigma|D,I)$ are statistically well defined and can directly be used to calculate estimates of mean values and standard deviations (*14*). As a special case, we can derive an average structure with atom-wise error bars and are thus able to define an objective figure of merit for NMR structures (Fig. 4).

Bayesian and maximum likelihood approaches have already proven useful for data analysis and partial aspects of structure refinement in NMR spectroscopy and x-ray crystallography (*15*, *16*, *13*, *17*). Our results suggest that structure determination can be solved entirely in a probabilistic framework.

It is straightforward to apply our approach to other NMR parameters. In case of three-bond scalar coupling constants, for example, an appropriate forward model is the Karplus curve (*18*) involving three coefficients that are treated as nuisance parameters. However, our method is not restricted to NMR data and can be applied to other structure determination problems. Besides theoretical coherence, a rigorous probabilistic approach has decisive practical advantages. It has no free parameter and is stable for many more than the two nuisance parameters used in the example (*19*). Hence, tedious and time-consuming searches for optimal values are no longer necessary. Once the forward model to describe the data has been chosen, probability calculus uniquely determines the posterior distribution for all unknowns. It is then only a computational issue to generate posterior samples. Further intervention is not required, and structure determination attains objectivity.

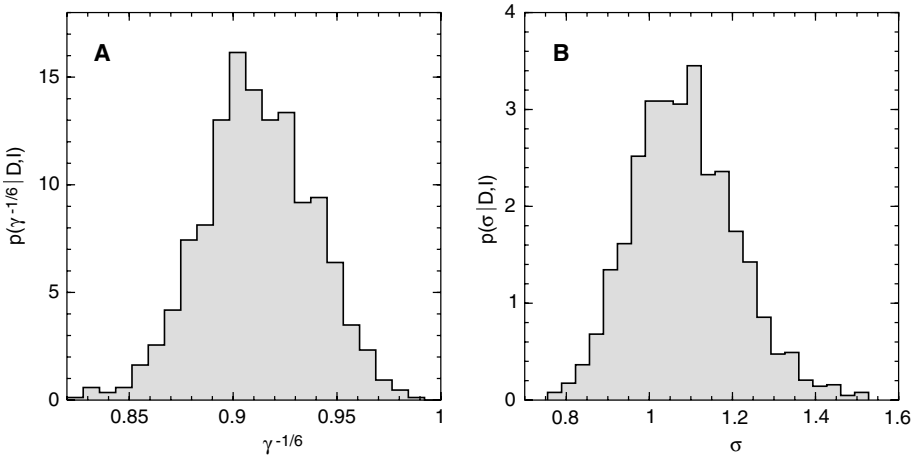

Fig. 3. Estimation of nuisance parameters. Posterior histograms compiled from MCMC samples for the scaling factor γ in the ISPA and for the width σ of the log normal error distribution. (**A**) Posterior histogram $p(\gamma^{-1/6}|D,I)$ for the inverse sixth power of γ. This factor corrects interproton distances to match the experimental distances best. (**B**) Posterior histogram $p(\sigma|D,I)$ for the error σ. In conventional approaches, this analog to the weight ($w_{data} \propto \sigma^{-2}$) can only be estimated via cross-validation or must be set empirically.

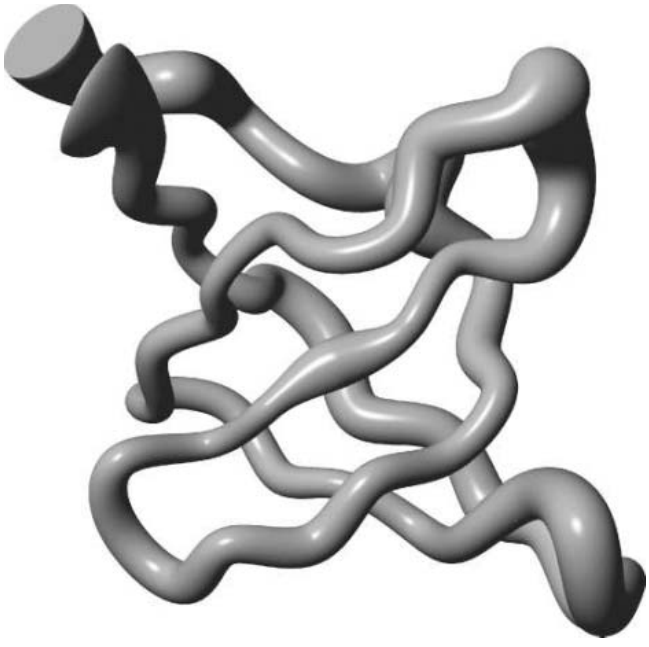

Fig. 4. Conformational uncertainty. MOLMOL "sausage" plot of the mean structure with atom-wise error bars indicated by the thickness of the sausage. The 20 most probable conformations (also shown in Fig. 2A) from the simulation of the joint posterior distribution $p(X,\gamma,\sigma|D,I)$ were used to calculate the average structure and its precision. The local precision ranges from 0.6 Å for secondary structure elements to 4.6 Å for loop regions (bottom and right-hand side) and termini (top). The average precision is 1.07 Å. The average precision of the structure ensembles calculated with CNS is 4.93 Å for the flat-bottom harmonic-wall potential and 5.04 Å for the harmonic potential.

References and Notes

1. S. Macura, R. R. Ernst, *Mol. Phys.* **41**, 95 (1980).
2. A. T. Brünger, M. Nilges, *Q. Rev. Biophys.* **26**, 49 (1993).
3. R. T. Cox, *Am. J. Phys.* **14**, 1 (1946).
4. E. T. Jaynes, *Probability Theory: The Logic of Science* (Cambridge Univ. Press, Cambridge, 2003).
5. Materials and methods are available as supporting material on *Science* Online.
6. T. K. Mal, S. J. Matthews, H. Kovacs, I. D. Campbell, J. Boyd, *J. Biomol. NMR* **12**, 259 (1998).
7. G. Lipari, A. Szabo, *J. Am. Chem. Soc.* **104**, 4546 (1982).
8. R. H. Swendsen, J.-S. Wang, *Phys. Rev. Lett.* **57**, 2607 (1986).
9. M. Habeck, M. Nilges, W. Rieping, *Phys. Rev. Lett.* **94**, 0181051 (2005).
10. M. E. Noble, A. Musacchio, M. Saraste, S. A. Courtneidge, R. K. Wierenga, *EMBO J.* **12**, 2617 (1993).
11. A. T. Brünger, *Nature* **355**, 472 (1992).
12. A. T. Brünger, G. M. Clore, A. M. Gronenborn, R. Saffrich, M. Nilges, *Science* **261**, 328 (1993).
13. P. D. Adams, N. S. Pannu, R. J. Read, A. T. Brünger, *Proc. Natl. Acad. Sci. U.S.A.* **94**, 5018 (1997).
14. M. H. Chen, Q. M. Shao, J. G. Ibrahim, *Monte Carlo Methods in Bayesian Computation* (Springer Verlag, New York, 2002).
15. R. B. Altman, O. Jardetzky, *Methods Enzymol.* **177**, 218 (1989).
16. M. Andrec, G. T. Montelione, R. M. Levy, *J. Magn. Reson.* **139**, 408 (1999).
17. G. Bricogne, *Methods Enzymol.* **276**, 361 (1997).
18. M. Karplus, *J. Am. Chem. Soc.* **85**, 2870 (1963).
19. W. Rieping, M. Habeck, M. Nilges, data not shown.
20. S. Geman, D. Geman, *IEEE Trans. Pattern Anal. Mach. Intell.* **6**, 721 (1984).
21. S. Duane, A. D. Kennedy, B. Pendleton, D. Roweth, *Phys. Lett. B* **195**, 216 (1987).
22. M. Nilges, M. J. Macias, S. I. O'Donoghue, H. Oschkinat, *J. Mol. Biol.* **269**, 408 (1997).
23. A. T. Brünger *et al.*, *Acta Crystallogr. D* **54**, 905 (1998).
24. R. Koradi, M. Billeter, K. Wüthrich, *J. Mol. Graph.* **14**, 51 (1996).
25. M. Nilges, S. I. O'Donoghue, *Prog. Nucl. Magn. Reson. Spectrosc.* **32**, 107 (1998).

26. The authors thank I. D. Campbell for kindly providing the experimental SH3 NMR data. This work was supported by European Union grants QLG2-CT-2000-01313 and QLG2-CT-2002-00988. The 20 most likely structures and the restraint list used in the calculation have been deposited in the Protein Data Bank under accession code 1ZBJ. The structure determination program is available from the authors on request to M.N.

Supporting Online Material

www.sciencemag.org/cgi/content/full/309/5732/303/DC1
Materials and Methods
Fig. S1

31 January 2005; accepted 16 May 2005
10.1126/science.1110428

Crossmodal Interactions Between Olfactory and Visual Learning in *Drosophila*

Jianzeng Guo[1] and Aike Guo[1,2]*

Different modalities of sensation interact in a synergistic or antagonistic manner during sensory perception, but whether there is also interaction during memory acquisition is largely unknown. In *Drosophila* reinforcement learning, we found that conditioning with concurrent visual and olfactory cues reduced the threshold for unimodal memory retrieval. Furthermore, bimodal preconditioning followed by unimodal conditioning with either a visual or olfactory cue led to crossmodal memory transfer. Crossmodal memory acquisition in *Drosophila* may contribute significantly to learning in a natural environment.

Information received by the nervous system through multiple sensory modalities must be processed in an integrated manner. Extensive crossmodal interaction during sensory processing and perception has been found in psychophysical studies, functional imaging of the human brain, and electrophysiological recordings from monkeys (*1*). Odor localization in *Drosophila* requires visual feedback during free flight (*2*), which suggests dynamic crossmodal sensory processing. Crossmodal interaction during memory acquisition has also been suggested by the finding that honeybees exposed to sequential color and scent conditioning can recall a specific color when they encounter a particular scent (*3*). In the present study, we aimed to explore possible crossmodal interactions during learning in *Drosophila*. Previous studies of *Drosophila* learning using unimodal sensory cues have shown robust visual learning of colors, patterns, and textures (*4*–*7*), and olfactory learning of distinct odors (*8*–*11*). Using a modified version of the classical visual flight simulator (*12*), we simultaneously applied visual and olfactory cues during reinforcement learning (*13*).

We first examined reinforcement learning (Fig. 1A) using an olfactory learning paradigm analogous to visual operant conditioning (*4*–*7*). Individual flies were trained to associate a particular odor-related flight orientation in the dark with a punishment (noxious heat stimulus). As shown in Fig. 1B, the fly frequently shifted its orientation from one 90° sector to another during the pretraining period (6 min), with no preference between 3-octanol (OCT, 1.96%) and 4-methylcyclohexano1 (MCH, 1.96%). The flies were then exposed to a training session (two 4-min periods separated by a 2-min test period) during which a noxious heat stimulus was switched on whenever OCT-related flight orientation enters the frontal 90° sector of fly's visual field. Posttraining test (8-min session in the absence of heat application) showed that the flies exhibited persistent preference for MCH (Fig. 1B). Course-control maneuvers of the tethered flight were evaluated quantitatively using the "preference index" (PI) defined as $PI = (t_c - t_h)/(t_c + t_h)$, where t_c is the time the fly was oriented toward a sector not associated with heat, and t_h is the time the fly was oriented toward a sector that was associated with heat during training (*13*). As shown in Fig. 1C, PI before the training (blocks 1 to 3) was close to zero, whereas PI during training (blocks 4, 5, 7, and 8) and during the test after training (blocks 9 to 12, "test PI") were significantly positive. A similar

[1]Institute of Neuroscience, Shanghai Institutes for Biological Sciences; Key Laboratory of Neurobiology, Chinese Academy of Sciences, Shanghai 200031, China. [2]State Key Laboratory of Brain and Cognitive Science, Institute of Biophysics, Chinese Academy of Sciences, Beijing 100101, China.

*To whom correspondence should be addressed. E-mail: akguo@ion.ac.cn

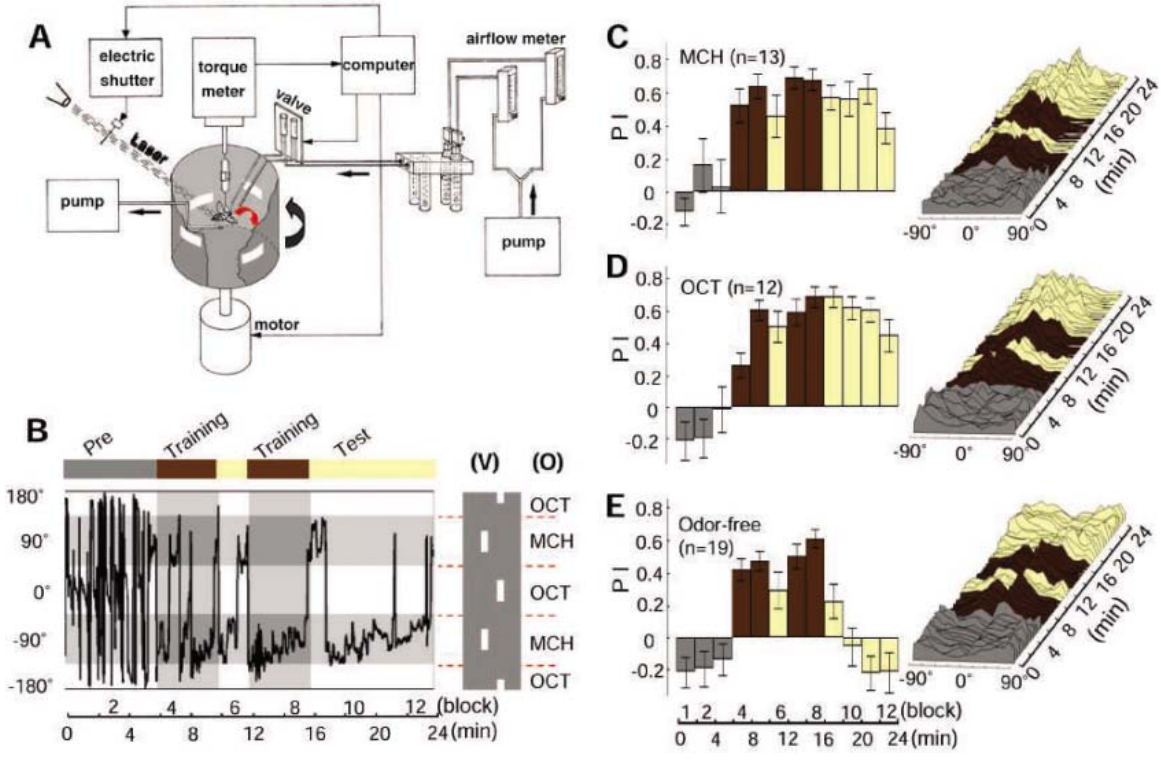

Fig. 1. Olfactory operant conditioning in the flight simulator. (**A**) The flight simulator and the operant conditioning procedure have been described previously (*12*). A description of the modifications for using them in olfactory conditioning is provided in the SOM (*13*). (**B**) A representative trace of flight path of a single fly with time in arena position (–180° to 180°) during preconditioning ("pre"), training, and test period, for unimodal olfactory conditioning in the dark. Shown on the right are corresponding visual (V) and olfactory (O) cue locations in the arena. (**C**) Summary of olfactory operant conditioning. Single *CS* flies were trained to prefer OCT to MCH. The test PI (average of PIs for block 9 to 12) was significantly positive ($P < 0.001$). (Right) The diagram of the relative amount of time spent by all tested flies in different directions between –90° and +90°. (**D**) Similar to (C), but *CS* flies were trained to prefer MCH to OCT. (**E**) Similar to (C), but the airflow was odor-free. Test PI was not significantly different from zero ($P > 0.05$). All *P* values were based on one-sample *t* test. n, the total number of flies examined.

preference for OCT rather than MCH was found when the flies were trained to avoid MCH (Fig. 1D). Also shown in Fig. 1, C and D, are angular histograms of flight path at 0.5-min intervals, indicating the relative amount of time spent by all flies in different directions between –90° and +90° relative to the preferred odor (the responses over four quadrants from –180° to +180° were pooled into two quadrants from –90° to +90° relative to the preferred direction). In control experiments using odor-free airflow, flies failed to learn to associate the airflow with the punishment, with test PIs not significantly different from zero (Fig. 1D).

Crossmodal facilitation of visual and olfactory perception has been found in human studies (*14*). There is the "principle of inverse effectiveness," in which crossmodal enhancement of perception is more pronounced when individual sensory stimuli are minimally effective (*15*). Moreover, flies' motor response to simultaneously presented visual and olfactory cues closely approximates the linear superposition of the response to each stimulus presented in isolation (*16*). We thus inquired whether *Drosophila* learning exhibits crossmodal facilitation of memory acquisition by testing visual or olfactory memory near the threshold level of conditioning stimuli. The threshold level of visual or olfactory learning in the flight simulator was defined by the magnitude of the conditioning cue at which the test PI becomes statistically not different from zero. For unimodal visual (V) learning, we trained the fly to associate punishment with either one of two white horizontal bars (on a dark background) located at different vertical positions defined by their center of gravity (COG) (*7*), alternatively presented in one of four quadrants in the visual field. The test PIs dropped to zero between 5° and 7° COG separation for both *WTB* (*wild-type Berlin*) and CS (*Canton-S*) wild-type flies (Fig. 2A, top). For determining the threshold of unimodal olfactory (O) learning in the flight simulator, the percentage concentration of the two odors (OCT and MCH) applied was varied from 0.99% to 0%. Flies failed to associate odor with punishment when the odor concentration was reduced from 0.59 to 0.39% for both *WTB* and *CS* flies (Fig. 2A, bottom).

To examine crossmodal facilitation, we applied bimodal conditioning by training single flies to associate the punishment with simultaneously presented visual and olfactory cues, which consisted of a fixed pairing of odor application and a particular flight orientation associated with the visual cue. When the subthreshold cue intensity for unimodal learning (5° for COG separation and 0.39% for odor concentration) was used for bimodal conditioning, highly significant test PI values for both *CS* and *WTB* flies were found (Fig. 2B). This apparent facilitation of learning via bimodal conditioning was not simply due to the addition of airflow in visual learning or of visual stimulation during olfactory learning, because the flies failed to exhibit significant learning when odor-free airflow (0%) or zero visual cue (0°) was used (Fig. 2C). Finally, to address whether acquisition of unimodal memory can be enhanced by the presence of simultaneous conditioning with a different sensory stimulus, which would imply crossmodal interaction during memory acquisition, we examined flies' memory with the unimodal cue below its threshold level for unimodal learning after the bimodal conditioning described above. We found significant memory retrieval during the test period (block 10 to 12) with either the subthreshold visual cue (5°) or the olfactory cue (0.39%) after bimodal conditioning with these cues (Fig. 2D). These results extend the notion of synergism in memory acquisition from unimodal to bimodal learning.

Previous flight simulator studies have shown that robust "sensory preconditioning" of flies by exposure to simultaneous color and shape visual cues without reinforcement led to the transfer of memory from the color to the shape cue, or vice versa, after pairing of the single (color or shape) cue with the punishment (*17*). In the present study, we examined this concept of memory transfer from unimodal to bimodal memory acquisition, using a similar sensory preconditioning paradigm. Single flies were

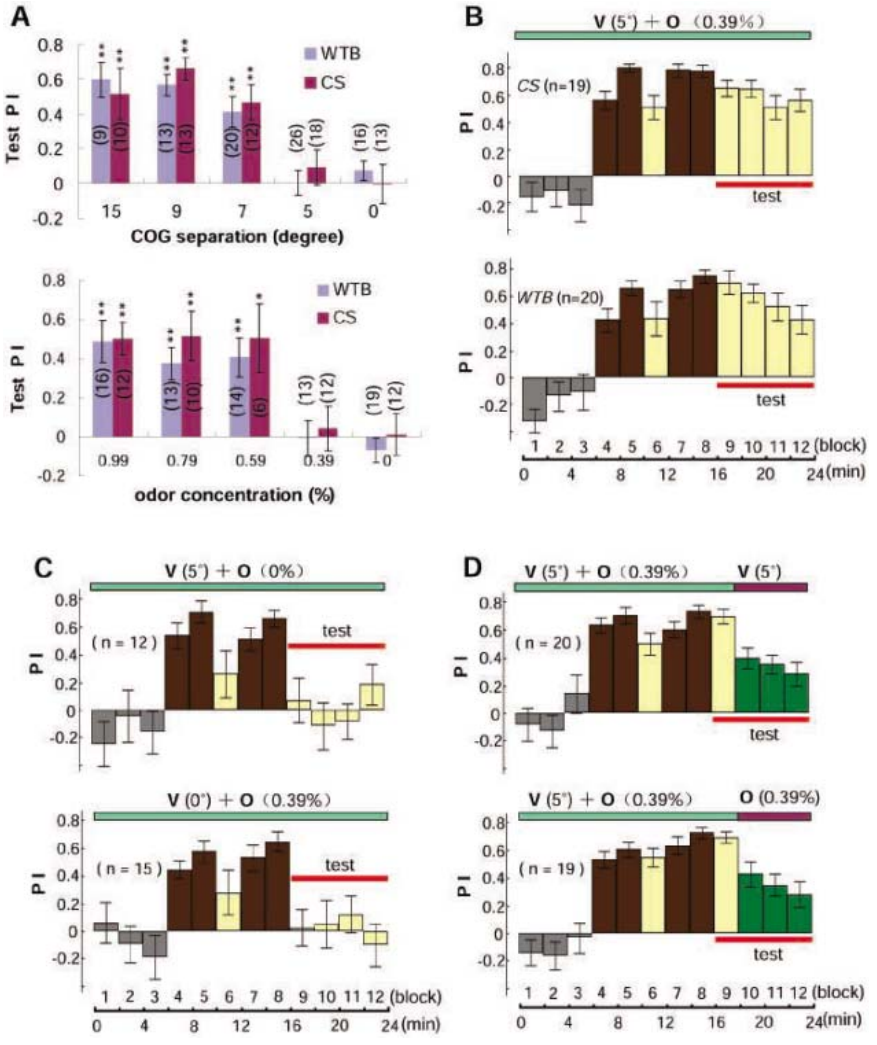

Fig. 2. Crossmodal enhancement in memory acquisition. (**A**) (Top) The threshold of visual learning. Five visual cue separations (ΔCOG from 0° to 15°) were tested. The average PI values during the test period (test PI) for 5° and 0° were not significantly different from zero ($P > 0.05$). $^{**}P < 0.01$; $^{*}P < 0.05$. (Bottom) The threshold of olfactory learning. Five concentrations of MCH/OCT (from 0 to 0.99%) were examined. Test PI for 0.39% and 0% was not significantly different ($P > 0.05$). The number in parentheses refers to the total number of flies examined. (**B**) Flies were conditioned with paired visual (5°) and olfactory (0.39%) cues. The test PI for *CS* (top) and *WTB* (bottom) was significant ($P < 0.001$). (**C**) Control experiments with the visual cue (5°), together with odor-free airflow (top), and with olfactory cue (0.39%), together with visual cue separation of 0° ΔCOG (bottom). The test PI was not significant ($P > 0.05$). (**D**) The same as in (B), except that the PI was examined during the test period for unimodal memory below its threshold. Test PI (blocks 10 to 12) for visual (V, 5°, top) or olfactory (0.39%, bottom) cue alone were significantly positive ($P < 0.001$).

allowed to fly without reinforcement (unconditioned stimulus, US^-) for eight 2-min blocks with the simultaneous presentation of fixed pairs of visual and olfactory cues (COG separation of 30°, OCT or MCH concentration at 1.96%). The flies were then conditioned (US^+) by pairing the heat punishment with the same visual cue, followed by memory acquisition test (US^-, 3 blocks) with the olfactory cue that was associated with the visual cue during preconditioning. Alternatively, the flies were conditioned by the olfactory cue after bimodal cue preconditioning and tested for memory acquisition with the associated visual cue used in preconditioning. We observed significant crossmodal transfer of memory between vision and olfaction (Fig. 3A). Note that it is necessary to present visual (V) and olfactory (O) cues concurrently during sensory preconditioning, because sequential presentation of the visual and olfactory cues (V/O, each for 50 ms) without interruption during preconditioning resulted in no transfer of memory after the single-cue conditioning (Fig. 3B).

Sensory preconditioning without reinforcement may represent a form of "incidental learning" (*18*), in which two equally salient stimuli are presented simultaneously in an equivalent manner, in contrast to the temporally asymmetric presentation of conditioned and unconditioned stimuli. We thus inquired whether crossmodal transfer of memory to unconditioned cue (either V, US^- or O, US^-; Fig. 3A) requires the presence of the memory for the conditioned cue (either O, US^+ or V, US^+). We performed reversal conditioning experiments in which the conditioned flies were punished during a brief postconditioning period by noxious heat stimulus whenever they assumed flight orientations that previously had been "safe." Flies were conditioned to prefer one of the two horizontal bars in standard training sessions and then subjected to a single 1-min reverse conditioning (RC) session (16 to 17 min) (Fig. 3C, top). Subsequent tests of memory acquisition showed that preference for the previously conditioned cue was completely abolished. Similar experiments for olfactory conditioning also showed the effectiveness of 1-min RC in abolishing the memory for the conditioned olfactory cue. Control experiments using no visual stimulation (dark, D) or no odor (stopping odor delivery, S) during the 1-min postconditioning block showed the persistence of memory for the conditioned cue (Fig. 3C, bottom). The test PIs for all RC experiments on unimodal visual or olfactory learning are summarized in Fig. 3D.

Next, we examined whether memory transfer still occurs in flies subjected to RC experiments. Flies preconditioned with simultaneous visual and olfactory cues (0 to 16 min) were then subjected to the visual cue conditioning (16 to 26 min) (Fig. 3E). Subsequent 1-min RC (26 to 27 min) on the visual cue resulted in a complete absence of memory for the olfactory cue that was paired with the conditioned visual cue during preconditioning, suggesting no memory transfer from vision to olfaction. Control experiments using no visual stimulation (dark, D) during the 1-min postconditioning block (26 to 27 min) in the absence of RC punishment showed the persistence of memory

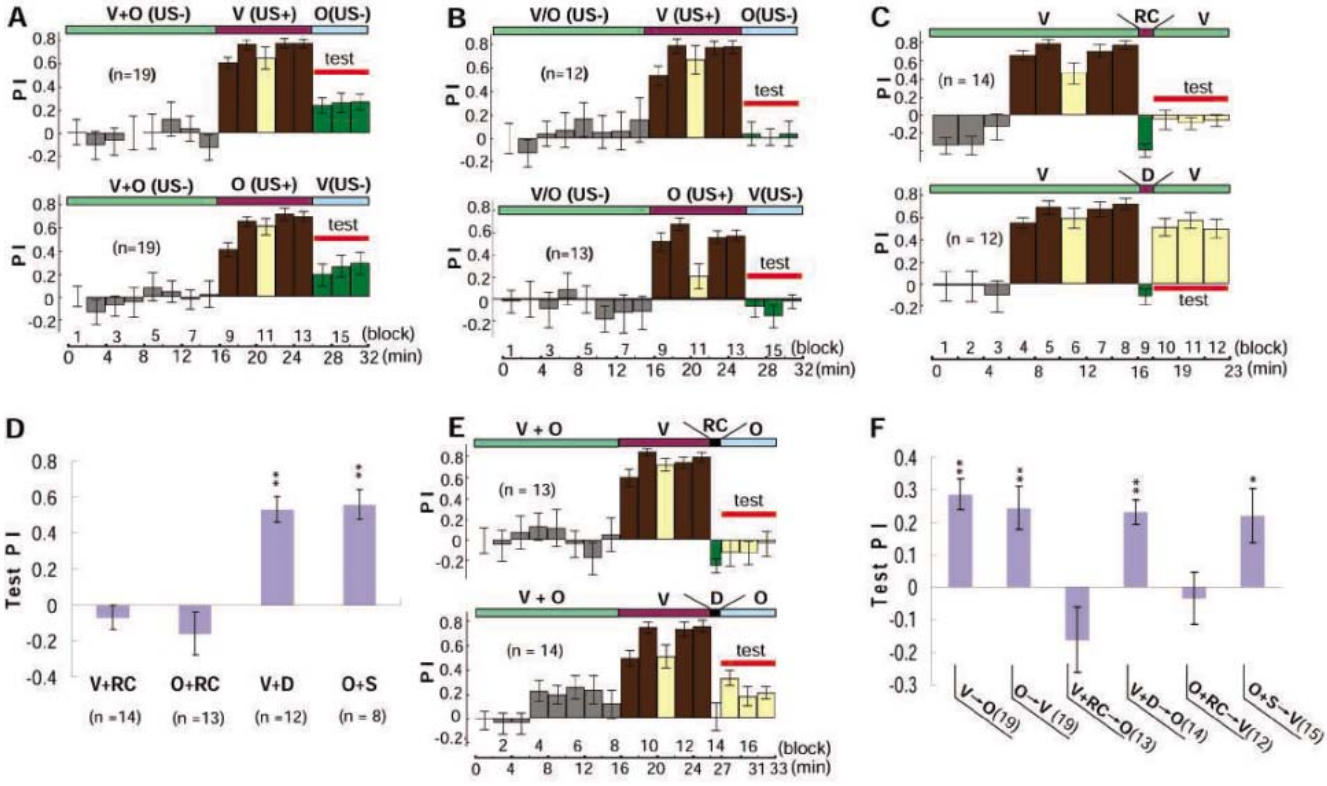

Fig. 3. Crossmodal memory transfer. (**A**) (Top) Individual *CS* flies were subjected to bimodal stimuli of ΔCOG = 30° and OCT/MCH (1.96%) for 16 min without reinforcement (O + V, US^-), followed by unimodal visual training (V, US^+), with an intervening 2-min test period. The test PI for retrieval with the olfactory cue (O, US^-) was significantly positive ($P < 0.001$). (Bottom) The test PI (V, US^-) was significantly positive ($P < 0.01$) after olfactory unimodal training. Similar results were obtained from *WTB* flies (not shown in figure). (**B**) Similar to (A), except that the visual and olfactory cues were presented alternately during preconditioning (50 ms each). The mean test PI (top: O, US^-; bottom: V, US^-) was not significant ($P > 0.05$). (**C**) (Top) RC after visual conditioning caused memory erasure; the test PI was not significant ($P > 0.05$). (Bottom) One-min darkness (D) did not impair memory, with positive test PI ($P < 0.001$). (**D**) Summary of all results showing that RC caused memory erasure (test PIs not significant, $P > 0.05$), stopping of the odor delivery for 1 min (at 16 to 17 min, O + S) did not cause memory erasure, with positive test PI ($P < 0.001$). (**E**) (Top) RC after visual conditioning (V + RC) caused failure of memory transfer from V to O (V→O), with insignificant test PI ($P > 0.05$). (Bottom) One minute of darkness after visual conditioning (at 26 to 27 min, V + D) caused no failure of memory transfer; the test PI was significant ($P < 0.001$). (**F**) Summary of all experiments similar to that in (A) and (E), together with data on the effects of the RC on olfactory training (O + RC), which caused failure of memory transfer (O→V), with insignificant test PI ($P > 0.05$). Stopping the odor delivery (26 to 27 min, O + S) caused no failure of memory transfer; the test PI was significant ($P < 0.05$). **$P < 0.01$, * $P < 0.05$ (One-sample *t* test).

transfer from vision to olfaction (Fig. 3E, bottom). Data for all memory transfer experiments are summarized in Fig. 3F. Thus, persistent memory for the conditioned cue is essential for crossmodal memory transfer.

The neural circuits and cellular mechanisms underlying the crossmodal enhancement and transfer of memory are unknown. Further understanding requires the elucidation of visual and olfactory circuits and their interconnection, as well as the locus for storage of visual and olfactory memory. It is possible that "multisensory integrative neuron" may also exist in the *Drosophila* brain and that crossmodal interaction between different sensory modalities may also be achieved through synchronized activity between modality-specific brain regions (*19*). Crossmodal interaction between sensory systems can enhance the detection and discrimination of external objects and can provide information about the environment that is unobtainable by a single modality in isolation. Our findings indicate that individual flies make use of crossmodal interactions between two sensory systems during operant conditioning, which further suggests that crossmodal interactions using multiple sensory systems may also facilitate learning in the natural environment. These results provide a basis for further studies of the circuit mechanisms underlying crossmodal interactions during memory acquisition.

References and Notes

1. G. A. Calvert, *Cereb. Cortex* **11**, 1110 (2001).
2. M. A. Frye, M. Tarsitano, M. H. Dickinson, *J. Exp. Biol.* **206**, 843 (2003).
3. M. V. Srinivasan, S. W. Zhang, H. Zhu, *Nature* **396**, 637 (1998).
4. M. Heisenberg, R. Wolf, B. Brembs, *Learn. Mem.* **8**, 1 (2001).
5. L. Liu, R. Wolf, R. Ernst, M. Heisenberg, *Nature* **400**, 753 (1999).
6. S. Tang, A. Guo, *Science* **294**, 1543 (2001).
7. S. Tang, R. Wolf, S. Xu, M. Heisenberg, *Science* **305**, 1020 (2004).
8. R. J. Greenspan, *Neuron* **15**, 747 (1995).
9. J. Dubnau, T. Tully, *Annu. Rev. Neurosci.* **21**, 407 (1998).
10. S. Waddell, W. G. Quinn, *Trends Genet.* **17**, 719 (2001).
11. R. L. Davis, *Neuron* **44**, 31 (2004).
12. A. Guo *et al.*, *Learn. Mem.* **3**, 49 (1996).
13. Materials and methods are available as supporting material on *Science* Online.
14. J. A. Gottfried, R. J. Dolan, *Neuron* **39**, 375 (2003).
15. B. E. Stein, M. A. Meredith, *Merging of the Senses* (MIT Press, Cambridge, MA, 1993).
16. M. A. Frye, M. H. Dickinson, *J. Exp. Biol.* **207**, 123 (2004).
17. B. Brembs, M. Heisenberg, *J. Exp. Biol.* **204**, 2849 (2001).
18. G. Hall, *Anim. Learn. Behav.* **24**, 233 (1996).
19. B. van Swinderen, R. J. Greenspan, *Nat. Neurosci.* **6**, 579 (2003).
20. Supported by the National Science Foundation of China (NSFC) (30270341), Multidisciplinary Program (Brain and Mind) of the Chinese Academy of Sciences (CAS), Major State Basic Research Program (G2000077800), and CAS (KJCX1-09-03). We thank M.-m. Poo for invaluable advice, Y.-q. Peng for programming, and C.-y. Yuan for assistance.

Supporting Online Material

www.sciencemag.org/cgi/content/full/309/5732/307/DC1
Materials and Methods

18 February 2005; accepted 11 May 2005
10.1126/science.1111280

MicroRNA Expression in Zebrafish Embryonic Development

Erno Wienholds,[1] Wigard P. Kloosterman,[1] Eric Miska,[2,3] Ezequiel Alvarez-Saavedra,[2] Eugene Berezikov,[1] Ewart de Bruijn,[1] H. Robert Horvitz,[2] Sakari Kauppinen,[4] Ronald H. A. Plasterk[1]*

MicroRNAs (miRNAs) are small noncoding RNAs, about 21 nucleotides in length, that can regulate gene expression by base-pairing to partially complementary mRNAs. Regulation by miRNAs can play essential roles in embryonic development. We determined the temporal and spatial expression patterns of 115 conserved vertebrate miRNAs in zebrafish embryos by microarrays and by in situ hybridizations, using locked-nucleic acid–modified oligonucleotide probes. Most miRNAs were expressed in a highly tissue-specific manner during segmentation and later stages, but not early in development, which suggests that their role is not in tissue fate establishment but in differentiation or maintenance of tissue identity.

Current estimates of miRNA gene numbers in vertebrates are as high as 500 (*1*), of which many are conserved, and miRNAs may regulate up to 30% of genes (*2*). The miRNA first discovered, *lin-4*, is involved in developmental timing in the nematode *Caenorhabditis elegans* (*3*). In mammals, miRNAs have been implicated in hematopoietic lineage differentiation (*4*) and homeobox gene regulation (*5*). Zebrafish that are defective in miRNA processing arrest in development (*6*). Recently, miRNAs were shown to be dispensable for cell fate determination, axis formation, and cell differentiation but are required for brain morphogenesis in zebrafish embryos (*7*). Together, these findings indicate that miRNAs can play essential roles in development. However, little is known about the individual roles of most miRNAs. To focus future miRNA studies, we determined the spatial and temporal expression patterns of 115 conserved vertebrate miRNAs (see online Material and Methods; table S1; table S2) in zebrafish embryos.

First, we determined the temporal expression of miRNAs during embryonic development by microarray analysis (Fig. 1A and fig. S1A). Up to segmentation [12 hours post fertilization (hpf)], most miRNAs could not be detected. Most miRNAs became visible 1 to 2 days after fertilization and showed strong expression when organogenesis is virtually completed (96 hpf). In adults, the majority of miRNAs remained expressed (Fig. 1A). In addition we determined the expression of miRNAs in dissected organs of adult fish. For some miRNAs, a high degree of tissue specificity was observed (figs. S1B and S2, and table S3).

In situ hybridization of miRNAs had thus far not been possible in animals. Recently LNA (locked-nucleic acid)–modified DNA oligonucleotide probes have been shown to increase the sensitivity for the detection of miRNAs by Northern blots (*8*). By Northern blots analysis and in situ hybridization, using LNA probes, we detected predominantly mature miRNAs, which were reduced in dicer knockout zebrafish (fig. S3). We used these LNA probes for the whole-mount in situ detection of the conserved vertebrate miRNAs in zebrafish embryos and made a catalog of miRNA expression patterns (fig. S4 and database S1).

Most miRNAs (68%) were expressed in a highly tissue-specific manner. For example, miR-140 was specifically expressed in the cartilage of the jaw, head, and fins, and its presence was entirely restricted to those regions (Fig. 1B and database S1). Representative examples are shown (Fig. 1C) of six miRNAs that were expressed in different organ systems: nervous system, digestive system, muscles, circulatory system, sensory organs, and excretory system. Even within organs, there is specificity, as exemplified in Fig. 1D, where miR-217 can be seen to be expressed in the exocrine pancreas, and miR-7 in the endocrine pancreas (Langerhans islets). More than half of the miRNAs (43) were expressed in (specific regions of) the central nervous system (fig. S4). Many miRNA genes are clustered in the genome and, therefore, are probably expressed as one primary transcript, and indeed, we observed that many such clustered genes showed identical or overlapping expression patterns (figs. S4 and S5). We compared the in situ data with microarray

[1]Hubrecht Laboratory, Centre for Biomedical Genetics, 3584 CT Utrecht, the Netherlands. [2]Howard Hughes Medical Institute, Department of Biology and McGovern Institute for Brain Research, Massachusetts Institute of Technology, Cambridge, MA 02139, USA. [3]Wellcome Trust, Cancer Research UK Gurdon Institute, University of Cambridge, Cambridge CB2 1QN, UK. [4]Wilhelm Johannsen Centre for Functional Genome Research, Institute of Medical Biochemistry and Genetics, University of Copenhagen, DK-2200 Copenhagen N, Denmark.

*To whom correspondence should be addressed. E-mail: plasterk@niob.knaw.nl

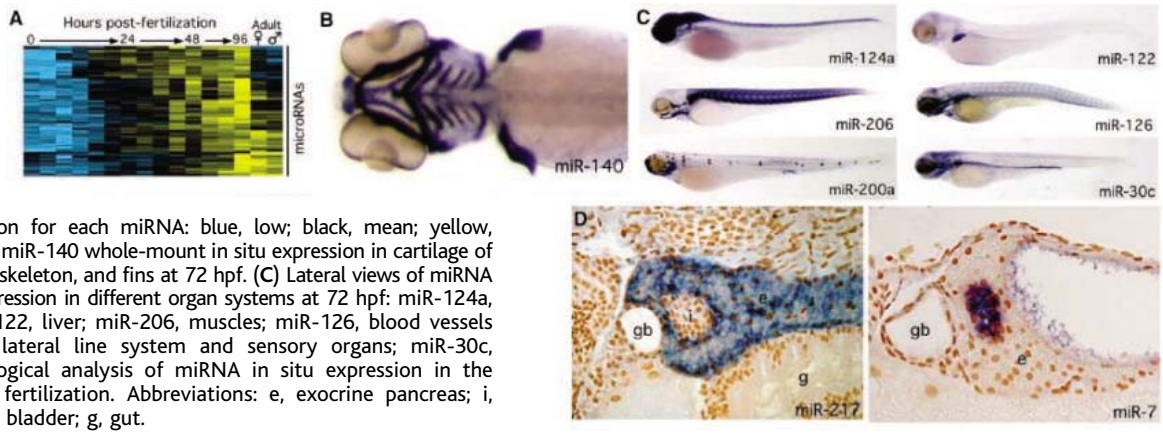

Fig. 1. miRNA expression in zebrafish embryonic development. (**A**) Microarray expression levels of 90 (of the 115) miRNAs during embryonic development. Colors indicate relative and mean-centered expression for each miRNA: blue, low; black, mean; yellow, high. (**B**) Ventral view of miR-140 whole-mount in situ expression in cartilage of pharyngeal arches, head skeleton, and fins at 72 hpf. (**C**) Lateral views of miRNA whole-mount in situ expression in different organ systems at 72 hpf: miR-124a, nervous systems; miR-122, liver; miR-206, muscles; miR-126, blood vessels and heart; miR-200a, lateral line system and sensory organs; miR-30c, pronephros. (**D**) Histological analysis of miRNA in situ expression in the pancreas 5 days after fertilization. Abbreviations: e, exocrine pancreas; i, pancreatic islet; gb, gall bladder; g, gut.

data for zebrafish and mammals (fig. S2 and table S3). Up to 77% of the in situ expression patterns were confirmed by at least one of the microarray data sets. In addition, miRNA in situ data showed patterns that cannot easily be detected by microarrays. For example, some miRNAs were expressed in hair cells of sensory epithelia (fig. S6).

In conclusion, we here describe the first comprehensive set of miRNA expression patterns in animal development. We found these patterns to be remarkably specific and diverse, which suggests highly specific and diverse roles for miRNAs. Most miRNAs are expressed in a tissue-specific manner during segmentation and later stages but were not detected during early development. Although we cannot exclude a role for undetectable early miRNAs, this observation indicates that most miRNAs may not be essential for tissue fate establishment but rather play crucial roles in differentiation or the maintenance of tissue identity.

References and Notes

1. E. Berezikov *et al.*, *Cell* **120**, 21 (2005).
2. B. P. Lewis, I. H. Shih, M. W. Jones-Rhoades, D. P. Bartel, C. B. Burge, *Cell* **115**, 787 (2003).
3. R. C. Lee, R. L. Feinbaum, V. Ambros, *Cell* **75**, 843 (1993).
4. C. Z. Chen, L. Li, H. F. Lodish, D. P. Bartel, *Science* **303**, 83 (2004).
5. S. Yekta, I. H. Shih, D. P. Bartel, *Science* **304**, 594 (2004).
6. E. Wienholds, M. J. Koudijs, F. J. van Eeden, E. Cuppen, R. H. Plasterk, *Nat. Genet.* **35**, 217 (2003).
7. A. J. Giraldez *et al.*, *Science* **308**, 833 (2005).
8. A. Valoczi *et al.*, *Nucleic Acids Res.* **32**, e175 (2004).

9. We thank D. Jongejan, F. van Eeden, S. Schulte-Merker, J. Bakkers, S. Chocron, N. Tolstrup, M. Bjørn, M. Bonde Mogensen, A. Hansen, W. Herzog, and ZFIN for technical assistance and/or help with annotation. We thank Exiqon for generously providing the LNA-modified probes. H.R.H. is an investigator of the Howard Hughes Medical Institute. This work was supported by a grant from the Netherlands Organization for Scientific Research (NWO) (E.W. and R.H.A.P.).

Supporting Online Material
www.sciencemag.org/cgi/content/full/1114519/DC1
Materials and Methods
Figs. S1 to S6
Tables S1 to S3
Database S1

6 May 2005; accepted 13 May 2005
Published online 26 May 2005;
10.1126/science.1114519
Include this information when citing this paper.

Ant Nestmate and Non-Nestmate Discrimination by a Chemosensory Sensillum

Mamiko Ozaki,[1]*† Ayako Wada-Katsumata,[1]* Kazuyo Fujikawa,[1] Masayuki Iwasaki,[2] Fumio Yokohari,[2] Yuji Satoji,[1] Tomoyosi Nisimura,[1] Ryohei Yamaoka[1]

In animal societies, chemical communication plays an important role in conflict and cooperation. For ants, cuticular hydrocarbon (CHC) blends produced by non-nestmates elicit overt aggression. We describe a sensory sensillum on the antennae of the carpenter ant *Camponotus japonicus* that functions in nestmate discrimination. This sensillum is multiporous and responds only to non-nestmate CHC blends. This suggests a role for a peripheral recognition mechanism in detecting colony-specific chemical signals.

The struggle to maintain order in societies has led social animals, including human beings, to evolve and develop various means of communication. Ants have developed a sophisticated chemical communication system that enables them to reject non-nestmate conspecifics and to accept nestmates (*1*, *2*). Many behavioral experiments have suggested that their aggressive behavior against non-nestmates is evoked by contact chemosensory detection of differences between colony-specific chemical signals (*3*–*8*). Despite this well-defined behavior, the sensory mechanism for nestmate and non-nestmate discrimination has been unclear. It is thought that a "neural template" of nestmate recognition cues is formed that represents a constantly changing, experience-derived memory (*9*, *10*). By comparing the chemosensory discriminators or "labels" of encountered individuals with the "template" previously acquired, ants decide between acceptance or aggression (*11*, *12*). For such a decision rule by "template-label matching," several models have been proposed (*13*–*15*). They are constructed on a threshold-response hypothesis (*2*) in which some neural mechanism in the brain sets a threshold of similarity between template and label, thus regulating aggression.

For the carpenter ant, *C. japonicus*, cuticular CHC blends consist of at least 18 compounds in colony-specific ratios (Fig. 1A). To investigate how these organisms discern nestmate from non-nestmate signals, we developed a bioassay whereby a glass bead was used as a surrogate ant. The aggressive behavior of worker ants toward encountered non-nestmates was mimicked by a glass bead inoculated with either cuticle extract or a CHC fraction derived from the non-nestmate body surface (Fig. 1B). No aggression was elicited in response to extract from the nestmate body surface. There was a significant difference (t test; $P < 0.001$) in ant aggression against nestmate and non-nestmate compounds. About 40% of the ants became ag-

[1]Department of Applied Biology, Faculty of Textile Science, Kyoto Institute of Technology, Matsugasaki, Sakyo-ku, Kyoto 606-8585, Japan. [2]Department of Earth System Science, Faculty of Science, Fukuoka University, Fukuoka 814-0180, Japan.

*These authors contributed equally to this work.
†To whom correspondence should be addressed. E-mail: mamiko@kit.ac.jp

gressive in response to the non-CHC fractions, regardless of their origin (Fig. 1C). Thus, similar to other social insects (*16*), the colony-specific CHC blend was the most important recognition-discriminating factor in *C. japonicus*.

Behavioral observations of ants suggest that aggression depends on antennal contact with non-nestmate compounds. Electrophysiological recordings show that typical taste sensilla in antennae did not respond to CHCs, but one type of sensillum (Fig. 2A) did respond to contact stimulation with the non-nestmate CHC blend (Fig. 3A). (Because CHCs are highly lipophilic, we used 0.1% Triton X-100 to dissolve CHCs into stimulus solutions). Response to the non-nestmate CHC blend gradually adapted to the control level but usually lasted longer than 10 s. This type of sensillum responded neither to the CHC blend nor to crude extract of nestmates. This electrophysiological response was observed in both an antenna attached to a head capsule and an antenna separated from the head (Fig. 3B). More than 75% of the tested sensilla responded to the crude extract or the purified CHCs of non-nestmates (Fig. 3C). Only 12% responded to the crude extract of nestmates, and only 24% responded to the purified CHCs of nestmates. The non-nestmate–derived non-CHC fraction elicited a response in only 30% of the tested sensilla, whereas the nestmate-derived non-CHC fraction did not elicit any response. When a mixture of nestmate and non-nestmate CHCs were tested, impulses diminished faster than those induced by non-nestmate CHCs. Moreover, this type of sensillum responded to CHC blends of different ant species (4 of 4 to *Formica japonica*, 4 of 4 to *Lasius japonicus*, and 23 of 29 to *Camponotus obscuripes*).

Scanning electron microscopy revealed that this type of sensillum is relatively thick (approximately 20 μm in length and 4 μm in diameter) and multiporous (Fig. 2B). Multiporous chemosensilla are generally assumed to be olfactory rather than contact chemosensory (*17*). However, in a few parasitic bees, a particular type of multiporous sensillum is presumed to act as a contact chemosensory organ for host discrimination (*18*). We found that ant sensilla that are sensitive to non-nestmate CHC blend also house a large number (about 200) of putative receptor neurons (Fig. 2C). Such a large number of receptor neurons might facilitate the resolution of small differences in the multiple-component chemical cues encountered by the sensillum and also might integrate the chemical information as a unit (*19*). A single sensillum responded to non-nestmate CHCs with different shapes of impulses (Fig. 3A), which suggests that several neurons in a sensillum could simultaneously respond to several compounds in the non-nestmate CHC blend.

The electrophysiological (Fig. 3) and behavioral (Fig. 1) results suggest that this sensillum might have a direct role in nestmate and non-nestmate discrimination in this ant species. There was not a full match between the behavioral (Fig. 1Cc) and electrophysiological (Fig. 3Cc) effects of the nestmate-derived non-CHC fraction to indicate the involvement of other types of sensilla. However, because this sensillum showed a response specificity for non-nestmate blends, even in isolated antenna preparations, the effect is generated peripherally and does not require feedback from the brain.

Analysis of the antennal extract of *C. japonicus* identified a 12-kD protein with an N-terminal amino acid sequence similar to that in members of the chemosensory protein (CSP) family (fig. S1A). Generally, receptor neurons in insect chemosensilla are surrounded by an aqueous lymphatic fluid. Thus, water-insoluble stimulants such as CHCs require water-soluble carriers to access receptor neurons (*20*). To obtain the complete sequence of the CSP, cDNA was derived from poly(A)-rich RNA isolated from the flagellum where CHC-sensitive sensilla were abundant. Reverse transcription polymerase chain reaction was used with degenerate primers and amplified a 580–base pair cDNA sequence (fig. S1B) consisting of 102 amino acid residues (fig. S2) (CjapCSP) (DNA Data Bank of Japan, accession number AB182637). CjapCSP showed 63% identity with two other *Hymenoptera* CSPs (LhumCSP and PdomCSP-1) and 30% to 40% identity with other CSPs (fig. S3). Histochemical staining with antiserum against recombinant CjapCSP (Fig. 3D) showed localization beneath the cuticle in the flagellum (Fig. 3Da) and also inside the CHC-sensitive antennal sensillum (Fig. 3Dc), although sensillar specificity in localization was not clear.

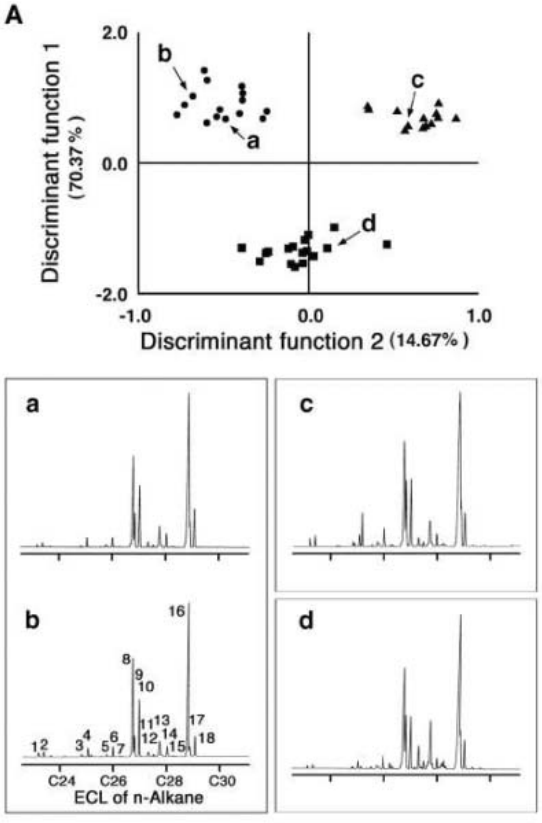

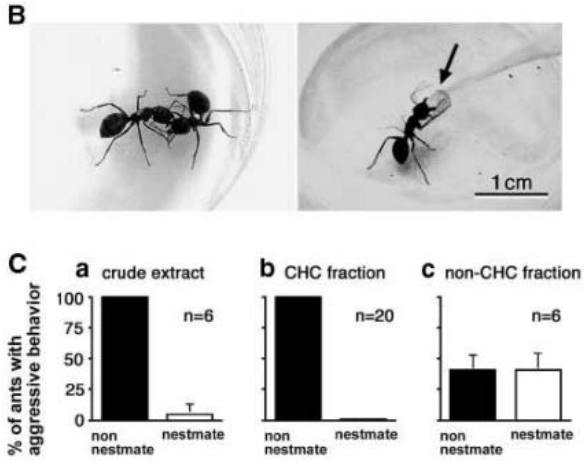

Fig. 1. Ant CHC profiles and behavioral responses. (**A**) (Top) Discriminant analysis of individual CHC profiles of three different colonies according to Dietemann *et al*. (*22*). (Bottom) CHC profiles of individuals belonging to each colony are indicated by the same symbols forming a cluster, which suggests similarity among them; (a and b) CHC profiles of different individuals within a colony; (c and d) CHC profiles of individuals in different colonies. Peak 1: tricosene; 2: *n*-tricosane; 3: pentacosene; 4: *n*-pentacosane; 5: hexacosene; 6: *n*-hexacosane; 7: 5,7,12- and 7,9,12-trimethylpentacosane; 8: 9-heptacosene; 9: 7-heptacosene; 10: *n*-heptacosane; 11: 13-methylheptacosane; 12: 5-methylheptacosane; 13: 7,15-dimethylheptacosane; 14: *n*-octacosane; 15: 5,7,12-trimethylheptacosane; 16: 9-nonacosene; 17: 7-nonacosene; 18: *n*-nonacosane. (**B**) Photographs of *C. japonicus* encountering a non-nestmate ant and a glass bead (arrow) covered with the CHC blend derived from non-nestmates. (**C**) The ratio of ants showing aggressive behavior to crude extract, CHC fraction, and non-CHC fraction from the non-nestmates (closed columns) or the nestmates (open columns). Twenty ants of one colony were tested for the stimuli derived from the same or a different colony. Reciprocal tests converting the colonies for the test ant and the test stimulus were also carried out, and data were statistically evaluated in a, b, and c, using 6, 20, and 6 colonies, respectively.

To determine whether CjapCSP is a carrier protein for *C. japonicus* CHCs, an aqueous buffer solution was added to CHCs (Fig. 4). Buffer solution alone did not dissolve CHCs, as determined by gas chromatography. However, buffer containing 10 or 100 μM CjapCSP did dissolve CHCs (0.9 ± 0.5 or 2 ± 0.8 μg/ml CHCs) at the given ratio. Buffer containing 100 μM bovine serum albumin (BSA) dissolved very little CHC (0.1 ± 0.2 μg/ml) in comparison. This was observed for CHC blends derived from three different colonies. When CjapCSP was used to dissolve CHCs in the stimulus solution, electrophysiologically recorded responses from CHC-sensitive sensilla indicated that only non-nestmate CHCs were stimulative (Fig. 3A). Thus, with CjapCSP as a carrier, lipohilic CHCs might be transferred to stimulate receptor cells.

Our data suggest that specialized sensilla in the antenna appear to have almost all-or-none sensitivity to non-nestmate or nestmate CHC blends. To discriminate between non-nestmates and nestmates by their CHC patterns of multiple components, a sensillum would be expected to have multiple receptor neurons. In accordance with olfactory coding by receptor neurons, each receptor neuron in the sensillum might express a different receptor molecule. Each CHC component might interact with more than one receptor molecule; therefore, each CHC component might activate several neurons. The receptor neurons must simultaneously be desensitized to stimulation by nestmate CHC blends. Desensitization of receptor neurons can occur by down-regulation of receptor molecules, by inhibition among receptor neurons or at the receptor molecule level, or even by sensory adaptation of receptor neurons. In any case, when a receptor neuron is desensitized to a stimulant, it shows an increased electrophysiological threshold (*21*). Even if all of the receptor neurons in a sensillum are desensitized to nestmate CHCs, some neurons can still respond to non-nestmate CHC components, concentrations of which are higher than the increased threshold levels. However, it was difficult to precisely evaluate the desensitization property of every receptor neuron because temporal and kinetic analysis of impulses to the multiple CHC components was not possible. If enough of the pure compounds that constitute the nestmate CHC blend could be obtained, more precise behavioral and electrophysiological analyses would be allowed. It also remains possible that ants obtain chemo-

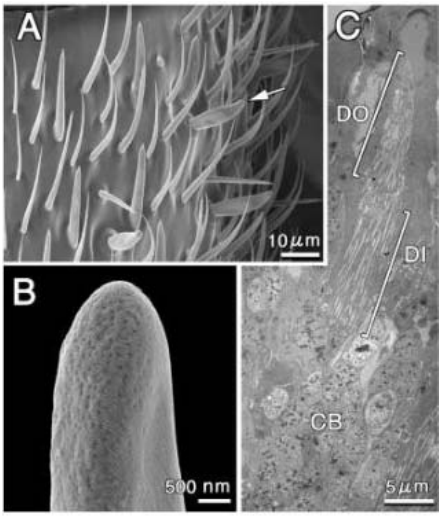

Fig. 2. CHC-sensitive sensillum and CPS localization. (**A**) Scanning electron micrograph (SEM) of the antennal surface at low magnification. The non-nestmate-CHC-sensitive sensillum is indicated by an arrow. (**B**) SEM of the tip of the non-nestmate-CHC-sensitive sensillum at high magnification. (**C**) Transmission electron micrograph of a longitudinal section beneath the cuticular apparatus of non-nestmate-CHC-sensitive sensillum. DO, dendritic outer segments; DI, dendritic inner segments; CB, cell bodies of the receptor neurons.

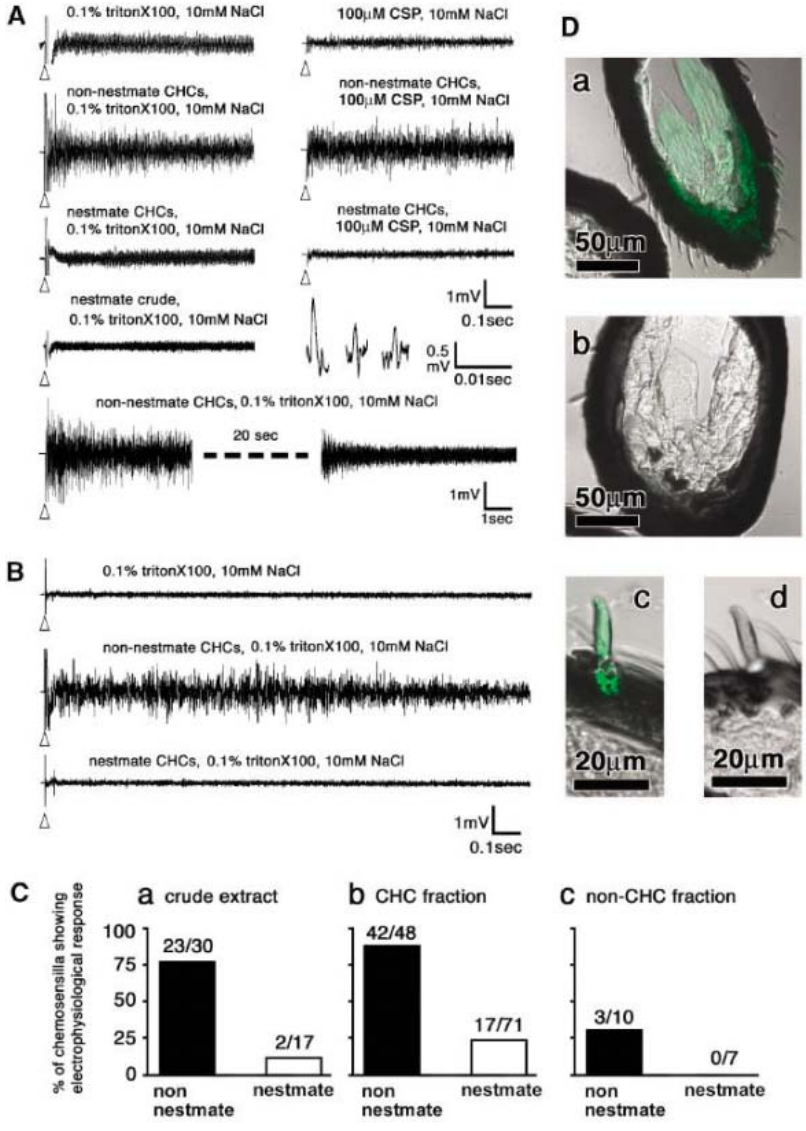

Fig. 3. Sensillum responses to CHCs. (**A**) (Left, top to bottom) Responses of the identified sensillum in a head-attached antenna preparation to indicated mixtures containing crude extract, CHCs, or CSP. A long response recording (20 s in the middle of the impulse recording is omitted) shows adaptation to non-nestmate CHCs dissolved in 10 mM NaCl containing 0.1% Triton X-100. Three distinguishable units of impulses are shown. Arrowheads indicate beginning of stimulation. The ants used for electrophysiological experiments were randomly chosen from seven colonies, and reciprocal tests converting the colonies for the test ant and the test stimulus were carried out. (**B**) Responses in an antenna preparation separated from the head to the indicated mixtures. (**C**) The ratio of sensilla in which impulses were observed in response to crude extract, CHC fraction, and non-CHC fraction derived from non-nestmates (closed columns) or nestmates (open columns). Fractions represent ratio of number of responding sensilla to number of tested sensilla. (**D**) Cross sections of flagellum (a) and scapus (b) stained with antiserum to CjapCSP. Longitudinal sections of the CHC-sensitive sensillum stained with antiserum to CjapCSP (c) and preimmune serum (d) as control. The photomicrographs are superimposed phase-contrast images and fluorescent images in which CjapCSP localization is indicated by green fluorescence.

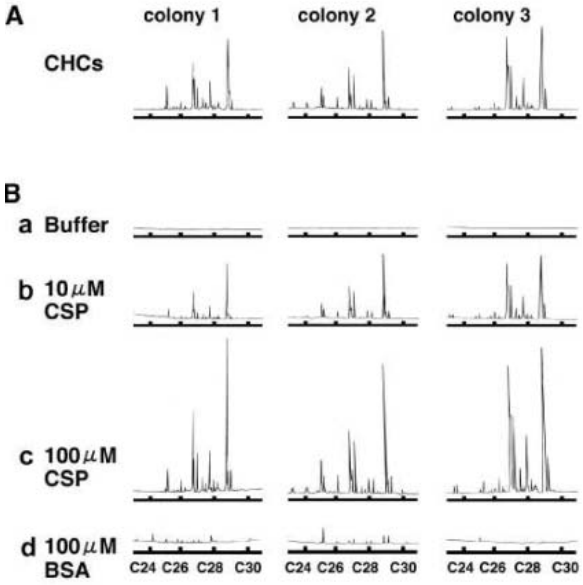

Fig. 4. CSP dissolves CHCs. (**A**) Gas chromatograms for the original CHC profiles from colonies 1 to 3. (**B**) (a, b, and c) CHC profiles dissolved in the buffer with 0, 10, and 100 μM CjapCSP, respectively; (d) CHC profiles dissolved in the buffer with 100 μM BSA as control. $n = 10$ for each assay using colony-specific CHC blend; the chromatograms are an average drawing of them.

sensory information from nestmate CHCs through other types of sensilla.

References and Notes

1. S. Lahav, V. Soroker, A. Hefetz, R. K. Vander Meer, *Naturwissenschaften* **86**, 246 (1999).
2. M. S. Obin, R. K. Vander Meer, *Anim. Behav.* **38**, 430 (1989).
3. R. W. Howard, in *Insect Lipids: Chemistry, Biochemistry, and Biology*, D. W. Stanley-Samuelson, D. R. Nelson, Eds. (Univ. Nebraska Press, Omaha, 1993), pp. 179–226.
4. E. O. Wilson, in *The Insect Societies* (Belknap Press of Harvard Univ. Press, Cambridge, MA, 1971).
5. B. Hölldobler, C. D. Michener, in *Evolution of Social Behavior: Hypothesis and Empirical Tests*, H. Markl, Ed. (Verlag Chemie GmbH, Weinheim, 1980), pp. 35–57.
6. M. D. Breed, B. Bennet, in *Kin Recognition in Animals*, D. J. C. Fletcher, C. D. Michener, Eds. (Wiley, New York, 1987), pp. 243–285.
7. R. K. Vander Meer, L. Morel, in *Pheromone Communication in Social Insects: Ants, Wasps, Bees, and Termites*, R. K. Vander Meer, M. D. Breed, K. E. Espelie, M. L. Winston, Eds. (Westview Press, Boulder, CO, 1998), pp. 79–103.
8. R. Yamaoka, *Physiol. Ecol. Jpn.* **27**, 3152 (1990).
9. R. K. Vander Meer, D. Saliwanchik, B. Lavine, *J. Chem. Ecol.* **15**, 2115 (1989).
10. S. Lahav, V. Soroker, R. K. Vander Meer, A. Hefetz, *J. Chem. Ecol.* **27**, 927 (2001).
11. R. C. Lacy, P. W. Sherman, *Am. Nat.* **121**, 489 (1983).
12. P. W. Sherman, W. G. Holmes, in *Experimental Behavioral Ecology*, B. Hölldobler, M. Lindauer, Eds. (G. Fischer Verlag, Stuttgart, 1985), pp. 437–460.
13. R. Crozier, M. W. Dix, *Behav. Ecol. Sociobiol.* **4**, 217 (1979).
14. W. M. Getz, *J. Theor. Biol.* **99**, 585 (1982).
15. W. M. Getz, R. F. Chapman, *Int. J. Neurosci.* **32**, 963 (1987).
16. M. D. Breed, in *Pheromone Communication in Social Insects*, R. K. Vander Meer, M. D. Breed, K. E. Espelie, M. L. Winston, Eds. (Westview Press, Boulder, CO, 1998), pp. 57–78.
17. R. A. Steinbrecht, in *Atlas of Arthropod Sensory Receptors*, E. Eguchi, Y. Tominaga, Eds. (Springer-Verlag, Tokyo, 1999), pp. 155–176.
18. N. Isidoro, R. Romani, F. Bin, *Microsc. Res. Tech.* **55**, 350 (2001).
19. W. M. Getz, R. P. Akers, *Behav. Neural Biol.* **61**, 191 (1994).
20. M. Tegoni, V. Campanacci, C. Cambillau, *Trends Biochem. Sci.* **29**, 257 (2004).
21. J. Dolzer, K. Fischer, M. Stengl, *J. Exp. Biol.* **206**, 1575 (2003).
22. Materials and methods are available as supporting material on *Science* Online.

23. We thank T. Amakawa and Y. Endo for their technical advice and R. K. Vander Meer, R. Menzel, and P. Pelosi for their critical reading and indispensable discussion on the paper. This work was supported by grants from ProBRAIN and KAKENHI 17207003 (M.O.), JSPS (A.W.-K.), and MEXT 142090131 (R.Y.).

Supporting Online Material

www.sciencemag.org/cgi/content/full/1105244/DC1
Materials and Methods
Figs. S1 to S3
References and Notes

15 September 2004; accepted 20 May 2005
Published online 9 June 2005;
10.1126/science.1105244
Include this information when citing this paper.

Bone Marrow Stromal Cells Generate Muscle Cells and Repair Muscle Degeneration

Mari Dezawa,[1]* Hiroto Ishikawa,[1] Yutaka Itokazu,[1] Tomoyuki Yoshihara,[1] Mikio Hoshino,[2] Shin-ichi Takeda,[3] Chizuka Ide,[1] Yo-ichi Nabeshima[2]

Bone marrow stromal cells (MSCs) have great potential as therapeutic agents. We report a method for inducing skeletal muscle lineage cells from human and rat general adherent MSCs with an efficiency of 89%. Induced cells differentiated into muscle fibers upon transplantation into degenerated muscles of rats and mdx-nude mice. The induced population contained Pax7-positive cells that contributed to subsequent regeneration of muscle upon repetitive damage without additional transplantation of cells. These MSCs represent a more ready supply of myogenic cells than do the rare myogenic stem cells normally found in muscle and bone marrow.

Cell transplantation therapy offers hope for the treatment of intractable muscle degenerative disorders. Embryonic stem (ES) cells and stem cells derived from muscle have been considered as candidates for transplantation therapy (*1*–*7*). Although they have great potential, they face limitations inherent in procurement from fetal tissue, including problems relating to histocompatibility and ethical concerns. Although muscle stem cells and satellite cells can be isolated from adult and prenatal tissues (*2*, *4*–*6*), the number of cells that can be harvested may be limited. Bone marrow is another source of myogenic stem cells (*3*, *8*); however, because the stem cell population is very small, the problem of inadequate tissue supply for therapeutic scale again arises.

Because bone marrow stromal cells (MSCs) are easy to isolate and expand rapidly from patients without leading to major ethical and technical problems, they have great potential as therapeutic agents. However, despite their potential for use in cell transplantation therapy, practical application to human muscle degenerative diseases depends on the ability to control their differentiation into functional skeletal muscle cells with high efficiency and purity. Recently we reported that efficient induction of neurons, without glial differentiation, from human and rat MSCs could be achieved by Notch1 intracellular domain (NICD) gene transfer and administration of certain trophic factors (*9*). Further addition of glial cell line–derived neurotrophic factor (GDNF) effectively induced dopamine-producing cells and resulted in functional recovery when those cells were grafted into the brains of Parkinson's disease model rats (*9*). Here we report a method to systematically and efficiently induce skeletal muscle lineage cells

[1]Department of Anatomy and Neurobiology, [2]Department of Pathology and Tumor Biology, Kyoto University Graduate School of Medicine, Yoshidakonoe-cho, Sakyo-ku, Kyoto, 606-8501 Japan. [3]Department of Molecular Therapy, National Center of Neurology and Psychiatry, Kodaira, 187-8502 Tokyo, Japan.

*To whom correspondence should be addressed. E-mail: dezawa@anat2.med.kyoto-u.ac.jp

with high purity from a large population of adherent MSCs, rather than from a rare subpopulation of myogenic stem cells contained in the bone marrow. The induced population effectively differentiated into mature myotubes with some cells persisting as Pax7-positive satellite cells that continued to function in host muscle to restore degenerating muscles in the absence of repeated transplantations. Because our induction system uses a large population of adherent MSCs, which can be easily isolated and expanded, functional skeletal muscle cells including satellite cells can be obtained on a therapeutic scale in a short time period.

General adherent MSCs were established as described [(*10*), Note1]. After three passages, induction was initiated. The induction procedure and corresponding phase contrast images taken at each step are shown (Fig. 1, A and B). Human and rat MSCs plated at a set cell density ([(*10*), Note1] were treated with basic fibroblast growth factor (bFGF), forskolin (FSK; known to up-regulate intracellular cyclic adenosine 3′,5′-monophosphate), platelet-derived growth factor-AA (PDGF), and neuregulin for 3 days (cells at this stage are referred to as C-MSCs). The C-MSCs were then transfected with an NICD expression plasmid by lipofection followed by G418 selection and allowed to recover to 100% confluency (referred to as CN-MSCs). Although MyoD expression was detected in CN-MSCs (Fig. 2J), the frequency of spontaneous cell fusion (the fusion index) was very low ["percentage nuclei incorporated in myotubes (*11*)" was <0.1%] in both rat and human CN-MSCs 5 days after cells reached 100% confluency. To confirm the potential of CN-MSCs to differentiate into multinucleated myotubes, we supplied cells with either 2% horse serum or ITS (insulin-transferrin-selenite) serum-free medium, both of which promote differentiation of myoblasts to myotubes (*11*, *12*). The fusion index was ~24% at 5 days after administration of 2% horse serum or 12% by ITS serum-free medium (Fig. 1A). A much higher production of differentiated myotubes was observed based on the appearance of a muscle phenotype that mainly arose from the spontaneous differentiation of original MSCs (*13*). Because horse serum is not appropriate for clinical usage, and cell survival and myotube formation were unsatisfactory in ITS serum-free medium, we searched for alternative conditions. We found that the supernatant of the original MSCs was also an effective inducer, with a fusion index of about 20% at 5 days after administration and plateauing at ~40% 14 days after induction (Fig. 1C). In the following experiments, we used MSC supernatants for the fusion induction and refer to CN-MSCs treated with supernatant of MSCs as M-MSCs (muscle-MSCs). Rat CN-MSCs and M-MSCs displayed the same features as human MSC-derived cells. Some multinucleated cells in both rat and human M-MSCs exhibited spontaneous contraction in vitro. Furthermore, these multinucleated cells expressed MyoD, myogenin (Fig. 2, A and B), skeletal myosin (Fig. 2F), myosin heavy chain (MHC) (Fig. 2, A, B, and D), and troponin (Fig. 2E), exhibiting skeletal myotube characteristics (*11*). The multinucleated cells appeared postmitotic as determined by p21 immunostaining (Fig. 2C, arrows) and 5-bromo-2′-deoxyuridine (BrdU) incorporation (Fig. 2D) (*12*). In addition to multinucleated cells and MyoD-positive mononucleated cells, cells immunopositive for Pax7 (Fig. 2F, arrows) and c-MetR (Fig. 2E, arrows), both markers for muscle satellite cells (*14*, *15*), were detected. These data suggest that M-MSCs consist of skeletal muscle lineage cells.

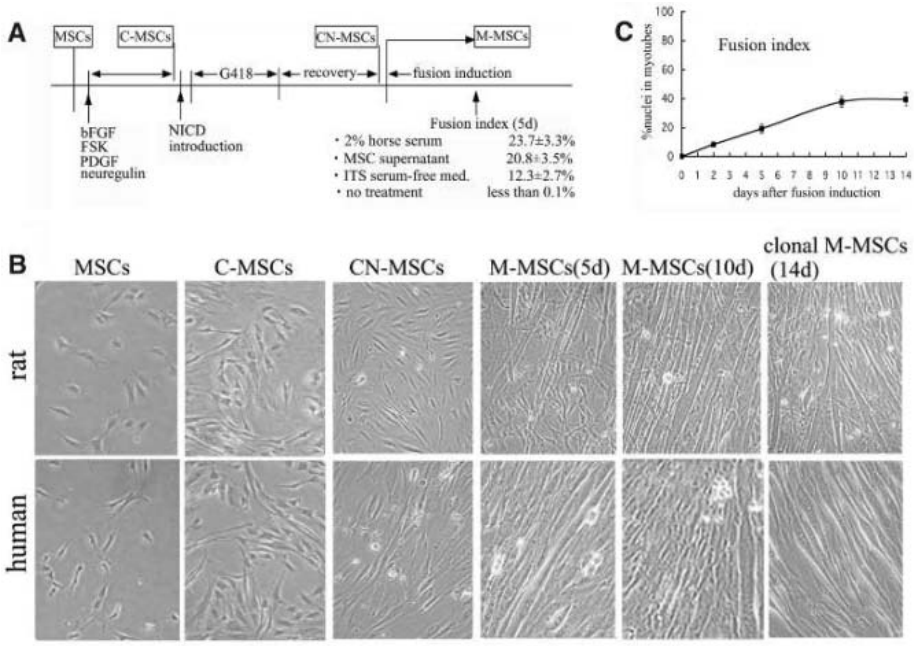

Fig. 1. Induction of skeletal muscle lineage cells. (**A**) Schematic diagram of the induction process. When human CN-MSCs reached 100% confluency, fusion induction was initiated. Fusion indexes were estimated after 5 days in human M-MSCs. For the cytokine treatment, omission of bFGF resulted in a major reduction of the fusion index in human M-MSCs (5 days; 0.5 ± 0.1%). Singular omission of Neuregulin, PDGF, or FSK singly resulted in fusion indexes of 1.8 ± 0.6%, 2.1 ± 0.4%, and 2.5 ± 0.7%, respectively. (**B**) Phase contrast microscopy of rat and human cells at each step and of clonal-M-MSCs (14 days). (**C**) Fusion indexes of human M-MSCs upon administration of human MSC supernatant.

Although most M-MSCs seemed to consist of skeletal muscle lineage cells, the possible existence of nonmuscle elements could not be neglected. We therefore subjected human and rat M-MSCs to single-cell clonal culturing (clonal-M-MSCs) and showed that ~89% of viable clones formed multinucleated cells at 14 days in vitro (Fig. 1B). Our results indicated that a large majority of proliferation-competent cells in M-MSCs possess myogenic potential. Clonal-M-MSCs were also shown to develop into MHC, skeletal myosin and MyoD-expressing multinucleated cells, MyoD-positive mononucleated cells, and Pax7-positive mononucleated cells as observed in their parental M-MSC population (Fig. 2, G and H). The ratios of MyoD-, myogenin-, and Pax7-positive cells to the total clonal-M-MSC cell number are shown in Fig. 2I.

To understand the induction events leading from MSCs to M-MSCs, we investigated the expression of genes related to myogenesis in these cells by means of reverse transcription–polymerase chain reaction (RT-PCR) (Fig. 2J). In MSCs, Pax3, Six1, and Six4 were detected, whereas Pax7, MyoD, and myogenin were not. In C-MSCs, Pax3 was down-regulated, whereas Pax7 expression was detected [(*10*), Note 2], which persisted in CN-MSCs and M-MSCs. Expression of MyoD and myogenin was found in CN-MSCs and M-MSCs. These results were confirmed by Western blot analyses (Fig. 2K). Myf6/MRF4, a marker for mature skeletal muscle (*16*), was detectable only in M-MSCs (Fig. 2J). Whereas expression of Six1 and Six4 persisted in M-MSCs, another myogenic factor, myf5, was not detected in any MSC-derived cells (Fig. 2J). This induction process mimicked some aspects of conventional skeletal muscle development in that Pax3, Pax7, MyoD, Myogenin, and Myf6/MRF4, all of which are related to muscle development (*11*, *12*, *14*, *16*), could be detected in a sequential manner. However, because the characteristics of MSCs used in this induction system are different from those of the conventional myogenic progenitor cells, it is possible that some of the mechanisms might differ, especially in the initial step in which MSCs are converted to MyoD-positive CN-MSCs. For this initial step, cytokine pre-

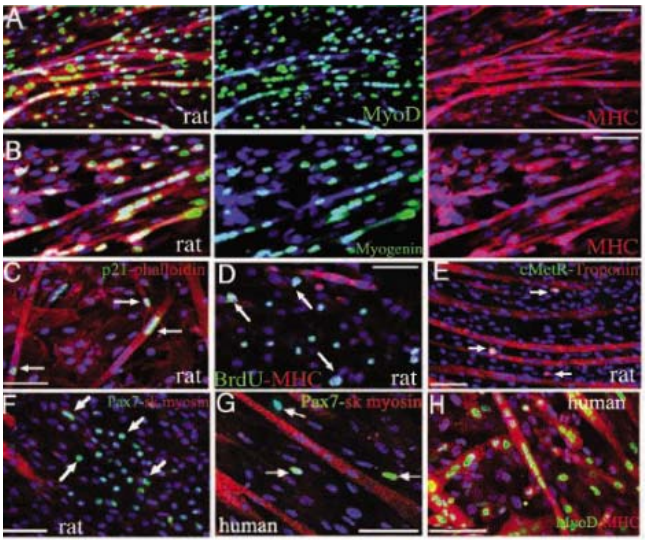

I	2 day	5 day
Pax7	17.9±1.7	3.3±0.8
MyoD	65.3±2.8	67.2±1.2
Myogenin	11.0±1.1	19.1±1.5

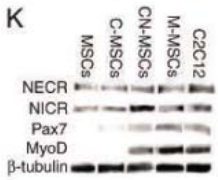

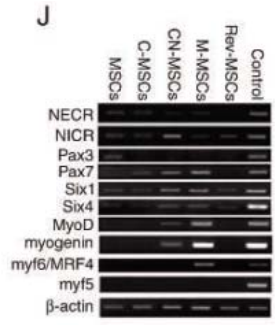

Fig. 2. Characterization of induced cells. (**A** to **H**) Immunocytochemical analysis of rat M-MSCs (10 days) (A to F) and human clonal-M-MSCs (14 days) (G and H). In (D), arrows indicate BrdU-incorporated mononucleated cells after 2 hours' incubation. Bars, 50 μm. (**I**) Ratios of Pax7-, MyoD-, and Myogenin-positive cells in rat clonal-M-MSCs. (**J**) RT-PCR and (**K**) Western blot of rat MSCs, C-MSCs, CN-MSCs and M-MSCs (5 days), and Rev-MSCs (5 days after fusion induction). In RT-PCR, the positive control (Control) is C2C12 cells, except for Pax3, which used ES cells. Notch extracellular region (NECR; corresponding to endogenous Notch) and intracellular region (NICR; corresponding to endogenous plus exogenous Notch) were detected in MSCs, suggesting that MSCs are endogenously expressing a small amount of Notch. After transfection with an NICD expression plasmid (CN-MSCs), NICR was up-regulated. The down-regulation of NECR in Rev-MSCs corresponds to the neuronal induction data in our previous report; when MSCs are first transfected with NICD, endogenous expression of Notch is down-regulated (*9*). β-tubulin was used as a loading control.

treatment and the subsequent NICD transfection are critical for MSC-derived cells to acquire competence for myogenic induction. Indeed, when we reversed the order of cytokine treatment and NICD transfection, muscle-lineage markers were not detected (Fig. 2J; Rev-MSCs), nor were multinucleated cells observed (*17*). The expression profiles of Notch and Hes genes during myogenic induction processes and effects of Notch/Hes signaling in the muscle induction system are described in (*10*), Note 3. Furthermore, we induced re-expression of NICD in CN-MSCs and estimated its effects on myogenic differentiation by analyzing the expression of MyoD and the fusion induction [(*10*), Note 3].

Bone marrow contains a small population of myogenic stem cells known to express c-Kit, CD45 and CD34 (*2*–*7*). However, the major population of MSCs is negative to these markers [(*10*), Note 1]. To exclude the possibility that the production of muscle-lineage cells was due to the vast proliferation of myogenic stem cells contained in MSCs, we isolated human MSCs negative for c-Kit, CD45, and CD34 by fluorescence-activated cell sorting (FACS) and subjected them to the induction process (Fig. 3A). We confirmed that isolated cells could also be driven to become muscle-lineage cells as efficiently as the unsorted MSCs. The data from rat MSCs were essentially identical to those from human MSCs. Thus, in our system, it appears that the major population of MSCs, rather than a small fraction of bone marrow–derived myogenic stem cells, contributes to the production of muscle lineage cells.

We next tested the differentiation of clonal-M-MSCs in vivo by transplantation into animals. Human clonal-M-MSCs were labeled by means of a green fluorescent protein (GFP)–encoding retrovirus and then transplanted by local injection (L.I.) into muscles or by intravenous injection (I.V.) into immunosuppressed rats whose gastrocnemius muscles were damaged with cardiotoxin pretreatment (*18*). Two weeks after transplantation, GFP-labeled clonal-M-MSCs incorporated into newly formed immature myofibers, and most of the GFP-positive myofibers exhibited centrally located nuclei in both L.I.- (*17*) and I.V.- (Fig. 3, B and D) treated animals. The incorporation ratios of human and rat GFP-positive cells at 2 weeks are indicated in (*10*), Note 4. Four weeks after transplantation, 60 to 70% of the GFP-positive myofibers exhibited mature characteristics with peripheral nuclei just beneath the plasma membrane (Fig. 3, E to G). Functional differentiation of grafted human clonal-M-MSCs was also confirmed by the detection of human dystrophin in GFP-labeled myofibers (Fig. 4A). In both L.I.- and I.V.-treated animals (4 weeks after injection), GFP-labeled human-derived cells were not detected in the host brain, heart, liver, kidney, and nondamaged muscles (*17*), suggesting that transplanted cells incorporate only into the damaged tissues. However, in the lung, a small number of rat and human GFP-positive cells were detected in the I.V.-treated animals (4 weeks), but not in the L.I.-treated animals. These findings indicate that clonal-M-MSCs are able to incorporate into damaged muscles and contribute to regenerating myofiber formation, regardless of the transplantation method.

In addition, some of the transplanted cells were observed between the plasma membrane and laminin-positive basal lamina that surround distinct myofibers (Fig. 3I). Because these cells expressed the satellite cell marker Pax7 (*14*) (Fig. 3H), they might be retained as satellite cells and/or developed into satellite cells in the host muscle. The ratios of transplanted Pax7/GFP-positive cells within total Pax7-positive satellite cells (transplanted and host satellite cells) are described in (*10*), Note 4. It is believed that muscle satellite cells contribute to regenerating myofiber formation upon muscle damage (*19*). We examined whether the transplanted satellite-like cells were able to function as satellite cells in vivo. Four weeks after transplantation of human clonal-M-MSCs (I.V.), cardiotoxin was readministered into the same muscles without additional transplantation just after the muscles were biopsied. The biopsies confirmed that 60 to 70% of GFP-positive myotubes displayed peripheral nuclei (Fig. 4A). Two weeks after the second cardiotoxin treatment (6 weeks after initial transplantation), we observed many regenerating GFP-positive myofibers with centrally located nuclei (Fig. 4B), and 16.5 ± 4.7% (mean ± SD; n = 4) of myofibers in the damaged area were GFP-positive. These results suggest that the Pax7-positive cells retained in the host muscle function as satellite cells, contributing to muscle repair. This implies that, upon transplantation of clonal-M-MSCs to muscles of patients, cells retained as satellite cells in clonal M-MSCs should be able to continue to contribute to future muscle regeneration. Similar characteristics were observed with rat clonal-M-MSCs (*17*).

Transplantation of muscle-lineage cells offers a potential therapeutic approach for the treatment of muscle degenerative disorders such as Duchenne muscular dystrophy. We therefore locally injected GFP-labeled human clonal-M-MSCs into cardiotoxin-pretreated

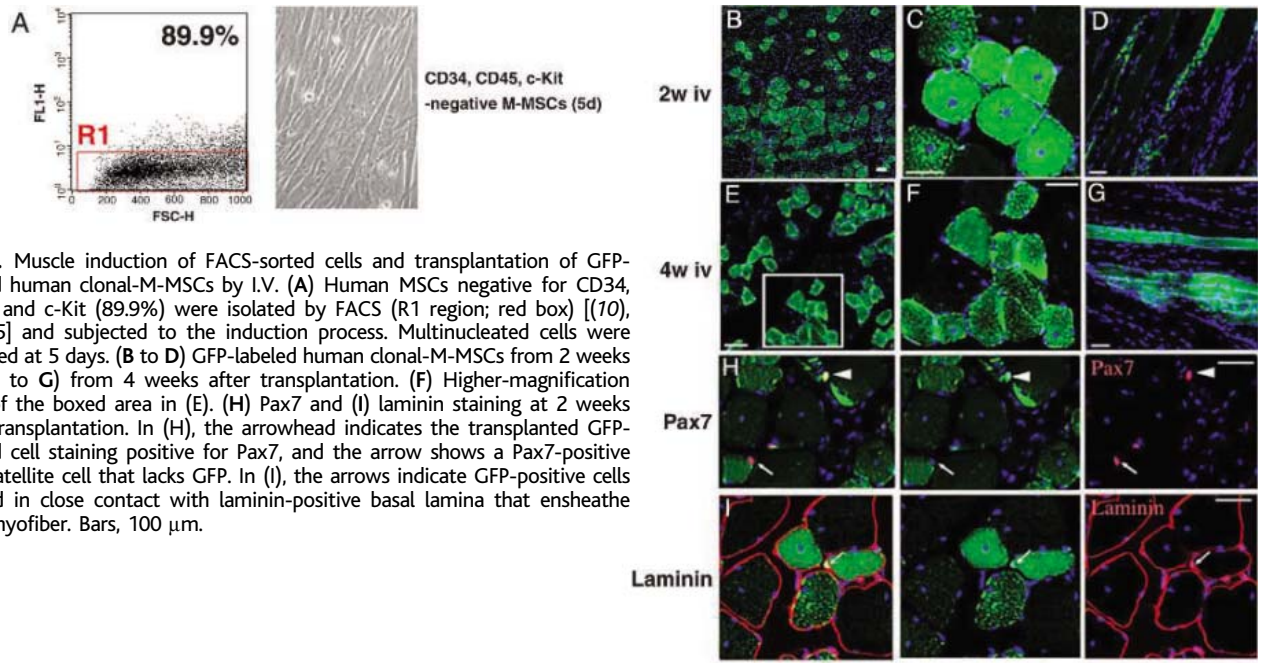

Fig. 3. Muscle induction of FACS-sorted cells and transplantation of GFP-labeled human clonal-M-MSCs by I.V. (**A**) Human MSCs negative for CD34, CD45, and c-Kit (89.9%) were isolated by FACS (R1 region; red box) [(*10*), Note 5] and subjected to the induction process. Multinucleated cells were observed at 5 days. (**B** to **D**) GFP-labeled human clonal-M-MSCs from 2 weeks and (**E** to **G**) from 4 weeks after transplantation. (**F**) Higher-magnification view of the boxed area in (E). (**H**) Pax7 and (**I**) laminin staining at 2 weeks after transplantation. In (H), the arrowhead indicates the transplanted GFP-labeled cell staining positive for Pax7, and the arrow shows a Pax7-positive host satellite cell that lacks GFP. In (I), the arrows indicate GFP-positive cells located in close contact with laminin-positive basal lamina that ensheathe each myofiber. Bars, 100 μm.

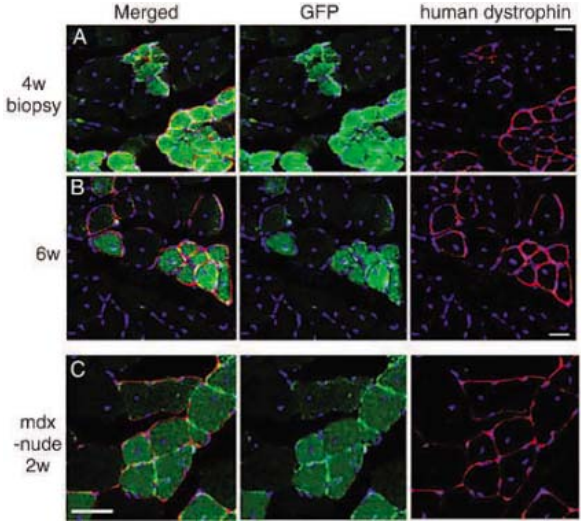

Fig. 4. Regeneration of human clonal-M-MSC transplanted rat (**A** and **B**) and mdx-nude mouse (**C**) gastrocnemius muscles after cardiotoxin treatment. (A) Specimen obtained from biopsy at 4 weeks by I.V. transplantation. Human dystrophin (red) is expressed by GFP-labeled transplanted cells. (B) After biopsy, cardiotoxin was administered and 2 weeks later (6 weeks after human clonal-M-MSC transplantation), gastrocnemius muscles were examined. Human dystrophin could be detected in GFP-labeled regenerating muscle fibers with centrally located nuclei. (C) Expression of human dystrophin in GFP-labeled cells in mdx-nude mouse gastrocnemius muscle after 2 weeks. Bars, 100 μm.

muscles of mdx-nude mice, which genetically lack dystrophin expression. Immunohistochemistry revealed the incorporation of transplanted cells into newly formed myofibers, which expressed human dystrophin 2 weeks after transplantation (Fig. 4C).

Compared to the various stem cell systems that have been reported (*1*, *20*–*22*), our MSCs offer several important advantages. First, MSCs can easily be obtained from patients or bone marrow banks and can be expanded efficiently in vitro. In the case of MSCs derived from inherited muscle dystrophy patients, genetic manipulation is possible after the isolation and expansion of MSCs. Second, transplantation of MSC-derived cells should encounter fewer ethical problems, because the use of these cells avoids the embryonic stem cell controversy and is in theory similar to bone marrow transplantation, which is currently in wide use for patients with leukemia, refractory anemia, etc. Third, autologous transplantation of MSC-derived muscle cells or transplantation of these cells with the same HLA (human leukocyte antigen) subtype from a healthy donor should minimize the risks of rejection. Because our induction system does not depend on a rare stem cell population, but can use the general population of adherent MSCs, which can be easily isolated and expanded, functional skeletal muscle cells can be obtained within a reasonable time on a therapeutic scale. At present, there are no effective therapeutic approaches for muscle dystrophy. Although the mechanism of muscle induction by NICD introduction remains to be clarified, we believe that our MSC differentiation system may contribute substantially to a major advance toward eventual cell-based therapies for muscle disease.

References and Notes

1. J. Rohwedel *et al.*, *Dev. Biol.* **164**, 87 (1994).
2. P. A. Dreyfus *et al.*, *Am. J. Pathol.* **164**, 773 (2004).
3. D. Suva *et al.*, *J. Cell. Physiol.* **198**, 110 (2004).
4. A. Polesskaya, P. Seale, M. A. Rudnicki, *Cell* **113**, 841 (2003).
5. Y. Torrente *et al.*, *J. Cell Biol.* **162**, 511 (2003).
6. A. Asakura, P. Seale, A. Girgis-Gabardo, M. A. Rudnicki, *J. Cell Biol.* **159**, 123 (2002).
7. J. R. Beauchamp *et al.*, *J. Cell Biol.* **151**, 1221 (2000).
8. G. Ferrari *et al.*, *Science* **279**, 1528 (1998).
9. M. Dezawa *et al.*, *J. Clin. Invest.* **113**, 1701 (2004).
10. Materials and methods are available as supporting material on *Science* Online.
11. N. Yoshida, S. Yoshida, K. Koishi, K. Masuda, Y. Nabeshima, *J. Cell Sci.* **111**, 769 (1998).
12. V. Andres, K. Walsh, *J. Cell Biol.* **132**, 657 (1996).
13. Y. Jiang *et al.*, *Nature* **418**, 41 (2002).
14. P. Seale *et al.*, *Cell* **102**, 777 (2000).
15. D. D. Cornelison, B. J. Wold, *Dev. Biol.* **191**, 270 (1997).
16. E. Bober *et al.*, *J. Cell Biol.* **113**, 1255 (1991).
17. M. Dezawa *et al.*, data not shown.
18. S. Fukada *et al.*, *J. Cell Sci.* **115**, 1285 (2002).
19. R. Bischoff, in *The Satellite Cell and Muscle Regeneration*, A. G. Engel, C. Franszini-Armstrong, Eds. (McGraw-Hill, New York, 1994), pp. 97–118.
20. M. A. LaBarge, H. M. Blau, *Cell* **111**, 589 (2002).
21. M. R. Wada, M. Inagawa-Ogashiwa, S. Shimizu, S. Yasumoto, N. Hashimoto, *Development* **129**, 2987 (2002).
22. Z. Qu, J. Huard, *Gene Ther.* **7**, 428 (2000).
23. We are grateful to N. Hashimoto and T. Partridge for providing the mdx-nude mice, R. Kageyama for pCI-neo Hes6, R. Yu and M. M. Taketo for critical reading of the manuscript, and M. Yoshida for technical assistance. This work was supported by Health and Labor Sciences Research Grants for "Research on Psychiatric and Neurological Diseases and Mental Health" and The Research Grant (16-B) for Nervous and Mental Disorders, both from the Ministry of Health, Labor and Welfare.

Supporting Online Material
www.sciencemag.org/cgi/content/full/309/5732/314/DC1
Materials and Methods
Figs. S1 to S7
Tables S1 and S2
References

28 January 2005; accepted 13 May 2005
10.1126/science.1110364

Comparative Genomic Hybridization

The microarray-based Comparative Genomic Hybridization (CGH) products and services are for the detection of DNA copy number changes on the whole-genome level or at ultra-high resolution using fine-tiling arrays for selected chromosomal regions. Array CGH is a widely used technique for cancer research and the identification of chromosomal abnormalities associated with congenital developmental disorders. A change in DNA copy number results when part or all of a chromosome is amplified or deleted. Cancer researchers use array CGH to identify sets of copy number changes associated with a particular cancer or its severity and to develop not only diagnostic tests but also new drug therapies. NimbleGen combines its high-capacity 385,000 probe microarrays with its long oligonucleotide probes designed with matched melting temperatures to produce high-resolution array CGH products. A novel isothermal probe selection strategy enables consistent detection of copy number changes in any non-repetitive region of the genome, thus affording researchers flexibility in their experiments and enabling detection of single- and multiple-copy changes.

NimbleGen Systems For information 608-218-7623 www.nimblegen.com

Immunoprecipitation System

Catch and Release v2.0 is faster, simpler, and more reproducible than traditional immunoprecipitation. The product contains a proprietary resin in a microfuge-compatible spin column, and enables recovery of denatured or non-denatured proteins to overcome many of the drawbacks of traditional bead-based immunoprecipitation. It has been successfully tested on both rabbit and mouse antibodies with a wide variety of lysate preparations from many different cell types.

Serologicals Corp For information 678-728-2018 www.serologicals.com

Cell Culture Media

Three formulas of BioWhittaker PowerCHO CD Cell Culture Media are now available to fill the increasing need for chemically defined Chinese hamster ovary (CHO) cell expression media. CHO cells are an important and popular vehicle for generating biologically active recombinant protein. Serum-free cell culture media that are chemically defined allow users to exert more control over cell culture conditions and avoid the use of animal-derived fetal bovine serum (FBS). Although FBS is routinely used in cell culture work, pressure is increasing to avoid its use due to its expense and potential regulatory liability in therapeutic applications. PowerCHO Media are chemically defined protein-free formulas that are optimized to support high-density growth with maximal protein expression in a CHO suspension culture. They contain only non-animal components.

Cambrex For information 800-638-8174 www.cambrex.com

Text Analysis and Data Visualization Software

A major upgrade has been released of RefViz, a text analysis and data visualization tool for the researcher's desktop. RefViz 2 works seamlessly with ResearchSoft bibliographic management software EndNote, ProCite, and Reference Manager, and is available for Mac OS X and Windows. Refviz 2 introduces Reference Retriever, a convenient interface for searching multiple data sources simultaneously. Reference Retriever identifies and retrieves relevant references from each data source, removes duplicates, and automatically creates data visualization. It eliminates the need to perform the same search on multiple data sources. RefViz provides researchers with a powerful way to explore reference collections visually for major themes and topics. An at-a-glace summary reveals trends and associations in the references, providing an additional level of analysis that allows researchers to find the most relevant citations for their papers.

Thomson ResearchSoft For information 760-438-5526 www.researchsoft.com

Centrifugal Concentrators

The miVac range of affordable centrifugal concentrators is designed to meet the requirements for careful and speedy drying in molecular biology applications. Special methods for drying aqueous and alcohol-based samples are included in all the miVac models. These concentrators range in capacity from six to 12 stacked shallow-well microplates or 64 to 200 microcentrifuge tubes of 1.5-ml size. They feature a full LCD display with digital controls and programming of time and temperature. A range of matching vacuum pumps is also available, including two-head and four-head diaphragm pumps and an ultra-low vacuum Scroll-type pump. These instruments will allow scientists working with DNA, RNA, peptides, oligonucleotides, and proteins to safely and swiftly concentrate or dry their samples.

Genevac For information +44-1473-240000 www.mivac.co.uk

For more information visit GetInfo, *Science*'s new online product index at *http://science.labvelocity.com*

From the pages of GetInfo, you can:
- Quickly find and request free information on products and services found in the pages of *Science*.
- Ask vendors to contact you with more information.
- Link directly to vendors' Web sites.

High Throughput Microarrays

The High Throughput microArray (HTA) products include a standard format slide (Slide1), a 12-well slide to simultaneously process 12 samples (Slide 12), and a specialized 96-well HTA Plate in 3 × 8 strip-well format with detachable wash collars to temporarily increase well volumes. HTA wells feature a 36 mm^2 printable surface area with low rim height (Z axis) for rapid spotting and sensitized scanning. With low-autofluorescence comparable to glass, HTA products are manufactured under stringent conditions to assure reproducibility. Polymer platforms are featured in three different surface chemistries for DNA, protein, and tissue immobilization.

Greiner Bio-One For information 800-884-4703 www.gbo.com/bioscience

Newly offered instrumentation, apparatus, and laboratory materials of interest to researchers in all disciplines in academic, industrial, and government organizations are featured in this space. Emphasis is given to purpose, chief characteristics, and availability of products and materials. Endorsement by *Science* or AAAS of any products or materials mentioned is not implied. Additional information may be obtained from the manufacturer or supplier by visiting www.science.labvelocity.com on the Web, where you can request that the information be sent to you by e-mail, fax, mail, or telephone.

POSITIONS OPEN

School of Medicine
TEMPLE UNIVERSITY

ANGIOGENESIS RESEARCHER

Temple University School of Medicine is currently seeking a Researcher (Ph.D. or M.D.) at the **ASSISTANT** or **ASSOCIATE PROFESSOR** level who is trained in cell or molecular biology (preferably with a history of grant funding) and whose research interests lie in the area of vascular biology as related to cancer and its treatment. Areas of interest would be factors which control proliferation of the vascular endothelium, specified markers for the vascular endothelium, the role of vascular endothelium in controlling tumor cell growth, and the use of kininogen derivatives as adjuncts to cancer therapy, etc.

DNA REPAIR RESEARCHER

We wish to recruit a Researcher (Ph.D. or M.D.) at the **ASSISTANT** or **ASSOCIATE PROFESSOR** level who is trained in cell/molecular biology or molecular pathology/genetics (preferably with a history of grant funding) and whose research interests lie in DNA repair/recombination genes that are involved in drug resistance, breast, and/or ovarian carcinogenesis, etc.

Please send curriculum vitae and bibliography to: **Henry Simpkins, M.D., Ph.D., Professor and Chairperson, Department of Pathology and Laboratory Medicine** or **Robert Coleman, M.D., Professor and Director, Sol Sherry Thrombosis Research Center, Temple University School of Medicine, 3401 North Broad Street, Philadelphia, PA 19140.** *Temple University is an Equal Opportunity/Affirmative Action Employer and strongly encourages applications from women and minorities.*

NEUROINFORMATICS POSTDOCTORAL POSITION
Yale University

The **POSTDOCTORAL FELLOW** will work as part of an interdisciplinary team on cutting-edge neuroinformatics projects as part of the national Human Brain Project, in a collaboration between the Yale Center for Medical Informatics and the Yale Department of Neurobiology. Candidates should have a Ph.D. in the neurosciences, biomedical informatics, computer science, or a related field, and significant computer programming experience. Projects focus on developing neuroscience databases and neuroinformatics tools, and on related neuroinformatics research. Please e-mail curriculum vitae, a statement of interests, and the names of three references to: **Perry Miller, M.D., Ph.D., Director, Center for Medical Informatics** at **e-mail: perry.miller@yale.edu (telephone: 203-737-2903; website: http://ycmi.med.yale.edu)** or to: **Gordon Shepherd, M.D., Ph.D., Department of Neurobiology** at **e-mail: gordon.shepherd@yale.edu (telephone: 203-785-4336; website: http://senselab.med.yale.edu/senselab/).** *Applications from women and members of minority groups are encouraged.*

BIO-ORGANIC CHEMISTRY POSTDOCTORAL: Looking for a highly motivated and creative individual with a strong background in peptide chemistry to join a multidisciplinary team within the National Science Foundation Industry/University Cooperative Research Center for biocatalysis and bioprocessing of macromolecules. The successful candidate will conduct research in enzyme-catalyzed routes to oligopeptides. She/he must have strong synthetic and characterization (nuclear magnetic resonance, liquid chromatography, mass spectrometry, MALDI) skills and a recent Ph.D. in bio-organic chemistry or related field. A competitive salary is offered commensurate with qualifications and experience. Send resume and copies of publications to:

Professor Richard A. Gross
Polytechnic University
Six Metrotech Center
Brooklyn, NY 11201
Website: http://chem.poly.edu/gross/

POSITIONS OPEN

DEPARTMENT OF RADIOLOGY
The University of Pennsylvania's School of Medicine

Seeks candidates for an **ASSISTANT PROFESSOR** position in the nontenure research track. Responsibilities include the development of an experimental research program in breast cancer in collaboration with breast cancer investigators at the University of Pennsylvania. Applicants must have a Ph.D. degree. Must also have at least two years of postdoctoral experience and/or experience as a faculty member and researcher. Expertise in the design, implementation, and validation of 1H nuclear magnetic resonance (NMR) pulse sequences for selective detection of lactate and choline in the presence of lipid is required. The successful candidate will lead an NMR spectroscopy program in breast cancer that will complement and interact closely with an ongoing world class breast cancer detection MRI program at this institution. Documentation of previous publication and funding in this field is desired. Please submit curriculum vitae and a letter of interest to:

Jerry Glickson, Ph.D., c/o Radiology Administration, University of Pennsylvania SoM, HUP, 3400 Spruce Street, 1 Silverstein, Philadelphia, PA 19104. Curricula vitae can be sent to **e-mail: glickson@mail.med.upenn.edu.**

The University of Pennsylvania is an Equal Opportunity/Affirmative Action Employer. Women and minority candidates are strongly encouraged to apply.

COORDINATOR
Chemistry and Biochemistry

The NUCLEUS Program is designed to provide science majors, including those from underrepresented groups, with a network of support that will foster academic success. The Coordinator will manage ongoing student services of the program including professional and peer mentoring, advisement, and tutoring. Bachelor's degree in a technical or scientific discipline required; graduate degree with training in scientific research preferred. At least three years experience in undergraduate support services or teaching is required. Skill in proposal writing desirable. Visit **website: http://www.udel.edu/udjobs** for more information. Send resume and names and contact information of three professional references to: **Susan Cheadle, Chemistry and Biochemistry, 105 Brown Laboratory, University of Delaware, Newark, DE 19716.** Review of applications will commence on July 11, 2005. This is a grant-funded position. *The University of Delaware is an Equal Opportunity Employer that encourages applications from Minority Group Members and Women.*

POSTDOCTORAL POSITION

A Postdoctoral position is immediately available at Texas Tech University to study adenosine triphosphate synthase, the world's smallest rotary motor, utilizing a variety of biochemical, biophysical, and molecular-biological techniques. Ph.D. is required; experience in biochemistry and/or biophysics is highly desirable. Position is NIH-funded; salary is competitive and commensurate with experience. Applicants should send curriculum vitae and the names and addresses of three references to: **Dr. Joachim Weber, Texas Tech University, Department of Chemistry and Biochemistry, Box 41061, Lubbock, TX 79409-1061** or by **e-mail: joachim.weber@ttuhsc.edu.**

SENIOR SCIENTIST, FOREST BIODIVERSITY
The International Plant Genetic Resources Institute

This position is based at The International Plant Genetic Resources Institute's (IPGRI) headquarters near Rome, Italy. The closing date for applications is 29 July 2005 or until the vacancy is filled.

Please consult the IPGRI website for a detailed job description, conditions of service, and application details at **website: http://www.ipgri.cgiar.org.**

Positions @ NIH
THE NATIONAL INSTITUTES OF HEALTH

NATIONAL INSTITUTE OF ALLERGY AND INFECTIOUS DISEASES
POSTDOCTORAL POSITIONS

The Laboratory of Viral Diseases invites applications for postdoctoral fellows to join research groups involved in basic studies on herpesviruses, papillomaviruses, and flaviviruses. The seven re search laboratories within the Laboratory of Viral Diseases focus on mechanisms involved in viral entry, gene expression, viral replication, and pathogenesis using diverse viral systems. Successful applicants will be part of the integrated LVD research community and have access to state of the art facilities. Currently positions are available in the following sections:

Molecular Genetics Section
The MGS focuses on addressing the molecular mechanisms of herpes simplex virus gene expression. The emphasis of the research group is on cellular activators and coactivators involved in viral immediate early gene expression during the lytic replication cycle and during viral reactivation from latency. **(Thomas Kristie, email: tkristie@nih.gov)**

DNA Tumor Virus Section
The DNA TVS focuses on the study of papillomavirus transcription and replication. Particular emphasis is on the molecular mechanisms by which papillomaviruses maintain and segregate their episomal genomes by tethering them to mitotic chromosomes. **(Alison McBride, email: amcbride@nih.gov)**

Viral Pathogenesis Section
The VPS is focused on characterizing the humoral immune response to flavivirus infection and vaccination, with an emphasis on West Nile and dengue viruses. Using a variety of biochemical and genetic approaches, our group is investigating the mechanisms and circumstances that contribute to determining the fate of flaviviruses once bound by antibody.
(Ted C. Pierson, email: piersontc@niaid.nih.gov)

Applicants should have a PhD and less than 5 years of postdoctoral experience. Interested applicants must submit a CV, a statement of research interests, and the names of three references by electronic mail directly to the indicated Senior Investigator.

STAFF CLINICIAN POSITION IN DIABETES

The Diabetes Unit in the Laboratory of Clinical Investigation at the National Center for Complementary and Alternative Medicine (NCCAM), National Institutes of Health (NIH) is seeking a staff clinician to conduct patient-oriented research in the intramural program at the Clinical Center of NIH. Applicants must possess an M.D. or D.O. degree, have a current U.S. medical license, be board certified in Internal Medicine, and board certified/eligible in Endocrinology and Metabolism. Prior experience in clinical research and a strong publication record are essential. The successful applicant will write clinical research protocols and conduct patient-oriented research exploring metabolic and vascular physiology and outcomes relevant to elucidating the mechanisms of action, safety, and potential efficacy of complementary and alternative medicine approaches for the treatment of diabetes, obesity, and cardiovascular diseases. Experience with glucose clamps and in vivo endothelial function studies is advantageous. Salary and benefits will be commensurate with experience.

NCCAM provides state-of-the-art research facilities in the intramural program at NIH in addition to a collegial and nurturing working environment. By **September 15**, please forward your CV, bibliography, list of three references, and a cover letter summarizing your scientific interests and experience to: **Michael J. Quon, M.D., Ph.D. Chief, Diabetes Unit, LCI, NCCAM, National Institutes of Health, Building 10, Room 6C-205, 10 Center Drive MSC 1632, Bethesda, Maryland 20892-1632, Fax (301) 402-1679, Email: quonm@nih.gov**

Section Of Brain Electrophysiology And Imaging
Full-time Neuroimaging Research Position For Physicians

The National Institute of Alcohol Abuse and Alcoholism (NIAAA), a major research component of the National Institutes of Health (NIH) and the Department of Health and Human Services (DHHS), offers a full-time research position for a senior physician at one of the premier research sites in the United States: the 300-acre Bethesda campus of the NIH, near Washington D.C. which houses state-of-the-art neuroimaging facilities (MRI, MRS and PET) dedicated to research as well as a twelve bed clinical alcoholism research unit and out patient program. The strong scientific environment and outstanding equipment resources at NIH make this a unique opportunity for an outstanding scientist/physician. The position is open to MDs trained in psychiatry, child psychiatry, neurology or other relevant fields. Senior physicians are hired at the Staff Clinician level. The successful candidate will be part of a multidisciplinary team using neuroimaging to understand the neural basis of motivation and affect particularly as it relates to alcoholism. The laboratory has a strong interest in using neuroimaging to understand brain development through adolescence and early adulthood and is part of a larger clinical research program focused on medications development. In addition to collaborative work within the team, there is opportunity for outstanding candidates to develop their own projects. Competitive stipends depend on level of experience.

For consideration, send letter of interest outlining experience and research goals, CV, and the names and addresses of six individuals who may be contacted for recommendation letters to: **Cathy Little, Administrative Laboratory Manager, LCTS, DICBR, NIAAA, NIH, Building 10-Hatfield CRC, Room 2-2352 NE; 9000 Rockville Pike, Bethesda MD 20892-1540 USA, or email clittle@niaaa.nih.gov. Applications will be accepted until August 18, 2005.**

WWW.NIH.GOV

NATIONAL INSTITUTE OF ALLERGY AND INFECTIOUS DISEASES
TENURE/TENURE TRACK POSITION

With nation-wide responsibility for improving the health and well being of all Americans, the Department of Health and Human Services oversees the biomedical research programs of the National Institutes of Health (NIH) and those of NIH's research Institutes.

The National Institute of Allergy and Infectious Diseases (NIAID), a major research component of the NIH and the Department of Health and Human Services, is recruiting for a Tenure/Tenure Track position in the Laboratory of Host Defenses (LHD). The LHD studies immune functions essential for host defense against infection (inherited immune deficiencies) and those required for immune homeostasis (autoimmunity associated with excessive inflammation). The LHD seeks an M.D. or M.D., Ph.D. physician scientist to develop an independent translational research program related to the genetic basis, pathophysiology, diagnosis and treatment of inherited abnormalities of immunity and/or of autoimmune diseases associated with excessive inflammation. An emphasis on clinical aspects of innate immunity including phagocytic cells, natural killer cells, dendritic cells, toll-like receptors or other pattern recognition receptors is desirable, though clinically related studies of the interface of innate and acquired immunity is also acceptable. The applicant should have a strong track record of basic research of the genetic basis of disease and alterations in signaling pathways responsible for inherited immune dysfunction. The applicant must possess expertise and experience in the design and conduct of diagnostic and therapeutic clinical trials studying and treating such diseases. Strong clinical credentials in a specialty area relevant to the proposed translational research program (relevant specialties include but are not limited to infectious disease, allergy-immunology, rheumatology, pulmonary diseases, or hematology) are required. The program of study proposed by the applicant must include both laboratory components and the conduct of clinical protocols to assess new diagnostic and therapeutic modalities to diagnose and treat inherited diseases associated with immune deficiency and/or autoimmunity associated with excessive inflammation. Applicants particularly suitable for this program are those who have knowledge and experience in the development and clinical application of novel cellular therapies or gene therapy, cytokines, monoclonal antibodies or other novel biologic agents to correct defects in immunity, to achieve immune tolerance or to reduce abnormal inflammation.

The applicant must provide evidence in the submitted materials that the applicant has a current license to practice medicine in one of the states of the United States or must have the all the credentials required by the State of Maryland for licensing to allow the practice of medicine. These credentials must include but are not limited to having a Doctor of Medicine or Doctor of Osteopathy degree from an accredited school in the U.S. or Canada, or a Doctor of Medicine or equivalent degree from a foreign medical school that provided education and medical knowledge substantially equivalent to accredited schools in the U.S. as demonstrated by permanent certification by the Educational Commission for Foreign Medical Graduates (ECFMG).

To be considered for this position, you will need to submit a curriculum vitae, bibliography, 3 letters of reference, a detailed statement of research interests, and a hardcopy of selected publications to **Thomas A. Fleisher, MD, Chairperson, NIAID Search Committee, c/o Mrs. Lynn Novelli, DIR Committee Coordinator, 10 Center Drive MSC 1356, Building 10, Rm. 4A-26, Bethesda, Maryland 20892-1356.** Completed applications **MUST be received by Friday, August 19, 2005.** For additional information on this position, and for instructions on submitting your application, please see our website at: **www.niaid.nih.gov.**

Tenure-Track Investigator
Membrane Protein Biochemistry

The Intramural Research Program at NINDS invites applications to fill a faculty position at the level of tenure-track investigator in the area of eukaryotic membrane protein biochemistry and structure. We seek a creative, interactive scientist to establish an independent research program focused on mechanistic and structural investigations of eukaryotic membrane proteins, with a particular emphasis on solving problems associated with the high level production, purification and stability of eukaryotic membrane proteins. Candidates working on G-protein coupled receptors are particularly encouraged to apply. A PhD and at least four years postdoctoral experience are required. The position includes salary, a competitive start-up package, as well as an annual operating budget to support the research program. Laboratory space will be provided in the 5625 Fishers Lane research facility in Rockville, MD, which is located several miles from the main NIH campus in Bethesda, MD. Applicants should send curriculum vitae including bibliography, statement of research interests and the names of three references to: **Story Landis, PhD, Director, NINDS, NIH, c/o Peggy Rollins, Building 35, Room GA908, 35 Convent Drive, MSC-3716, Bethesda, MD 20892-3716. Applications must be postmarked by August 31, 2005.**

Postdoctoral Training Positions
Translational Cancer Genomics

The Oncogenomics Section, at the National Cancer Institute, NIH, has two post-doctoral training positions available in translational genomics. Ongoing research efforts involve genomic and proteomic approaches to the investigation of Neuroblastoma. Using these approaches we have identified prognostic markers and potential new therapeutic targets in cancers. The candidate will work on combining molecular and genomic approaches to validate these targets both in vitro and animal models to bring these reagents to the clinic. The candidate should hold either a Ph.D. or M.D. degree and have an interest in oncology and significant experience in genomics and the microarray technology. Experience in mouse/animal models is preferred. Candidates should have less than five years post-doctoral experience.

Correspondence, names of references and CV should be sent to **Dr. Javed Khan, Advanced Technology Center, National Cancer Institute, Room 225B, 8717 Grovemont Circle, Gaithersburg, MD 20877, or via email at khanjav@mail.nih.gov**

UNIVERSITÄT BASEL

Zoological Institute of the University of Basel

invites applications for a

Assistant Professorship Tenure-Track in Zoology/Evolutionary biology

The Zoological Institute provides a collaborative research environment with strength in integrative biology. The successful candidate will perform independent research in the area of biology of animals within the framework of evolution and participate in the zoology teaching program. She/He will develop strong links within the department of environmental sciences and with the emerging foci of system biology and biology of infection at the University of Basel. Candidates must hold a PhD degree and have a substantial postdoctoral experience. A strong commitment to excellence in teaching and research is essential. The position includes an attractive package with full salary, assistant positions and a running budget. The appointment will be made at the level of an assistant professor tenure-track. As the University of Basel would like to increase its female staff, women are strongly encouraged to apply.

Applicants should send a curriculum vitae, copies of 3 selected publications, a brief description of past and proposed research, a statement about teaching philosophy, and the names of 3 potential referees by 15 August 2005, to:
Prof. Dr. Hans-Jakob Wirz
Dekan der Philosophisch-Naturwissenschaftlichen Fakultät der Universität Basel
Klingelbergstrasse 50, CH-4056 Basel, Switzerland.

For further information, please visit: http://www.unibas.ch/ or
http://www.zoo.unibas.ch/ or contact Prof. Dr. Dieter Ebert, Zoologisches Institut der Universität Basel, Vesalgasse 1, CH-4051 Basel, Switzerland (Tel: ++61 267 03 60; E-mail: Dieter.Ebert@unibas.ch).

UNI
BASEL

THE CLEVELAND CLINIC FOUNDATION
LERNER RESEARCH INSTITUTE

FACULTY POSITIONS
IN DEPARTMENT OF CELL BIOLOGY
Diabetes, Obesity, Metabolic Syndrome

The Department (**www.lerner.ccf.org/cellbio/**) is undergoing substantial expansion and will be hiring several new faculty at all ranks. Particular focus for this round of recruitment will be research broadly related to the cell biology of diabetes, obesity, or metabolic syndrome, including islet cell transplantation. Applicants with M.D., Ph.D. or dual degrees will be considered, with co-appointment to appropriate clinical departments available. Applicants must have strong potential to develop an active, independent research program. Outstanding facilities, generous start-up funds, and ongoing operational support are available. The Department's 19 primary faculty members lead strong programs in signaling, cell adhesion and growth regulation, apoptosis, intracellular trafficking, vascular biology, oxidative stress, regulation of gene expression, and regulation of mRNA translation and splicing. There is a strong tradition of collaborative research and well-developed training programs for both postdoctoral fellows and Ph.D. students. Interactions with outstanding clinical programs, including diabetes, bariatric surgery, cardiovascular medicine, and regenerative medicine are readily available, and all faculty are members of the Cell Biology Graduate Training Program at Case Western Reserve University School of Medicine.

Candidates should submit complete curriculum vitae, list of publications, brief statement of research interests, and three letters of reference to: **Roy L. Silverstein, M.D., Chairman, Department of Cell Biology, Lerner Research Institute, The Cleveland Clinic Foundation [NC10], 9500 Euclid Ave, Cleveland, OH 44195.** For specific questions contact **Ms. Teri Schantz 216-444-5221**, **schantt@ccf.org**.

The Cleveland Clinic Foundation is an Equal Opportunity/ Affirmative Action Employer.

Virology Faculty Position
Department of Microbiology and Molecular Genetics
Michigan State University

The Department of Microbiology and Molecular Genetics, Michigan State University, seeks applications for an academic-year, **tenure-track assistant or associate professor position in molecular virology**. Areas of interest include virus replication strategies, mechanisms of pathogenesis, host responses to infection, molecular evolution, tumor virology and zoonotic diseases. A doctoral degree (PhD, DVM or MD) and a minimum of two years of postdoctoral research experience are required.

The successful candidate will join a department with strong basic research programs in microbial biology and pathogenesis, eukaryotic cell biology and molecular genetics. He or she will be expected to establish an extramurally funded research program, mentor graduate students, and interact collaboratively with other faculty in the department and university. State of the art research space is available, including BSL-2 and BSL-3 labs. The department is jointly administered by the Colleges of Veterinary Medicine, Human Medicine, Osteopathic Medicine and Natural Science, and the Michigan Agricultural Experiment Station. This position will be affiliated with the College of Veterinary Medicine and the Michigan Agricultural Experiment Station. Further information on the department is available at **www.mmg.msu.edu**.

Salary will be commensurate with experience. Applicants should submit a letter of application, curriculum vitae, statement of research goals, copies of pertinent reprints and contact information (address, e-mail and phone) for three referees to: **Dr. Susan Conrad, Virology Search Committee Chairperson, Department of Microbiology and Molecular Genetics, 2209 Biomedical Physical Sciences, Michigan State University, East Lansing, MI 48824-4320; Fax: (517) 353-8957; Tel: (517) 353-5161; Email: mmgchair@msu.edu.** Applications may also be submitted electronically. For full consideration, applications should be received by August 31, 2005, but will be accepted until the position is filled.

Michigan State University is an Affirmative Action/Equal Opportunity Employer. Women and minority candidates are particularly encouraged to apply.

DIRECTOR, CENTER FOR BIOINFORMATICS AND COMPUTATIONAL BIOLOGY

National Institute of General Medical Sciences (NIGMS)
National Institutes of Health (NIH)
Department of Health and Human Services (DHHS)

The Challenge: A significant challenge for the biomedical research community is the integration of the vast amount of accumulating scientific data in order to develop predictive understanding of basic biological processes. The ability to meet this challenge will be critically dependent on advances in bioinformatics and computational biology. To this end, in 2001, NIGMS established a Center that is responsible for stimulating and funding research in areas of importance for NIGMS. The Center supports research on bioinformatics, databases, and data mining; on modeling of complex biological systems; on algorithmic development and software engineering; and on mathematical biology, among other areas. In addition, the Center is responsible for managing the NIH Biomedical Information Science and Technology Initiative (BISTI), an agency-wide effort to stimulate and coordinate use of computer science and technology to address problems in biology and medicine. Finally, the Center plays a major role in coordinating and directing the Bioinformatics and Computational Biology component of the NIH Roadmap for Medical Research. **The institute is seeking a leader in this field to direct the Center and the BISTI efforts, and to coordinate the work of both with other interested federal agencies and the broader scientific community.** Information about the Center and BISTI is available at: **http://www.nigms.nih.gov/about_nigms/cbcb.html**.

Position Requirements: Candidates must have an M.D., Ph.D. or equivalent degree in a field relevant to the position. The ideal candidate will have considerable research experience demonstrating a strong understanding of both computation and biological issues. In addition, candidates should possess recognized research management and leadership abilities. The position will be filled under Title 42, offering a competitive salary commensurate with qualifications and experience, within the range of $125,304 to $175,700. A recruitment or relocation bonus may be available. Relocation expenses will be paid. An intramural research program is possible, subject to negotiation.

How to Apply: The official vacancy announcement is available at: **http://www.nigms.nih.gov/about/job_vacancies.html**. To be considered for this position, send to the address below a CV, bibliography, the names and contact information of 4 references, and **a "vision statement," not to exceed 3 pages, that presents your views of the most significant challenges and opportunities in bioinformatics and computational biology relevant to NIGMS that you would seek to address should you be selected for this position.**

nigmsjobs@mail.nih.gov or FAX to **301-451-5686**
Applications must be received by midnight on the closing date: **Thursday, August 4, 2005**

You may contact **Stephanie Klingenberg**, Human Resources Specialist, with questions about this vacancy on **301-594-2233**.

DHHS, NIH, and NIGMS are Equal Opportunity Employers.

Virginia Tech

The **Department of Biomedical Sciences and Pathobiology, Virginia-Maryland Regional College of Veterinary Medicine** (**http://www.vetmed.vt.edu/Organization/Departments/DBSP/index.asp**) invites applications for **three tenure track faculty openings** in the area of **Viral Pathogenesis** as part of an interdisciplinary program focused on emerging and re-emerging infectious diseases. Areas of particular interest include, but are not limited to, molecular mechanisms of pathogenesis for viral diseases of public health concerns and zoonotic viral diseases, and animal models for human viral diseases.

Appointees will be expected to establish and maintain internationally recognized, extramurally funded research programs, to collaborate amongst themselves and/or with existing faculty members on campus, and to participate in graduate and professional student (DVM) education. Rank is open. Candidates for Assistant Professor with a good publication record and funding history during their postdoctoral training are strongly encouraged to apply. Associate/Full Professor candidates must be nationally or internationally recognized virologists with sustained extramurally funding records and strong publication records. Generous start-up packages will be provided. The appointees will be housed in the college's Center for Molecular Medicine and Infectious Disease (CMMID; **http://www.vetmed.vt.edu/Organization/Centers/CMMID/index.htm**) on campus.

Core lab facilities covering DNA sequencing, microarrays, and proteomics are available through the Virginia Bioinformatics Institute on campus (**http://www.vbi.vt.edu**). Also, the Institute of Biomedical and Public Health Sciences has sustainable resources available to support infectious disease research (**http://www.ibphs.vt.edu**).

Applications must be submitted using the Virginia Tech website at **https://jobs.vt.edu**. Use the search engine to select posting number **042512**. Fill out the application form, and upload supporting documents including a cover letter, curriculum vitae, statement of research goals, and names and contact information for 3 references. The statement of research goals should include an explanation of how collaborative research fits in with your overall career goals. Further position information is also available at this site.

Individuals with disabilities desiring accommodation in the application process or those with inquiries about the positions should contact **Dr. Stephen Boyle; Chair, Virology Search Committee; Department of Biomedical Sciences and Pathobiology; 1410 Prices Fork Road, Virginia Tech, Blacksburg, VA 24061; smboyle@vt.edu; 540-231-4641**.

Virginia Tech is an Equal Opportunity/Affirmative Action Employer.

FELLOWSHIPS

CLIFFORD G. SHULL
Fellowship Program

The Clifford G. Shull Fellowship Program is aimed at attracting new scientific talent to the Oak Ridge National Laboratory (ORNL) and its neutron science programs, making it possible for these outstanding new scientists to continue on the path to excellence while substantially contributing to ORNL and U.S. Department of Energy missions and goals. The Shull Fellowship is open to fields of science and engineering that further advances in neutron science. Shull Fellows are expected to provide valuable stimuli to the research efforts of the Laboratory, make available the most recent developments of university science and engineering departments, and represent the Laboratory to its sponsors and collaborators in the scientific community.

The Shull Fellowship Program is directed to recent doctoral degree recipients of exceptional ability who show clear and definite promise of becoming outstanding leaders in scientific research and development. The Program will provide them with the opportunity to:

- Develop neutron science programs in areas of national importance
- Pursue research programs within their areas of interest and expertise
- Collaborate with Laboratory R&D staff and distinguished scientists
- Have access to Laboratory expertise, facilities, and programs

Shull Fellows carry out and develop research programs to enhance the knowledge of the structure or dynamical behavior of advanced materials using neutron scattering as a primary tool; work with scientists in ORNL and other research institutions on collaborative research programs using neutron scattering experiments; educate and promote the use of neutron scattering to new user communities; publish research results in scientific journals; and assist Spallation Neutron Source and High Flux Isotope Reactor instrument scientists and design teams in the development of new instrumentation to meet research program goals.

Each applicant must be the recipient of an earned doctorate and must be no more than three years beyond the doctorate. Applicants should not have previously served more than one postdoctoral appointment. Current ORNL postdoctoral appointees and staff members cannot be considered as valid applicants. A Ph.D. in materials science, materials engineering, chemistry, physics, biology or a related field is required. Candidates with expertise in nano materials are particularly welcome, and those with strong processing or characterization skills are also encouraged to apply. Previous experience in neutron or X-ray scattering techniques is a plus. Strong written and oral communication skills and the desire to work in a team environment on scientifically challenging problems are required.

ORNL is an equal opportunity employer and is committed to workforce diversity; women and minorities are strongly encouraged to apply. Applicants need not be U.S. citizens.

For more information and to apply online: **www.sns.gov/shullfellowship**. Applications will be accepted until August 1, 2005.

SNS
SPALLATION NEUTRON SOURCE

Ludwig Maximilians Universität München

LMU

The **Gene Center and** the **Department of Chemistry and Biochemistry of the Ludwig-Maximilians-University of Munich (LMU**) invites applications for a

Tenure-track Professor (W2) of Biochemistry

The position is initially for 5 years but can be converted to tenure after a positive evaluation.

Candidates must have an outstanding record of internationally recognized research accomplishments in Organismic Biochemistry, ideally with an emphasis on the molecular mechanisms of cell differentiation and development. Possible model organisms include C. elegans, Drosophila, or mouse.

Candidates are expected to conduct an independent research program that complements existing research efforts, to obtain extramural funding, and to participate in the innovative teaching program of the Center (lectures may be given in English). Primary selection criteria are research excellence, teaching ability and potential for scientific interactions. The Gene Center offers a stimulating and interdisciplinary research environment, and is committed to expand the research focus in the above area.

Applicants should submit a curriculum vitae (with list of publications, invited lectures, teaching experience), a research summary, a concise research proposal for the next five years, and the three most relevant publications to: **Dekan der Fakultaet für Chemie und Pharmazie, Prof. Dr. F. Bracher, Ludwig-Maximilians-Universitaet, Butenandtstr. 5-13, Haus F, 81377 Muenchen, Germany**.

The Ludwig-Maximilians-University of Munich seeks to increase the proportion of women. Disabled candidates will be preferred if they are equally qualified. The candidate must be less than 52 years old at the starting date of the contract. Exceptions are possible (Art. 12. Abs. 3 Satz 2 BayHSchlLG).

Deadline for applications is **August 31, 2005**.

Bergen Center for Computational Science
COMPUTATIONAL BIOLOGY UNIT

University of Bergen

GROUP LEADER – BIOINFORMATICS

The Computational Biology Unit (CBU) at the University of Bergen, Norway, is seeking an experienced and competent bioinformatics scientist to lead a new research group. The bioinformatics environment in Bergen currently consists of seven research groups and about 40 staff and students. Salary and professional resources are internationally competitive.

For more information about the position and about CBU, please refer to **http://www.cbu.uib.no/jobs/**, or contact the head of CBU, professor Inge Jonassen (Inge.Jonassen@bccs.uib.no).

Evaluation of applications commences September 1st 2005.

香港浸會大學
HONG KONG BAPTIST UNIVERSITY

SCHOOL OF CHINESE MEDICINE

Full-time Chinese Medicine Programme Unit

Professor/Associate Professor/Assistant Professor (PR005/05-06)

Founded in 1999, the School of Chinese Medicine is a young and fast-growing School among the seven Faculties/Schools of the Hong Kong Baptist University. It now has a number of vacancies for positions at the Professor, Associate Professor and Assistant Professor levels. The appointees are expected to conduct teaching and research as well as provide academic leadership in their respective fields. One of the successful appointees may have to oversee the operation of the Full-time Programme Unit of the School.

Applicants must have a doctoral degree (PhD and/or MD) in a relevant discipline with teaching and research experience in Chinese Medicine, Biomedical Science, Chinese Pharmacy/Pharmacology or related fields. Proficiency in both English and Putonghua is a must.

Starting salary will be commensurate with qualifications and experience.

Application Procedure:
Applicants are invited to write in response to the requirements and fill in the application forms which are obtainable from [http://www.hkbu.edu.hk/~pers]. Application, together with copies of transcripts/testimonials should be sent to the Personnel Office, Hong Kong Baptist University, Kowloon Tong, Hong Kong [Fax: (852) 3411-5001; E-mail: recruit@hkbu.edu.hk]. Applicants are requested to send in three samples of their most recent publications and request two referees to send in confidential letters of reference to the Personnel Office direct. Please quote **PR** number on the application, confidential reference letters and any subsequent correspondence. Details of the University's Personal Information Collection Statement can be found at [http://www.hkbu.edu.hk/~pers/job].

The University reserves the right not to make an appointment for the post advertised, and the appointment will be made according to the terms & conditions then applicable at the time of offer.

Closing Date: 13 August 2005

Science
AAAS

Life Science Editor for *Science*

Join the dynamic team at *Science* as a full time associate editor for the biological sciences in our Washington, DC, USA or Cambridge, UK office. We are looking for a life scientist with broad interests, a lively curiosity, and experience in cutting-edge research in one or more of the following fields: evolutionary genomics, evo-devo, microbial ecology, biological chemistry, systems biology, bioinformatics, computational or quantitative biology, and neuroscience. Responsibilities include managing the review, selection, and editing of manuscripts, soliciting reviews and special issues, and fostering contacts and communication with the scientific community. Editors are expected to travel to scientific meetings. A Ph.D., postdoctoral experience, and multiple publications are required. Previous editorial experience is not necessary.

For consideration, send a resume and cover letter, along with salary requirements, to:

AAAS
Human Resources Department
Suite #101
1200 New York Avenue
Washington, DC 20005

Applications can also be sent by e-mail to **hrtemp@aaas.org** or Fax to **202-682-1630**. Visit us at: **www.aaas.org**.

Nonsmoking work environment. EOE.

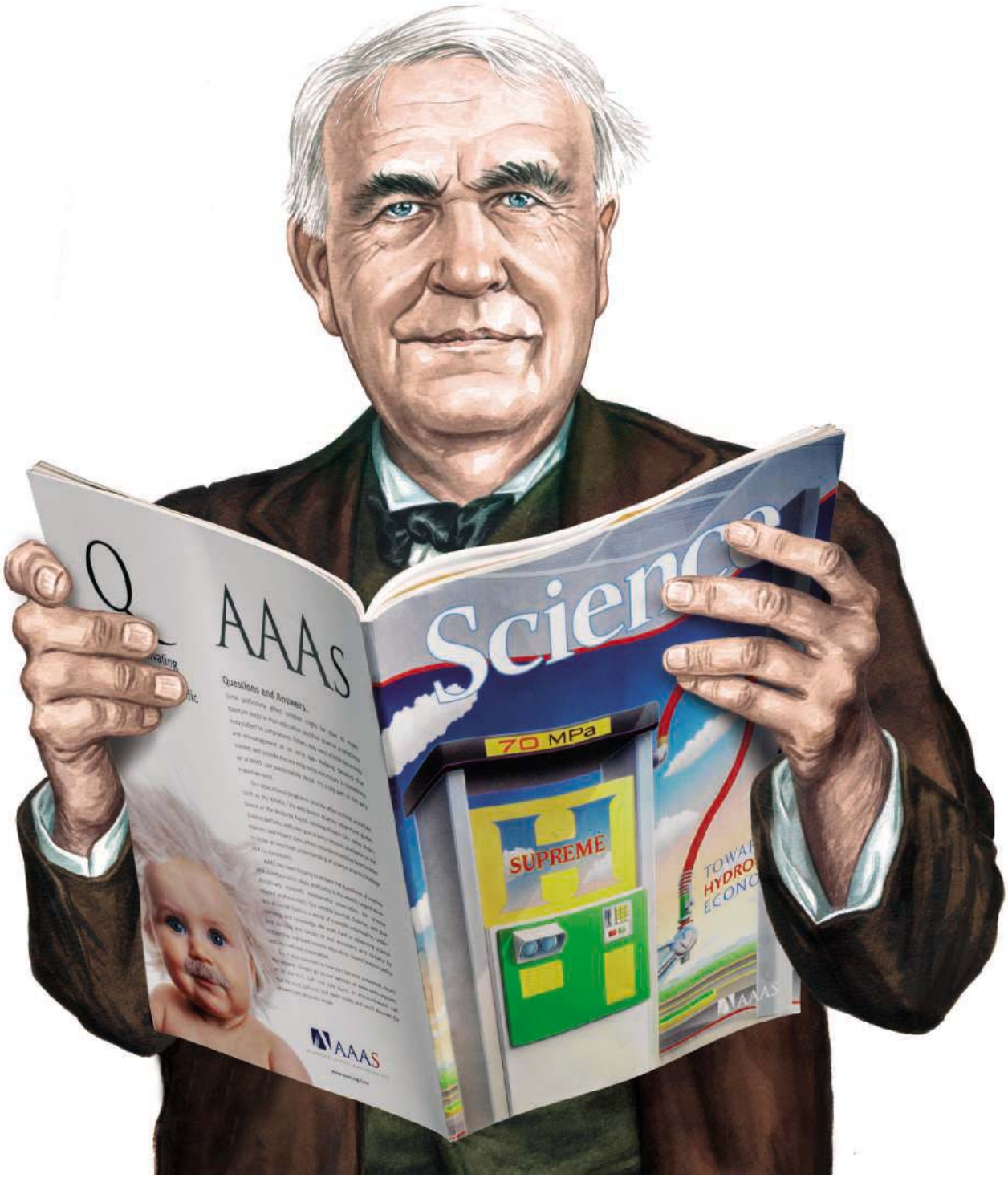

Thomas Edison
1847–1931
Founder of *Science*

TENURE-TRACK FACULTY POSITIONS IN BIOCHEMISTRY

The Division of Molecular Biology and Biochemistry, School of Biological Sciences, University of Missouri-Kansas City invites applications for two full-time tenure-track faculty positions. One position may be filled at the level of **Associate** or **Full Professor** if a particularly outstanding candidate with commensurate experience is identified; the second position will be filled at an assistant professor level. Candidates with research interests in metabolic pathway discovery/engineering or in protein dynamics/folding/interactions are of particular interest but outstanding scientists in other areas will receive careful consideration. We seek outstanding scholars with demonstrable abilities in research and teaching, and exemplary communication skills. Candidates for a more senior appointment are expected to have an established record of research productivity and funding. The School of Biological Sciences offers highly competitive salaries, start-up funds and laboratory space, and maintains state-of-the-art core facilities and shared instrumentation supporting a wide array of applications, including protein crystallography, NMR, proteomics, and genomics. For more information please visit our web-site: **www.umkc.edu/sbs**. Applicants should supply a *curriculum vitae*, reprints of 2-3 recent publications, a summary of current and future research plans, and arrange to have three letters of recommendation sent to us. Review of applications will begin immediately, and will continue until the positions have been filled. **MBB Search Committee, Division of Molecular Biology and Biochemistry – BSB 503, University of Missouri-Kansas City, 5007 Rockhill Road, Kansas City, MO 64110-2499**.

The University of Missouri Kansas City is an EO/AA Employer.

UNIVERSITY OF DELAWARE

One of the oldest institutions of higher education in this country, the University of Delaware today combines tradition and innovation, offering students a rich heritage along with the latest in instructional and research technology. The University of Delaware is a Land-Grant, Sea-Grant, Urban-Grant and Space-Grant institution with its main campus in Newark, DE, located halfway between Washington, DC and New York City. Please visit our website at **www.udel.edu.**

Assistant/Associate Professor of Plant Pathology

Department of Plant and Soil Sciences
College of Agriculture and Natural Resources

The Department invites applications for a tenure-track faculty position at the Assistant or Associate professor level. The appointment will be an academic year appointment beginning September 1, 2006 with approximately 70% research and 30% teaching. The successful candidate will be expected to develop a vigorous, extramurally-funded research program with a high potential for unique fundamental discoveries and will teach the introductory plant pathology course. All areas of plant pathology will be considered. Applications are particularly welcomed from candidates interested in host plant resistance, mycology, epidemiology, and molecular plant pathology. Candidates whose research would be enhanced by existing faculty in agronomy, horticulture, plant breeding, plant pathology, and molecular biology of plant/microbe interactions are particularly encouraged to apply. We also encourage applicants with an interest in collaborating with other faculty, extension personnel, and industrial partners in the application of basic research to address national and regional needs in the areas of plant pathology and crop improvement. Competitive salary/start up packages, modern greenhouse and plant growth facilities, and state-of-the-art facilities for microarray/gene chip analysis, proteomics, bioimaging and computational biology are available. Candidates must have a Ph.D. and demonstrated excellence in innovative research. Postdoctoral training preferred. Applicants should forward a curriculum vitae, a statement of research interests and future plans, and provide names for five references to: James A. Hawk, Chair, Plant Pathology Search, c/o Kathy Fleischut, University of Delaware, 531 South College Avenue, 152 Townsend Hall, Newark, DE 19717-1303. Email: kathyfl@udel.edu. The review of applications will commence on September 1, 2005. The curriculum vitae and letters of reference shall be shared with department faculty.

The UNIVERSITY OF DELAWARE is an Equal Opportunity Employer that encourages applications from Minority Group Members and Women.

POSITIONS OPEN

The Department of Medicine at the University of California San Francisco (UCSF) is recruiting physician-scientists engaged in translational research. Candidates must have an M.D. or M.D./Ph.D. degree and demonstrated potential to lead a first-rate and independent research program. Board certification in internal medicine is required. Appointments will be made at the **ASSISTANT/ASSOCIATE PROFESSOR** level in the In-Residence series, depending upon qualifications. The candidate will also become a member of the graduate program in biomedical sciences. Please send curriculum vitae to:

Joseph M. McCune, M.D., Ph.D.
Chair, Search Committee
Gladstone Institute of Virology and Immunology
1650 Owens Street
San Francisco, CA 94158

UCSF is an Affirmative Action/Equal Opportunity Employer. The University undertakes affirmative action to assure equal employment opportunity for underutilized minorities and women, for persons with disabilities, and for Vietnam-era veterans and special disabled veterans.

The Department of Psychiatry and Behavioral Sciences at Stanford University School of Medicine is seeking two full-time faculty members in the area of psychopharmacology. One of these positions will be at the **ASSISTANT, ASSOCIATE,** or **FULL PROFESSOR** level and based at the Veterans Affairs Palo Alto Health Care System, the second position will be at the **ASSISTANT PROFESSOR** level and based in the Stanford University Hospital and Clinics. Applicants must hold an M.D. or equivalent degree and board certification in general psychiatry. Applicants should forward curriculum vitae and the names and addresses of five references to:

K. Thomas
Faculty Affairs Administrator
401 Quarry Road
Stanford, CA 94305-5717
E-mail: kann@stanford.edu

Stanford University is an Equal Opportunity/Affirmative Action Employer.

POSITIONS OPEN

FACULTY POSITION PHARMACOLOGY/TOXICOLOGY

The Department of Pharmacology and Toxicology at Morehouse School of Medicine invites applications for a faculty position at the **ASSISTANT/ASSOCIATE PROFESSOR** level. Candidates must hold a Ph.D. and/or M.D. degree, and a strong record of research accomplishments. The successful applicant is expected to develop an independently funded research program and to participate in teaching medical and graduate students. Preference will be given to candidates with medical school teaching experience. Please send curriculum vitae, a description of research interests, and three references to: **Evan F. Williams, Ph.D., Chair, Faculty Search Committee, Department of Pharmacology and Toxicology, Morehouse School of Medicine, 720 Westview Drive, SW, Atlanta, GA 30310-1495. E-mail: ewilliams@msm.edu.**

POSTDOCTORAL RESEARCH POSITIONS in the Department of Microbiology and Immunology and Sylvester Cancer Center at the University of Miami School of Medicine are available to study innate immune responses to viral and malignant disease. The first position requires a Ph.D. with experience in virology, immunology, and/or vaccine development and evaluation. Projects involve developing novel oncolytic viruses for the treatment of malignant disease and nanoparticle based strategies for the prevention and treatment of pathogen-associated disease. The second position would require a Ph.D. with experience in *Drosophila* genetic systems with an interest in innate immunity. For consideration, please send curriculum vitae to: **Dr. Glen N. Barber** at **e-mail: gbarber@med.miami.edu.**

POSITIONS OPEN

POSTDOCTORAL TRAINEE POSITIONS
Stem Cell Research
University of Wisconsin–Madison

Outstanding candidates in all areas of stem cell research are sought for a new NIH-funded interdisciplinary postdoctoral training program. A major strength of this program is the range of stem cell expertise at the University of Wisconsin–Madison, including: (1) cutting-edge basic research examining mechanisms of pluripotency and differentiation of stem cells; (2) a broad range of translational research exploring stem cell-based therapies for degenerative diseases of the brain, heart, blood, pancreas, and more; (3) the WiCell Research Institute, which cultures and distributes five of the federally approved human embryonic stem (ES) cell lines; (4) one of only two National Primate Centers in the country that currently derive new primate ES cell lines; and (5) an active bioethics program. Program details, list of available mentors, and application procedures are available at **website: http://www.stemcells.wisc.edu.** Application deadline: August 1, 2005.

Applicants must be U.S. citizens or permanent residents. Applications from women and minorities are especially encouraged.

IMAGE PROGRAMMER II

Supervise/develop three-dimensional medical imaging software to support visualization of magnetic resonance imaging on a multi-platform environment, for real-time interventional procedures using cardiac magnetic resonance images.

Requirements: M.S. in biomedical engineering/computer science, three years design and development of medical image rendering, using interface design and data communication with auxiliary systems to support visualization of magnetic resonance imaging utilizing Linux, Silicon graphics workstation. Equivalent combined degree/experience acceptable.

Send resume to: **Johns Hopkins University, Baltimore, Maryland** at **e-mail: mritter@jhmi.edu.**

The Coca-Cola Company

The Coca-Cola Company is a 119 year-old company, the owner of the world's most recognized trademark and the world leader in nonalcoholic beverages. The Company has Innovation Centers on 4 continents and presently has the following opportunities for scientists at the corporate offices in Atlanta, Georgia:

Biological Chemistry: Selected candidates will have a PhD degree with expertise in cell biology, signal transduction and membrane chemistry along with working knowledge of organic chemistry and nutritional science. Qualified candidates are expected to have a minimum of 10 years experience in industrial or academic research with a track record of innovation as reflected by products, patents and publications. Experience and capability in the initiation and management of internal as well as external research projects are essential.

Neuroscience: Selected candidates will have a PhD degree with expertise in central processing of sensory information as is relevant to perception of food and beverage attributes. Qualified candidates are expected to have a minimum of 10 years experience in industrial or academic research with a track record of innovation as reflected by products, patents and publications. Experience and capability in the initiation and management of internal as well as external research projects are essential.

The Coca-Cola Company offers a competitive salary, excellent benefits and an opportunity to work in an exciting interdisciplinary team environment. For consideration, please send or fax your resume to **Attn: Diane Vogel: 404-253-4752 (FAX); divogel@na.ko.com (email).**

All candidates must be US citizens or permanent residents. Minority applicants are encouraged to apply.

Sant Chair for Marine Science
Smithsonian Institution, National Museum of Natural History

The National Museum of Natural History (NMNH) of the Smithsonian Institution is inviting applications for the Sant Chair for Marine Sciences, made possible by a generous gift from Mr. and Mrs. Roger Sant. This senior-level position has recently been established as part of the Museum's new Ocean Science Initiative (**www.mnh.si.edu/ocean**). The Museum has a large faculty of scientists concerned with investigating and documenting marine biodiversity and is home to unparalleled collections that comprise over 33 million specimens of marine organisms. It is part of the Smithsonian Marine Science Network, with facilities in Maryland, Florida, Belize and Panama providing outstanding opportunities for field research. In partnership with the Congress and the National Oceanic and Atmospheric Administration (NOAA), it is currently developing a dramatic new Ocean Hall, which will become the Museum's most prominent hall and is scheduled to open in September 2008.

Applications are invited from researchers who have an outstanding record of leadership and accomplishment in collections-based research in the marine sciences, including systematics, evolution, ecology, or paleobiology. The successful candidate will be responsible for articulating and advancing the Ocean Science Initiative and stimulating new multi-investigator collaborations involving NMNH, the Smithsonian Marine Science Network, and affiliated scientists from the National Marine Fisheries Service of NOAA. He/she is expected to maintain an active program of high-profile research and train graduate and postdoctoral research personnel.

This is a Smithsonian Trust position. Trust employees enjoy a comprehensive benefit program including a lucrative TIAA-CREF retirement program that is fully vested. Salary range is $124,736 - $149,200. The position is located in the National Museum of Natural History in Washington, DC.

For complete announcement and application instructions, go to **http://www.si.edu/ohr**; the announcement number is **EX-05-12**.

The Smithsonian is an Equal Opportunity Employer.

Tenure-Track Faculty Position in Biophotonics
Center for Cell Analysis and Modeling
University of Connecticut Health Center

The Center for Cell Analysis and Modeling (**http://www.ccam.uchc.edu/**) at the University of Connecticut Health Center is a multidisciplinary center that develops new photonic, microscopy, and computational approaches for the study of cellular systems. We are seeking an addition to our faculty whose research program focuses on development of new optical methods to investigate the physical bases for cell biological processes such as cell motility, intracellular trafficking, cell differentiation or signal transduction. Areas of special interest include: nanofabrication, nanomanipulation, micro- and nano-sensors, single molecule microscopy, non-linear optical contrast mechanisms, and new modalities for sub-cellular functional imaging down to the nanometer spatial and millisecond time scales. The successful candidate will also have an appointment in an appropriate basic science department and will be encouraged to develop collaborations with other investigators in the biological, physical and clinical sciences. Approximately 80% time will be available for research. Opportunities to participate in training of graduate students in cell biology, physical sciences, and engineering disciplines will also be available. Salary and startup package will be commensurate with experience and level of appointment.

The closing date for receipt of applications is **October 1, 2005**. Applicants should submit a letter of application, curriculum vitae, research plan, and statement of teaching interests, and names (with address and e-mail address) of at least three references. Applications should be e-mailed in RTF or PDF format to **biophotonics@uchc.edu.**

The University of Connecticut is an Equal Opportunity/Affirmative Action Employer. Women and people from diverse racial, ethnic, and cultural backgrounds are strongly encouraged to apply.

POSITIONS OPEN

DIVISION OF INTEGRATIVE ORGANISMAL BIOLOGY
National Science Foundation

The National Science Foundation (NSF)'s Division of Integrative Organismal Biology (IOB) is seeking qualified candidates for several current positions as **PROGRAM DIRECTOR:** extensive cyber experience and biological expertise in the general area of organismal biology, especially in the areas of animal development, neuronal and glial mechanisms, computational neuroscience, behavioral neuroscience, and neuroendocrinology. Program Directors are responsible for program planning and administration, and for furthering the goals of the NSF and IOB. More information about IOB can be found on their **website: http://www.nsf.gov/div/index.jsp?div=IOB.** Positions may be filled on a permanent basis, one or two year Visiting Scientist (VSEE), or a federal temporary appointment with a salary range of $88,369 to $137,713, depending on qualifications and experience. Alternatively, this position may be filled under the terms of the Intergovernmental Personnel Act (IPA). Applicants must possess a Ph.D. in biology or in an equivalent discipline, plus six or more years of successful research, research administration, or managerial experience beyond the Ph.D. Familiarity with NSF policies and practices, administrative experience, and recognized stature among peers are desirable.

Individuals interested in the permanent position should apply to announcement E20050091 and individuals interested in the rotator position should apply to announcement E20050092-Rotator. Additional information on the VSEE and IPA program can be obtained at **website: http://www.nsf.gov/about/career_opps.** Technical questions should be directed to: **Dr. Tom E. Brady, Division Director** at **telephone: 703-292-8420** or **e-mail: tbrady@nsf.gov** or **Dr. Judith Verbeke, Deputy Division Director** at **telephone: 703-292-8420** or **e-mail: jverbeke@nsf.gov.**

NSF is an Equal Opportunity Employer committed to employing highly qualified staff that reflects the diversity of our nation.

SENIOR BIOLOGIST
Vanderbilt Screening Center for GPCRs, Ion Channels, and Transporters

The Vanderbilt Screening Center for G protein-coupled receptors (GPCRs), Ion Channels, and Transporters invites applications for the position of senior staff biologist. The Vanderbilt Center is a new, state-of-the-art high-throughput screening (HTS) facility that is part of the ten-member Molecular Libraries Screening Center Network (MLSCN) funded by the National Institutes of Health. The successful candidate will work as a member of a multidisciplinary team focused on discovering novel small molecular tools for the advancement of basic and drug-discovery research. Candidates should have a Ph.D. in biology, chemistry, or related discipline with a research focus on ion channels, GPCRs, or transporters. Candidates with a Master's degree plus five years of relevant experience will also be considered. Excellent personal, supervisory, training, organizational, and communication skills are essential. Applications should be submitted electronically to: **Dave Weaver** at **e-mail: david.weaver@vanderbilt.edu.**

POSTDOCTORAL POSITION
Human Cancer Gene Therapy

Federally funded laboratory program conducting human clinical trials and basic research in T cell gene therapy for prostate, melanoma, breast, colon cancers. Advanced retroviral vector development and engineering T cell effector responses. Contact: **Dr. R.P. Junghans, Roger Williams Medical Center/Boston University School of Medicine** via **e-mail: mjamison@rwmc.org** with resume, research summary, names of three references.

The Department of Physiology at the University of Pennsylvania's School of Medicine seeks candidates for an **ASSISTANT PROFESSOR** position in the non-tenure research track. Applicants must have a Ph.D. or equivalent degree and have demonstrated excellent qualifications in research.

The candidate must have evidence of research experience in cell culture and free radical chemistry.

The successful candidate will be expected to develop an independent research program in signaling by oxygen radicals and will also be responsible for the direction of a funded research program in mechanism of oxygen radical production in lung ischemia and for participating in collaborative research programs of the Institute for Environmental Medicine.

Application materials must be submitted by August 31, 2005.

Please submit curriculum vitae, a brief statement of research interests, and three reference names to:

Susan Turbitt
Institute for Environmental Medicine
University of Pennsylvania,
School of Medicine
3620 Hamilton Walk
Philadelphia, PA 19104-6068
Fax: 215-898-0868
E-mail: turbitt@mail.med.upenn.edu

The University of Pennsylvania is an Equal Opportunity/Affirmative Action Employer. Women and minority candidates are strongly encouraged to apply.

POSTDOCTORAL POSITIONS: DEVELOPMENT, FUNCTIONAL GENOMICS, AND CHROMATIN

As part of an interdisciplinary research team (**website: http://compbio.med.wayne.edu**) you will be using advanced, molecular, fluorescence activated cell sorter (FISH), chromatin immunoprecipitation (CHIP), microarray, real-time, and computational technologies to determine how chromatin structure and RNA are used to reprogram our genome. Self-motivated individuals trained in molecular spermatogenesis, genetics, cytogenetics, and/or biochemistry with expertise in FISH, CHIP, and microarrays are especially encouraged to apply. Applicants should forward their curriculum vitae and three letters of reference to:

Dr. S.A. Krawetz, C.S.
Mott Center for Human Growth and Development
Wayne State University
School of Medicine
275 E. Hancock
Detroit, MI 48201
E-mail: steve@compbio.med.wayne.edu

Wayne State University is an Equal Opportunity/Affirmative Action Employer.

POSTDOCTORAL POSITIONS
Baylor College of Medicine

Two Postdoctoral Research positions are available immediately to study estrogen receptor action. One position is to study the regulation of cell signaling on estrogen receptor function and interaction with coactivators and corepressors. The second position is to study mechanisms of ligand-dependent estrogen receptor down regulation by the 26S proteasome. See **website: http://public.bcm.tmc.edu/mcb/faculty/smith_c.html** for more details of the laboratory's research interests and recent publications.

Required qualifications: Ph.D. with strong background in molecular biology and/or cell biology. Salary commensurate with experience.

To apply send (preferably by **e-mail: carolyns@bcm.tmc.edu**) a letter of application including a short description of research experience and interests, curriculum vitae, and names and contact information for three references to: **Carolyn Smith, Ph.D., Department of Molecular and Cellular Biology, Baylor College of Medicine, One Baylor Plaza, Houston, TX 77030.** *Baylor College of Medicine is an Equal Opportunity/Affirmative Action/Equal Access Employer.*

THE GENOMICS RESEARCH CENTER
Academia Sinica, Taipei, Taiwan

Nominations and applications are invited for all levels of **RESEARCH** and **TECHNICAL POSITIONS** in the following areas: chemical biology (synthetic organic chemistry and drug discovery), cell-based research (cell biology related to cancer and infectious diseases), key technology development (nanobiotechnology, new methods for detection, analysis, and profiling), biotech incubation center (technology transfer, evaluation, and business development).

For consideration, please send a copy of curriculum vitae, including a list of publications, two to three references, and a cover letter describing your area of interest, and for a **PRINCIPAL INVESTIGATOR** position, a brief statement of research plan to:

Dr. Chi-Huey Wong, Director
Genomics Research Center
Academia Sinica
128 Academia Road, Section 2
Nankang District, Taipei 115
Taiwan
Telephone: +886-2-2789-9922
Fax: +886-2-2789-9923
E-mail: chwong@gate.sinica.edu.tw
Website: http://www.genomics.sinica.edu.tw/

METALLOPROTEIN ENGINEERING POSTDOCTORAL: Searching for a highly motivated and creative individual with a strong background in protein engineering to join a multidisciplinary team within the National Science Foundation Industry/University Cooperative Research Center for Biocatalysis and Bioprocessing of Macromolecules. The successful candidate will design and synthesize metalloproteins with new catalytic properties using various strategies that include both targeted and combinatorial protein engineering. He/she must have a recent Ph.D. in biochemistry or a closely related field. A competitive salary is offered commensurate with qualifications and experience. Send resume and copies of publications to:

Professor Richard A. Gross
Polytechnic University
Six Metrotech Center
Brooklyn, NY 11201
Website: http://chem.poly.edu/gross/

POSTDOCTORAL POSITIONS: Several Postdoctoral positions funded by the National Institutes of Health are available, to study the roles of insulin, nitric oxide, and protein tyrosine phosphatases in regulation of vascular smooth muscle cell signaling and neointima formation in vascular injury. Our projects address important basic science questions and also have relevance to clinical problems. Experience in molecular biology and/or rat and mouse surgery is essential. Competitive salaries are offered. Please send curriculum vitae and the names of three references to: **Dr. Aviv Hassid, Department of Physiology, University of Tennessee, 894 Union Avenue, Memphis, TN 38163. E-mail: ahassid@tennessee.edu; fax: 901-448-7126.** *The University of Tennessee is an Equal Employment Opportunity/Affirmative Action/Title IV/Title IX/Section 504/ADA/ADEA Institution in the provision of its education and employment programs and services.*

San Francisco, California: **POSTDOCTORAL RESEARCH FELLOW** position available at University of California San Francisco, Division of Nephrology. *Must be U.S. citizen or permanent resident* and eligible for NIH training grant. Please send curriculum vitae to:

Dr. Stephen L. Gluck
513 Parnassus Avenue
Box 0532
San Francisco, CA 94143-0532
E-mail: glucksl@medicine.ucsf.edu

Careers in Drug Discovery

A *Science* Advertising Supplement

Marie Curie
1867–1934

Issue date 29 July
Limited space still available.
Reserve Now!

Need to attract great scientists?

Then talk to someone who knows science.

Special Bonus Distributions:

- Drug Discovery Technology, 8-11 August, Boston, MA
- *Science* Career Fair, 10 August, Boston, MA

Qualified circulation of 129,590[1] plus our pass-along readers brings total global weekly readership to over 710,000.[2]

ScienceCareers.org postings available – 7 websites for the price of one!
Your print recruitment ad can be placed on our website, ScienceCareers.org, for a nominal fee. Ads posted are also searchable on the following websites:

- Biocompare
- National Postdoctoral Association (NPA)
- Stanford University School of Medicine
- *Science*'s Signal Transduction Knowledge Environment (STKE)
- *Science*'s Aging Knowledge Environment (SAGE)
- *Science*'s Next Wave.

1 *Science* June 2004 BPA Publisher's Statement.
2 *Science* June 2004 circulation as applied to 14 January 2000 Harvey Readership Survey and 2002 Harvey Cumulative Report, publisher's own data.

To advertise contact:
U.S. Daryl Anderson
phone: 202-326-6543
e-mail: advertise@sciencecareers.org

Europe and International
Tracy Holmes
phone: +44 (0) 1223 326 500
e-mail: ads@science-int.co.uk

Japan
Jason Hannaford
phone: +81 (0) 52 789-1860
e-mail: jhannaford@sciencemag.jp

ScienceCareers.org
We know science AAAS

MARKETPLACE

MARKETPLACE

Believe it!

DNA Sequencing for $2.50 per reaction.

- Read length up to 900 bases.
- High quality electropherograms.
- Fast turnaround.
- Plasmid and PCR purification available.

$2.50 per reaction!

Polymorphic exclusively uses ABI 3730XL sequencers.
Data delivered via secure FTP, email or CD.
No charge for standard sequencing primers.
96 sample minimum order.
96 well plates only- no tubes.

POLYMORPHIC
Polymorphic DNA Technologies, Inc.℠

www.polymorphicdna.com
info@polymorphicdna.com

1125 Atlantic Ave., Ste. 102
Alameda, CA 94501

888.362.0888

For more information please visit
www.polymorphicdna.com